Middle Miocene climate change: marine palaeoecology and organic geochemistry in the Porcupine Basin

(IODP Site U1318, eastern North Atlantic Ocean)

Midden-Miocene klimaatsveranderingen: mariene paleo-ecologie en organische geochemie in het Porcupine Bekken

(IODP Site U1318, oostelijke Noord-Atlantische Oceaan)

Cecilia Wilhelmina Quaijtaal, 2017

Dissertation submitted for the degree of Doctor in Science: Geology

Supervisor: Prof. Dr. Stephen Louwye

Co-supervisor: Prof. Dr. Timme H. Donders

GHENT UNIVERSITY

FACULTY OF SCIENCES

Members of the examination committee

Prof. Dr. Marc De Batist (Ghent University, Belgium): chair
Prof. Dr. David Van Rooij (Ghent University, Belgium): secretary
Prof. Dr. Matthew Pound (Northumbria University, United Kingdom)
Prof. Dr. Ir. Stefan Schouten (Utrecht University / NIOZ, the Netherlands)
Prof. Dr. Elie Verleyen (Ghent University, Belgium)
Prof. Dr. Thijs Vandenbroucke (Ghent University, Belgium)
Dr. Kenneth Mertens (Ifremer, France)
Prof. Dr. Timme Donders (Utrecht University, the Netherlands): supervisor
Prof. Dr. Stephen Louwye (Ghent University, Belgium): supervisor

Willemijn Quaijtaal carried out the research with financial support of the Research Foundation – Flanders (FWO grant number G.0179.11N).

Please refer to this thesis as:
Quaijtaal, W., 2017, Middle Miocene climate changes: marine palaeoecology and organic geochemistry in the Porcupine Basin (IODP Site U1318, eastern North Atlantic Ocean). PhD thesis, Ghent University, Ghent, Belgium.

Front cover:
Painting by **Annemarie van Dijk**, picture by **Matthijs Quaijtaal**.

Research highlights

- The middle Miocene deposits of IODP Leg 307 Site U1318 were investigated using magnetostratigraphy, biostratigraphy using organic-walled dinoflagellate cysts (dinocysts) and calcareous nannoplankton, and stable carbon- and oxygen isotope stratigraphy. The results indicate that the sediments accumulated between ~16.6–12.7 Ma. The sampling resolution was ~17 ka. Four positive excursions were measured in benthic foraminiferal stable oxygen isotope ratios: Mi-2 (16.1 Ma), Mi-2a (14.8 Ma), Mi-3 (13.7 Ma) and Mi-4 (12.9 Ma). These events indicate cooling and / or glaciation.
- A palaeoecological assessment of Mi-3 and Mi-4, based on dinocyst assemblages, shows a decrease in sea-surface temperature and sea level during both events. Mi-3 seems associated with an increase in productivity, indicated by an acme of the heterotrophic, but also low-salinity-tolerant dinocyst species *Palaeocystodinium golzowense*. Dinocyst diversity decreases during Mi-4. Decreases in sea-surface temperature correlate to minima in June solar insolation, implying a strong role for orbital forcing of the Mi-events.
- Six acritarch species new to science were recorded and described: *Cometesphaera bullatio* gen. et sp. nov., *Cymatiosphaera*? *deverteuilii* sp. nov., *Platycystidia manumii* sp. nov., *Porcupinea collaris* gen. et sp. nov., *Porcupinea indentata* gen. et sp. nov. and *Pusillisphaera solaris* gen. et sp. nov.. Their biostratigraphic ranges and palaeoecological preferences were determined.
- The first middle Miocene sea-surface temperature record from the North Atlantic Ocean was generated using the organic geochemical palaeothermometers TEX_{86} and $U^{K'}_{37}$ and a qualitative record based on dinocysts (SST_{dino}). SST_{dino} compares well to the TEX_{86} record. Based on a good correlation to the benthic foraminiferal stable isotope record from Site U1318 and a lead of the SST_{dino} and $U^{K'}_{37}$ temperatures relative to TEX_{86}-temperatures (SST_{TEX86}), it was concluded that SST_{TEX86} represents subsurface rather than surface temperatures. The most prominent event is Mi-3 with ca. 6°C cooling. Comparison with available atmospheric CO_2 reconstructions and the orbital parameters shows that sustained cooling and northern hemisphere glaciation are only possible at CO_2 lower than 280 ppm, combined with minima in the orbital parameters eccentricity and obliquity amplitude modulation.

Table of contents

Acknowledgments

First of all I want to thank my 'SST' team: Stephen, Stefan and Timme.
Stephen: Bedankt voor al je steun en raad. Ik heb zoveel van je geleerd over het Mioceen, dinocysten en de wondere wereld van de acritarchen, en er is nog steeds zoveel bij te leren. Tussen alle vergaderingen en lessen door had je of maakte je altijd tijd voor me, of we belden met elkaar. Ik weet dat ik soms eigenwijs en koppig kan zijn, maar het is op tijd afgeraakt!
Timme: Grazie mille voor alle warme welkomsten in Utrecht! Het is spijtig dat we zo weinig met de pollen hebben kunnen doen, maar ik heb zoveel gehad aan je input, suggesties, commentaren en het hart onder de riem wanneer dat nodig was. Het heeft al mijn manuscripten zoveel verbeterd!
Stefan: Dankjewel dat ik op het NIOZ mijn analyses mocht doen. Het was fijn dat we altijd tussendoor iets nieuws konden uitproberen om te zin of het werkte op mijn sedimenten. Bedankt voor je rake opmerkingen voor hoofdstuk 5!

Then there are some other colleagues that I want to acknowledge.
Zonder **Steven Tesseur** zou er geen stabiele koolstof- en zuurstofisotopencurves zijn. Hij heeft alle foraminifera gepickt en geanalyseerd. Dankjewel voor de gezellige tijd op kantoor samen, en de lunches in de resto.
Stijn De Schepper, bedankt voor de samenwerking in het manuscript dat helaas niet heeft mogen zijn. Wie weet, ooit nog?
Many thanks to all the members of the **examination committee**, my thesis has improved so much from all the input I got.
In special I would like to thank Honorary Professor **Jean-Pierre Henriet**, who passed away in April, this year. Without him there would be no IODP expedition 307 in the Porcupine Basin. He was always interested in my stories about Porcupine when I met him in the corridors.
Dan zijn er nog mijn andere kantoorgenootjes **Koen, Annelies en Sabine.** Ook jullie vergezelden mij vaak naar de resto. Ik weet dat ik soms wat te veel klets, maar ik vond het erg gezellig!
Terugkerend thema: de resto. Ook **Gerben, Ingrid** en **Lieven** gingen vaak mee. Bedankt voor alle koffie, de chats, de kattenpraat en wat al niet meer. En Ingrid, heel erg bedankt voor mijn Griekse kadootje Lena, ik ben zo blij met haar!
Als laatste van 't unief zijn er dan nog alle andere collega's, van de groep: **Achilles, Bert, Daan, Dirk, Jan B, Jan M, Jacques, Julie, Kenneth, Leonard, Pieter, Thijs, Thomas S, Thomas V, Vanessa,** en de andere groepen: **Ann-Eline, Elien, Emmanuel, Hans, Kurt, Marc, Mathijs, Tim, Thomas, Stan, Wim**.

Hiernaast wil ik iedereen op het NIOZ bedanken die me daar met van alles geholpen heeft: **Anchelique, Jort, Monique, Marianne** en **Ellen**. **Lisa**, thanks for sharing your office with me during my visits!

Furthermore there are plenty of people that I need to thank outside university. I have been writing my thesis at very unconventional places: sitting in an ambulance, at the ice rink during the break of a shorttrack competition, at the dispatching room of a big event, and there are probably plenty more weird spots. Therefore it is in order to thank all the people tolerating me for doing so, and for tolerating me being a lousy friend during the last months.

De Gentse afdeling van het Rode Kruis is mijn tweede familie sinds ik hierheen ben verhuisd. Ik heb me altijd welkom gevoeld, ondanks mijn andere achtergrond en opleidingen. Ik heb zoveel lol gehad tijdens de preventieves dat ik hoop dat ik nog vele jaren aan mijn staat van dienst kan toevoegen. Natuurlijk kan ik niet iedereen persoonlijk bedanken, maar een dikke merci aan het 'minicomité' **Wim V, Dorien, Tom, Wouter, Karolien, Jeroen** en **Wim B**, mijn voorganger als materiaalverantwoordelijke **Emma** en onze secretaresse **Nancy**. Hiernaast veel dank aan het Rode Kruis van Dendermonde om mij op te vangen na weeral een verhuis.

Een van mijn Rode Kruis-collega's wil ik special bedanken. M2 voor H622? **Kris**, ik weet dat je er niet van houdt in de aandacht te staan, maar je hebt het verdiend. Je bent een van mijn beste vrienden de laatste jaren. Je bent er altijd geweest voor me. Je was er wanneer ik in de put zat, mezelf had buitengesloten, hebt voor Lena gezorgd als ik naar het buitenland moest, onze vrijdagmiddag/avond dinertjes en drankjes, onze gekke ambulanceshifts samen, Wacken, de opleiding Dringende Geneeskundige Hulpverlening… Ik kan niet in woorden uitdrukken hoe dankbaar ik daarvoor ben. H622 out.

Ich möchte also meine Freunden vom Wacken Resque Squad danken für die schöne Zeiten. Ins besonders danke ich **Bjorn** und **Raoul**. Sehe euch in Wacken, Rain or Shine!

Then there are what I call the "expat knitters". I am happy that I got to know you all: **Adina** (mew!), **Babs** (thanks for giving me the best Christmas present ever!), **Diana** (I love the vegan cupcakes) and later **Jan** (ok, you don't knit. Thanks for having me over and fixing my laptop), and many more… De Oost-Vlaamse dames hier in de buurt: ik geniet zo van onze breiavondjes! Verder wil ik al mijn Diva- en Karmazusjes bedanken om er voor elkaar te zijn!

Aan iedereen van mijn schaatsclub, bedankt voor de fijne tijd tot nu toe, BK medailles, wie had dat ooit gedacht? Bedankt aan iedereen met wie ik keer op keer heb mogen meerijden naar wedstrijden of Breda. **Petra**, zonder jou was ik nooit gaan schaatsen! Bedankt voor alles toen je hier in Gent was. Van de LangeBaan Schaatsclub Gent LBSG een duim voor special **Koen, Marc, Jean-Luc, Gert, Henk, Kenny, An, Seppe, Michiel, Andreas** en **Ids**. Voor de collega's van de kortebaan ShortTrackclub Kristallijn Gent STKG zijn dat **Maarten, Fabienne, Jill, Freddy, Antoine, Willem, Kristof** en **Tony** (Masters powerrrr!).

Verder zijn er nog een paar belangrijke vrienden die ik met heel mijn hart wil bedanken.

Johan, het is onwaarschijnlijk dat we allebei in België zijn beland, maar ik ben er heel blij mee! We waren maar een treinreis van elkaar verwijderd en je hebt me opgebeurd toen ik het soms even niet meer zag zitten. Bedankt voor het uitleggen van geologische zaken aan een 'domme bioloog', de etentjes en biertjes samen!
Alje, ook al is het lang geleden dat we elkaar hebben gesproken, jij hebt me door de eerste, moeilijke tijd in België heen gesleept, met knuffels en je heerlijke eten. Dankjewel.
Een boel kudo's aan **Vera en Paula**, en **Joost**. Jullie zijn mijn connectie met Nijmegen, en het was met een grens tussen ons niet altijd makkelijk om elkaar te blijven zien, maar ik ben zo blij dat ik jullie in mijn leven heb, en dat voor al een heel lange tijd.

Dan nog mijn dank aan heel mijn **familie**, en mijn **grootouders** (ja, ik ben eindelijk klaar nu!). Ook een dankjewel aan **Rita**, en **René** en **Gina**, voor alles dat jullie voor Raf en mij doen.

I cannot thank my brother **Matthijs** enough. I have bothered him plenty of times with questions regarding the English language and he has always tried to help me, even though he detests scientific English. Thanks bro! Lots of hugs to **Terje** too!

Lieve **papa en mama**, dankjulliewel voor jullie eeuwige steun. Om te proberen te begrijpen wat ik nu eigenlijk allemaal deed. De ritjes heen en weer naar België, met eten! De Skypejes. Jullie geduld (heb je al een datum?). Mama, bedankt dat je het schilderij voor mijn kaft wilde maken. Ik wilde dat jullie dichterbij woonden…

Lieve **Lena**, dankjewel voor alle knuffels, je gezelschap op mijn werkkamer thuis, je teken dat ik genoeg had gewerkt wanneer je op mijn papierwerk of toetsenbord kwam liggen. Je hebt wat lekkers verdiend!

Natuurlijk wordt het beste tot het laatst bewaard. Mijn liefste **Raf**, onverwacht stond je daar in mijn leven. Wat had ik het afgelopen jaar zonder jou gemoeten? Echt, het was me niet gelukt. Jouw grenzeloze steun, die kleine push die nodig was om me terug in gang te doen schieten, je eindeloze stroom aan grapjes… De afgelopen vijf maanden zijn misschien een kleine hel geweest met de ene deadline na de andere, een verbouwing en een halve verhuis, maar we hebben het gehaald. Ik hoop dat ik jou ook zo door jouw thesis heen kan slepen, en dat we onder het motto “wat denk je dat ik ga doen???” nog heel veel langer mogen doorgaan. Ik hou van je, dikke kus!

List of abbreviations

ATNTS	Astronomically Tuned Neogene Time Scale
BWT	Bottom water temperature
CCA	Canonical correspondence analysis
CM	^{13}C maximum
CNC	Continental slope current
DSDP	Deep Sea Drilling Project
EF	England finder
ENAW	Eastern North Atlantic water
FOV	Fields of view
GDGT	Glycerol dialkyl glycerol tetraether
HO	Highest occurrence
IODP	Integrated Ocean Drilling Program
ka	Kilo-annum, thousand years
kyr	Kilo years, thousand years
LO	Lowest occurrence
Ma	Mega-annum, million years
MAT	Mean annual air temperature
mbsf	Meters below sea floor
mcd	Meters composite depth
Mi-	Miocene isotope-
MMCO	Middle Miocene Climatic Optimum
MMCT	Middle Miocene Climatic Transition
Myr	Million years
N/O	Neritic/Oceanic
NH	Northern hemisphere
P/G	Peridinioid/Gonyaulacoid
PCA	Principal component analysis
S/D	Sporomorph/Dinocyst
SEM	Scanning electron microscope
SH	Southern hemisphere
SSP	Sea surface productivity
SSS	Sea surface salinity
SST	Sea surface temperature
W/C	Warm/Cold
wt.%	Weight percentage

Samenvatting

Het Mioceen is een geologische tijdsperiode van 23.03 tot 5.33 miljoen jaar geleden (Ma). Deze periode wordt gekenmerkt door twee intervals met elk een verschillend klimaatregime. De eerste is het relatief warme midden Miocene klimaatsoptimum (MMCO; 17–14.5 Ma), die wordt gevolgd door een periode van afkoeling, de midden Miocene klimaatstransitie (MMCT). Het MMCO is de warmste periode van de laatste 34 miljoen jaar. Echter, dat warme klimaat was niet constant, maar werd tijdelijk onderbroken door periodes van afkoeling. Aan het einde van het MMCO werd die afkoeling echter permanent tijdens het MMCT, een periode van stapsgewijze afkoeling en/of glaciatie. Deze periodes van afkoeling gaan samen met 7 positieve excursies van stabiele zuurstofisotopen gemeten op benthische foraminiferen: de Miocene isotopen(Mi-)zonering of events. Mi-2 en Mi-2a spelen zich af tijdens het MMCO, Mi-3 en Mi-4 zijn onderdeel van het MMCT. Mi-3 heeft van al deze Mi-events de meeste impact. Verschillende oorzaken van de Mi-events zijn onderzocht, maar een reductie van de hoeveelheid CO_2 in de atmosfeer of een combinatie van minima in de aardbaanparameters eccentriciteit en amplitudemodulatie van obliquiteit zijn de meest aannemelijke verklaringen. CO_2 alleen is niet voldoende om een dergelijke permanente transitie als het MMCT te veroorzaken. Daarom zijn er data nodig om de effecten van verschillende oorzaken uit elkaar te halen. Vooral van de Noord Atlantische Oceaan zijn er geen temperatuurdata die zowel het MMCO als het MMCT overspannen.

Het Porcupine Bekken in de oostelijke Noord Atlantische Oceaan, voor de kust van Ierland biedt een goede locatie voor studie van het midden Mioceen. In 2005 werd er een boring gezet door het 'Integrated Ocean Drilling Program' om het ontstaan van de koudwaterkoralen in de omgeving te onderzoeken. Onderzoekssite U1318 ligt op 409 meter waterdiepte op de continentale marge en staat onder invloed van de Noord Atlantische stroming, die onder invloed van glaciatie minder sterk zou kunnen zijn.

Een studie op lage resolutie liet al zien dat eencellige mariene algen uit het Porcupine Bekken, dinoflagellaten, sterk reageren onder invloed van de Mi-events. Deze dinoflagellaten reageren gevoelig op veranderingen in oppervlaktewatertemperatuur, -saliniteit, -productiviteit en afstand tot de kust. Tijdens hun seksuele voortplanting maken dinoflagellaten rustcystes, zogenaamde dinocysten. Deze zijn gemaakt van een sterk resistent materiaal zodat ze goed bewaard blijven in sedimenten. Dinocysten worden daarom vaak gebruikt om mariene paleo-ecologie te reconstrueren. Voor deze studie zullen we dan ook dinocysten op hoge resolutie gebruiken om de biotische respons op de Mi-events te monitoren. Aanvullend worden ze hier tevens gebruikt voor biostratigrafie.

Omdat dinocysten enkel relatieve temperatuur weergeven worden aanvullend twee organisch geochemische methodes gebruikt om kwalitatieve temperatuurreconstructies te maken. De TEX_{86} index is gebaseerd op het temperatuursafhankelijke aantal cyclopentaanringen in de vetzuren van de celmembranen van Thaumarchaeota. Thaumarchaeota zijn chemoautotrofe eencelligen die in de gehele waterkolom voorkomen, maar voornamelijk in de bovenste 200 meter. Aanvullend wordt de $U^{K'}_{37}$ index gebruikt, die gebaseerd is op het temperatuursafhankelijke aantal dubbele bindingen in alkenonen. Alkenonen zijn moleculen die worden geproduceerd door haptophyten, fotoautotrofe algen die een van de belangrijkste groepen fytoplankton zijn.

Verder worden voor deze studie stabiele zuurstof ($\delta^{18}O$)- en koolstofisotopen ($\delta^{13}C$) gemeten op benthische foraminiferen, heterotroof plankton dat op de zeebodem leeft en een kalkskeletje maakt. Deze isotopen worden gebruikt omdat bepaalde veranderingen en pieken in isotopencurves

mondiaal waar te nemen zijn. Sommige van deze pieken zijn gecorreleerd aan magnetostratigrafie, een methode die ook beschikbaar is voor Site U1318. De intensiteit van het paleomagnetische signaal van het Porcupine Bekken is echter zeer laag, wat de interpretatie lastig maakt. Door de veranderingen in de curves van het Porcupine Bekken te vergelijken met curves van andere goed gedateerde onderzoekssites is het mogelijk om het ouderdomsmodel voor Site U1318 te valideren of te verbeteren.

Een palynologische studie op hoge resolutie tijdens het MMCT laat zien dat tijdens Mi-events Mi-3a, Mi-3b en Mi-4 oppervlaktewatertemperaturen en het zeeniveau daalden. Mi-3a en Mi-3b gaan samen met een stijging in oppervlaktewaterproductiviteit, en een sterke toename van de heterotrofe dinocyst *Palaeocystodinium golzowense*. Deze wordt waarschijnlijk veroorzaakt door een versterking in opwelling van diepe wateren door sterkere westenwindgordels tijdens koude periodes. Mi-3b is het meest uitgesproken event. Koude periodes vallen samen met juni-insolatie minima wat impliceert dat de aardbaanparameters sterke invloed hebben op het veroorzaken van de Mi-events. Zeespiegelveranderingen doorheen de tijd correleren goed met zeespiegelveranderingen in de westelijke Noord Atlantische Oceaan. Verder is de paleo-ecologie van vijf fossiele dinocystensoorten bepaald door middel van multivariate statistiek.

Tijdens deze palynologische studie is extra aandacht besteed aan kleine palynomorfen. Acritarchen zijn palynomorfen met een zeer waarschijnlijke mariene oorsprong waarvan de biologische affiniteit onbekend is. Desondanks kunnen ze worden gebruikt als biostratigrafische marker, maar ook als indicator van verschillende omgevingsvariabelen in het verleden. Zes nieuwe soorten zijn ontdekt: *Cometesphaera bullatio* gen. nov. et sp. nov., *Cymatiosphaera*? *deverteuilii* sp. nov., *Platycystidia manumii* sp. nov., *Porcupinea collaris* gen. nov. et sp. nov., *Porcupinea indentata* gen. nov. et sp. nov. en *Pusillisphaera solaris* gen. nov. et sp. nov.. Het biostratigrafische bereik van deze soorten is bepaald, evenals de omgevingsvoorkeuren. *Cymatiosphaera*? *deverteuilii* en *Porcupinea indentata* hebben een voorkeur voor koudere oppervlaktewateren, terwijl *Cometesphaera bullatio* en *Platycystidia manumii* eerder in warme oppervlaktewateren gedijen.

Ondanks dat het ouderdomsmodel sterk verbeterd werd door toevoeging van biostratigrafische punten op basis van dinocysten en kalkschalig nannoplankton in de eerste studie, bleef er onduidelijkheid in de magnetostratigrafie door de lage intensiteit van het signaal. Daarom is ervoor gekozen om Site U1318 aanvullend te dateren door middel van isotopenstratigrafie. Tijdens het midden Mioceen zijn er twee verschillende stabiele isotopenstratigrafieën beschikbaar die globaal te correleren zijn. Er is een benthische koolstof- en zuurstofisotopensignaal gegenereerd op basis van de foraminiferen *Cibicidoides pachyderma* en *Uvigerina* sp.. Eerst is het signaal van site U1318 met de eerste methode vergeleken met een hoge-resolutiesignaal uit de Stille Oceaan, dat gedateerd is met astronomische datering, een zeer betrouwbare methode. Hieruit bleek dat het oude ouderdomsmodel onjuist was. Vervolgens is het signaal vergeleken met de andere stratigrafische methode die gekoppeld is aan magnetostratigrafie. Hieruit bleek dat de oude interpretatie van de magnetostratigrafie onjuist was. Twee keer is een periode van drie magnetosubchrons geherinterpreteerd als één. Hiermee komt de nieuwe ouderdom van het onderzochte deel van Site U1318 uit op 16.60–12.75 Ma, met een resolutie van ongeveer 29 ka.

De laatste studie integreert relatieve oppervlaktetemperaturen op basis van dinocystenassemblages met twee organisch geochemische temperatuurcurves en de benthische zuurstofisotopencurve uit de vorige studie. Deze temperatuurstudie is de eerste van de Noord Atlantische Oceaan, en laat een graduele afkoeling zien van 27°C rond 16.4 Ma naar 18°C tegen 12.8

Ma. Hiernaast zijn er cyclische veranderingen van 2–4°C te observeren. De relatieve temperaturen op basis van dinocysten volgen de veranderingen in de organisch geochemische temperaturen goed. De gelijkenis van de organisch geochemische temperaturen op basis van de TEX_{86} proxy met de benthische zuurstofisotopencurve is opvallend. Het verschil tussen temperaturen gereconstrueerd met TEX_{86} en met de $U^{K'}_{37}$, samen met de goede correlatie tussen TEX_{86} temperaturen en de benthische zuurstofisotopen doet vermoeden dat de TEX_{86} eerder temperaturen onder het wateroppervlak dan oppervlaktetemperatuur weergeven. Alle vier Mi-events in het bereik van deze studie zijn waar te nemen in de temperatuurcurves, maar Mi-3 is het meest prominent met een afkoeling van ca. 6°C. Vanaf Mi-3 gaan seizoensgebonden afkoeling en opwarming ook voor op jaarlijkse afkoeling en opwarming, waarschijnlijk in respons op opbouw en smelt van continentaal ijs op het noordelijk halfrond. Tevens is de temperatuurgradiënt tussen pool en evenaar groter vanaf Mi-3 als gevolg van grotere seizoenaliteit. Een vergelijking met de aardbaanparameters en een compilatiecurve van atmosferische CO_2 laten zien dat een permanente afkoeling en mogelijke glaciatie op het noordelijk halfrond enkel mogelijk zijn bij CO_2 lager dan 280 ppm in combinatie met minima in de aardbaanparameters eccentriciteit en amplitudemodulatie van obliquiteit.

Summary

The Miocene is an Epoch from 23.03 to 5.33 million years ago (Ma). This period is characterized by two periods with a distinct climatic regime. The first period is the relatively warm Middle Miocene Climatic Optimum (MMCO; 17–14.5 Ma) that is followed by a period of cooling: the Middle Miocene Climatic Transition (MMCT). The MMCO is the warmest period of the last 34 Ma. The warm MMCO climate was not constant however, but was temporarily interrupted by periods of cooling. At the end of the MMCO cooling became permanent during the MMCT, a period of stepwise cooling and/or glaciation. These periods of cooling are coeval with 7 positive excursions of stable oxygen isotopes measured on benthic foraminifera: the Miocene isotope (Mi-) zonation or events. Mi-2 and Mi-2a are set during the MMCO; Mi-3 and Mi-4 occur during the MMCT. Of these Mi-events, Mi-3 had the most impact. Several causal factors of the Mi-events have been investigated, but a reduction in atmospheric CO_2 or a combination of minima in the orbital parameters eccentricity and obliquity amplitude modulation are the most plausible. CO_2 alone does not suffice to cause such a permanent transition as the MMCT. Therefore, it is necessary to collect more data to separate the effects of the different causal factors. Especially the North Atlantic Ocean is understudied and no temperature records covering both the MMCO and MMCT are available.

The Porcupine Basin, located in the eastern North Atlantic Ocean, offshore Ireland, provides a good location for a study on the middle Miocene. In 2005 the 'Integrated Ocean Drilling Program' drilled the basin to investigate the origins of the cold water corals in the region. Site U1318 is located on the continental margin at 409 m water depth and is influenced by the North Atlantic Current, which likely reduced its influence during past glaciations.

A low-resolution study already showed that unicellular marine algae from the Porcupine Basin, dinoflagellates, strongly react under influence of the Mi-events. These dinoflagellates react sensitively to changes in sea surface temperature, salinity, productivity and coastal proximity. Dinoflagellates produce a resting cyst during their sexual reproduction: dinocysts. These consist of a very resistant material, so they preserve very well in sediments. Hence, dinocysts are often used to reconstruct marine palaeoecology. For this study dinocysts will be applied to monitor the biotic response to the Mi-events in a high resolution. In addition, dinocysts are used here for biostratigraphical purposes.

Since temperatures reconstructed using dinocysts only provide relative information, two additional organic geochemical methods will be applied to reconstruct temperature qualitatively. The TEX_{86} index is based on the temperature dependent number of cyclopentane rings in the cell membranes of Thaumarchaeota. Thaumarchaeota are unicellular chemoautotrophs that live in the entire water column, but predominantly in the upper 200 meters. Additionally the $U^{K'}_{37}$ index is applied, which is based on the temperature dependent number of double bonds in alkenones. Alkenones are molecules produced by haptophytes, photoautotrophic algae that are one of the most important groups of phytoplankton.

Furthermore, stable carbon- ($\delta^{13}C$) and oxygen isotopes ($\delta^{18}O$) will be measured on benthic foraminifera, heterotrophic plankton that lives on the bottom of the sea and builds a calcareous shell, or test. These isotopes are applied because certain changes and peaks in isotope curves can be observed globally. Some of these peaks are correlated to magnetostratigraphy, a tool that is also available at Site U1318. The intensity of the palaeomagnetic record of the Porcupine Basin however is very low, complicating the interpretation. By comparing the changes in the isotopic curves of the

Porcupine Basin to curves of other, well-dated sites it is possible to validate or improve the age model of Site U1318.

A high-resolution palynological study of the MMCT shows that during Mi-events Mi-3a, Mi-3b and Mi-4 sea surface temperatures and sea level decreased. Mi-3a and Mi-3b are accompanied by an increase in surface productivity and an acme of the heterotrophic dinocyst *Palaeocystodinium golzowense*. This acme is likely caused by an enhancement of upwelling through stronger westerlies during colder periods. Mi-3b is the most pronounced event. Cooling periods co-occur with minima in June insolation, implying a strong role for orbital forcing of the Mi-events. Sea-level changes through time correlate very well to sea-level changes in the western North Atlantic Ocean. Furthermore, the palaeoecology of five fossil dinocyst species was determined using multivariate statistics.

During this palynological study extra attention was given to smaller palynomorphs. Acritarchs are palynomorphs with an unknown biological affinity, but with a likely marine origin. Regardless they can be used as biostratigraphic markers, but also as indicators of various past environmental factors. Six new species were discovered: *Cometesphaera bullatio* gen. nov. et sp. nov., *Cymatiosphaera*? *deverteuilii* sp. nov., *Platycystidia manumii* sp. nov., *Porcupinea collaris* gen. nov. et sp. nov., *Porcupinea indentata* gen. nov. et sp. nov. and *Pusillisphaera solaris* gen. nov. et sp. nov.. Their biostratigraphical ranges were determined, as well as their environmental preferences. *Cymatiosphaera*? *deverteuilii* and *Porcupinea indentata* prefer colder surface waters, whereas *Cometesphaera bullatio* and *Platycystidia manumii* prefer warmer surface waters.

Regardless of the large improvements made to the age model by adding biostratigraphic tie-points from dinocysts and calcareous nannoplankton during the first study, uncertainty regarding the magnetostratigraphy remained because of the low intensity of the signal. Therefore, Site U1318 was additionally dated using isotope stratigraphy. There are two different stable isotope stratigraphies available for the middle Miocene that are globally correlatable. A benthic carbon- and oxygen isotope signal was created using the foraminiferal species *Cibicidoides pachyderma* and *Uvigerina* sp.. Firstly the U1318 signal was compared to a high-resolution curve from the Pacific Ocean that was dated using astronomical tuning, a very reliable method of dating. This showed that the existing age model was incorrect. Subsequently the signal was compared to the other isotope stratigraphy that is linked to magnetostratigraphy. This indicated that the existing interpretation of the magnetostratigraphy was incorrect too. Twice a period of three magnetosubchrons was reinterpreted as one. The new age of this investigated part of Site U1318 is now 16.60–12.75Ma, with a temporal resolution of ca. 29 ka.

The last study integrates relative surface temperatures based on dinocyst assemblages with two organic geochemical temperature curves and the benthic oxygen isotope curve from the previous study. This temperature study is the first of the North Atlantic Ocean, and it shows a gradual cooling from 27°C at 16.4 Ma to 18°C at 12.8 Ma. In addition, cyclical changes of 2–4°C can be observed. The relative temperatures based on dinocysts keep track of the changes in organic geochemical temperatures. The similarity of the organic geochemical temperatures based on the TEX_{86} proxy with the benthic isotope curve is remarkable. The difference between temperatures reconstructed with TEX_{86} and with $U^{K'}_{37}$, in combination with the good correlation between TEX_{86} temperatures and the oxygen isotopes suggests that the TEX_{86} represents subsurface rather than surface temperatures. All four Mi-events within the range of this study are depicted in the temperature curves, but Mi-3 is the most prominent event with a cooling of 6°C. From Mi-3 onwards seasonal cooling and warming precede annual cooling and warming, probably as a response to waxing and waning of a continental northern hemisphere ice sheet. Moreover, the temperature gradient from pole to equator is larger

from Mi-3 onwards because of increased seasonality. A comparison to the orbital parameters and a compilation curve of atmospheric CO_2 shows that a permanent cooling and northern hemisphere glaciation are only possible at CO_2 below 280 ppm combined with minima in the orbital parameters eccentricity and obliquity amplitude modulation.

Chapter 1.
Introduction

Willemijn Quaijtaal

Unpublished

Introduction

1. The Miocene

The Miocene is an Epoch from 23.03 to 5.33 million years ago (Ma). The middle Miocene (15.97–11.63 Ma) is characterized by two different intervals with a distinct climatic regime. The first is the Middle Miocene Climatic Optimum (MMCO), which is followed by the Middle Miocene Climatic Transition (Figure 1.1). The MMCO (17–14.7 Ma; *Holbourn et al.,* 2015) is considered the warmest interval of the last 34 Ma with temperatures being 4–8°C higher than preindustrial values (*Goldner et al.*, 2014; *Herold et al.*, 2012). However, the climate of the MMCO was not uniform, but interrupted with punctuated short-lived cooling and/or glaciation events. These cooling and/or glaciation events during the MMCO and MMCT are accompanied by positive excursions in stable isotope ratios as measured in benthic foraminifera (see below for an explanation): the Miocene isotope (Mi-) zones or events (*Miller et al.*, 1998, 1991). Seven Miocene Mi-events and subzones have been defined (Figure 1.1). Mi-2 and Mi-2a occur during the MMCO, while Mi-3 and Mi-4 characterize the MMCT.

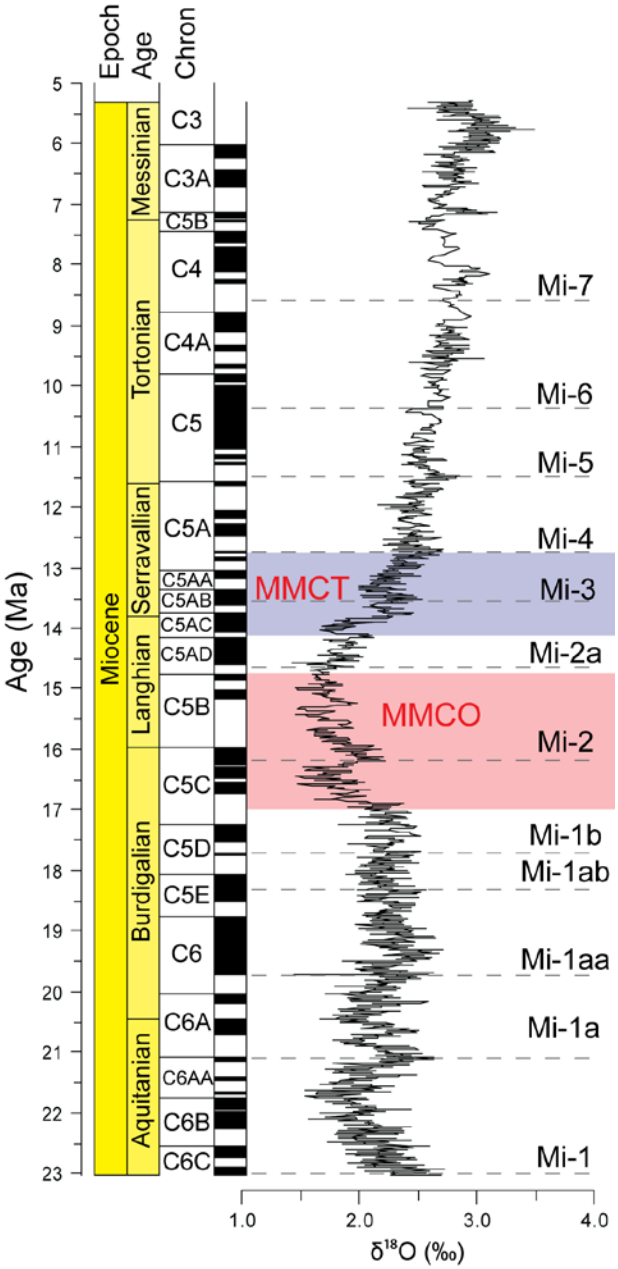

Figure 1.1: The global benthic $\delta^{18}O$ stack (5-point running average) of *Zachos et al.* (2008) versus age. General Miocene stratigraphy and magnetostratigraphy are given. The approximate timing of the MMCO (in red) and MMCT (in blue) are given and all Miocene Mi-events of *Miller et al.* (1991) are plotted (grey dashed lines) using the ages for the Mi-events of *Boulila et al.* (2011).

Global climate eventually toppled unequivocally during the MMCT. The MMCT is strictly defined from 14.2–13.8 Ma according to *Shevenell et al.,* 2004, but this definition does not fully implement the maximum extent of middle Miocene cooling. Therefore, in this study the MMCT is defined as the interval between the start of the Mi-3 (14.2 Ma) excursion and the maximum extent of Mi-4 (12.9 Ma) (Figure 1.1).

Mi-3 is considered the most severe of the middle Miocene Mi-events. It can be associated with expansion of the East Antarctic ice sheet, and possible sea-ice growth on the Arctic Ocean *(Moran et al.*, 2006), southern hemisphere sea surface temperature cooling of 6–7°C (*Shevenell et al.*, 2004), a sea-level lowering of 25–40m (*Westerhold et al.*, 2005), aridification of the northern hemisphere and mid-latitudes (*Eronen et al.*,

2012; *Pound et al.*, 2012) and species turnover in terrestrial and marine biota (*Flower and Kennett*, 1994).

The most likely causal mechanism for the Mi-events is a combination of minimum nodes in eccentricity and obliquity amplitude modulation (e.g. *Abels et al.*, 2005; *Westerhold et al.*, 2005). This specific orbital configuration is favourable for continental ice sheet expansion, as observed during the Eocene–Oligocene transition and the initiation of the first Cenozoic ice sheets on Antarctica (*Coxall et al.,* 2005) In addition, drawdown of atmospheric CO_2 (*Badger et al.*, 2013; *Kürschner et al.*, 2008; *Pagani et al.*, 2005) is a likely forcing mechanism. However, modelling studies and reconstructions of the continental climate of northwestern Europe indicate that CO_2 alone cannot be the sole forcing factor.

Since the middle Miocene climate is very similar to that of 'business as usual' projections of the end of the 21st century (*IPCC*, 2014). It is therefore important to assess the drivers and patterns of the middle Miocene climate. For example, no reliable high-resolution northern hemisphere palaeotemperature record exists that spans both the MMCO and MMCT and integrates both deep sea and surface cooling signals. This type of record is imperative to understand the differences between the Mi-events and assess different forcing factors involved.

2. Study objectives

Since the middle Miocene climate is a potential analogue to projected future changes, and because the northern hemisphere is so understudied, the main goal of this study is to study the climate and ecological turnover of the North Atlantic Ocean during this period. Special focus lies on the timing and magnitude of climate change in the eastern north Atlantic, which is particularly sensitive due to variability of the North Atlantic Current (NAC) and has a key role in the onset and terminations of glaciations.

A first objective is to study the palaeoecology and the response to the MMCT of an important group of marine primarily producers, dinoflagellates, on a high temporal resolution. It was already shown that dinoflagellates (mostly surface-dwelling algae) show a large, punctuated species turnover during the middle Miocene (e.g. *de Verteuil and Norris*, 1996; *Louwye et al.*, 2008). Dinoflagellates respond sensitively to changes in surface temperature, salinity, productivity and coastal proximity (see below) and their fossil resting cysts are often used to reconstruct marine palaeoenvironments (e.g. *Sluijs et al.*, 2005). Therefore, to assess additional forcing factors during the middle Miocene, such as productivity, dinoflagellates are an ideal tool.

A second objective is to study the evolution of northern hemisphere sea-surface temperature during the middle Miocene using the independent palaeothermometers TEX_{86} and $U^{K'}_{37}$.

A last objective is to combine all the assembled data to further elucidate the tempo and mode of the changes occurring during the middle Miocene.

3. Study Site

3.1. Choice of study site

To achieve the objectives, a drill site needed to be found with several properties: 1) preferably on the continental shelf for the most optimal distribution of dinoflagellate habitats, 2) relatively complete, since many drill sites suffer from hiatuses associated with the 'middle Miocene unconformity', a widespread erosional event, and 3) a relatively recent drilling, to avoid post-drilling growth of micro-organisms that could affect the organic geochemical signals.

Several drill sites have been considered. Ocean Drilling Project Leg 154 (Ceara Rise, western tropical Atlantic Ocean) is relatively complete and has benthic foraminiferal $\delta^{13}C$ and $\delta^{18}O$ records available for global correlation (*Shackleton et al.,* 1997), but this is a relatively old drilling. Furthermore, the water depths of the drill sites are deeper than 2000m, complicating assessment of dinocyst assemblages because of the oceanic setting, and by possible long-distance transport of dinocysts.

Another assessed drill site is site M29A of special-missions platform IODP Leg 313 at the New Jersey shallow shelf. Although the location suffers from hiatuses (*Browning et al.,* 2013), the location is shallow and should be ideal for palynology. As ample pollen would be present, the connection between the marine and continental realms could be assessed. Twenty-three samples of Site M29A were analyzed palynologically, but the site is too shallow to be easily examined: there was too much amorphous organic matter, plenty of pollen but many were filled with pyrite and there were few dinocysts (unpublished data). One-hundred and thirty samples were examined organic geochemically (Supplementary Figure 1.1), but because of the shallow depth, switching between the marine TEX_{86} and the continental mean annual air temperature palaeothermometer MBT/CBT further complicates the interpretation. Assessment of $U^{K'}_{37}$ temperatures was not possible because of contamination from the drilling method (unpublished data).

A third possible location was Integrated Ocean Drilling Program Leg 307, Site U1318, in the Porcupine Basin, offshore southwestern Ireland in the eastern North Atlantic Ocean. *Louwye et al.* (2008) determined a late Burdigalian to late Serravallian age (16.75–12.01 Ma) for the relatively complete middle Miocene sediments, using magnetostratigraphy and biostratigraphy based on organic-walled dinoflagellate cysts. More importantly, the preliminary low-resolution palaeoenvironmental study using dinocysts showed distinct assemblage changes that could be related to the Mi-events, deeming this study site very suitable to assess the biotic response to the climatic changes during the MMCO and the MMCT on a high resolution.

3.2. The Porcupine Basin: general background

The study area is located in the Porcupine Seabight (Figure 1.2), a failed rift system that originated during the opening of the North Atlantic Ocean during the Middle to Late Jurassic. It is enclosed by the Precambrian and Palaeozoic rocks of the Slyne Ridge (north), the Irish Mainland Shelf (east) and the Goban Spur (south) and connected to the North Atlantic and the Porcupine Abyssal Plain through a small opening in the southeast (See Figure 1.2). During the middle Miocene the British Isles were still connected to continental Europe and there was no connection to the North Sea through the English Channel (Figure 1.3). The Porcupine Basin is filled with 12 km of Late Palaeozoic to Quaternary sediments (*Ryan et al.*, 2009), mainly supplied from the Irish and Celtic shelves (*Rice et al.*, 1991).

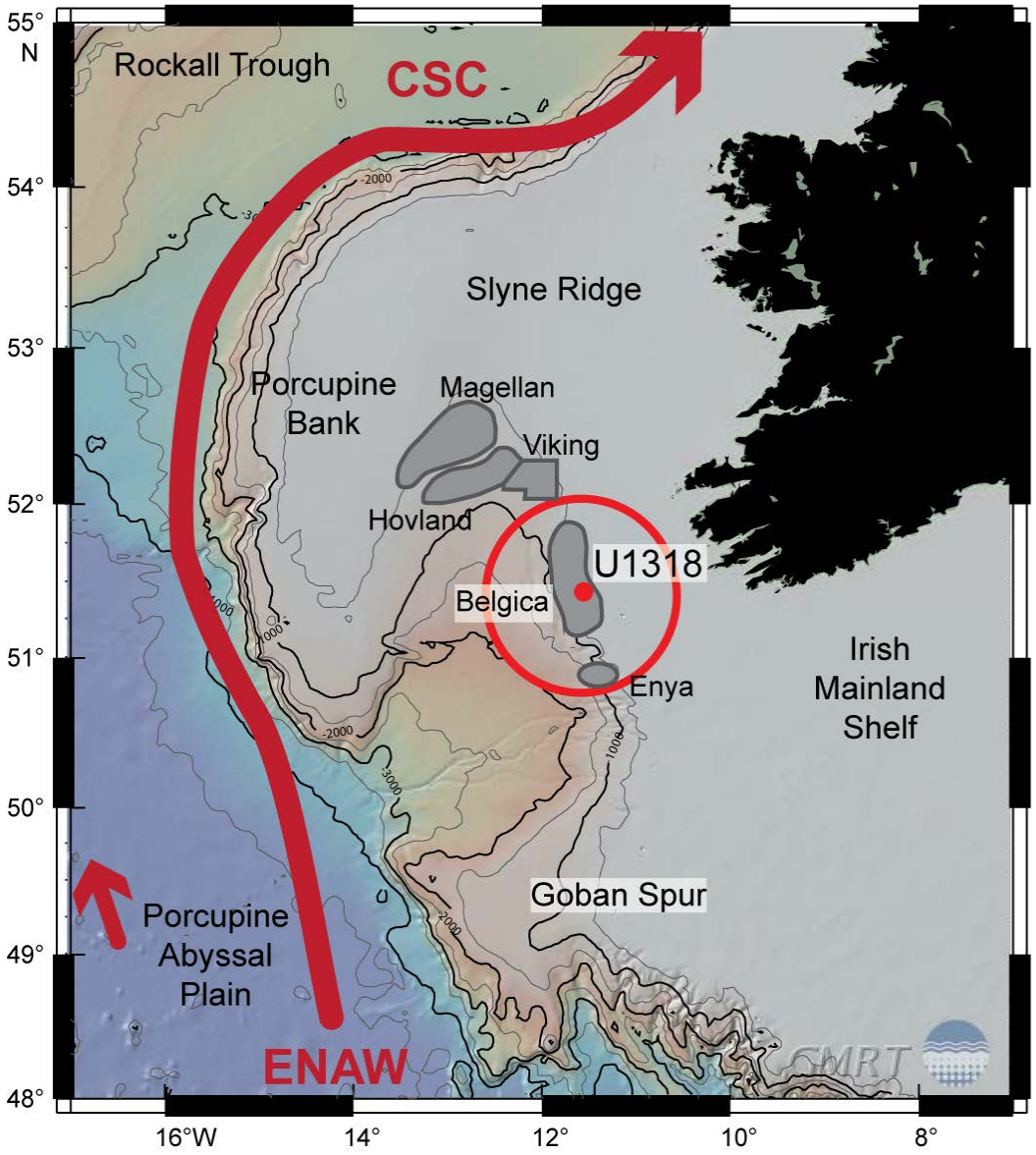

Figure 1.2: Location of drill Site U1318 and the most important geographic features (coral mound provinces in grey). Dark red lines indicate the most important surface currents. Background bathymetry created using the Global Multi-Resolution Topography (GMRT) Map tool: http://www.marine-geo.org/tools/GMRTMapTool/.

Nowadays, the main water source at intermediate depths down to 800 m is Eastern North Atlantic Water (ENAW) and the Shelf Edge Current or Continental Slope Current (CSC; See Figure 1.2), underlain by Mediterranean Outflow Water. At greater depths Labrador Sea water and Norwegian Sea Deep Water have been observed (*Raddatz et al.*, 2011, and references therein). For the Miocene these water masses are less clear, but deep and intermediate waters were most likely dominated by Southern Component Water (an analogue of the modern Antarctic Bottom Water; AABW) or Southern Component Intermediate Water respectively, supplemented by two warmer water masses with higher salinity: Northern Component Water, though in very small volumes, and Tethyan Outflow Water (*Woodruff and Savin*, 1989; *Wright et al.*, 1992). However, at a certain point prevailing bottom water currents would have ceased and been replaced with *'vigorous bottom currents due to the introduction of Norwegian Sea Water in the North Atlantic Ocean'* (*Van Rooij et al.*, 2003). There is nonetheless still much uncertainty regarding the Miocene hydrography at the Porcupine Basin.

Figure 1.3: Palaeogeography of Europe at ca. 13 Ma. Image adapted from www.deeptimemaps.com.

The Porcupine Seabight is renowned for its cold-water corals that were already discovered in the 19th century (*Thomson*, 1873). Using seismic profiling it became apparent that there are several coral mounds of up to 200–250 m high and over 1500–5000 m long, enclosed by sediment drifts (*De Mol et al.*, 2002; *Hovland et al.*, 1994; *Van Rooij et al.*, 2003, 2009) that are spread over three distinct mound provinces: the Belgica, Hovland and Magellan provinces (Figure 1.2)(*De Mol et al.*, 2002; *Huvenne et al.,* 2007; *Van Rooij et al.*, 2003). *De Mol et al.* (2002) and *Van Rooij et al.* (2003) assumed initiation of mound growth commenced during the Pliocene, but despite seismic data collected during many cruises there was much uncertainty about the age of origin, internal structures and growth of these coral mounds.

In May 2005 the Challenger mound (Belgica mound province) was drilled by the Integrated Ocean Drilling Program (IODP) during Leg 307: *'Modern Carbonate Mounds: Porcupine Drilling'*. The mound itself was drilled to reveal the internal structure of the mound, two additional sites were drilled for stratigraphic and correlative purposes, and provided the unique possibility to produce a near-shore high resolution palaeoclimate record across the Miocene MMCO and MMCT. IODP Site U1318 (51°26.16'N, 11°33.0'W; 409 m water depth; Figure 1.2) was drilled on the upper slope edge of the continental margin to assess the three most important seismic units: P1, P2 and P3 (See Figure 1.4 and Chapter 2, figure 2.3). The three seismic units are separated by erosive boundaries: unit P1 and P2 are separated by unconformity reflectors (RD) RD2, unit P2 and P3 are separated by the RD 3 reflector (*Van Rooij et al.*, 2003). According to *Van Rooij et al.*, (2003), unit P1 is of early to middle Miocene age, the very local unit P2 of middle Miocene to middle Pliocene age and unit P3 of Quaternary age; RD2 is of supposedly early middle Miocene age and RD1 of middle Pleistocene age. More detailed information on the geology and sedimentary processes at the Porcupine Seabight can be found in *Huvenne et al.* (2009), *Stoker et al.* (2005), *Shannon et al.* (2007) and *Van Rooij et al.* (2007).

Site U1318 is composed of three different holes: U1318A (51°26.162'N, 11°33.018'W), U1318B (51°26.148'N, 11°33. 019'W) and U1318C (51°26.150'N, 11°33.040'W). Hole U1318B is the deepest

and reaches into seismic unit P1, but suffers from a core gap. This gap was filled by coring Hole U1318C. A composite record was created based on physical properties (e.g. magnetic susceptibility), gamma ray attenuation density and natural gamma ray radiation, aided by biostratigraphy and lithologic contacts (*Expedition 307 Scientists*, 2006).

3.3. The Porcupine Basin: lithostratigraphy

Site U1318 consists of three lithostratigraphic units: Units 1, 2 and 3 (See Figure 1.4). Unit 1 is a clayey succession that is not lithified, and corresponds to seismic unit P3. It is subdivided into subunits 1a, 1b and 1c with distinct boundaries corresponding to shifts in the magnetic susceptibility. Unit 2 corresponds to the lowermost part of seismic unit P3 and consists of olive-grey, coarsening upwards fine- to medium grained sands interbedded with dark yellowish brown silty clay. Additionally, lithoclasts and mollusc and shell fragments can be observed. Lithostratigraphic unit 3 is of most interest, since the samples for this research were all taken from this unit. It is sectioned into three subunits that are divided based on their calcium carbonate contents. Subunits 3A and 3B correspond to seismic unit P2, subunit 3C corresponds to seismic unit P1. All subunits are moderately lithified. Subunit 3A consists of greenish grey to light greenish grey silty clays that are interbedded with well-sorted greenish grey fine-grained sand and greenish grey to grey silt with erosive boundary at their bases. The top of the subunit contains well-sorted fine-grained sands overlain by a prominent bivalve bed, whereas the base is defined by a sharp erosive boundary at 127.3 mbsf (Hole U1318C). Subunit 3A has relatively high carbonate contents (27–50 wt.%). Subunit 3B contains very homogeneous greenish grey silty clay, with abundant bioturbation. Carbonate contents increase from ~10 wt.% in the lower half to ~20 wt.% in the upper half. Subunit 3C is characterized by greenish grey silty clay to fine sands that fine upwards from the middle to the upper part of the subunit. The subunit has moderate carbonate contents (~35 wt.% at the bottom to ~25 wt.% at the top), with the exception of several extremely lithified beds. These have carbonate contents of ~70 wt.%; two beds are partly dolomitized (*Expedition 307 Scientists*, 2006).

3.4. The Porcupine Basin: potential problems

There is one downside to the Porcupine Basin as study site: there are existing problems with the age-depth model, specifically the weak intensity of the palaeomagnetic signal causing problems for magnetostratigraphy. These issues can be resolved by measuring stable carbon- and oxygen isotope ratios of benthic foraminifera, in addition to calcareous nannoplankton and dinocyst stratigraphy. Several excursions in benthic stable carbon- and oxygen isotopes are globally correlatable (*Woodruff and Savin,* 1991). Similarly, the Mi-events are the maxima of positive oxygen isotope excursions that provide a global connection. The Mi-events can furthermore be correlated to the magnetostratigraphy, providing additional certainty regarding the magnetostratigraphy of the Porcupine Basin. Additionally, calcareous nannoplankton and dinocyst stratigraphy will be applied.

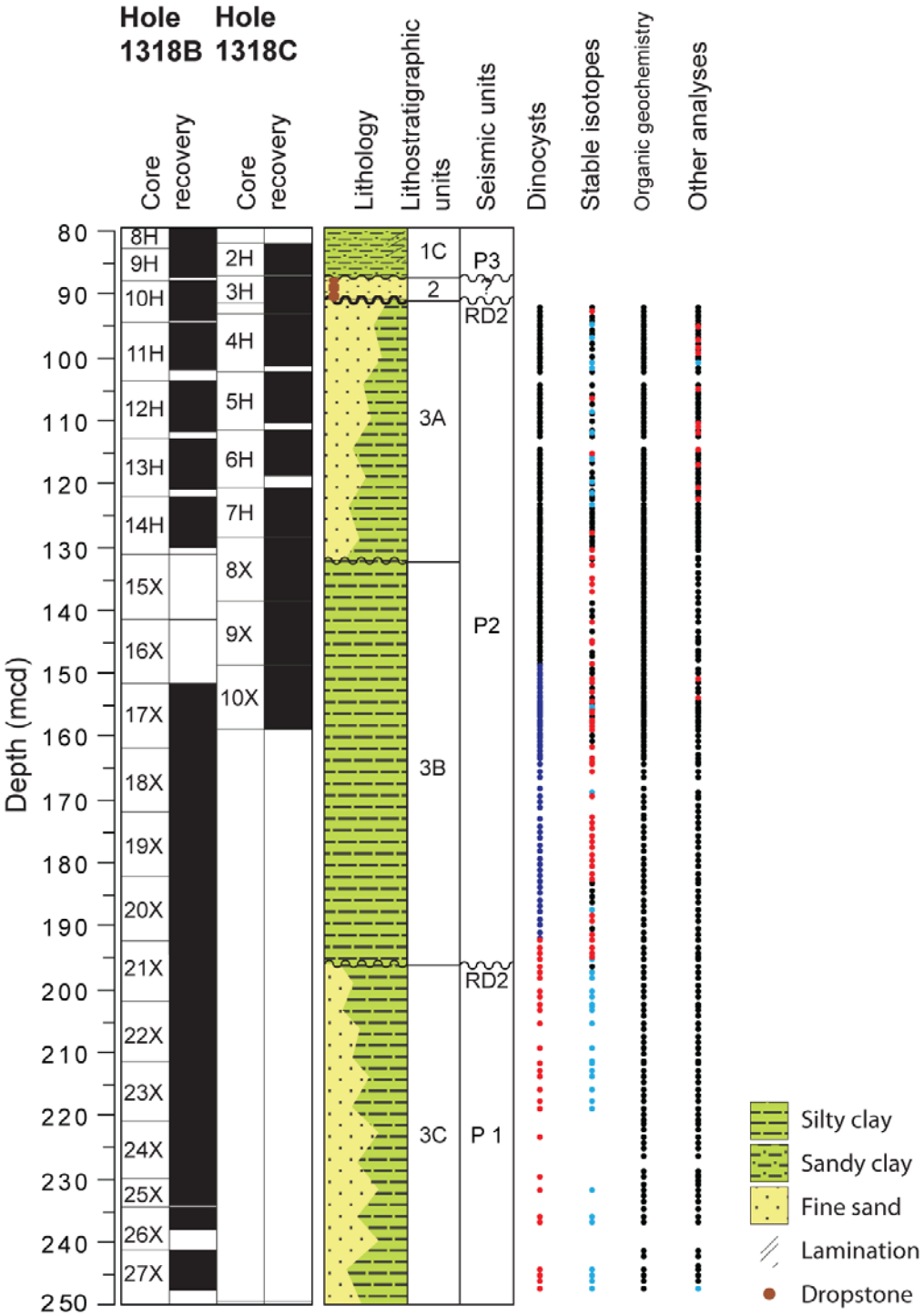

Figure 1.4: Core recovery (black), lithology, lithostratigraphic interpretation and position of seismic units of Holes U1318B and U1318C. Wavy lines indicate unconformities. The positions of all analyzed samples is given. Dinocysts: samples for Chapter 2 in black, additional samples for Chapter 3 in blue, more additional samples for Chapter 5 and 6 in red. Stable carbon and oxygen isotope analyses: light blue circles are analyses on *Cibicidoides pachyderma*, red circles are analyses on *Uvigerina* sp., black circles represent analyses on both taxa. Other analyses: red circles represent weight % material >63 µm,only, blue cirkles represent Planktonic/Benthic foraminiferal ratios only, black circles represent both analyses.

4. Sampling strategy

For this study a sampling resolution was targeted where at least the orbital parameter obliquity with a cycle of ca. 40 ka could be resolved. Based on the age model of *Louwye et al.* (2008) a sample spacing of 50 cm would result in a resolution of ~16 ka. Initially, Mi-events Mi-3 and Mi4 were targeted and 194 samples were taken in May 2011. Thirty of the lowermost sample would contain the sediments before Mi-3; these were sampled at 100 cm intervals. However, based on revisions in the age-depth model discussed in Chapter 2 it became apparent that the sediments of Site U1318 could also contain the MMCO, including Mi-2 and Mi-2a. Therefore, in September 2013 the remainder of the core was sampled with 50 cm intervals, and sample spacing of the interval that was sampled at 100 cm intervals was increased to 50 cm. Because it was impossible to study all 128 new samples in the time frame of this study, the resolution of analyzes on the lower part of Site U1318 is lower.

In total, 222 samples were analyzed palynologically; 245 samples were analyzed organic geochemically using two palaeothermometers (TEX_{86} and $U^{K'}_{37}$); stable carbon and oxygen isotope ratios were measured on 145 samples, and 199 samples were assessed for Planktonic/Benthic foraminifer ratios and the weight percentage of material >63 µm. An overview of all samples can be found in Figure 1.4

5. Study tools

5.1. Palynology

The principal tool that is applied is palynology. Palynology sensu lato is the study of resistant organic microfossils that remain after chemical maceration of sediments using hydrochloric and hydrofluoric acid (*Wood et al.*, 1996). Examples of palynomorphs are pollen, spores, organic-walled dinoflagellate cysts or dinocysts, acritarchs and chitinozoans. For this research mainly dinocysts and acritarchs will be used, although pollen and spores, as well as several other palynomorphs will also aid in the biostratigraphic assessment of the deposits and the reconstruction of the palaeoenvironment.

5.1.1. Organic-walled dinoflagellate cysts

Organic-walled dinoflagellate cysts are produced by dinoflagellates. Dinoflagellates are unicellular algae belonging to the superphylum Alveolata, SAR supergoup (former kingdom Protista) in the domain Eukaryota. They are characterized by having two flagella and a so-called dinokaryon: a cell nucleus where chromosomes remain condensed throughout the entire cell cycle rather than during mitosis only (*Fensome et al.*, 1993). Dinoflagellates occur in all sorts of aquatic environments, but mostly live in the marine realm, where they are one of the most important groups of primary producers together with diatoms and haptophytes. The majority of dinoflagellates are photosynthetic, but there are also dinoflagellates that combine photosynthesis and predation on other algae (mixotrophy) or dinoflagellates that are solely heterotrophic (*Dale*, 2001). Dinoflagellates are, like most phytoplankton, good indicators of climate change in the marine realm, and they can provide information regarding temperature, salinity, productivity, nutrient availability, sea-level change, upwelling, stratification, influx of fresh water etc. (*Hays et al.*, 2005).

Meroplanktonic dinoflagellates (ca 10–15% of all recent marine species; *Dale*, 2001) are dinoflagellates that produce a resting cyst or hypnozygote as part of their sexual reproduction in their life cycle (Figure 1.5). This hypnozygote contains the cell, together with nutritional starch grains and lipids (*Dale and Dale*, 2002). Dinocysts are formed within the thecal plates of the motile dinoflagellate and might therefore reflect morphological features present on the motile stage (Figure 1.6; *Fensome*

et al., 1996). The taxonomy of dinocysts is entirely based upon morphology, hence the species are morphospecies. Their identification is based on the tabulation pattern of thecal plates, the sulcus and cingulum where the flagellae of the motile form are located (Figure 1.6), cyst shape, ornamentation, spiny outgrowths called processes, and the opening in the dinocyst where the rested motile stage leaves the hypnozygote (*Fensome et al.*, 1996). This opening is called an archaeopyle, and the position and shape are unique for a 'morphogenus'. The hypnozygote behaves like a sediment particle and sinks to the bottom until the motile cell leaves the resting cyst and resumes a planktonic habit (*Evitt*, 1985). The hypnozygote is left in the sediment. Organic-walled resting cysts are made of dinosporin, a highly resistant molecule; other dinocysts are siliceous or calcareous (*Fensome et al.*, 1993). Hence, dinocysts generally preserve very well.

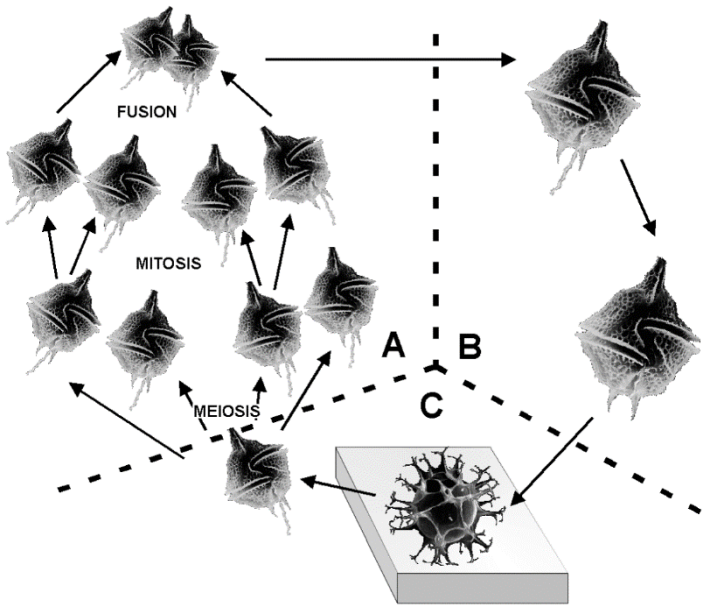

Figure 1.5: Simplified dinoflagellate life cycle from *Rochon* (2009). A: vegetative, haploid stage where cell division is mitotic. When gametes are formed, these will fuse to form a diploid zygote. B: Pelagic motile zygote (planozygote) in which the cyst is formed. This planozygote will eventually lose motility. C: Hypnozygote, or dinocyst in which a mandatory resting period will occur. From this cyst the diploid motive dinoflagellate excysts and form new haploid vegetative cysts through meiosis.

Dinocysts generally represent the surface water conditions their motile counterparts lived in. Through culture, sediment trap and core top studies the ecological affinities of extant (non-extinct) dinocyst species can be determined. The ecology of fossil dinocysts on the other hand has to be derived through more indirect methods such as comparison with species with known affinities, geographical distribution and multivariate statistics (*De Schepper et al.*, 2011, and references therein). This way dinocysts can be used to reconstruct parameters like past temperature, salinity, nutrient availability, productivity, coastal proximity and sea ice cover (Figure 1.7) (e.g. *De Schepper et al.*, 2011; *de Vernal et al.*, 2013; *Pross and Brinkhuis*, 2005; *Radi and de Vernal*, 2008; *Sluijs et al.*, 2005; *Versteegh*, 1994; *Zonneveld et al.*, 2013).

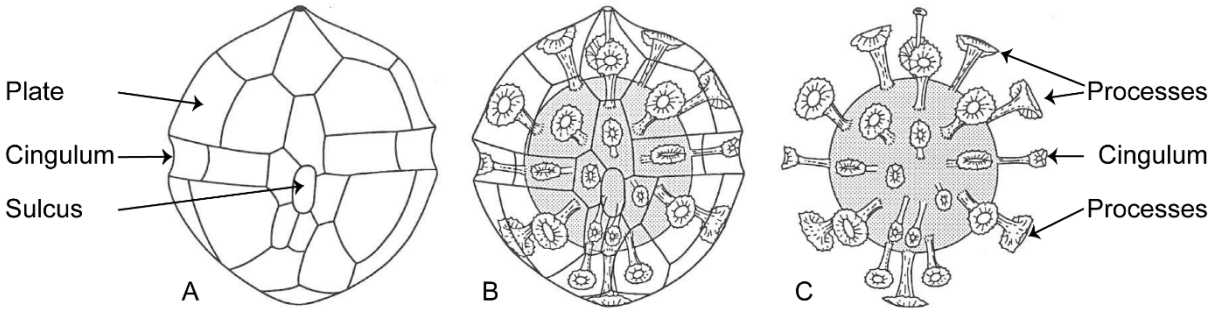

Figure 1.6: Transition from theca to dinocyst (adapted from *Evitt* (1985)). A: ventral view of the theca, in which the planozygote resides. B: dinocyst inside the theca. C: Dinocyst after disintegration of the theca. Some morphological features are indicated with arrows.

Due to their preservational properties and global distribution dinocysts are also excellent tools for biostratigraphy. Dinocysts appear consistently in the palynological record from the Middle Triassic (*MacRae et al.*, 1996) and due to their rapid evolution they are suitable as high-resolution biostratigraphic markers (*Williams et al.*, 2004).

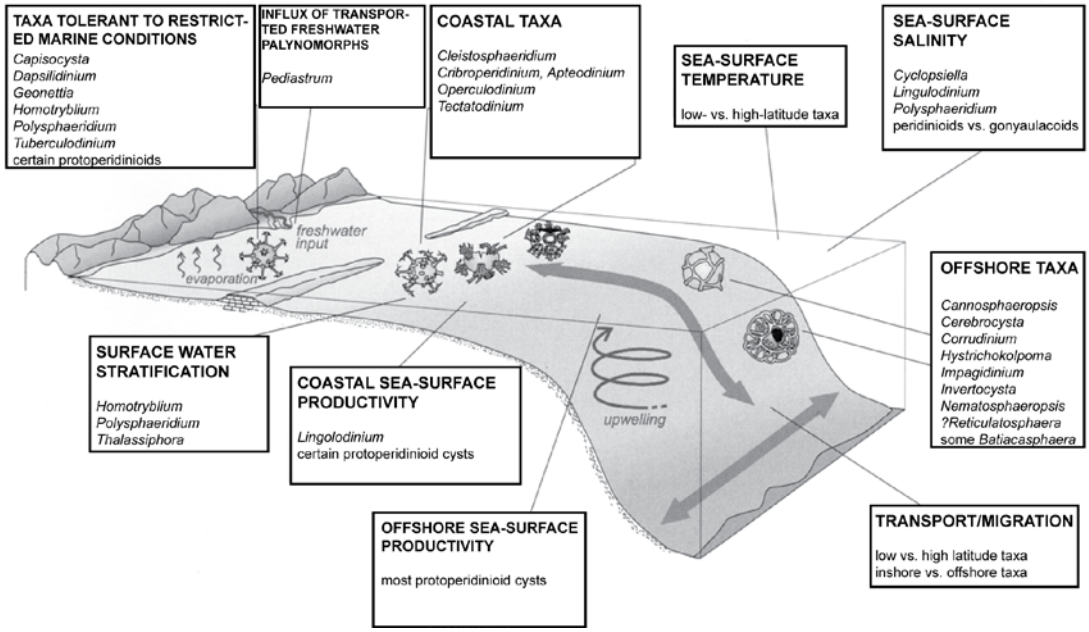

Figure 1.7: Typical Neogene palynomorphs that indicate specific environmental conditions (adapted from *Pross and Brinkhuis* (2005)).

5.1.2.Acritarchs

Acritarchs are palynomorphs with an unknown biological affinity, and are per definition regarded as *incertae sedis*. Acritarchs are most likely produced by marine phytoplankton and are generally small (ca. 15–80 µm; *Strother*, 1996). An acritarch usually consists of a single body that may be ornamented, and have an irregular excystment structure, a pylome that cannot be compared to the regular archaeopyles of dinocysts (Figure 1.8). Due to their diversity they have a great potential as biostratigraphic marker species, and they are particularly used in the Palaeozoic. In the Neogene, acritarchs are applied more and more often for biostratigraphy, especially in the North Atlantic and North sea regions (e.g. *De Schepper et al.*, 2017; *Head and Norris*, 2003; *Louwye*, 1999; *Schreck et al.*, 2012). Furthermore, acritarchs can also be applied as environmental indicators, for e.g.

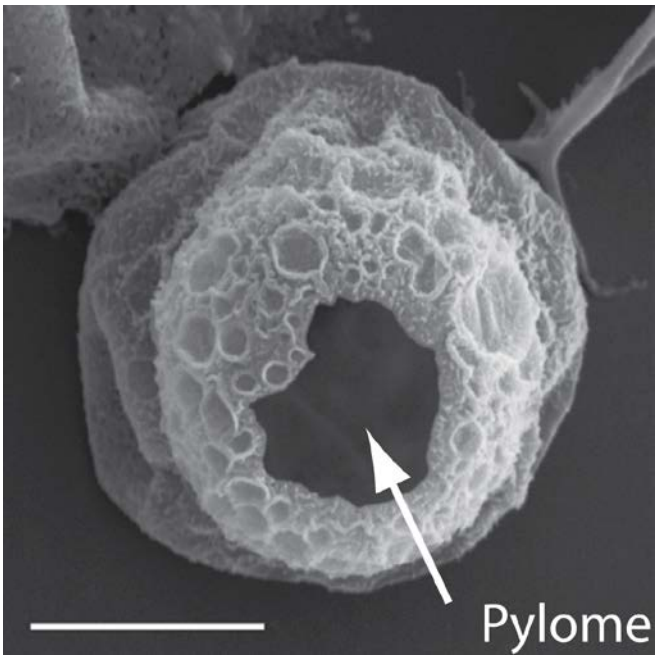

Figure 1.8: Scanning electron microscopic photograph of the acritarch *Cometesphaera bullatio* (*Quaijtaal et al.*, 2014). The scale bar represents 10 µm.

shallow and highly energetic waters or marginal marine environments (*Louwye and Laga*, 2008) or warm-water environments (*Head*, 2003).

5.2. Organic geochemistry

Organic geochemistry provides us with independent methods (i.e. a direct conversion to temperature, independent from other factors that need to be calculated first) to reconstruct temperature. Another advantage of these methods apart from being independent is that they can be applied when foraminifera, a commonly used source for carbonate chemistry-based temperature reconstructions, are absent due to dissolution. Two methods of reconstructing early to middle Miocene sea-surface temperatures (SST) using so-called 'palaeothermometermolecules' will be applied: the TEX_{86} temperature proxy and the $U^{K'}_{37}$ method.

5.2.1. TEX_{86}

The TetraEther indeX of tetraethers consisting of 86 carbon atoms (TEX_{86}) is based on the temperature-dependent number of cyclopentane rings, or so-called moieties, built in within the cell membrane of Thaumarchaeota (formerly Group I Crenarchaeota). Thaumarchaeota belong to the domain Archaea and constitute a major part of the marine picoplankton. They have a chemoautotrophic habit, using ammonia as nutrient source, and live throughout the water column, predominantly in the upper photic zone <200 m (*Schouten et al.*, 2013, and references therein). The cell membranes of Thaumarchaeota consist of glycerol dialkyl glycerol tetraethers (GDGTs; Figure 1.9). It was found that with increasing temperature the amount of cyclopentane moieties in GDGTs increases (*Schouten et al.*, 2013, and references therein). In 2002 the TEX_{86} temperature proxy was presented, where TEX_{86} = ([GDGT-2] + [GDGT-3] + [crenarchaeol regio-isomer]) / (GDGT-1] + [GDGT-2] + [GDGT-3] + [crenarchaeol regio-isomer]). Sea-surface temperature was subsequently defined as SST= 56.2*TEX_{86} − 10.8 (*Schouten et al.*, 2002). Because of the non-linear relationship between TEX_{86} and SST, *Kim et al.* (2010) defined two new temperature equations: one for the lower temperature range, and one for higher temperatures. The equation for higher temperatures, as expected during the early to middle Miocene, is SST = 68.4*log(TEX_{86}) + 38.6. An advantage of using GDGT's is that they are not affected as much by lateral transport in comparison to alkenones (*Mollenhauer et al.*, 2007; *Shah et al.*, 2008).

However, it became apparent that the input of continental (branched) GDGTs (Figure 1.9) through soil organic matter influx significantly influences SST reconstructions using the TEX_{86} proxy. The branched isoprenoid tetraether (BIT) index was defined to quantify the amount of terrestrial GDGTs (*Hopmans et al.*, 2004), where BIT = ([GDGT-I] + [GDGT-II] + [GDGT-III]) / ([crenarchaeol] + [GDGT-I] + [GDGT-II] + [GDGT-III]). Sediments with BIT values >0.3 are generally considered unsuitable for temperature reconstructions using TEX_{86}. The BIT index is also a valuable method to track soil organic matter influx as a result of sea-level and run-off changes. The TEX_{86} can also be influenced by the presence of methanotrophic or methanogenic archaea. Two methods of analysing this are the Methane index: MI = ([GDGT-1] + [GDGT-2] + [GDGT-3]) / ([GDGT-1] + [GDGT-2] + [GDGT-3] + [crenarchaeol] + [crenarchaeol region-isomer]) (*Zhang et al.*, 2011) and the Ring Index; RI = 0*[GDGT-0] + 1*[GDGT-1] + 2*[GDGT-2] + 3*[GDGT-3] + 4*[crenarchaeol] + 4*[crenarchaeol region-isomer] (*Zhang et al.*, 2016).

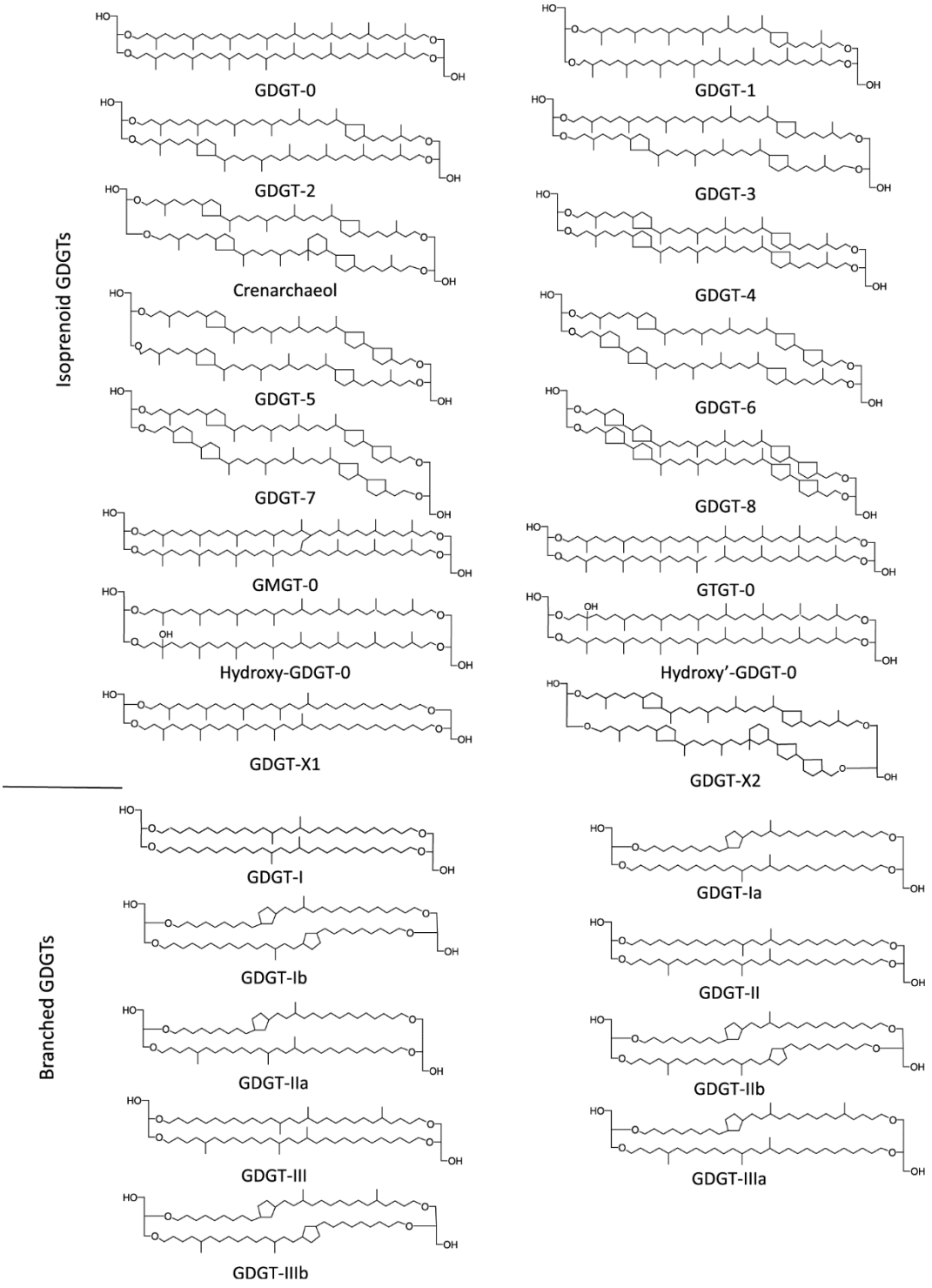

Figure 1.9: Molecular structure of all different isoprenoid (top) and branched (bottom) Glycerol Dialkyl Glycerol Tetraethers (GDGTs) (from *Schouten et al.* (2013)).

5.2.2. $U^{K'}_{37}$

The $U^{K'}_{37}$ sea-surface temperature proxy is based on long-chain di- and trisaturated methyl and ethyl ketones, also called alkenones, produced by haptophyte algae, a group of photosynthetic unicellular algae to which coccolithophores belong (*Brassell et al.*, 1986; *Prahl and Wakeham*, 1987). The number of double bonds in alkenones with 37 carbon atoms decreases with increasing SST. The $U^{K'}_{37}$, or alkenone unsaturation index is defined as follows: $U^{K'}_{37}$ = [37:2] / [37:2 + 37:3] (*Prahl and Wakeham*, 1987). SST is calculated from the $U^{K'}_{37}$ by the following calculation: SST = ($U^{K'}_{37}$ − 0.044) / 0.033 (*Müller et al.*, 1998) based on core top calibrations. One disadvantage of using the $U^{K'}_{37}$ SST-proxy is that there is a maximum temperature that can be reconstructed (29°C).

5.3. Stable isotopes

Foraminifera are primarily marine unicellular zooplankton, belonging to the domain Eukaryota, supergroup Rhizaria, with either a planktonic (living in surface waters) or a benthic (living in or on ocean sediments) habitat. They build a calcareous ($CaCO_3$) shell – also called a test – that is preserved in marine sediments. Foraminifera are frequently used to assess past climate by analysing their stable carbon and oxygen ratios. Stable isotopes occur naturally and are variations of elements with (an) extra neutron(s) and ratios are measured as $\delta_{sample} = ((R_{sample}-R_{standard}) / (R_{standard}))*1000$, where R is the ratio between two stable isotopes. For oxygen these are ^{16}O and ^{18}O and their ratios $\delta^{18}O$, for carbon they are ^{12}C and ^{13}C and their ratios $\delta^{13}C$. Foraminiferal stable isotopic values of tests are used because they generally reflect the isotopic composition of the sea water they live in: planktonic foraminifer tests for surface waters, and benthic tests for deep water. The isotopes of sea water are continuously under the influence of climate change (Figure 1.10). Surface water $\delta^{18}O$ is being influenced by evaporation, input of freshwater, sea-ice growth and global ice volume, whereas deep water $\delta^{18}O$ is mainly influenced by global ice volume. Both are influenced by temperature, and a combination of planktonic and benthic $\delta^{18}O$ can be used to assess water column structure. The $\delta^{13}C$ of surface and deep waters is mainly influenced by productivity (through photosynthesis and respiration), atmospheric CO_2 and carbon burial and weathering. Water masses each have their specific $\delta^{13}C$ and $\delta^{18}O$ and can be traced through especially benthic foraminiferal stable isotopes. Additionally, during incorporation into the foraminiferal shell stable isotopes are affected processes within the cell (vital effects)(e.g. *Ezard et al.*, 2015; *Katz et al.*, 2003).

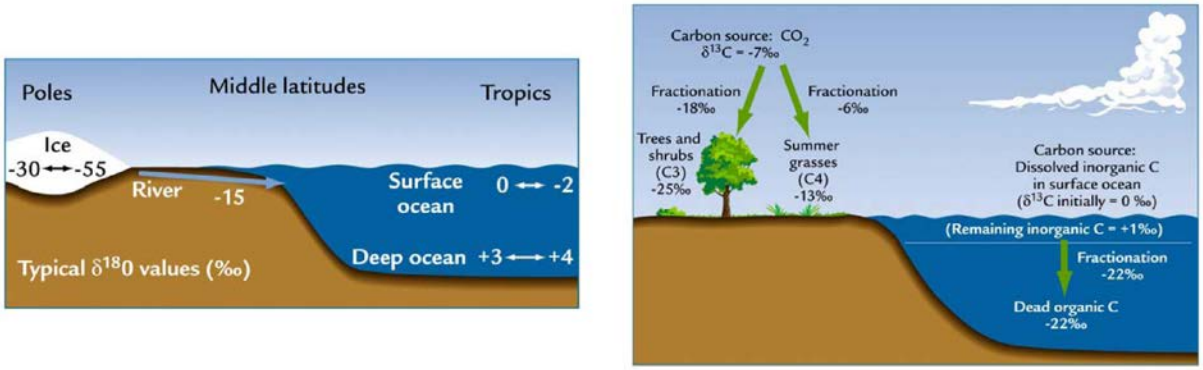

Figure 1.10: Typical $\delta^{18}O$ and $\delta^{13}C$ values of different sources. Fractionation processes are given for $\delta^{13}C$ (from *Ruddiman* (2001))

In addition, and used within this thesis, benthic foraminiferal stable carbon and oxygen isotopes can also be applied as stratigraphic tools. For the Miocene, *Woodruff and Savin* (1991) established a carbon and isotope stratigraphy based on a global compilation of stable carbon and oxygen isotope records, resulting in seven $\delta^{13}C$ maxima and seven positive and negative $\delta^{18}O$ excursions that can be applied for global correlation. Additionally there are the nine Miocene stable oxygen isotope (Mi-) zones or events defined by *Miller et al.* (1991, 1998). The main advantage of these Mi-zones is that they are correlated to magnetostratigraphy, a method that was previously measured at the Porcupine Basin (*Louwye et al.*, 2008).

6. Outline

In Chapter 2 the MMCT of the North Atlantic realm is examined palynologically. Past changes in sea-surface temperature, productivity, diversity and coastal proximity are assessed using qualitative indexes based on dinocysts and other palynomorphs. Additionally, the existing chronostratigraphic framework is improved using biostratigraphy of dinocysts and calcareous nannoplankton. The palaeoecology of several dinocysts with unknown ecological affinities is assessed using multivariate statistics.

Chapter 3 describes six new species and three new genera of acritarchs from the Porcupine Basin: *Cometesphaera bullatio* gen. et sp. nov., *Cymatiosphaera*? *deverteuilii* sp. nov., *Platycystidia manumii* sp. nov., *Porcupinea collaris* gen. et sp. nov., *Porcupinea indentata* gen. et sp. nov. and *Pusillisphaera solaris* gen. et sp. nov.. The biostratigraphic ranges of these acritarchs are discussed, and their palaeoecology is analysed using multivariate statistics. The usefulness of these acritarchs demonstrates the importance of sieving using a 10µm mesh to avoid the loss of such important information.

Chapter 4 presents a revised age model for the Porcupine Basin based on stable carbon and oxygen isotope stratigraphy. The stable isotope records are created from the benthic foraminifera *Cibicidoides pachyderma* and *Uvigerina* spp. and will be compared to the initial isotopic framework of *Woodruff and Savin* (1991) and a high-resolution record from the Pacific Ocean with a reliable, orbitally-tuned age model. Comparison with the Miocene oxygen isotope zones of *Miller et al.* (1991, 1998) will provide correlation to the magnetostratigraphic framework.

The first early to middle Miocene sea-surface temperature record from the North Atlantic Ocean is presented in Chapter 5. SSTs are reconstructed quantitatively using the organic geochemical proxies TEX_{86} and $U^{K'}_{37}$ and compared with qualitative SST derived from the Warm/Cold dinocyst index and benthic stable oxygen isotopes. These combined records will be compared to a compilation record of atmospheric CO_2 and solar insolation to assess the influence of orbital and greenhouse gas forcing during four different periods of cooling and/or glaciation.

The general results, conclusions and recommendations are summarized in Chapter 6. This chapter furthermore discusses the limitations of the TEX_{86} temperature proxy when using it for ecological purposes. The main problem lies in the variable depth habitat of the producers of the molecules used in the reconstruction method, the Thaumarchaeota. It provides a possible solution on how to overcome these problems by using an additional microfossil group, i.e. planktonic foraminifera.

7. References

Abels, H.A., Hilgen, F.J., Krijgsman, W., Kruk, R.W., Raffi, I., Turco, E., Zachariasse, W.J., 2005. Long-period orbital control on middle Miocene global cooling: Integrated stratigraphy and astronomical tuning of the Blue Clay Formation on Malta. Paleoceanography 20, PA4012.

Badger, M.P.S., Lear, C.H., Pancost, R.D., Foster, G.L., Bailey, T.R., Leng, M.J., Abels, H.A., 2013. CO_2 drawdown following the middle Miocene expansion of the Antarctic Ice Sheet. Paleoceanography 28, 42–53.

Boulila, S., Galbrun, B., Miller, K.G., Pekar, S.F., Browning, J. V., Laskar, J., Wright, J.D., 2011. On the origin of Cenozoic and Mesozoic "third-order" eustatic sequences. Earth-Science Reviews 109, 94–112.

Brassell, S.C., Eglinton, G., Marlowe, I.T., Pflaumann, U., Sarnthein, M., 1986. Molecular stratigraphy: a new tool for climatic assessment. Nature 320, 129–133.

Browning, J.V., Miller, K.G., Sugarman, P.J., Barron, J., McCarthy, F., Kulhanek, D., Katz, M.E., Feigenson, M.D., 2013. Chronology of Eocene-Miocene sequences on the New Jersey shallow shelf: Implications for regional, interregional, and global correlations.: Geosphere 9, 1–23.

Coxall, H.K., Wilson, P. a, Pälike, H., Lear, C.H., Backman, J., 2005. Rapid stepwise onset of Antarctic glaciation and deeper calcite compensation in the Pacific Ocean. Nature 433, 53–57.

Dale, B., 2001. The sedimentary record of dinoflagellate cysts: looking back into the future of phytoplankton blooms. Scientia Marina 65, 257–272.

Dale, B., Dale, A.L., 2002. Environmental applications of dinoflagellate cysts and acritarchs, in: Haslett, S.K. (Ed.), Quaternary Environmental Micropalaeontology. Arnold, London, pp. 207–240.

De Mol, B., Van Rensbergen, P., Pillen, S., Van Herreweghe, K., Van Rooij, D., McDonnell, A., Huvenne, V., Ivanov, M., Swennen, R., Henriet, J.P., 2002. Large deep-water coral banks in the Porcupine Basin, southwest of Ireland. Marine Geology 188, 193–231.

De Schepper, S., Beck, K.M., Mangerud, G., 2017. Late Neogene dinoflagellate cyst and acritarch biostratigraphy for Ocean Drilling Program Hole 642B, Norwegian Sea. Review of Palaeobotany and Palynology 236, 12–32.

De Schepper, S., Fischer, E.I., Groeneveld, J., Head, M.J., Matthiessen, J., 2011. Deciphering the palaeoecology of Late Pliocene and Early Pleistocene dinoflagellate cysts. Palaeogeography, Palaeoclimatology, Palaeoecology 309, 17–32.

De Vernal, A., Rochon, A., Fréchette, B., Henry, M., Radi, T., Solignac, S., 2013. Reconstructing past sea ice cover of the Northern Hemisphere from dinocyst assemblages: Status of the approach. Quaternary Science Reviews 79, 122–134.

de Verteuil, L., Norris, G., 1996. Miocene dinoflagellate stratigraphy and systematics of Maryland and Virginia. Micropaleontology, supplement 42, 1–172.

Eronen, J.T., Fortelius, M., Micheels, A., Portmann, F.T., Puolamäki, K., Janis, C.M., 2012. Neogene aridification of the northern hemisphere. Geology 40, 823–826.

Evitt, W.R., 1985. Sporopollenin Dinoflagellate Cysts. Their Morphology and Interpretation. American Association of Stratigraphic Palynologists Foundation, Dallas, Texas.

Expedition 307 Scientists, 2006. Site U1318, in: Ferdelman, T.G., Kano, A., Williams, T., Henriet, J.-P., the Expedition 307 Scientists (Eds.), Proceedings of the Integrated Ocean Drilling Program. Integrated Ocean Drilling Program Management International, Washington, D.C., pp. 1–57.

Ezard, T.H.G., Edgar, K.M., Hull, P.M., 2015. Environmental and biological controls on size-specific $\delta^{13}C$ and $\delta^{18}O$ in recent planktonic foraminifera. Paleoceanography 30, 1–23.

Fensome, R.A., Taylor, F.J.R., Norris, G., Sarjeant, W.A.S., Wharton, D.I., Williams, G.L., 1993. A classification of living and fossil dinoflagellates. Micropaleontology Special Publication 7, 351.

Fensome, R.A., Riding, J.B., Taylor, F.J.R., 1996. Chapter 6. Dinoflagellates, in: Jansonius, J., McGregor, D.C. (Eds.), Palynology: Principles and Applications. American Association of Stratigraphic Palynologists Foundation, Dallas, Texas, pp. 107–169.

Flower, B.P., Kennett, J.P., 1994. The middle Miocene climatic transition: East Antarctic ice sheet development, deep ocean circulation and global carbon cycling. Palaeogeography, Palaeoclimatology, Palaeoecology 108, 537–555.

Goldner, A., Herold, N., Huber, M., 2014. The challenge of simulating the warmth of the mid-Miocene climatic optimum in CESM1. Climate of the Past 10, 523–536.

Hays, G.C., Richardson, A.J., Robinson, C., 2005. Climate change and marine plankton. Trends in Ecology & Evolution 20, 337–344.

Head, M.J., 2003. Neogene occurrences of the marine acritarch genus *Nannobarbophora* Habib and Knapp, 1982 emend., and the new species *N. gedlii*. Journal of Paleontology 77, 382–385.

Head, M.J., Norris, G., 2003. New Species of Dinoflagellate Cysts and Other Palynomorphs From the Latest Miocene and Pliocene of DSDP Hole 603C, Western North Atlantic. Journal of Paleontology 77, 1–15.

Herold, N., Huber, M., Müller, R.D., Seton, M., 2012. Modeling the Miocene climatic optimum: Ocean circulation. Paleoceanography 27, PA1209.

Holbourn, A., Kuhnt, W., Kochhann, K.G.D., Andersen, N., Meier, K.J.S., 2015. Global perturbation of the carbon cycle at the onset of the Miocene Climatic Optimum. Geology 43, 123–126.

Hopmans, E.C., Weijers, J.W.H., Schefuß, E., Herfort, L., Sinninghe Damsté, J.S., Schouten, S., 2004. A novel proxy for terrestrial organic matter in sediments based on branched and isoprenoid tetraether lipids. Earth and Planetary Science Letters 224, 107–116.

Hovland, M., Croker, P.F., Martin, M., 1994. Fault-associated seabed mounds (carbonate knolls?) off western Ireland and

north-west Australia. Marine and Petroleum Geology 11, 232–246.
Huvenne, V.A.I., Bailey, W.R., Shannon, P.M., Naeth, J., di Primio, R., Henriet, J.-P., Horsfield, B., de Haas, H., Wheeler, A., Olu-Le Roi, K., 2007. The Magellan mound province in the Porcupine Basin. International Journal of Earth Sciences 96, 85–101
Huvenne, V.A.I., Van Rooij, D., De Mol, B., Thierens, M., O'Donnell, R., Foubert, A., 2009. Sediment dynamics and palaeo-environmental context at key stages in the Challenger cold-water coral mound formation: Clues from sediment deposits at the mound base. Deep-Sea Research I 56, 2263–2280.
IPCC, 2014. Climate Change 2014: Synthesis Report. Contribution of Working Groups I, II and III to the Fifth Assessment Report of the Intergovernmental Panel on Climate Change Geneva, Switzerland: IPCC.
Katz, M.E., Katz, D.R., Wright, J.D., Miller, K.G., Pak, D.K., Shackleton, N.J., Thomas, E., 2003. Early Cenozoic benthic foraminiferal isotopes: Species reliability and interspecies correction factors. Paleoceanography 18, doi:10.1029/2002PA000798.
Kim, J.H., van der Meer, J., Schouten, S., Helmke, P., Willmott, V., Sangiorgi, F., Koç, N., Hopmans, E.C., Damsté, J.S.S., 2010. New indices and calibrations derived from the distribution of crenarchaeal isoprenoid tetraether lipids: Implications for past sea surface temperature reconstructions. Geochimica et Cosmochimica Acta 74, 4639–4654.
Kürschner, W.M., Kvacek, Z., Dilcher, D.L., 2008. The impact of Miocene atmospheric carbon dioxide fluctuations on climate and the evolution of terrestrial ecosystems. Proceedings of the National Academy of Sciences of the United States of America 105, 449–53.
Louwye, S., 1999. New species of organic-walled dinoflagellates and acritarchs from the Upper Miocene Diest Formation, northern Belgium (southern North Sea Basin). Review of Palaeobotany and Palynology 107, 109–123.
Louwye, S., Foubert, A., Mertens, K., Van Rooij, D., The IODP Expedition 307 Scientific Party, 2008. Integrated stratigraphy and palaeoecology of the Lower and Middle Miocene of the Porcupine Basin. Geological Magazine 145, 321–344.
Louwye, S., Laga, P., 2008. Dinoflagellate cyst stratigraphy and palaeoenvironment of the marginal marine Middle and Upper Miocene of the eastern Campine area, northern Belgium (southern North Sea Basin). Geological Journal 43, 75–94.
MacRae, R.A., Fensome, R.A., Williams, G.L., 1996. Fossil dinoflagellate diversity, originations, and extinctions and their significance. Canadian Journal of Botany 74, 1687–1694.
Miller, K.G., Wright, J.D., Fairbanks, R.G., 1991. Unlocking the Ice House: Oligocene–Miocene Oxygen Isotopes, Eustasy, and Margin Erosion. Journal of Geophysical Research 96, 6829–6848.
Miller, K.G., Mountain, G.S., Browning, J. V., Kominz, M., Sugarman, P.J., Christie-Blick, N., Katz, M.E., Wright, J.D., 1998. Cenozoic global sea level, sequences, and the New Jersey Transect: Results From coastal plain and continental slope drilling. Reviews of Geophysics 36, 569–601.
Mollenhauer, G., Inthorn, M., Vogt, T., Zabel, M., Sinninghe Damsté, J.S., Eglinton, T.I., 2007. Aging of marine organic matter during cross-shelf lateral transport in the Benguela upwelling system revealed by compound-specific radiocarbon dating. Geochemistry, Geophysics, Geosystems 8, 1–16.
Moran, K., Backman, J., Brinkhuis, H., Clemens, S.C., Cronin, T.M., Dickens, G.R., Eynaud, F., Gattacceca, J., Jakobsson, M., Jordan, R.W., Kaminski, M., King, J., Koc, N., Krylov, A., Martinez, N., Matthiessen, J., McInroy, D., Moore, T.C., Onodera, J., O'Regan, M., Pälike, H., Rea, B., Rio, D., Sakamoto, T., Smith, D.C., Stein, R.R., St. John, K.E.K., Suto, I., Suzuki, N., Takahashi, K., Watanabe, M., Yamamoto, M., Farrell, J., Frank, M., Kubik, P.W., Jokat, W., Kristoffersen, Y., St John, K., Suto, I., Suzuki, N., Takahashi, K., Watanabe, M., Yamamoto, M., Farrell, J., Frank, M., Kubik, P.W., Jokat, W., Kristoffersen, Y., 2006. The Cenozoic palaeoenvironment of the Arctic Ocean. Nature 441, 601–605.
Müller, P.J., Kirst, G., Ruhland, G., von Storch, I., Rosell-Mele, A., 1998. Calibration of the alkenone paleotemperature index $U^{K'}_{37}$ based on core-tops from the eastern South Atlantic and the global ocean (60°N–60°S). Geochimica et Cosmochimica Acta 62, 1757–1772.
Pagani, M., Zachos, J.C., Freeman, K.H., Tipple, B., Bohaty, S., 2005. Marked decline in atmospheric carbon dioxide concentrations during the Paleogene. Science 309, 600–603.
Pound, M.J., Haywood, A.M., Salzmann, U., Riding, J.B., 2012. Global vegetation dynamics and latitudinal temperature gradients during the Mid to Late Miocene (15.97–5.33 Ma). Earth-Science Reviews 112, 1–22.
Prahl, F.G., Wakeham, S.G., 1987. Calibration of unsaturation patterns in long-chain ketone compositions for palaeotemperature assessment. Nature 330, 367–369.
Pross, J., Brinkhuis, H., 2005. Organic-walled dinoflagellate cysts as paleoenvironmental indicators in the Paleogene; a synopsis of concepts. Paläontologische Zeitschrift 79, 53–59.
Quaijtaal, W., Mertens, K.N., Louwye, S., 2014. Some new acritarch species from the lower and middle Miocene of Porcupine Basin, North Atlantic Ocean: biostratigraphy and palaeoecology. Palynology 39(1), 1–53.
Raddatz, J., Rüggeberg, A., Margreth, S., Dullo, W.-C., 2011. Paleoenvironmental reconstruction of Challenger Mound initiation in the Porcupine Seabight, NE Atlantic. Marine Geology 282, 79–90.
Radi, T., de Vernal, A., 2008. Dinocysts as proxy of primary productivity in mid–high latitudes of the Northern Hemisphere. Marine Micropaleontology 68, 84–114.
Rice, A.L., Billett, D.S.M., Thurston, M.H., Lampitt, R.S., 1991. The Institute Of Oceanographic Sciences Biology Programme In The Porcupine Seabight: Background And General Introduction. Journal of the Marine Biological Association of the United Kingdom 71, 281–310.
Rochon, A., 2009. The ecology and biological affinity of Arctic dinoflagellates and their paleoceanographical significance in the Canadian High Arctic. IOP Conference Series: Earth and Environmental Science 5, 12003, 1–6.

Ruddiman, W.F., 2001. Earth's Climate, Past and Future. Freeman.
Ryan, M.C., Helland-Hansen, W., Johannessen, E.P., Steel, R.J., 2009. Erosional vs. accretionary shelf margins: the influence of margin type on deepwater sedimentation: an example from the Porcupine Basin, offshore western Ireland. Basin Research 21, 676–703.
Schouten, S., Hopmans, E.C., Schefuß, E., Sinninghe Damsté, J.S., 2002. Distributional variations in marine crenarchaeotal membrane lipids: a new tool for reconstructing ancient sea water temperatures? Earth and Planetary Science Letters 204, 265–274.
Schouten, S., Hopmans, E.C., Sinninghe Damsté, J.S., 2013. The organic geochemistry of glycerol dialkyl glycerol tetraether lipids: A review. Organic Geochemistry 54, 19–61.
Schreck, M., Matthiessen, J., Head, M.J., 2012. A magnetostratigraphic calibration of Middle Miocene through Pliocene dinoflagellate cyst and acritarch events in the Iceland Sea (Ocean Drilling Program Hole 907A). Review of Palaeobotany and Palynology 187, 66–94.
Shackleton, N., Hall, M.A., 1997. The Late Miocene stable isotope record, Site 926. *In: Shackleton, N.J., Curry, W.B., Richter, C., Bralower, T.J. (eds.), Proceedings of the Ocean Drilling Program, Scientific Results* **154***, Ocean Drilling Program, College Station, Texas*, pp. 367–373.
Shah, S.R., Mollenhauer, G., Ohkouchi, N., Eglinton, T.I., Pearson, A., 2008. Origins of archaeal tetraether lipids in sediments: Insights from radiocarbon analysis. Geochimica et Cosmochimica Acta 72, 4577–4594.
Shannon, P.M., McDonnell, A., Bailey, W.R., 2007. The evolution of the Porcupine and Rockall Basins, offshore Ireland; the geological template for carbonate mound development. International Journal of Earth Sciences 96, 21–35.
Shevenell, A.E., Kennett, J.P., Lea, D.W., 2004. Middle Miocene Southern Ocean cooling and Antarctic cryosphere expansion. Science 305, 1766–1770.
Sluijs, A., Pross, J., Brinkhuis, H., 2005. From greenhouse to icehouse; organic-walled dinoflagellate cysts as paleoenvironmental indicators in the Paleogene. Earth-Science Reviews 68, 281–315.
Stoker, M.S., D. Praeg, B.O. Hjelstuen, J.S. Laberg, T. Nielsen, and P.M. Shannon, 2005. Neogene stratigraphy and the sedimentary and oceanographic development of the NW European Atlantic margin, Marine Petroleum Geology, 22, 977–1005.
Strother, P.K., 1996. Chapter 5. Acritarchs, in: Jansonius, J., McGregor, D.C. (Eds.), Palynology: Principles and Applications. American Association of Stratigraphic Palynologists Foundation, Dallas, Texas, pp. 81–106.
Thomson, C.W., 1873. The depths of the sea. MacMillan and Co, London.
Van Rooij, D., De Mol, B., Huvenne, V., Ivanov, M., Henriet, J.P., 2003. Seismic evidence of current-controlled sedimentation in the Belgica mound province, upper Porcupine slope, southwest of Ireland. Marine Geology 195, 31–53.
Van Rooij, D., Blamart, D., Richter, T., Wheeler, A., Kozachenko, M., Henriet, J.-P., 2007. Quaternary sediment dynamics in the Belgica mound province, Porcupine Seabight: ice-raftig events and countour current processes. International Journal of Earth Sciences 96, 121–140.
Van Rooij, D., Huvenne, V.A.I., Blamart, D., Henriet, J.-P., Wheeler, A., de Haas, H., 2009. The Enya mounds: a lost mound-drift competition. International Journal of Earth Sciences 98, 849–863.
Versteegh, G.J.M., 1994. Recognition of cyclic and non-cyclic environmental changes in the Mediterranean Pliocene: A palynological approach. Marine Micropaleontology 23, 147–183.
Westerhold, T., Bickert, T., Röhl, U., 2005. Middle to late Miocene oxygen isotope stratigraphy of ODP site 1085 (SE Atlantic): New constrains on Miocene climate variability and sea-level fluctuations. Palaeogeography, Palaeoclimatology, Palaeoecology 217, 205–222.
Williams, G.L., Brinkhuis, H., Pearce, M.A., Fensome, R.A., Weegink, J.W., 2004. Southern Ocean and global dinflagellate cyst events compared: index events for the Late Cretaceous Neogene, in: Exon, N.F., Kennett, J.P., Malone, M.J. (Eds.), Proceedings of the Ocean Drilling Program, Scientific Results Volume 189. pp. 1–98.
Wood, G.D., Gabriel, A.M., Lawson, J.C., 1996. Chapter 3. Palynological techniques - processing and microscopy, in: Jansonius, J., McGregor, D.C. (Eds.), Palynology: Principles and Applications. American Association of Stratigraphic Palynologists Foundation, Dallas, Texas, pp. 29–50.
Woodruff, F., Savin, S.M., 1989. Miocene Deepwater Oceanography. Paleoceanography 4, 87–140.
Woodruff, F., Savin, S.M., 1991. Mid-Miocene isotope stratigraphy in the deep sea: High-resolution correlations, paleoclimatic cycles, and sediment preservation. Paleoceanography 6, 755–806.
Wright, J.D., Miller, K.G., Fairbanks, R.G., 1992. Early and Middle Miocene stable isotopes: Implications for Deepwater circulation and climate. Paleoceanography 7, 357.
Zachos, J.C., Dickens, G.R., Zeebe, R.E., 2008. An early Cenozoic perspective on greenhouse warming and carbon-cycle dynamics. Nature 451, 279–283.
Zhang, Y.G., Zhang, C.L., Liu, X.L., Li, L., Hinrichs, K.U., Noakes, J.E., 2011. Methane Index: A tetraether archaeal lipid biomarker indicator for detecting the instability of marine gas hydrates. Earth and Planetary Science Letters 307, 525–534.
Zhang, Y.G., Pagani, M., Wang, Z., 2016. Ring Index : A new strategy to evaluate the integrity of TEX_{86} paleothermometry. Paleoceanography 31, 220–232.
Zonneveld, K.A.F., Marret, F., Versteegh, G.J.M., Bogus, K., Bonnet, S., Bouimetarhan, I., Crouch, E., de Vernal, A., Elshanawany, R., Edwards, L., Esper, O., Forke, S., Grøsfjeld, K., Henry, M., Holzwarth, U., Kielt, J.-F., Kim, S.-Y., Ladouceur, S., Ledu, D., Chen, L., Limoges, A., Londeix, L., Lu, S.-H., Mahmoud, M.S., Marino, G., Matsouka, K., Matthiessen, J., Mildenhal, D.C., Mudie, P., Neil, H.L., Pospelova, V., Qi, Y., Radi, T., Richerol, T., Rochon, A., Sangiorgi,

F., Solignac, S., Turon, J.-L., Verleye, T., Wang, Y., Wang, Z., Young, M., 2013. Atlas of modern dinoflagellate cyst distribution based on 2405 data points. Review of Palaeobotany and Palynology 191, 1–197.

Chapter 2.

Characterising the middle Miocene Mi-events in the Eastern North Atlantic realm:

A first high-resolution marine palynological record from the Porcupine Basin

Willemijn Quaijtaal, Timme H. Donders, Davide Persico, Stephen Louwye

The warm climate of the Miocene peaked during the middle Miocene Climatic Optimum (MMCO; 17–14.5 Ma). After the MMCO, global climate went through several short-lived cooling events: the Mi-events (Miocene isotope events). One of the more severe Mi-events is Mi-3, associated with East Antarctic Ice Sheet growth, species turnover in terrestrial and marine realms, Northern Hemisphere and mid-latitude aridification and Antarctic sea-surface temperature cooling. CO_2 reconstructions, as well as the aforementioned observations, suggest that a drawdown of CO_2 and/or changes in ocean circulation led to the changes surrounding Mi-3. A combination of eccentricity and obliquity amplitude modification minima, favourable conditions for ice growth, has also been suggested as a possible triggering mechanism. However, an exact cause cannot be pinpointed yet. High-resolution records necessary to investigate the exact order of events surrounding Mi-3 and the possible role of orbital forcing, a very likely trigger, are sparse.

Integrated Ocean Drilling Program (IODP) Leg 307 recovered such a high resolution record from the middle Miocene at the Porcupine Basin (offshore south-western Ireland). Well-preserved palynomorphs, mainly organic-walled dinoflagellate cysts, acritarchs and some pollen were extracted from Site U1318, and relative and absolute abundance changes were determined. Using dinocysts and calcareous nannoplankton the age model for the record was improved. Based on the palynology, the Mi-3a, Mi-3b and Mi-4 events were successfully identified and concomitant palaeoenvironmental change was observed. These events, although different in magnitude, can be associated with a decrease in sea-surface temperature, as well as with a likely fall in sea-level. Furthermore, possible palaeoenvironmental preferences of 5 dinocyst taxa were determined, based on observations from the record and multivariate statistics.

Published in: Palaeogeography, Palaeoclimatology, Palaeoecology (2014), vol. 399, 140–159.

Characterizing the middle Miocene Mi-events in the Eastern North Atlantic realm: a first high-resolution marine palynological record from the Porcupine Basin

1. Introduction

Over the last 65 million years (Myr) Earth's climate underwent a significant change: from a warm greenhouse climate in the Paleogene to a glaciated Icehouse World in modern times (e.g. *Zachos et al.*, 2001, 2008). From the Early Eocene Climatic Optimum onwards the climate started cooling and during the Eocene–Oligocene Transition Antarctica became glaciated for the first time in Cenozoic history (e.g. *DeConto and Pollard*, 2003; *Zachos et al.*, 2001). Climate remained relatively stable until the late Oligocene warming and the Mid Miocene Climatic Optimum (MMCO; 16–14.5 Ma; *Abels et al.*, 2005). After the MMCO climate started cooling again in gradual steps, eventually leading to the bipolar glaciated world as we know it now. A series of these brief glaciation periods, where Antarctica experienced major ice caps again (*Haywood et al.*, 2009; *Lewis et al.*, 2007; *Shevenell et al.*, 2004), has been identified in several Miocene isotope zones (e.g. *Miller et al.*, 1991, 1996). The positive increases in benthic stable oxygen isotopes ($\delta^{18}O$) in these zones, also referred to as the Miocene isotope events (Mi-events), indicate a drop in bottom water temperature and/or an increase in ice volume (See Figure 2.1). Mi-1 (23.13 Ma; *Abels et al.*, 2005) is considered the second largest climate aberration after the Eocene–Oligocene Transition and it is accompanied by accelerated turnover rates in certain groups of biota (*Zachos et al.*, 2001). After the MMCO the Mi-3 throughout Mi-7 events carried on the pattern of stepwise cooling. Of these events Mi-3 is considered to be the strongest event and $\delta^{18}O$ values did not return to pre-event values (e.g. *Zachos et al.*, 2001). The Mi-3 event was later split into Mi-3a (14.2 Ma) and Mi-3b (13.82; *Abels et al.*, 2005; *Miller et al.*, 1996), of which Mi-3a was relatively small in comparison to the second major Mi-3b event (*Abels et al.*, 2005, and references therein). During and

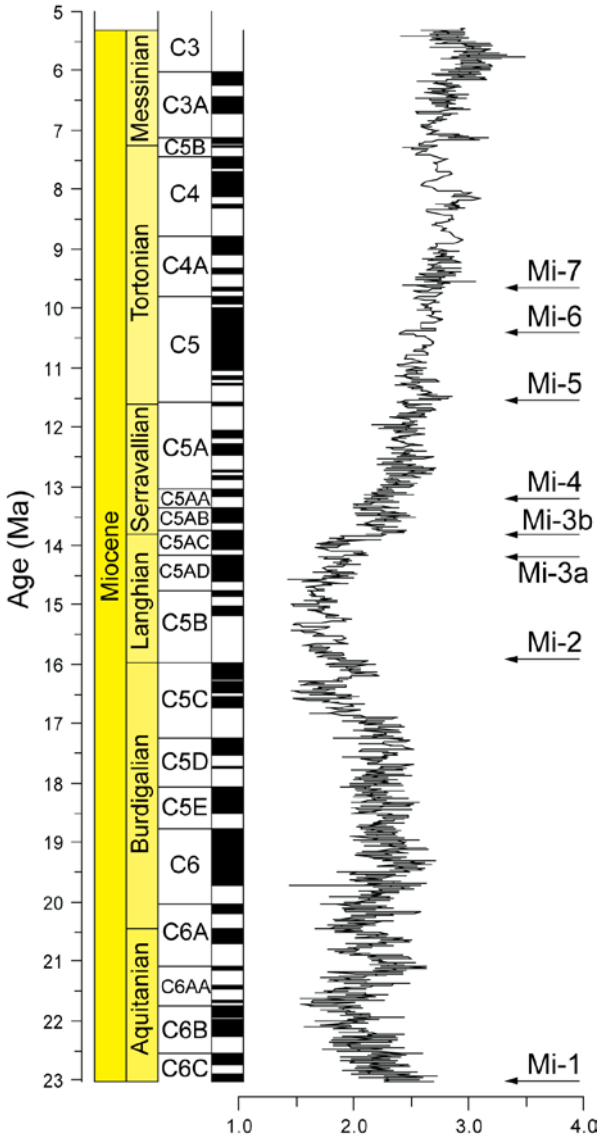

Figure 2.1: Overview of Mi-events 1–7 plotted versus age (Ma; ATNTS 2012) and benthic $\delta^{18}O$. Benthic $\delta^{18}O$ curve is a 5-pt. running average from the *Zachos et al.* (2008) benthic isotope stack, positioning of the Mi-events according to *Miller et al.* (1991, 1996).

after Mi-3 a series of environmental changes occurred, such as species turnover in both terrestrial and marine biota (*Flower and Kennett*, 1994), Northern Hemisphere and mid-latitude aridification (*Eronen et al.*, 2012; *Flower and Kennett*, 1994; *Pound et al.*, 2012) and a carbonate crash in the Caribbean (*Roth et al.*, 2000). Additionally, a shift towards heavier $\delta^{13}C$ values as measured in benthic foraminifers can be observed (*Woodruff and Savin*, 1991). Furthermore, in the Southern Hemisphere surface waters surrounding Antarctica cooled ca. 6–7°C and possibly also freshened (*Shevenell et al.*, 2004), and the tundra vegetation on Antarctica went extinct except for a few isolated communities (*Pound et al.*, 2012). *Moran et al.* (2006) even suggested local presence of sea ice in the Arctic Ocean, implying the first signs of bipolar glaciation. These findings, along with various CO_2 reconstructions, suggest that a drawdown of CO_2 and/or changes in ocean circulation (e.g. *Badger et al.*, 2013; *Kürschner et al.*, 2008; *Pagani et al.*, 2005; *Shevenell et al.*, 2004) led to the changes around Mi-3. However, most of the oceanic records that define and characterise the Mi-events have a relatively low resolution; an order of events and possible causal relationships is therefore hard to determine. The few available high-resolution records of the late middle Miocene suggest that the Mi-3b event (13.82 Ma ± 0.03; *Abels et al.*, 2005) coincides with minima nodes in eccentricity and obliquity amplitude modulation (*Abels et al.*, 2005; *Shevenell et al.*, 2004), a specific configuration that has previously been shown to be favourable for ice growth (*Coxall et al.*, 2005).

To assess whether orbital forcing truly has been a trigger for the Mi-events it is important to gather more high-resolution records, assessing factors such as surface water cooling, terrestrial-marine coupling, productivity changes, sea-level responses and changes in ocean circulation. Especially the biotic response is an important factor given that it links the carbon cycle to climatic processes. Preserved remains of dinoflagellates, an important group of predominantly photosynthetic aquatic micro-organisms (*Taylor*, 1987), can provide insight into surface water properties during the middle and late Miocene cooling. Dinoflagellates are single-celled algae belonging to the superphylum Alveolata, SAR supergoup (former kingdom Protista) in the domain Eukaryota that live in both freshwater and marine surface waters. Together with diatoms and coccolithophorids they form the largest marine phytoplankton group and are important as primary producers. Some dinoflagellates build a strongly resistant resting cyst (dinocyst) — which consists of organic, siliceous or calcareous material — as part of their life cycle (*Evitt*, 1985). It has become clear from a variety of studies that dinocysts are preserved very well, and that they record climatic and environmental change in the past and present through the environmental preferences of the living dinoflagellate (e.g. *Marret and Zonneveld*, 2003; *Pross and Brinkhuis*, 2005; *Rochon and Marret*, 2004; *Sluijs et al.*, 2005; *Zonneveld et al.*, 2013). Dinocysts are excellent proxies for the reconstruction of sea surface temperature (SST), salinity (SSS), productivity and upwelling intensity (SSP) and relative sea-level (e.g. *De Schepper et al.*, 2011; *Mertens et al.*, 2009; *Verleye and Louwye*, 2010). Changes in these properties can be deduced from either changes in the dinocyst assemblage composition or physiology (shape) of dinocysts.

No high-resolution dinocyst records across the Mi-3 and Mi-4 events are available and their potential for assessing the timing and mode of the Mi-events still has to be proven. *Donders et al.* (2009) have already suggested water mass changes and relative SST decreases based on a.o. a dinocyst record, concurrent with terrestrial cooling (based on pollen and organic biomarker evidence) for several of the Mi-events. However, that record from a continental borehole in the Netherlands is not continuously cored and thus not suited for high resolution analysis.

A low-resolution study by *Louwye et al.* (2008) on organic-walled dinocysts for the biostratigraphy and deposition history of the Porcupine Basin (offshore South-western Ireland; See Figure 2.2) at Site U1318, IODP Leg 307 revealed drastic dinocyst assemblage changes during the late

middle Miocene, possibly in relation to the Mi-events. The dinocyst assemblage shifted to a cooler, less productive and more oceanic environment after the MMCO. Based on sedimentation rates and the environmental response in the *Louwye et al.* (2008) study, we consider sediments from Site U1318 to be well-suited for a high resolution dinocysts study to reconstruct the detailed environmental succession across the short-lived Mi-events.

Here we report high-resolution quantitative dinocyst and palynofacies records of environmental conditions at Site U1318 between 14.4 Ma and 12 Ma. We investigate assemblage shifts, changes in species diversity and turnover and their environmental interpretation across this time interval, and compare their timing to existing records and interpretations of the Mi-events.

2. Material and methods

2.1. Material

2.1.1. Geological setting and stratigraphic framework

The Porcupine Basin is especially famous for its deep-water habitats (*Le Danois*, 1948; *Thomson*, 1873) and harbours several large carbonate mounds (*De Mol et al.*, 2002). These mounds are deep-water coral banks (*De Mol et al.*, 2002; *Foubert et al.*, 2005) and can be separated into three distinct provinces: 1) the Belgica mounds in the east, 2) the Hovland mounds in the north (*De Mol et al.*, 2002) and 3) the buried Magellan mounds in the northwest (*Huvenne et al.*, 2002, 2007; See Figure 2.2) and the adjacent Viking and buried Enya mounds (*De Cock, 2005*; *Van Rooij et al.,* 2009). It was assumed

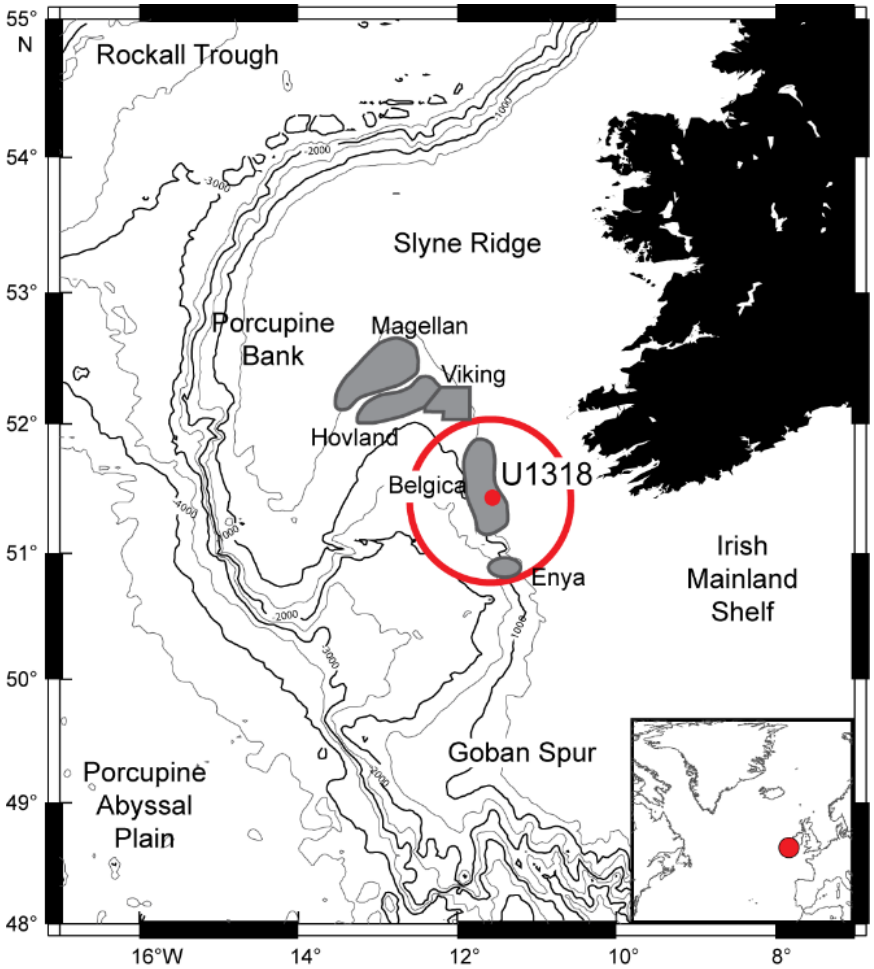

Figure 2.2: Location of Site U1318. Location of coral mound provinces are indicated by grey areas; provinces after *Foubert et al.* (2011).

that the initiation of mound growth most likely started in the Pliocene (*De Mol et al.*, 2002; *Van Rooij et al.*, 2003), but this could only be resolved when Integrated Ocean Drilling Program (IODP) Leg 307 '*Modern Carbonate Mounds: Porcupine Drilling'* drilled mound Challenger in the Belgica province in May 2005 (Site U1318). High-resolution seismic profiles of the Belgica mound province divide the sediments into three units (Figure 2.3): P1 being the lowermost unit, P2 being the intermediate unit and P3 being the uppermost unit (*Van Rooij et al.*, 2003). One of the coral mounds is rooted on unconformity reflector RD1 that separates units P1 and P3; unit P2 is absent at that location. Sites U1316 and U1317 were drilled in close vicinity to mound Challenger and through Mound Challenger respectively in order to gain more insight into coral mound growth and ecology. Site U1318 was drilled at a more upslope position in the Basin at a water depth of 409 m to determine the age of the RD1 reflector and to investigate the palaeoenvironment during the initiation of coral mound growth (*Expedition 307 Scientists*, 2006). The dinocyst biostratigraphy showed that the RD 1 reflector has a terminal middle Miocene or earliest late Miocene age (*Louwye et al.*, 2008), and can be correlated to the Ser4/Tor1 sequence boundary (10.5 Ma) of *Hardenbol et al.* (1998). Underlying sediments are of late early Miocene and middle Miocene age.

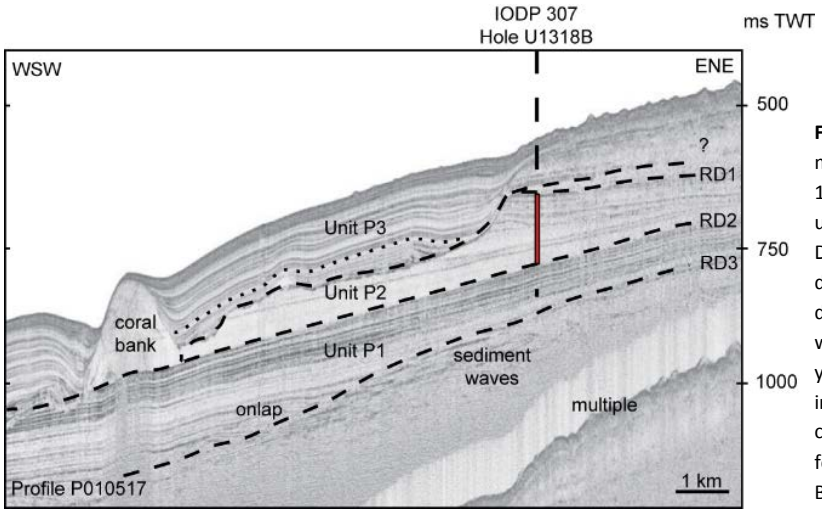

Figure 2.3: Seismic profile of the Belgica mound province, with location of drill site 1318B, seismic units P1, P2 and P3, and unconformity reflectors RD3, RD2 and RD1. Dashed lines indicate unconformity reflectors, dotted lines indicate the upper limit of drift deposits not observed in 1318B, dashed line with question mark indicates the position of a yet unmapped unconformity. Red rectangle indicates analysed interval. Seismic profile courtesy of Jean-Pierre Henriet, Renard Centre for Marine Geology, Ghent University, Belgium.

The lithology of Site U1318 can be divided into three stratigraphic units, 1, 2 and 3 (*Expedition 307 Scientists*, 2006; Figure 2.4). Unit 1 is an unlithified clayey succession that can be divided into three subunits with distinct boundaries that correspond to shifts in the magnetic susceptibility record. Unit 1 corresponds to seismic unit P3. Unit 2 consists of olive-grey, fine-grained to medium-grained sands interbedded with dark yellowish brown silty clay. The sands show a coarsening-upward trend. Lithoclasts, mollusc and shell fragments can also be observed in this unit. Unit 2 corresponds to the lowermost part of seismic unit P3 (*Expedition 307 Scientists*, 2006).

Unit 3, from which the samples for this study were taken, is divided into three moderately lithified subunits based on their carbonate content. Subunit 3A contains greenish grey to light greenish grey silty clays. These are interbedded with well-sorted greenish grey fine-grained sand and greenish grey to grey silt with erosive boundaries at their bases. Carbonate content is relatively high (27–50 wt%). The top of the subunit is defined by a prominent bivalve bed overlying well-sorted fine-grained sands. The base of the subunit is defined by a sharp erosive boundary at 127.3 mbsf in Hole 1318C. Subunit 3B is characterized by very homogeneous greenish grey silty clay. Carbonate content varies from ~20 wt% in the upper half of the unit to ~10 wt% in the lower half. Abundant bioturbation is present throughout the unit. Subunit 3A and 3B correspond to seismic unit P2 (Figure 2.3). Subunit 3C

consists of greenish grey silty clay to fine sand with a fining-upward trend from the middle to the upper part of the subunit. Carbonate content ranges from ~25 wt% at the top to 35 wt% at the bottom. Exceptions are several extremely lithified beds with ~70 wt% carbonate content. Two of these beds are partly dolomitised. Subunit 3C corresponds to seismic unit P1 (*Expedition 307 Scientists*, 2006; Figure 2.3).

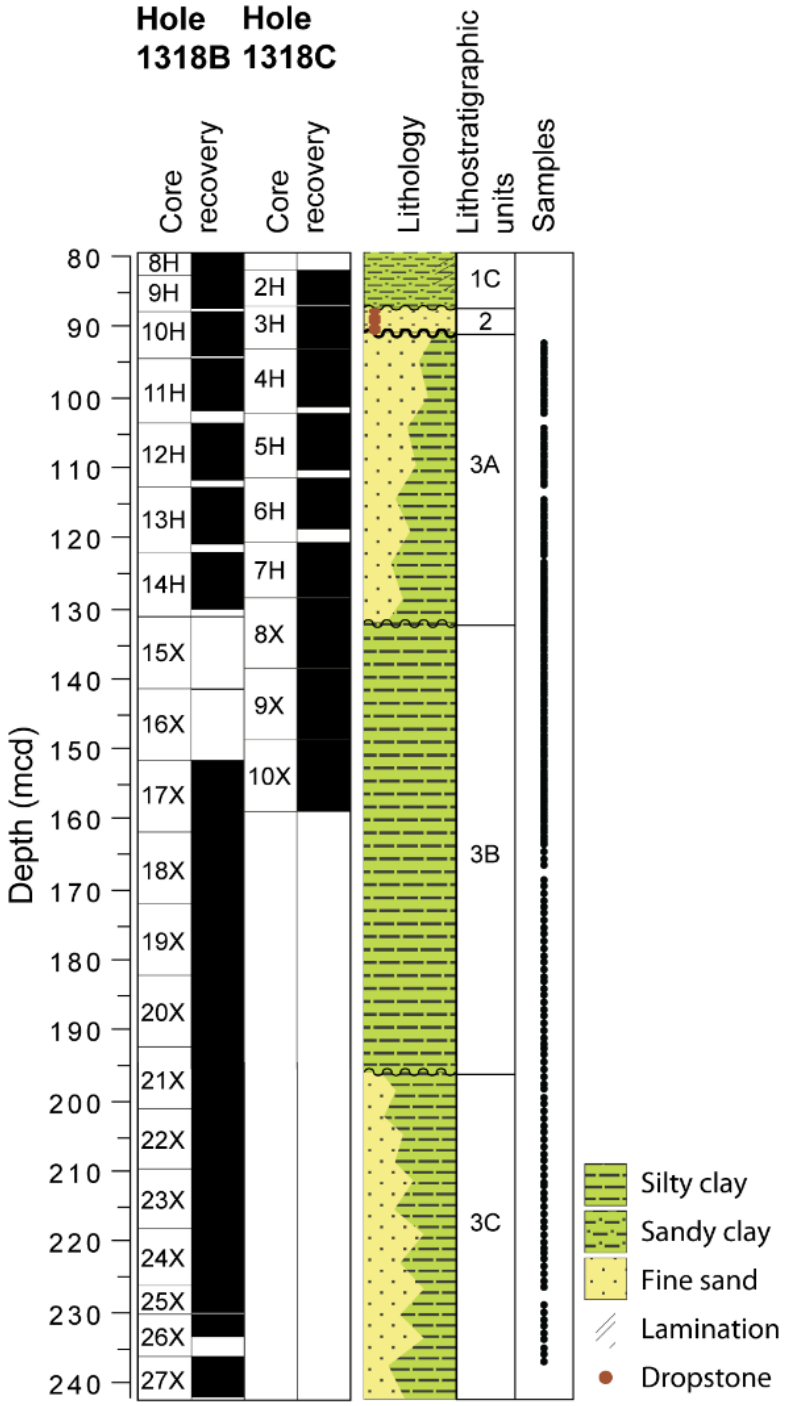

Figure 2.4: Core recovery (black), lithology, lithostratiphic interpretation and sample positions of drill sites 1318B and 1318C. Wavy lines indicate unconformities.

2.1.2.Samples

At Site U1318 three holes have been drilled: 1318A, 1318B and 1381C. Deepest of these is Hole 1318B (51°26.148'N lat., 11°33.019'W long.): 213 m sediment was recovered, although cores 15X and 16X recovered almost no sediments. A total of 72 samples was taken from Hole 1318B. In order to fill in the gap caused by the minimal recovery in cores 15X and 16X additional samples were analysed from Hole 1318C (51°26.150.4358'N lat., 11°33.040'W long.). The hole was drilled 25 m south of Hole 1318B and 84.15 m of sediment has been recovered. 52 samples from Hole 1318C were analysed, resulting in a total of 123 analysed samples (See Figure 2.4 for sample positioning). Average sample spacing is circa 22 ka.

2.1.3.Spliced record

Expedition 307 Scientists (2006) reconstructed a meters composite depth (mcd) scale for Site 1318 based on physical properties, especially magnetic susceptibility, gamma ray attenuation density and natural gamma radiation, with aid of biostratigraphy and lithologic contacts. An overview of splice tie-points can be found in table 10 of *Expedition 307 Scientists* (2006).

2.2. Methods

2.2.1.Palynological processing

Standard palynological preparation techniques have been used (*Wood et al.*, 1996). The samples were cleaned and oven-dried at 60°C. The material was then weighed and rehydrated with demineralised water. Ten to fifteen grams of dry weight material were tested for presence of carbonates and one or two *Lycopodium clavatum* tablets (batch no. 177745, X = 18584 ± 829 and batch no. 1031, X = 20848 ± 2186, see Supplementary Table 2.1) were added. Carbonates were removed using hydrochloric acid (HCl, 2N), the samples were then allowed to settle overnight and rinsed with demineralised water until pH neutral. Sand was removed after 4 hour etching with a small quantity of hydrofluoric acid (HF, 40%) and stepwise adding of demineralised water and decanting. The samples were then settled overnight and decanted again. The remaining silicates were then removed by adding HF and heating the samples in a 65°C water bath for two days. Demineralised water was added to stop the reaction and the samples were left to settle overnight. The samples were decanted and 2N HCl was added to remove fluorosilicates. The samples were heated at 65°C for two days, HCl was refreshed after a day. The residues were then placed in an ultrasonic bath for 30 seconds to break up clumps of amorphous organic matter and sieved over a 10 µm nylon mesh screen. The residue was transferred to a plastic vial with addition of several drops of $CuSO_4$ solution to prevent fungal growth. The vials were centrifuged at 2000 rpm for 5 min, water surpluses removed and one drop of homogenized residue was mounted on a microscopic slide in a drop of liquid glycerol gelatine. The slides were covered with a cover slip and sealed with nail polish. The samples are stored in the collection of the research Unit Palaeontology, Ghent University, Ghent, Belgium.

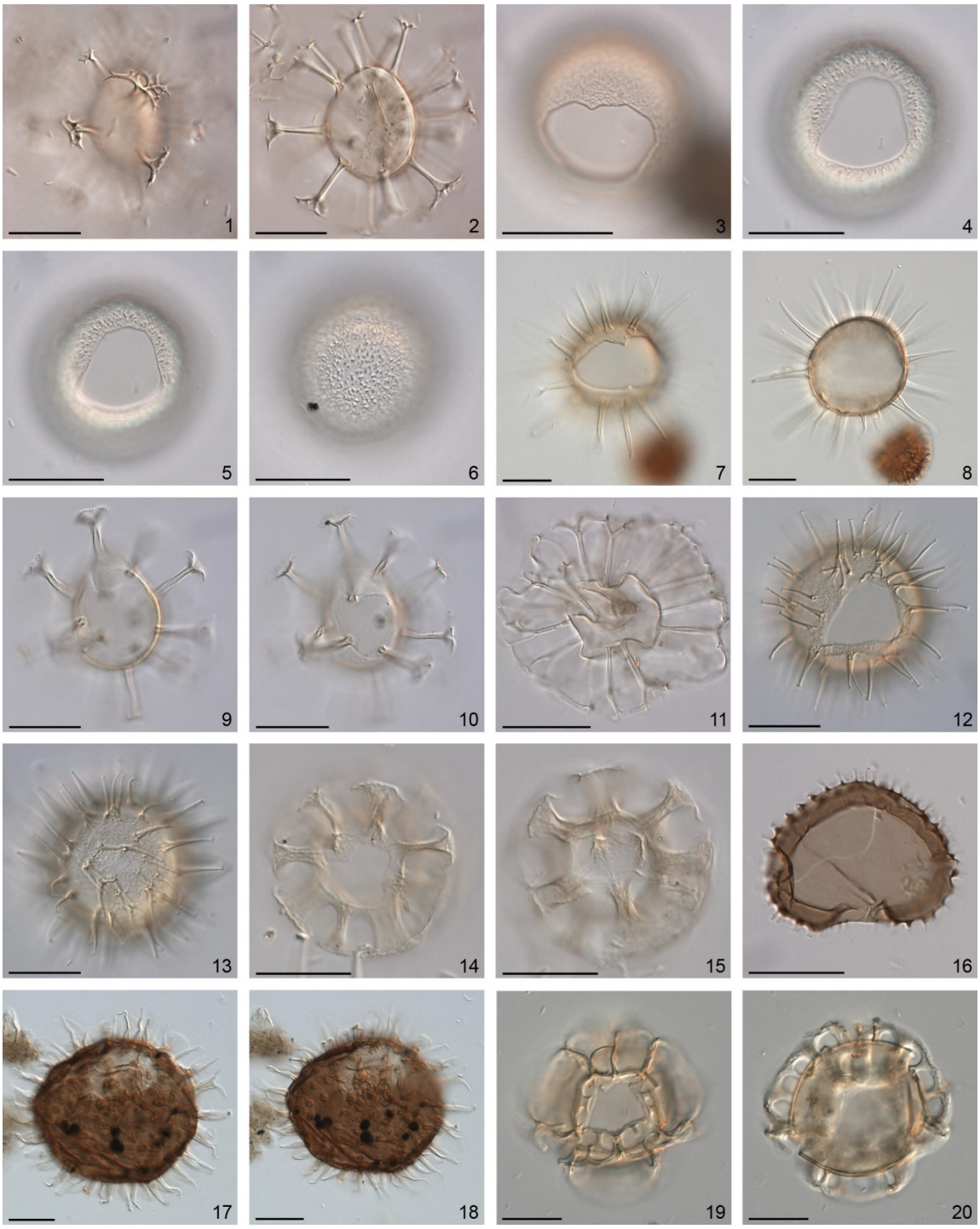

Plate 2.1: Photomicrographs of selected dinoflagellate cyst species. All images taken with interference contrast. Various magnifications. EF: England Finder coordinates. Scale bar: 20 µm. 1–2. *Achomosphaera andalousiensis*. Sample 307/1318B/12H1/30–32 cm/462/1, EF: U26-3. 1 high focus on process tips. 2 mid-focus. 3. *Batiacasphaera* complex. Sample 307/1318B/11H6/2–4 cm/459/1, EF: Y30-1. High focus on wall ornamentation. 4–6. *Habibacysta tectata*. Sample 307/1318B/11H4/3–4 cm/452/1, EF: U44-3. 4, 5 successively slightly differing high foci on archaeopyle. 6 low focus on ornamentation. 7–8. *Lingulodinium machaerophorum.* Sample 307/1318C/9X5/130–132 cm/698/1, EF: X14-4. 7 high focus on archaeopyle. 8 mid-focus. 9–10. *Melitasphaeridium choanophorum*. Sample 307/1318B/10H7/17–19 cm/442/1, EF: E32-1. 9 high focus on processes. 10 slightly lower focus on wall ornamentation, note slight thickenings on wall surface possibly reflecting tabulation. 11. *Nematopsphaeropsis labyrinthus*. Sample 307/1318B/12H5/80–82 cm/495/1, EF R43-3. Mid-focus. 12–13. *Operculodinium centrocarpum*. Sample 307/1318B/11H2/5–7 cm/445/1, EF: J31-2. 12 high focus on archaeopyle. 13 low focus on wall structure. 14–15. *Paucisphaeridium* sp. A. Sample 307/1318C/7H3/70-72 cm/651/1, EF: W39-1. 14 high focus on archaeopyle. 15 low focus on fibrous processes. 16. *Selenopemphix brevispinosa.* Sample 307/1318B/11H5/52–54 cm/457/1, EF: S41-4. High focus. 17–18. *Sumatradinium soucouyantiae*. Sample 307/1318B/14H1/140–142 cm/552/1, EF: Q25-1. 17 high focus on archaeopyle. 18 low focus on wall structure and processes. 19–20. *Unipontidinium aquaeductus*. Sample 307/1318C/7H3/120–122 cm/652/1, EF: K23-4. 19 high focus on archaeopyle. 20 mid-focus.

A minimum of 300 dinocysts was counted systematically, in non-overlapping traverses. Other palynomorphs such as acritarchs, chlorophytes, organic linings of foraminifers and pollen were counted as well (See Supplementary Table 2.1). After the systematic count the remainder of the slide was scanned for rare species and well-preserved specimens suitable for photomicrography. Slides were counted using a Zeiss AxioImagerA1 microscope at 400x magnification equipped with a Zeiss Axiocam MRc5 camera.

Taxonomy follows (*Fensome et al.*, 2008)*. Several dinocyst taxa have been grouped in complexes. The *Spiniferites*/*Achomosphaera* complex (cpx) contains all specimens of *Spiniferites* and/or *Achomosphaera* that have not been identified upon species level. *Spiniferites membranaceus* and *Spiniferites mirabilis* have been grouped together based on their similar morphology and ecological preferences (*Zonneveld et al.*, 2013). The *Batiacasphaera* complex contains specimens of the species *Batiacasphaera minuta*, *Batiacasphaera micropapillata* and *Batiacasphaera sphaerica*; species that are morphologically very similar and hard to distinguish under a light microscope reliably (*Schreck and Matthiessen*, 2013). *Capisocysta lata* and *Capisocysta lyellii* have been grouped because they are distinguished based on tabulation of the hypocyst, a feature that is not always clearly visible under the microscope.

* Post publication note: several species have been described or determined after publication of this paper. *Spiniferites* sp. B was identified as *Spiniferites pachydermus*, Dinocyst sp. A-D were later transferred to the acritarchs and acritarch sp. F was described as *Platycystidia manumii*. These are all described in Chapter 3. The other provisional taxa are illustrated in Plates 2.3 and 2.4.

2.2.2.Calcareous nannoplankton

Twenty-five samples were sent to the University of Parma for a biostratigraphical analysis of calcareous nannofossils. The samples were prepared following a standard smear slide preparation technique (*Bown*, 1998) and then studied using a Zeiss polarised microscope at 1250x magnification. A fixed number of fields of view (FOV = 100) were observed in each sample and semi-quantitative analyses were used to determine the highest and lowest occurrence events.

For every sample, the total abundance of calcareous nannofossils and the abundance of each individual nannofossil taxon were estimated as follows: A = abundant; >1 specimen per FOV; C = common; ≥1 specimen per FOV; F = few; <1 specimen per 2–10 FOV; R = rare; <1 specimen per 11–100 FOV; B = barren; no calcareous nannofossils present (see Supplementary Table 2.2).

2.2.3.Age model

The age model for Holes 1318B and 1318C (Figure 2.5) is mainly based upon the magnetostratigraphy of *Louwye et al.* (2008), but was updated to the new time scale of *Hilgen et al.* (2012). Depths in meters below sea floor were converted into meters composite depth. The shipboard measurements of inclination used for the magnetostratigraphy have to be interpreted with caution because of possible magnetic overprint gathered during drilling and bias and background noise in the cryogenic magnetometer. This creates an artificial magnetic inclination pointing downward. Sediments with low magnetic intensities such as carbonates are especially susceptible to this process (*Expedition 307 Scientists*, 2006). In addition, it is likely that magnetites have been destructed post-depositionally (*Louwye et al.*, 2008). To overcome the first problem, measurements were taken on discrete samples from Hole 1318B (*Louwye et al.*, 2008). Magnetic reversal points in Hole 1318C that occur in the part

that covers the core gap of Hole 1318B have been excluded since no discrete samples were taken from this hole.

The magnetostratigraphy was complemented with biostratigraphy. The dinocyst biostratigraphy is based upon lowest and highest occurrences (LO; HO) of dinocysts in this record. Biostratigraphical tie-points for the part of the record that was not analysed in high-resolution yet were taken from *Louwye et al.* (2008). The used biostratigraphical events were then correlated to well-dated and calibrated dinocyst bio-events from the North Atlantic Ocean and North Sea (*Dybkjær and Piasecki*, 2010; *Schreck et al.*, 2012). The Porcupine Basin is well-connected to the North Atlantic Ocean and therefore to the Iceland Sea, the study location of *Schreck et al.* (2012). A factor hampering correlation to the Iceland Sea might be latitude and therefore temperature. However, latitudinal temperature gradients during the Langhian and Serravallian were less steep than nowadays (*Pound et al.*, 2012) and temperatures in the Iceland Sea were still 12–20°C during our study period (*Schreck et al.*, 2013). The Porcupine Basin was less well-connected to the North Sea, since it was a semi-enclosed basin during the Miocene. Nonetheless, *Donders et al.* (2009) state that North Sea dinocyst zonations were largely comparable to the Mediterranean and a similar conclusion can therefore be drawn for the comparison with the North Atlantic Ocean. Regardless of possible comparison, the biostratigraphical events have only been used as a guideline in the age-model, not included in the model, due to the diachronous nature of most biostratigraphical events.

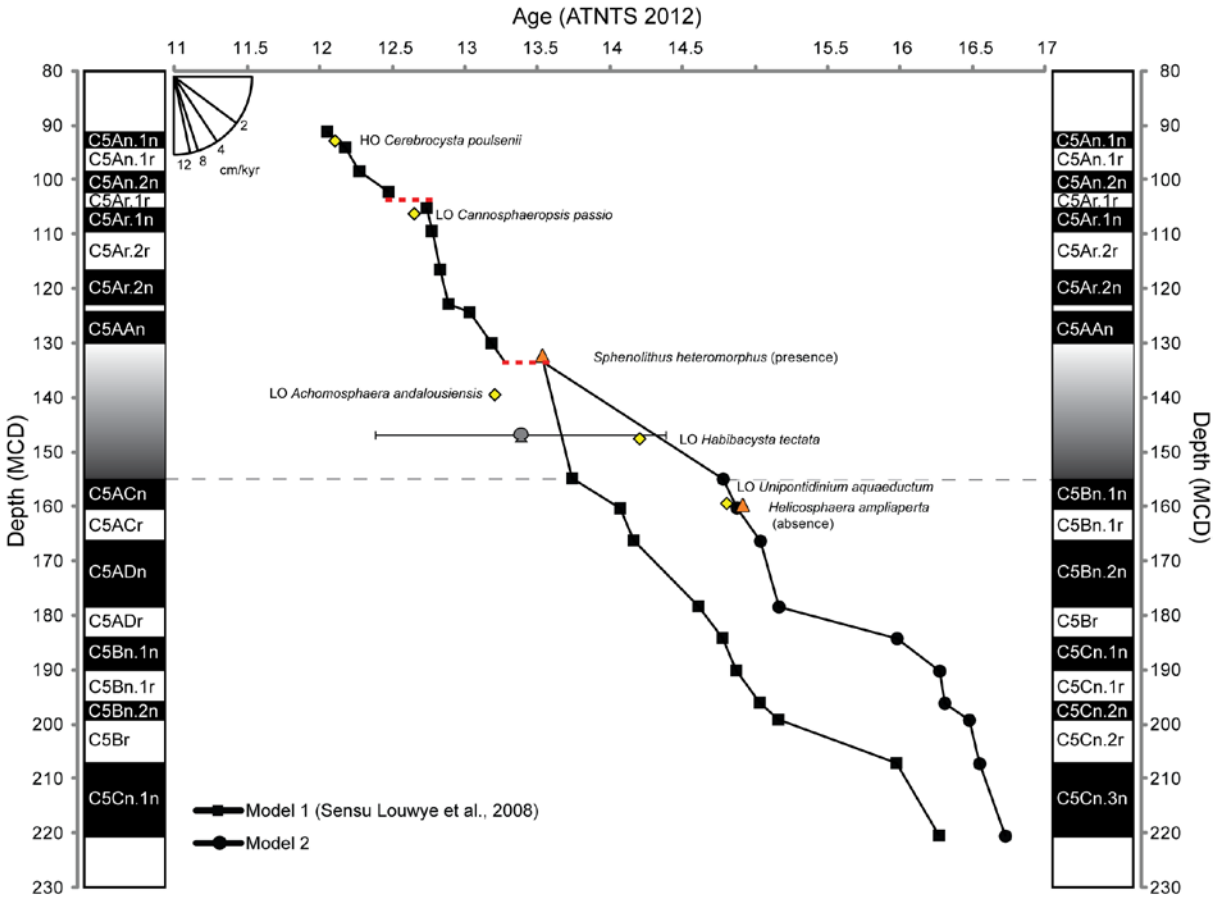

Figure 2.5: Age model and the different magnetostratigraphic interpretations for Site U1318. Red dashed line indicates a hiatus, black squares or circles indicate magnetostratigraphic tie-points, yellow diamonds indicate dinocyst biostratigraphic tie-points, orange triangles indicate nannoplankton presence or absence, grey mollusc indicates Sr-isotope age. Grey lines link the illustrated magnetostratigraphic interpretation to their associated age models.

The nannofossil biostratigraphical points represent the presence of *Sphenolithus heteromorphus* that provides a minimum age of the record at 131.81 mcd that is older than its HO, dated 13.53 Ma (*Hilgen et al.*, 2012), and the absence of *Helicosphaera ampliaperta* at 159.65 mcd that provides an age younger than its HO, dated at 14.91 Ma (*Hilgen et al.*, 2012). The latter age can be used regardless of it being an absence because a rough biostratigraphical study by the *Expedition 307 Scientists* (2006) confirms the presence of *Helicosphaera ampliaperta* in Hole 1318B. An additional contribution to the age model was provided by a strontium isotope measurement on mollusc fragments (*Kano et al.*, 2007). An overview of all the tie-points used for the age model can be found in Table 2.1.

For the uppermost part of the composite (90–122 mcd) the magnetostratigraphy was followed completely. However, for the part from 122 mcd downwards the magnetostratigraphical interpretation of *Louwye et al.* (2008) was off-set from the additional ages provided by the biostratigraphy. Therefore, the interpretation of the magnetostratigraphy was shifted by two magnetochrons towards an older age (see Figure 2.5). Other changes are the incorporation of the hiatus at ca. 133.2 mcd that separates lithostratigraphic units 3A and 3B. A previously unnoticed hiatus was found due to inconsistencies in sedimentation rates as deduced from the magnetostratigraphy (See Figure 2.5). Core photographs of core 1318B 12H1 shows an irregularity in the first 30 cm (104.31–104.60 mcd; Supplementary Figure 2.1). Gamma ray attenuation density also shows a positive increase at this point (*Expedition 307 Scientists*, 2006). A likely possibility is that it is a remainder of a mass transport deposit, since the corresponding seismic profile at the depth of the irregularity (See Figure 2.3) shows discontinuous higher amplitude reflections at the top of seismic unit P2. Another option is that it represents a coring artefact. The hiatus spans circa 300 ka. Sedimentation rates of the composite record are on average 5.8 cm/ka. Highest sedimentation rates ranging from 10.92–12.1 cm/ka can be found in the interval from 122.81–102.23 mcd and 16.9 cm/ka between 196.05–190.15 mcd.

Table 2.1
Magneto- and biostratigraphical tie-points. Tie-points in bold are used for the age model.

Bio-/magnetostratigraphical event	Age (Ma)	Site	Interpretation 1		Interpretation 2		Reference for age
			Depth (mbsf)	Depth (mcd)	Depth (mbsf)	Depth (mcd)	
Top C5An.1n	**12.049**	**1318B**	**86.2**	**91.14**	**86.2**	**91.14**	**ATNTS 2012**
HO *Cerebrocysta poulsenii* (this study)	12.1	1318B	87.795	92.735	87.795	92.735	*Schreck et al.*, 2012
Bottom C5An.1n	**12.174**	**1318B**	**89.1**	**94.04**	**89.1**	**94.04**	**ATNTS 2012**
Top C5An.2n	**12.272**	**1318B**	**94**	**98.43**	**94**	**98.43**	**ATNTS 2012**
Bottom C5An.2n	**12.474**	**1318B**	**97.8**	**102.23**	**97.8**	**102.23**	**ATNTS 2012**
LO *Cannosphaeropsis passio* (this study)	12.73	1318B	101.565	105.875	101.565	105.875	*Hilgen et al.*, 2012
Top C5Ar.1n	**12.735**	**1318C**	**99.1**	**105.2**	**99.1**	**105.2**	**ATNTS 2012**
Bottom C5Ar.1n	**12.77**	**1318C**	**103.3**	**109.4**	**103.3**	**109.4**	**ATNTS 2012**
Top C5Ar.2n	**12.829**	**1318C**	**110.8**	**116.51**	**110.8**	**116.51**	**ATNTS 2012**
Bottom C5Ar.2n	**12.887**	**1318B**	**117.1**	**122.81**	**117.1**	**122.81**	**ATNTS 2012**
Top C5AAn	**13.032**	**1318B**	**119.8**	**124.320**	**119.8**	**124.320**	**ATNTS 2012**
Bottom C5AAn	**13.183**	**1318B**	**125.5**	**130.020**	**125.5**	**130.020**	**ATNTS 2012**
LO *Achomosphaera andalousiensis* (*Louwye et al.*, 2008)	13.2	1318C	136.785	139.385	136.785	139.385	*Hilgen et al.*, 2012
Top C5ABn	13.363	N/A	N/A	N/A	N/A	N/A	ATNTS 2012
Sr-dated mollusc fragment	(12.74) 13.381 (14.624)	1318C	140.83	146.740	140.83	146.740	*Kano et al.*, 2007
Sphenolithus heteromorphus (presence)	> 13.52	1318C	127.29	131.810	127.29	131.810	*Hilgen et al.*, 2012
Bottom C5ABn	13.608	N/A	N/A	N/A	N/A	N/A	ATNTS 2012
Top C5ACn	**13.739**	**1318B**	**148.7**	**154.850**	N/A	N/A	**ATNTS 2012**
Bottom C5ACn	**14.07**	**1318B**	**154.2**	**160.350**	N/A	N/A	**ATNTS 2012**
Top C5ADn	**14.163**	**1318B**	**160.1**	**166.250**	N/A	N/A	**ATNTS 2012**
LO *Habibacysta tectata* (*Louwye et al.*, 2008)	14.2	1318C	141.595	147.505	141.595	147.505	*Schreck et al.*, 2012
Bottom C5ADn	**14.609**	**1318B**	**172.2**	**178.350**	N/A	N/A	**ATNTS 2012**
Top C5Bn.1n	**14.775**	**1318B**	**178**	**184.150**	**148.7**	**154.850**	**ATNTS 2012**
LO *Unipontidinium aquaeductus* (*Louwye et al.*, 2008)	14.8	1318B	153.22	159.370	153.22	159.370	*Dybkjær and Piasecki*, 2010
Bottom C5Bn.1n	**14.87**	**1318B**	**184**	**190.150**	**154.2**	**160.150**	**ATNTS 2012**
Helicosphaera ampliaperta (absence)	< 14.91	1318C	153.7	159.650	153.7	159.650	*Hilgen et al.*, 2012
Top C5Bn.2n	**15.032**	**1318B**	**189.9**	**196.050**	**160.1**	**166.250**	**ATNTS 2012**
Bottom C5Bn.2n	**15.16**	**1318B**	**193**	**199.150**	**172.2**	**178.350**	**ATNTS 2012**
Top C5Cn.1n	**15.974**	**1318B**	**201**	**207.150**	**178**	**184.150**	**ATNTS 2012**
Bottom C5Cn.1n	**16.268**	**1318B**	**214.3**	**220.450**	**184**	**190.150**	**ATNTS 2012**
Top C5Cn.2n	**16.303**	**1318B**	N/A	N/A	**189.9**	**196.050**	**ATNTS 2012**
Bottom C5Cn.2n	**16.472**	**1318B**	N/A	N/A	**193**	**199.150**	**ATNTS 2012**
Top C5Cn.3n	**16.543**	**1318B**	N/A	N/A	**201**	**207.150**	**ATNTS 2012**
Bottom C5Cn.3n	**16.721**	**1318B**	N/A	N/A	**214.3**	**220.450**	**ATNTS 2012**

2.2.4. Palaeoenvironmental indices

The composition of a fossil dinocyst assemblage depends on two main factors: the modern dinoflagellate assemblage and various taphonomic processes. Environmental parameters that influence the dinoflagellate assemblage are e.g. sea-surface temperature, -salinity, -productivity, trophic state of the environment and relative sea-level (e.g. *Zonneveld et al.*, 2013). To deduce the environmental variables, several indices are available. These indices do not give exact numbers, but an indication of relative environmental change based on the preferential habitat of dinoflagellate taxa. Taphonomic processes that influence the assemblage are e.g. sedimentary processes, transport, preservational processes and laboratory procedures (*Dale*, 1976, 1992, *Mertens et al.*, 2009a, 2009b, 2012; *Zonneveld et al.*, 2008) .

One factor might hamper our analysis specifically: the relative offshore location of the U1318 drill site. It is located at the upper slope on the transition from outer neritic to oceanic conditions. The assemblage does not solely contain oceanic species or outer neritic species and it should be assumed that dinocysts have been transported from the shelf. Our record therefore does not only reflect changes in the Porcupine Basin, but it is a more regional signal from the South-western Irish Shelf. Furthermore, some dinocysts can be indicative of multiple environmental factors. Especially cysts produced by heterotrophic dinoflagellates were found to represent more than one environmental factor in previous studies; these were excluded from all indices other than the P/G index (see below) since their heterotrophic feeding behaviour is probably the most important factor in their distribution (*Verity et al.*, 1993).

2.2.4.1. Sea-surface temperature

To assess relative SST the Warm/Cold index (W/C) can be used: W/C = nW / (nW + nC), where n is the number of specimens counted, W are warm-water indicating species and C are cold-water indicating species (*Versteegh*, 1994). The overview of species that indicate either warm or cold conditions *De Schepper* (2006) gave was complemented with other indicative species in the Porcupine Basin record (see Table 2.2). *De Schepper et al.* (2011) carried out a comparative study based on Pliocene and Pleistocene dinocyst and Mg/Ca temperature and compared the past and present records. This confirmed the correct environmental interpretation of most of the used species. The oceanic dinocyst *Impagidinium pallidum* however showed a wider temperature range for the past record than is known in present records. Nonetheless this species was kept as a cold-water indicator since changing temperature gradients and concomitant competition between species may have caused *Impagidinium pallidum* to migrate polewards in recent times.

Table 2.2
Indicative dinocyst and acritarch species arranged by their specific environmental preference.

Environmental factor	Dinocyst or acritarch species	Reference
Cold water	*Bitectatodinium tepikiense, Filisphaera filifera, Habibacysta tectata, Impagidinium pallidum*	*De Schepper*, 2006, and references therein
Warm water	*Bitectatodinium raedwaldii, Capisocysta lata, Impagidinium aculeatum, Impagidinium paradoxum, Impagidinium patulum, Impagidinium strialatum, Invertocysta* spp., *Lingulodinium machaerophorum*, *Melitapshaeridium choanophorum, Nannobarbophora gedlii, Operculodinium israelianum, Polysphaeridium zoharyi, Spiniferites hyperacanthus, Spiniferites mirabilis, Tectatodinium pellitum, Tuberculodinium vancampoe*	*Dale*, 1996; *De Schepper*, 2006, and references therein; *De Schepper et al.*, 2011; *Head*, 2003, 1998, 1997; *Marret and Zonneveld*, 2003
Neritic waters	*Achomosphaera andalousiensis, Capisocysta lata, Cleistosphaeridium placacanthum, Dapsilidinium pseudocolligerum, Dinopterygium cladoides* sensu Morgenroth (1966), *Geonettia cliniae*, *Homotryblium* spp., *Lingulodinium machaerophorum*, *Operculodinium* spp., *Polysphaeridium zoharyi*, *Spiniferites/Achomosphaera* complex, *Tectatodinium pellitum*, *Tuberculodinium vancampoae*	*De Schepper*, 2006; *Marret and Zonneveld*, 2003; *Pross and Brinkhuis*, 2005; *Zevenboom et al.*, 1994
Oceanic waters	*Cannosphaeropsis* spp., *Edwardsiella sexispinosa*, *Impagidinium* spp., *Nematosphaeropsis* spp.	*Dale*, 1996; *De Schepper*, 2006; *Sluijs et al.*, 2005

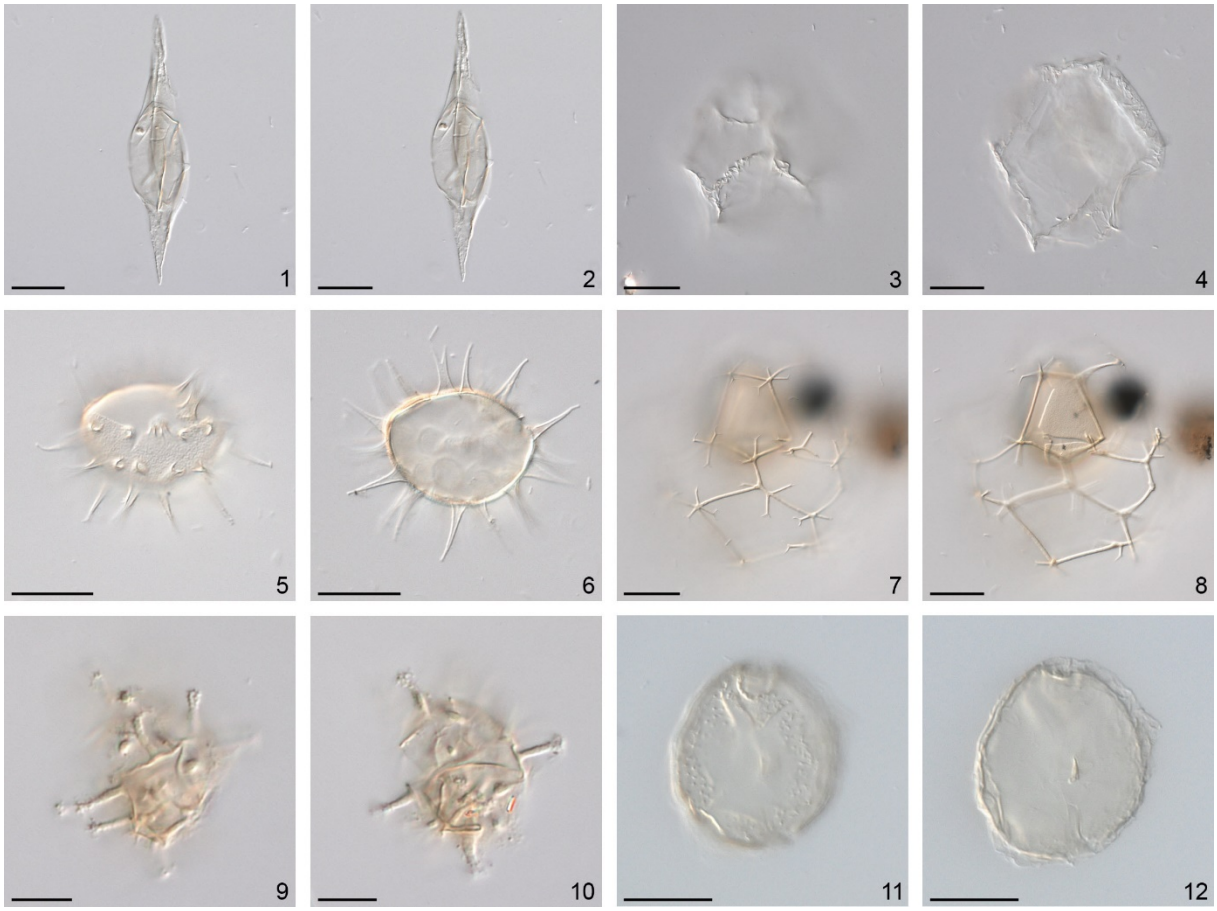

Plate 2.2: Photomicrographs of selected dinoflagellate cyst and acritarch species. All images taken with interference contrast. Various magnifications. EF: England Finder coordinates. Scale bar: 20 µm. 1–2. *Palaeocystodinium golzowense*. Sample 307/1318C/8X3/115–117 cm/672/1, EF: V26-4. 1, 2 slightly differing high foci on archaeopyle and horns. 3–4. *Impagidinium pallidum*. Sample 307/1318C/9X5/33–35 cm/696/1, EF: R29-1. 3 high focus. 4 mid-focus. 5–6. *Dapsilidinium pseudocolligerum*. Sample 307/1318C/7H2/120–122/649/1, EF: F40-1. 5 high focus. 6 mid-focus. 7–8. *Cannosphaeropsis passio*. Sample 307/1318B/10H7/17–19 cm/442/1, EF: Y20-4. 7 high focus on trabeculae. 8 lower focus on archaeopyle. 9–10. *Nannobarbophora gedlii*. Sample 307/1318B/13H2/43–45 cm/513/1, EF: S30-1. 9 high focus on processes. 10 mid-focus on central body, note possible excystment opening in left lateral position. 11–12. *Cyclopsiella granosa/elliptica*. Sample 307/1318C/7H2/120–122 cm/649/1, EF: W19-2. 11 high focus. 12 mid-focus.

2.2.4.2. Sea-surface productivity

A measure of SSP is the P/G index (P/G; *Versteegh*, 1994), where P/G = nP / (nP + nG). N is the number of specimens counted, P the peridinioid species and G the gonyaulacoid species. *Harland* (1973) introduced the gonyaulacoid ratio, using the number of *species* rather than the number of *specimens*, but later on the ratio was commonly used with the number of specimens (*Sluijs et al.*, 2005). The P/G ratio is based upon the assumption that most peridinioid species have a heterotrophic or mixotrophic feeding strategy. They often favour areas where diatoms — one of their main food sources — bloom on nutrients brought into the area by upwelling or river discharge (e.g. *Dale*, 1996). *Reichart and Brinkhuis* (2003) showed that the number of cysts of the extant peridinioid dinoflagellate genus *Protoperidinium* correlates well with other proxies that indicate upwelling and/or marine productivity. Therefore, an increased P/G ratio may be interpreted as surface-water conditions with enhanced nutrient availability. The same study by *Reichart and Brinkhuis* (2003) however also showed that oxidation of sediments can lead to selective degradation of cysts of *Protoperidium*. A similar conclusion

on selective preservation of other peridinioid species was drawn by *Zonneveld et al.* (2008). Absence of peridinioids might therefore point towards oxidative degradation of palynomorphs.

The species used representing P are *Barssidinium* spp., *Cristadinium* spp., *Echinidinium* spp., *Lejeunecysta* spp., *Palaeocystodinium* spp., round brown cysts (cysts with brown, smooth walls, a rounded outline and indications of an archaeopyle, mostly represented by the genus *Brigantedinium*), *Selenopemphix* spp., *Sumatradinium* spp. ad *Trinovantedinium* spp.. The species representing G are all other dinocysts, except for the goniodomacean species (e.g. *Capisocysta* spp. and *Tuberculodinium vancampooae*) and the polykrikacean *Polykrikos*.

2.2.4.3. Relative sea-level

To discern between ice volume and temperature changes in the benthic $\delta^{18}O$ signal during the Mi-events and concomitant glaciation it is of importance to detect associated sea-level variability. Most dinocysts have been associated with their own specific environment based on coastal proximity (e.g. *Brinkhuis*, 1994; *Pross and Brinkhuis*, 2005; *Sluijs et al.*, 2005). The goniodomaceans for example are associated with inner neritic, euryhaline environments (*Brinkhuis*, 1994; *Sluijs et al.*, 2005), whereas most species of the genus *Impagidinium* are linked to oceanic conditions. Two dinocysts indices are commonly used to reconstruct relative sea-level changes, the inner neritic/outer neritic index and the neritic/oceanic index. Because Site U1318 is located on the upper continental slope only the neritic/oceanic index (N/O; *Versteegh*, 1994) was applied: N/O = nN / (nN + nO), 'n' is the number of specimens counted, N the species associated with neritic environments and O the species associated with oceanic conditions. The species used in the N/O index are shown in Table 2.2.

The amount of terrestrial palynomorphs (pollen and spores) in a sample can be indicative of coastal proximity and is expressed as the sporomorph vs. dinocyst ratio (S/D) (*Versteegh*, 1994). The ratio is calculated as follows: S/D = nS / (nD + nS) where n is the number of counted specimens, S is represented by pollen and spores and D by dinocysts and marine acritarchs, whereby an increase in pollen and spores relative to dinocysts is interpreted as a sea level lowering as the site becomes more proximal to the coast. However, also changes in run-off due to precipitation changes can influence this ratio.

2.2.4.4. Diversity

Phytoplankton diversity is generally correlated with latitude, where diversity is lowest towards the poles as a result of lower temperatures (*Barton et al.*, 2010). For dinoflagellates, diversity has also proven to correlate with temperature (*Chen et al.*, 2011). The latter study also mentions availability of macronutrients and water-column stability as possible parameters. A comparable factor to water-column stability is shoreline proximity and concomitant factors as sedimentation rates and grain size (e.g. *Bradford and Wall*, 1984; *Patten*, 1962). There are several methods to express diversity. Richness (S) is the total number of dinocyst species in a sample, including species encountered during the scanning of the slide. A method that is often used to express diversity is the Shannon-Wiener index (H'): $\mathrm{H}' = -\sum_{i=1}^{S}(p_i)(\ln p_i)$ where S is the number of species and p_i the proportion of total sample belonging to the i^{th} species. The Shannon-Wiener index is based on information theory and tries to measure the amount of entropy (disorder) or order within a system (*Krebs*, 1998). An index based on the Shannon-Wiener index is evenness (E_H; E_H = H' / ln(S)). It compares an observed assemblage with a hypothetical community that exists of species that are equally abundant. In general, it expresses

whether an assemblage has a few common species along with some rare species ($E_H = 0$) or whether all species are equally represented within the assemblage ($E_H = 1$).

3. Results

3.1. Palynomorph assemblage

On average, 65% of the palynomorphs are dinocysts, making them the most abundant palynomorphs group (Figure 2.6). Other important palynomorphs are the acritarchs *Leiosphaeridia rockhallensis*, *Cyclopsiella elliptica/granosa*, *Cymatiosphaera* spp., *Nannobarbophora gedlii*, skolochorate acritarchs and to a lesser extent bisaccate pollen. Most of these occur regularly throughout the studied part of the composite record although *Leiosphaeridia rockhallensis* and *Cyclopsiella elliptica/granosa* have a more punctuated occurrence. *Leiosphaeridia rockhallensis* seems to have a relatively stable presence until ~12.73 Ma, where the relative abundance suddenly peaks to ~16% of the total palynomorph assemblage (Figure 2.6). This spike cannot be followed across the hiatus, but abundances remain higher than before 12.73 Ma and increase to over 20% at 12.23 Ma. *Cyclopsiella elliptica/granosa*, a shallow marine to near shore high energetic environment (*Louwye and Laga*, 2008; *Matsuoka and Head*, 1992) and possibly low-salinity tolerant species (*Brinkhuis*, 1994), shows a few peak

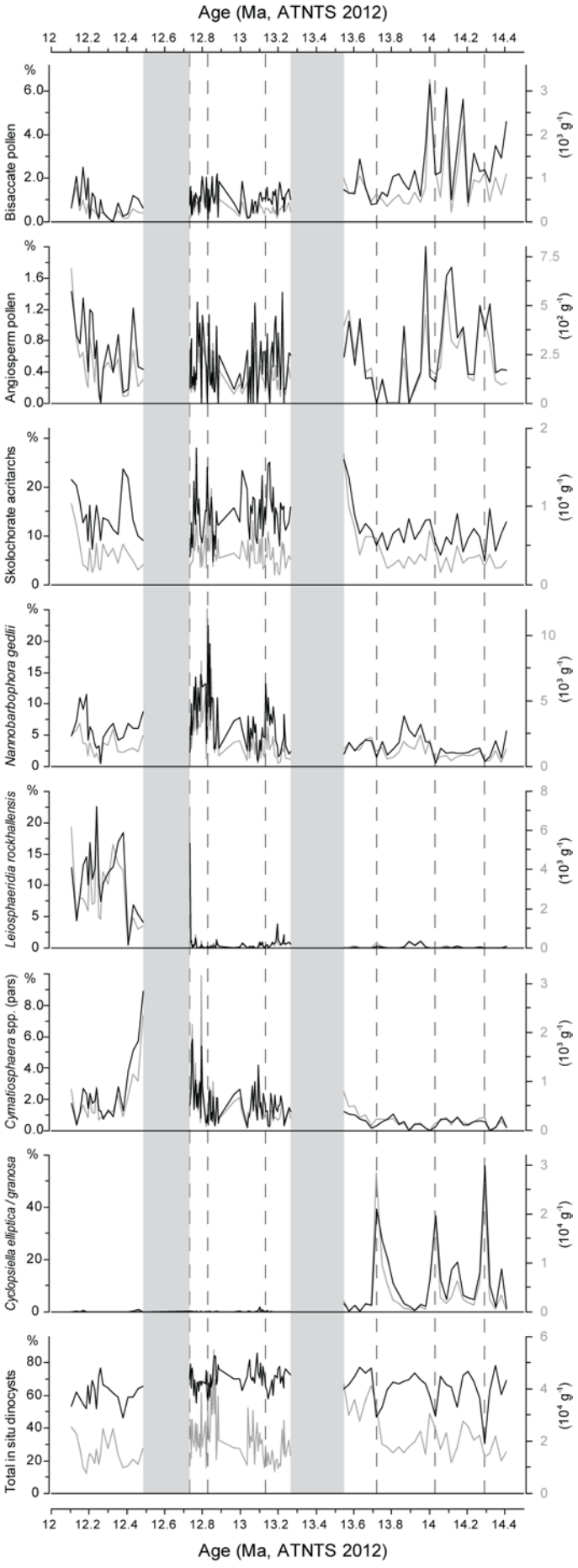

Figure 2.6: Most abundant palynomorphs versus age (Ma). Black solid lines indicate percentages of the total palynomorph assemblage, grey solid lines represent number of specimens per gram dry sediment. Grey area indicates the hiatus in the record, dark grey dashed lines provide tie-points with events mentioned in the text.

abundances in the lower part of the composite (~13.7–13.3 Ma; Figure 2.6). Three sharp peaks can be observed at 14.29, 14.03 and 13.72 Ma where it reaches 56, 37 and 39% respectively. Two minor peaks of ~17% can be observed at 14.38 and 14.15 Ma (Figure 2.6).

3.1.1.Organic-walled dinoflagellate cyst assemblage

Analysis of the Porcupine Basin dinocyst assemblage led to the identification of 134 taxa. Dinocyst preservation is moderate to exceptional. No preservation bias through oxidation is expected since peridinioid dinocysts were present in every sample. Reworking of dinocysts is stable and does not exceed 4% of the dinocyst assemblage including reworked specimens. The *Spiniferites*/*Achomosphaera* complex dominates all assemblages. Other common taxa are *Batiacasphaera hirsuta*, the *Batiacasphaera* complex, *Dapsilidinium pseudocolligerum*, *Habibacysta tectata*, *Labyrinthodinium truncatum*, *Nematosphaeropsis labyrinthus*, *Operculodinium centrocarpum*, *Paucisphaeridium* sp. A and *Paucisphaeridium* sp. B (Supplementary Figure 2.2). In the lower part of the record *Palaeocystodinium golzowense* becomes quite dominant, with a smaller peak with abundances up to 10% of the dinocyst assemblage at 14.29–14.09 Ma, but especially between 13.95 Ma and 13.58 Ma where it reaches up to 22% (Figure 2.8). The *Batiacasphaera* complex is not included in any of the palaeoenvironmental indices but shows some significant peaks: a variable increased abundance pattern from 13.26–12.74 Ma with relative abundances between ~10–20% and an increase at 12.49–12.35 Ma where it reaches abundances up to ~18%. *Batiacasphaera hirsuta* shows an increase to ~8% between 12.88 and 12.74 Ma. During that period *Paucisphaeridium* sp. B shows an increase as well, with relative abundances up to ~19%.

3.1.2.Sea-surface temperature

Relative SST as expressed by the W/C index shows a steadily decreasing trend from 14.38 Ma onwards (Figure 2.7). The index decreases from 0.68 to 0.18 around 13.78 Ma. This decreasing trend is accompanied by peaks in the cold-water species *Impagidinium pallidum* and an increase in abundance of *Lingulodinium machaerophorum*. The warm-water species *Capisocysta lata/lyellii*, *Impagidinium paradoxum*, *Spiniferites hyperacanthus* and *Spiniferites membranaceus/mirabilis* show a decline. Around 14.25 Ma a small decrease in the W/C can be observed, caused by a decrease in *Lingulodinium machaerophorum*, *Melitasphaeridium choanophorum* and *Polysphaeridium zoharyi*. Following this decrease the W/C index shows a small increase and then continues the decreasing trend.

Subsequently the W/C index fluctuatingly starts rising from 13.78 to 13.60 Ma to a value of ca. 0.4. These values persist after the hiatus. The higher values can also be observed by an increase in the warm-water dinocyst species *Capisocysta lata/lyellii*, *Impagidinium aculeatum*, *Impagidinium paradoxum*, *Impagidinium strialatum*, *Invertocysta tabulata* and *Spiniferites membranaceus/mirabilis*, and the acritarch *Nannobarbophora gedlii*. At 12.96 Ma SST decreases towards a minimum of 0.02, concomitant with increase in *Habibacysta tectata* up to ~30% of the dinocyst assemblage. The W/C index subsequently starts rising again until 12.73 Ma; after the hiatus relative SST is lower with a small increase at 12.38 Ma. *Invertocysta lacrymosa, Melitasphaeridium choanophorum, Nannobarbophora gedlii Polysphaeridium zoharyi* and *Tectatodinium pellitum,* all species associated with warmer SST show an increase in abundance as well. A colder interval is recorded around ~12.26 Ma, together with an increase in *Habibacysta tectata* and an increase in the warm-water species *Impagidinium paradoxum*, *Spiniferites membranaceus/mirabilis* and *Spiniferites hyperacanthus* (~10% of the assemblage). At the end of the analysed interval relative SST starts to rise again, as indicated by an increase in *Lingulodinium machaerophorum* and *Melitasphaeridium choanophorum*.

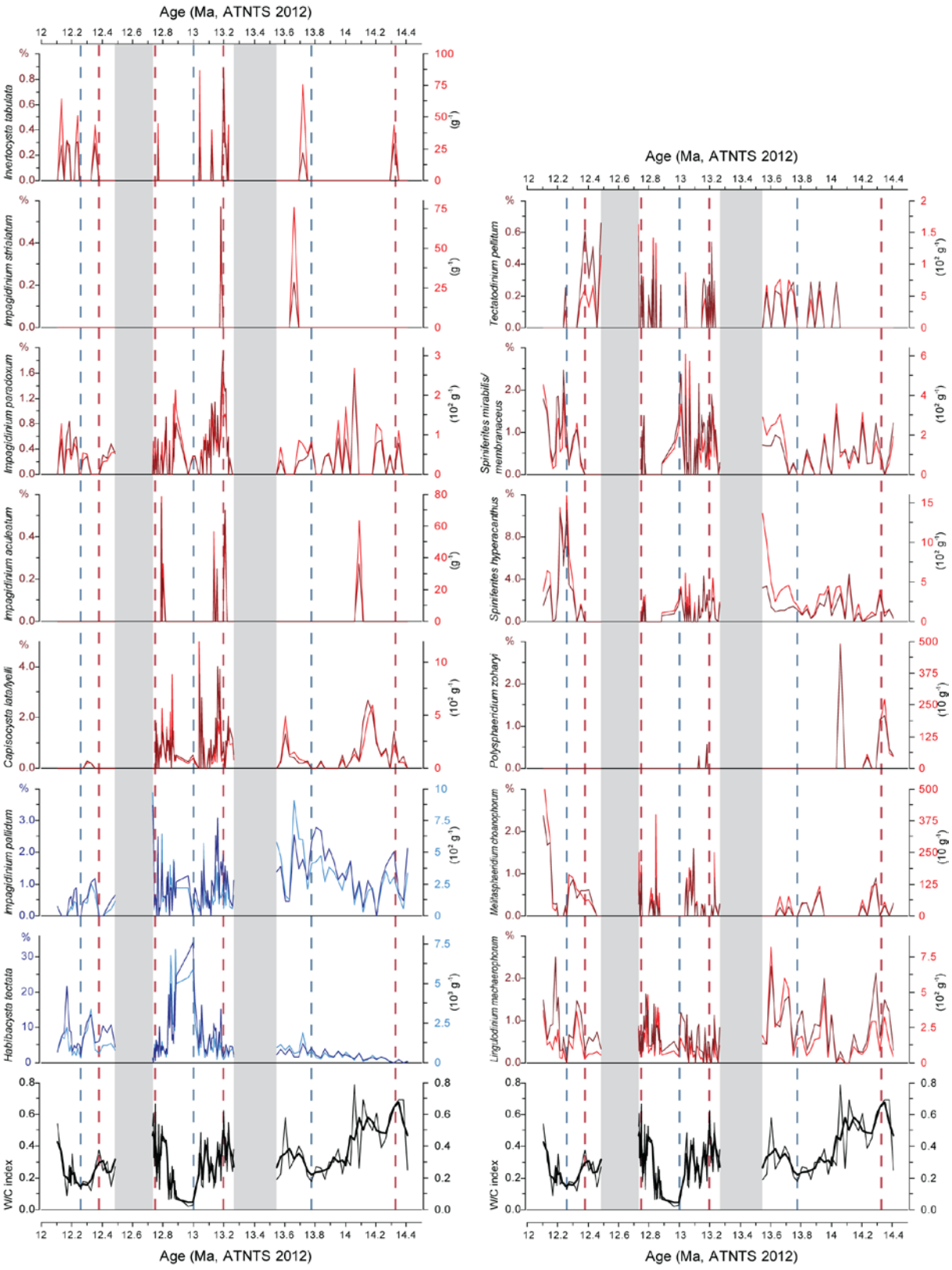

Figure 2.7: W/C-index and most abundant representative species versus age (Ma) with cold species in blue, warm species in red. Thick black line is a 3-point running average of the W/C-index. Darker colours for dinocysts indicate percentages of the total dinocyst assemblage, lighter colours represent the number of specimens per gram dry sediment. Grey area indicates the hiatus in the record, red dashed lines provide tie-points with warm events mentioned in the text, blue dashed lines indicate cold events mentioned in the text.

3.1.3.Sea-surface productivity

The heterotrophic species *Lejeunecysta marieae*, *Selenopemphix brevispinosa*, *Selenopemphix nephroides*, *Sumatradinium hamulatum* and *Sumatradinium soucouyantiae* are present throughout the record (Figure 2.8). The relative SSP, as indicated by the P/G index, is relatively low, except for a number of peaks described below.

A first small increase is recorded at 14.18 Ma. It is coincident with an increase in *Palaeocystodinium golzowense* and *Selenopemphix nephroides*. The next increase is the most noticeable event in the entire dinocyst record: a large increase in productivity from 14.03 to 13.55 Ma. Superimposed on this increase two pronounced peaks can be observed at 13.81 Ma and 13.66 Ma. The peak at 13.81 Ma is concurrent with an increase in the genera *Lejeunecysta* and *Palaeocystodinium*. *Palaeocystodinium* — mainly represented by *Palaeocystodinium golzowense*, *Palaeocystodinium minor* and *Palaeocystodinium miocaenicum* — increases to ~24% of the total dinocyst assemblage. The latter two species are also responsible for the increase at 13.66 Ma. The next small peak in the P/G ratio at 13.13 Ma coincides with an increase in *Palaeocystodinium minor* and *Selenopemphix nephroides*. The last, relatively minor peak can be found at 12.80 Ma. In contrast with the aforementioned peaks it is accompanied by an increase in absolute abundance of dinocysts belonging to the genera *Selenopemphix*,

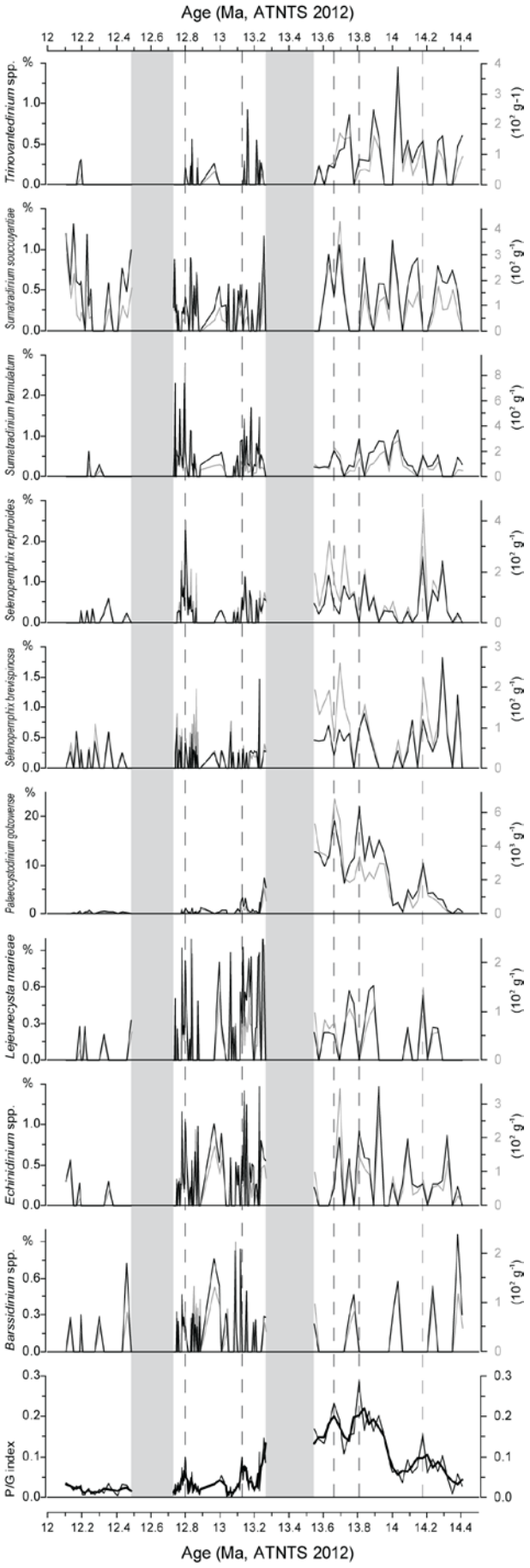

Figure 2.8: P/G-index and most abundant representative species versus age (Ma). Thick black line is a 3-point running average of the P/G-index. Black solid lines indicate percentages of the total dinocyst assemblage, grey solid lines represent number of specimens per gram dry sediment. Grey area indicates the hiatus in the record, dark grey dashed lines provide tie-points with events mentioned in the text.

Sumatradinium and round brown cysts. Especially *Selenopemphix nephroides* and *Selenopemphix quanta* show an increase in abundance. After this peak and across the hiatus relative SSP remains relatively low.

3.1.4.Relative Sea-Level

The N/O index indicates a possibly cyclic pattern that can be interpreted as changes from a more neritic to a more oceanic environment and vice versa (Figure 2.9). A first low in the N/O index is recorded at 14.29 Ma. Especially the genus *Impagidinium* increases, as well as *Lingulodinium machaerophorum*; the *Spiniferites/Achomosphaera* complex*, Cleistosphaeridium placacanthum* and the goniodomacean species, usually associated with inner neritic conditions, decrease. At 14.18 Ma the N/O index reaches a maximum due to an inverse trend in the aforementioned species, to subsequently decrease until 13.84 Ma. *Impagidinium* spp. increases towards this minimum, whereas *Cleistosphaeridium placacanthum, Dapsilidinium pseudocolligerum, Lingulodinium machaerophorum* and *Operculodinium* spp. decrease. The next N/O high occurs at 13.60 Ma, as indicated by an increase in goniodomacean species and *Lingulodinium machaerophorum*. The N/O index thereafter decreases towards 13.14 Ma, interrupted by a smaller peak in the N/O index. The initial N/O low at 13.18 Ma is accompanied by an increase in *Nematosphaeropsis labyrinthus* and *Impagidinium*; *Dapsilidinium pseudocolligerum* decreases. The interval with an increased N/O index coincides with an increase in goniodomacean species and *Tectatodinium pellitum*, to return to lower N/O index values again at 13.14 Ma. *Tectatodinium pellitum* declines and *Nematosphaeropsis labyrinthus* and *Impagidinium* spp. increase. Both taxa decline as the N/O index increases towards 13.04 Ma. Most neritic species show an increase, especially *Cleistosphaeridium placacanthum, Dapsilidinium pseudocolligerum, Operculodinium* spp. and *Spiniferites/Achomosphaera* complex. *Nematosphaeropsis labyrinthus* and *Impagidinium* spp. decrease towards 13.04 Ma, to increase again at the next low in N/O index at 12.88 Ma. There *Dapsilidinium pseudocolligerum, Lingulodinium machaerophorum,* the *Spiniferites/Achomosphaera* complex and the goniodomacean species drop in relative abundance. This pattern reverses at 12.86 Ma, with in addition an increase of *Operculodinium* spp. The next low in N/O index is at 12.79 Ma, contemporaneous with an increase in *Nematosphaeropsis labyrinthus* and *Impagidinium* spp. and a decrease in *Dapsilidinium pseudocolligerum, Operculodinium* spp. and the *Spiniferites/Achomosphaera* complex. The following peak shows a reversed pattern again. After the hiatus the N/O index is relatively high, with a peak in especially the *Spiniferites/Achomosphaera* complex at 12.41 Ma. *Nematosphaeropsis labyrinthus*, *Impagidinium* spp. and *Operculodinium* spp. decrease. At 12.29 Ma the N/O index declines, together with *Operculodinium* spp., the *Spiniferites/Achomosphaera* complex and *Tectatodinium pellitum*. *Cannosphaeropsis passio, Nematosphaeropsis labyrinthus* and *Impagidinium* spp. increase. At the end of the record the N/O index shows a rising trend.

The S/D index follows the general trends of the N/O index. However, because of the very low numbers of the index the ratio between signal and scatter is rather limited. There is one exception to the general trend: the large increase that can be found between 14.20 and 13.98 Ma. This increase consists of three separate peaks at 14.18, 14.09 and 14.00 Ma that are most likely caused by peaks in bisaccate pollen at that time (see Figure 2.6). Before the hiatus three smaller peaks can be found at 13.63, 13.07 and fluctuating values between 12.87 and 12.80 Ma. After the hiatus, from 12.49–12.25 Ma the index fluctuates, to reach maximum values again at 12.17 Ma.

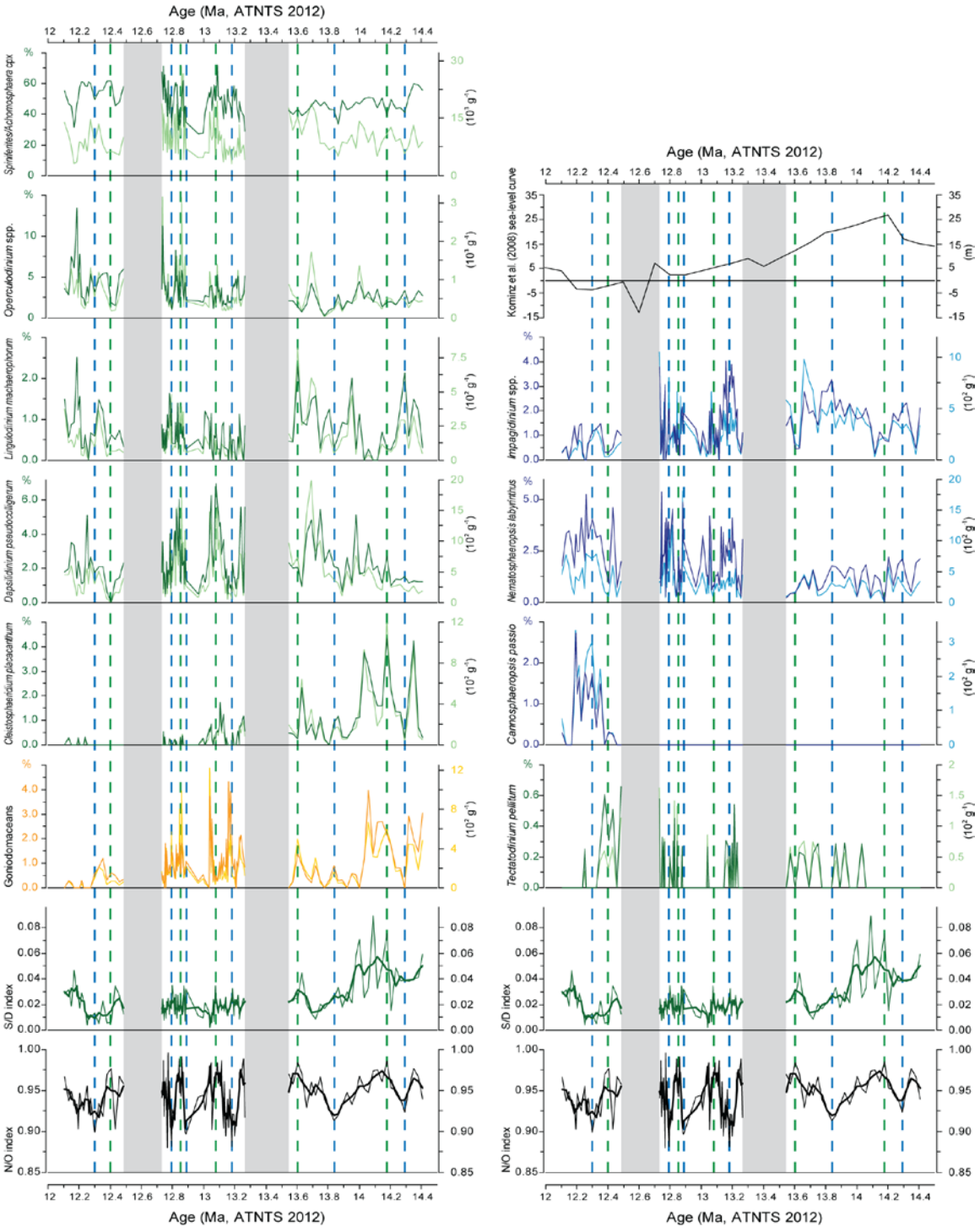

Figure 2.9: N/O-index, S/D-index and most abundant representative species versus age (Ma) with inner neritic species in orange, neritic species in green and outer neritic and oceanic species in blue. Thick line through N/O-index and S/D-index is a 3-point running average. Darker colors for dinocysts indicate percentages of the total dinocyst assemblage, lighter colours represent the number of specimens per gram dry sediment. Grey area indicates the hiatus in the record, green dashed lines provide tie-points with high N/O-index events mentioned in the text, blue dashed lines indicate low N/O-index events mentioned in the text. Kominz sea-level curve (middle estimate with inferred lowstands of sea level) from *Kominz et al.* (2008).

3.1.5.Diversity

Of the three indices used as a measure of diversity, richness shows the most variation (Figure 2.10). The average number of species is ~53, with a minimum of 36 of species at 12.49 Ma and a maximum of 70 species at 13.69 Ma. The latter peak also coincides with a higher number of dinocysts per gram of dry-weight sediment (see Figure 2.6), indicative of favourable conditions for dinocyst production. The Shannon-Wiener index and the evenness are relatively stable between 14.29 and 13.15 Ma. Then both signals decrease towards 13.04 Ma, where the richness has already started to decrease earlier. The Shannon-Wiener index and the evenness indicate a low diverse, unevenly distributed assemblage. All indices subsequently increase again, accompanied by an increase in the number of dinocysts per gram. Just before the hiatus diversity starts to decrease and remains low after. Towards the end of the record diversity starts recovering with a peak at 12.27 Ma, where the richness shows a steeper recovery than the Shannon-Wiener index and the evenness.

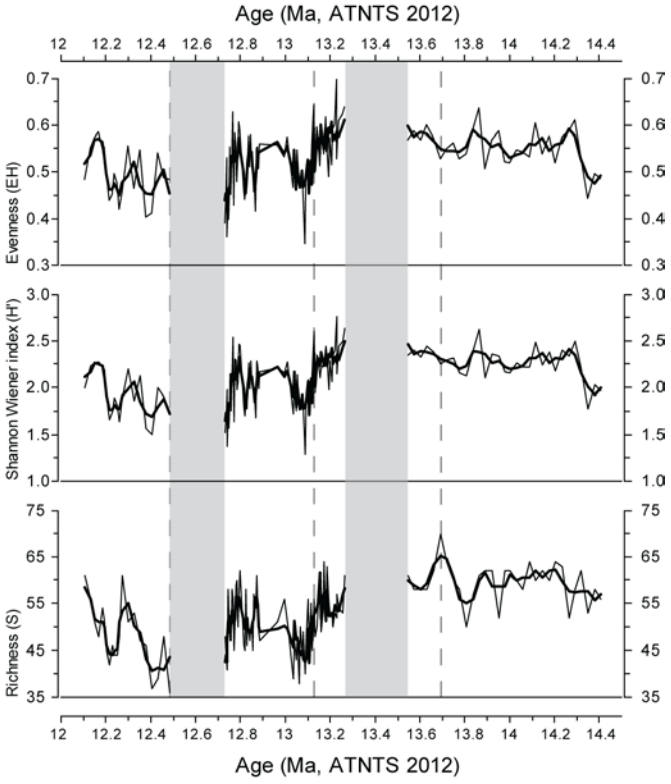

Figure 2.10: Richness, Shannon-Wiener index and evenness versus age (Ma). Thick black line is a 3-point running average of the indices. Grey area indicates the hiatus in the record, dark grey dashed lines provide tie-points with events mentioned in the text.

3.2. Multivariate statistics

Multivariate statistics can be applied to reduce a large dataset into a smaller number of factors that might influence the dataset. One of the most commonly used types of multivariate statistics for closed-sum biological assemblage data is the principal component analysis (PCA). A PCA reduces a dataset into linearly uncorrelated variables: the principal components. Because of the relatively large number of taxa the dataset was reduced manually by grouping most species by genus, except for palaeoecological indicator species. PCA analyses have been performed with Canoco software (*Ter Braak and Šmilauer*, 2002).

The PCA analysis resulted in the first two axes together explaining 72.3% of the variance in the dataset; the first axis explains 53.2%, the second axis explains another 19.1% (Figure 2.11). The third axis, not shown here, explains 10.3% of the variance. In the ordination bi-plot three taxa dominate the ordination: *Palaeocystodinium* spp.*, Habibacysta tectata* and the *Spiniferites/Achomosphaera* cpx, the most dominant species in the record. When zooming in on the centre of the plot a clear separation based on species specific palaeoecological preferences is not evident. Nonetheless, heterotrophic dinocyst species, as well as species indicative of colder environments plot on the right side of the first (x) axis, whereas warm-water species plot on the left side. On the secondary (y) axis most outer neritic or oceanic species plot on the upper part of the graph. This distribution suggests that the first axis represents a combination of sea-surface productivity and -temperature, whereas the second PCA

represents relative sea-level. This can be supported by removing the most important (first) ordination factor and comparing the second and the third axes (Supplementary Figure 2.3).

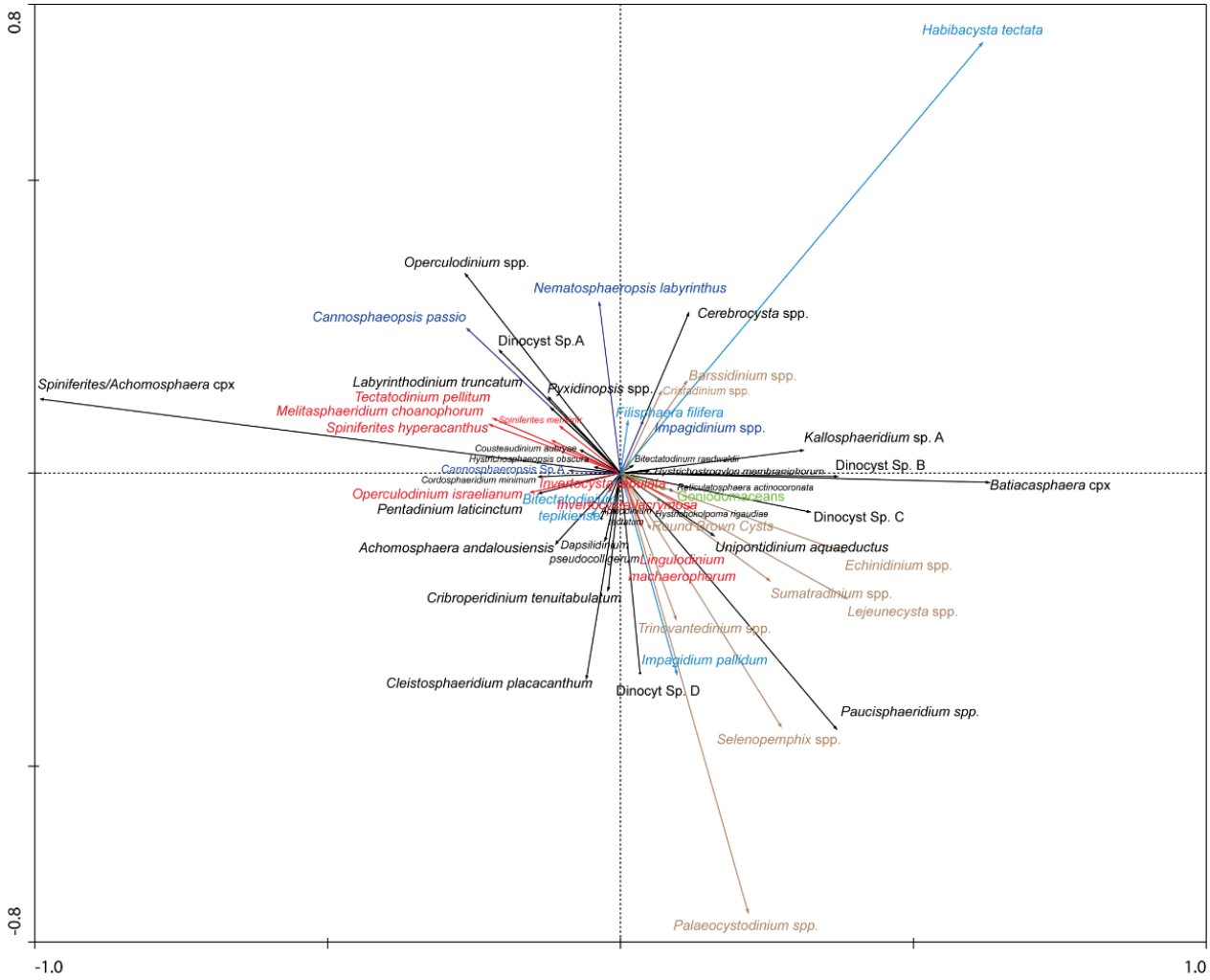

Figure 2.11: PCA bi-plot of the first and second PCA axes. Warm-water species indicated in red, cold-water species indicated in light blue, inner neritic species in green, outer neritic and oceanic species in dark blue, peridinioid species in brown. Variation explained by axis 1 53.2%, variation explained by axis 2 19.1%.

4. Discussion

4.1. Correlation to global events

A small change in all palaeoenvironmental indices can be found between 14.35 and 14.23 Ma (147.54–145.51 mcd). The W/C index decreases with 0.3, the N/O index decreases as well and the P/G index starts increasing. Based on our age model and comparison with the $\delta^{18}O$ record of DSDP Site 608 (*Miller et al.*, 1996) a possible comparable event would be Mi-3a (14.2 Ma; *Abels et al.*, 2005). The magnitude of the events is also fairly low, especially in comparison with the following two events, suggesting that this might indeed be Mi3-a. However, the event is located at the lower end of the record and it might be possible that the full extent is not covered.

The most prominent change in the Porcupine basin record is the drop in the W/C index and the increase in the P/G index from ~14.38 to 13.78 Ma (148.05–137.67 mcd; Figure 2.12). The most plausibly comparable global event would be the Mi-3b event (13.82 Ma; *Abels et al.*, 2005) within the Mi-3 zone of *Miller et al.* (1991) because of comparable timing and magnitude. This Mi-3 zone has its

base within Chronozone C5ABr, at the maximal $\delta^{18}O$ value of IODP Hole 608. However, there is no magnetostratigraphy available for that specific interval since there are no discrete measurements on Hole 1318C, and it is therefore not possible to determine the base of the Mi-3 zone as defined by *Miller et al.* (1991). Notwithstanding, when comparing our record to the $\delta^{18}O$ record of DSDP Site 608 and their definition of the Mi-zones (*Miller et al.*, 1991, 1996) it can be observed that the changes in W/C and P/G indices at the Porcupine Basin record correlate well to their Mi-3 zone (Figure 2.12). Furthermore, according to *Abels et al.* (2005) the Last Common Occurrence (LCO) of *Sphenolithus heteromorphus* is slightly younger than the Mi-3b event. There is still common to rare *Sphenolithus heteromorphus* present until at least 131.81 mcd. Although the exact LCO of *Sphenolithus heteromorphus* is unknown in this record, based on our new age model it is very likely that the shift in W/C index from 148.05–137.67 mcd can be attributed to Mi-3b. The base of the change towards a cooler environment is found at ~14.38 Ma in our record and culminates at 13.78 Ma. The base is older than the age *Abels et al.* (2005) provide for Mi-3b (13.82 Ma), but the culmination is slightly younger, so this suggests that our record well covers the Mi-3 zone and the later defined Mi-3b event.

The next low in W/C index can be found at ~13.05–12.96 Ma (124.92–123.61 mcd), close to the base of C5Ar.2n (Figure 2.12). The location of the Mi-4 zone by *Miller et al.* (1991)

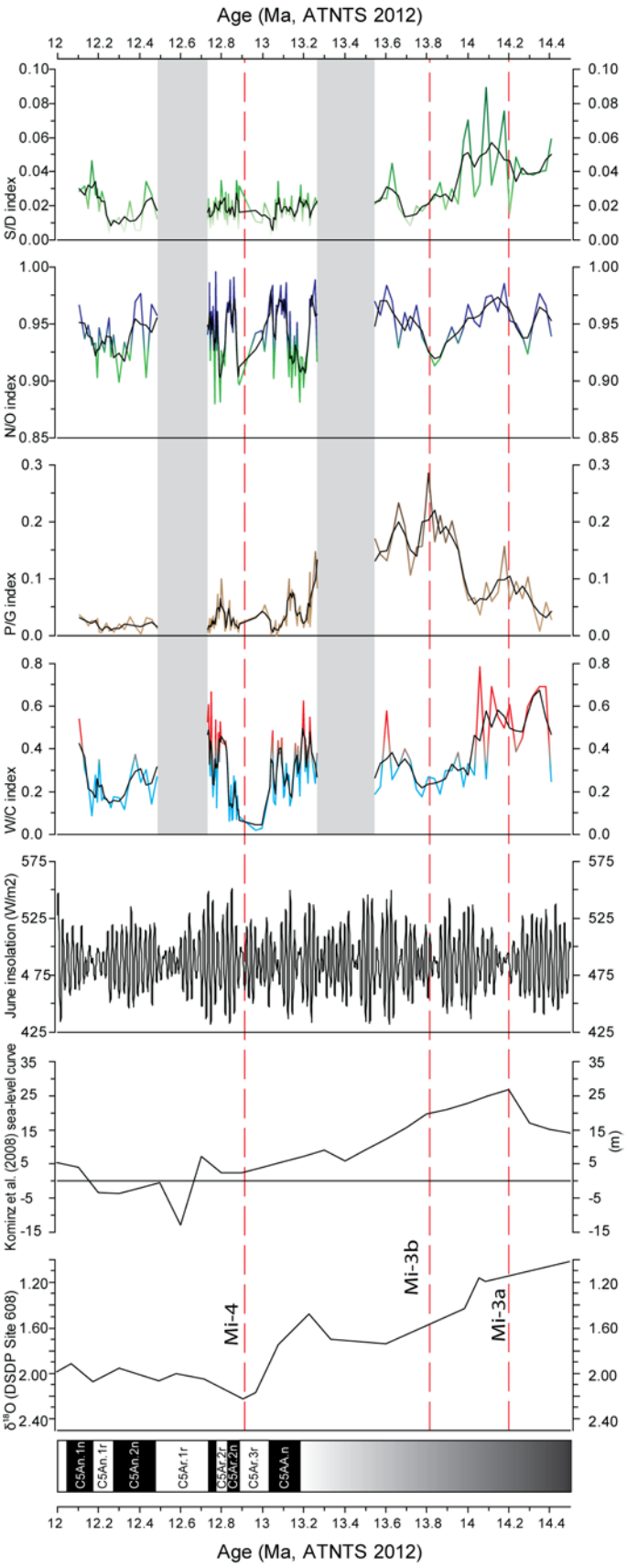

Figure 2.12: Magnetostratigraphy, $\delta^{18}O$ of DSDP Site 608, *Kominz et al.* (2008) sea-level curve, June insolation at the Porcupine Basin and palaeoecological indices versus age (Ma). Isotope data and positioning of the Mi-zones from *Miller et al.* (1991) and *Abels et al.* (2005), insolation data from *Laskar et al.* (2004). Red lines indicate the position of the Mi-zones. Thick black line is a 3-point running average of the indices.

at the base of the undifferentiated magnetosubchron C5Ar, as well as comparison with the $\delta^{18}O$ record of DSDP Site 608 suggests a correlation of the observed cooling in the Porcupine Basin record with the Mi-4 zone. The age of Mi-4 in our record is in discordance with the orbitally tuned age of 13.2 Ma of *Westerhold et al.* (2005). However, this datum falls within Chronozone C5Aar. Therefore we have chosen to retain the definition of Mi-4 by *Miller et al.* (1991).

Nonetheless, it has to be noted that this age model has not been orbitally tuned and that off-sets in timing of the aforementioned events might be possible in comparison to orbitally-tuned studies such as that of *Abels et al.* (2005).

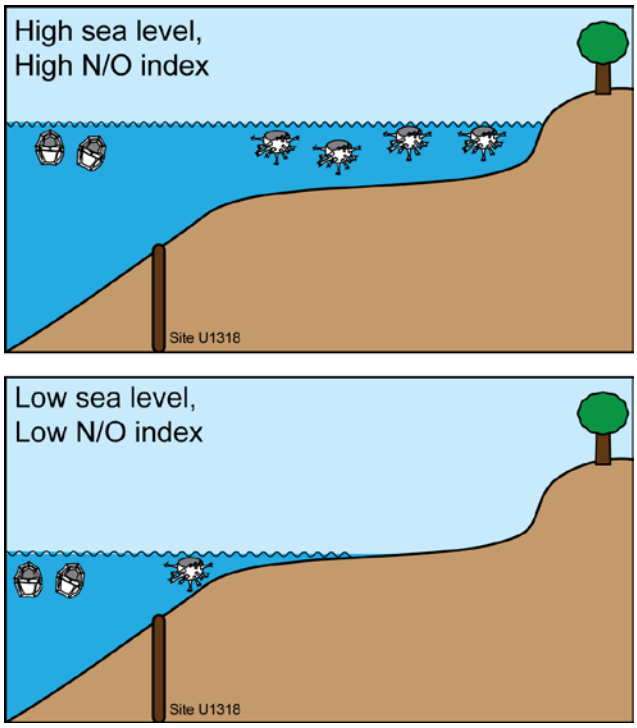

Figure 2.13: A. Illustration of the dinocyst assemblage composition during higher sea-level at the location of Site U1318. B. Figure illustrating the dinocyst assemblage composition during lower sea-level at the location of Site U1318.

4.2. Sea-Level

The S/D index shows a good correlation with the sea-level estimate curve of *Kominz et al.* (2008) (See Figure 2.9). This curve has been derived from backstripping of sediments from the New Jersey and Delaware coastal plain and provides a good comparison across the Atlantic Ocean. The N/O index does not show such a clear correlation since it shows more variance and individual events, and because of the difference in resolution between the N/O index and the curve of *Kominz et al.* (2008). Nonetheless, most of the individual events as shown by the 3-point running average of the N/O index correlate well with changes in the *Kominz et al.* (2008) curve. A low N/O index however — usually associated with high relative sea-level — is here correlated with lower reconstructed sea-levels. A possible explanation for this apparently negative correlation can be found in the location of Site U1318. The N/O index is mostly used in shelf settings where it is assumed that enhanced abundance of oceanic species indicates oceanographical changes related to sea-level rise that bring more oceanic dinocysts onto the shelf. However, since Site U1318 is located on the upper slope the catchment area is more susceptible to transport of dinocysts from the shelf. It can therefore be assumed that the oceanic dinocyst species are in-situ and that the neritic species are mostly transported from the shelf. In case of eustatic sea-level lowering the shelf will become smaller, and less neritic dinocysts will be transported from the shelf, resulting in a lower N/O index and vice versa (see Figure 2.13). The correlation with the reconstructed sea-level curve proves the usefulness of the N/O index in non-shelf studies. A similar reasoning can be applied to the S/D index given the correlation with the *Kominz et al.* (2008) sea-level curve: a high S/D index most likely corresponds to higher relative sea-level.

Furthermore, the N/O index exhibits certain cyclicity. The duration of the cycles is too short (90–580 ka) to link them to any of the cycles of *Hardenbol et al.* (1998), but they are most likely part of the Lan2/Ser1, Ser2 and Ser3 cycles and concomitant onshore sequence KW 3 of *Miller et al.* (1996). The part below the oldest hiatus probably represents Lan2/Ser1, the part between the two hiatuses Ser 2 and the part above the youngest hiatus Ser3. The cyclic behaviour could indicate that the record

is suitable for future time series analysis. Previous research has already proved the use of time series analysis on dinocyst records (e.g. *González et al.*, 2008; *Versteegh*, 1994). A comparison with the calculated June insolation at the latitude of Site U1318 (*Laskar et al.*, 2004) already shows that the coldest intervals as indicated by the W/C index correlate to low insolation intervals (see Figure 2.12). Peaks in the P/G index generally coincide with high insolation intervals, except before and during the *Palaeocystodinium* acme where individual peaks within the acme do or do not correlate. However, if time series analysis is to be applied, the age model will have to be refined with e.g. orbital tuning or additional biostratigraphy, because some cycles might be offset due to the gap in the magnetostratigraphy.

4.3. Regional palaeoenvironment

The Mi-3b event as indicated in the Porcupine Basin record shows a drastic change in the dinocyst assemblage. Relative sea-surface temperature shows a large decrease as the W/C index drops with 0.61, over half of its theoretical range. These decreasing SSTs in combination with sea-level lowering are concurrent with expansion of the cryosphere. As already suggested by *Flower and Kennett* (1994) and *Shevenell et al.* (2008), the East-Antarctic Ice Sheet is a likely candidate, and possibly seasonal expansion of the sea ice and icebergs on the northern hemisphere (*Moran et al.*, 2006). Based on sedimentology (*Expedition 307 Scientists*, 2006) and the dinocyst composition no evidence of sea-ice the Porcupine Basin can be found, as is the case with the Pleistocene sediments that contain frequent ice-rafted dropstones (*Expedition 307 Scientists*, 2006).

The other prominent change in the record is the apparent increase in primary productivity from 14.03 to 13.55 Ma as expressed by the P/G ratio. This increase is mainly characterised by an acme of the genus *Palaeocystodinium*. Comparable acmes and increased abundances were recorded in the North Sea Basin between 15.97 and 13.2 Ma (*Dybkjær and Piasecki*, 2010), in the Langhian of the Iceland Sea (*Schreck et al.*, 2013) and the equatorial Pacific Ocean (*T. Veenstra*, PhD candidate, Utrecht University, personal communication). The genus *Palaeocystodinium* is a peridinioid species and might have a heterotrophic feeding habit and therefore be indicative of enhanced primary productivity. *Sluijs et al.* (2008) have grouped the species together with other low-salinity-tolerant dinocysts in an assessment of Paleogene dinocysts. The increase in *Palaeocystodinium* at the Porcupine Basin might therefore be linked to sea-level lowering and thus a more proximal location to the continental margin. The N/O index during the acme indeed points towards lower relative-sea level, but no increase in terrestrial matter was observed from the S/D index coincident with the *Palaeocystodinium* acme. However, peaks in abundance of the shallow marine and possibly low-salinity tolerant acritarch *Cyclopsiella* and the inner neritic goniodomaceans before and after the acme might indeed point towards lower sea-surface salinity on the transition towards a lower sea-level. A possible cause for the acme might therefore be sea-level lowering and a coincident decrease in SSS.

Another option might be an increase in primary productivity if the species might have had a heterotrophic feeding habit. The lower sea level as indicated by the N/O index and a possible more proximal location might suggest an enhanced supply of nutrients. However, the S/D index shows an increase before and decreased values during the acme. A small supply of organic matter and nutrients could still have been present, but it is more likely that an additional nutrient resource was present. Changes in wind patterns could have caused upwelling that supplied the nutrients for enhanced primary productivity. Expansion of the cryosphere in the northern hemisphere as suggested by *Moran et al.* (2006) might have caused southward movement of the polar front and strengthened the northerlies. Strengthened northerlies might have caused enhanced upwelling, as has already been

observed at the Portuguese continental slope during the latest Quaternary (*Abrantes*, 1991). A lowering in sea-surface salinity in combination with upwelling due to shifted wind patterns thus are possible causes for the acme. Why specifically *Palaeocystodinium* reacts is unknown and other acmes will have to be studied into more detail to unravel the exact cause of this acme.

Mi-3a and Mi-3b are very similar in response. The magnitude of Mi-3a however is smaller and the duration shorter. However, it is uncertain if Mi-3a extends further into the part of Porcupine record that has not been analysed yet and these conclusions have to be approached with caution. The Mi-4 event appears to be a lot shorter than Mi-3b at the Porcupine Basin. Although it shows a drop towards even lower relative SST, the magnitude of the decrease is lower (~0.61 at Mi-3b versus ~0.46 at Mi-4). The relative sea-level lowering indicates that Mi-4 can most likely be associated with an extension of the cryosphere as well. The decrease in sea-surface temperature is also reflected in decreased dinocyst richness. The Shannon-Wiener index and the evenness are low, the latter indicating that a small group of taxa dominates the assemblage. This is most likely due to the smaller size of the shelf, decreasing specific shelf habitats and shelf species abundance. The small SSP peak prior to Mi-4 at 13.13 Ma is caused by the same species as during Mi-3b, but it is very minor compared to the *Palaeocystodinium* acme during Mi-3b. This indicates that there is less transport of nutrients and/or *Palaeocystodinium* dinocysts from the shelf and a smaller decrease in relative sea-level and concomitant lowering of the SSS in comparison to Mi-3b. Another possibility is that a strengthening of the northerlies and concomitant upwelling, as is a possibility during Mi-3b, does not occur. Hence, only a low-amplitude sea-level lowering and concomitant lowering of sea-surface salinity can be related to the minor increase in productivity.

Additional differences between Mi-3b and Mi-4, apart from the variation in magnitude, can be observed. While the decrease in W/C index around Mi-3b is caused by *Impagidinium pallidum, Habibacysta tectata* is responsible for the decrease across Mi-4. There is no large peak of *Palaeocystodinium* spp. and no increase in pollen and the S/D index at Mi-4 either. Moreover, the neritic species that occur during Mi-4 are different: *Cleistosphaeridium placacanthum* peaks during Mi-3b, while *Dapsilidinium pseudocolligerum* is more common across Mi-4. This indicates that different conditions must have prevailed during these Mi-events. According to *Pross and Brinkhuis* (2005) *Cleistosphaeridium placacanthum* has a more distal ecological preference than *Dapsilidinium pseudocolligerum*, and equally *Habibacysta tectata* has a neritic preference (*Head et al.*, 2004) in contrast with the more oceanic preference of *Impagidinium pallidum*. The occurrence of species associated with more neritic environments during Mi-4 indicates that the decrease in relative sea-level was smaller than at Mi-3b. This observation points to a less strong expansion of the cryosphere during Mi-4 compared to Mi-3b. Overall, Mi-4 does not have the large impact on the Porcupine Basin that Mi-3b had.

The difference in magnitude can also be observed in the global isotope stack of *Zachos et al.* (2008) where Mi-3 is clearly present whereas Mi-4 is not of large significance. A possible explanation is that these events have had different forcing mechanisms. *Westerhold et al.* (2005) have performed time-series analysis on their oxygen isotope record from the South-eastern Atlantic Ocean and found that Mi-events 3–7 correspond to minima in obliquity amplitude modification and eccentricity, except for the Mi-4 event. However, they do not address alternative causes for the Mi-4.

Although the number of pollen in the record is very small, the changes concomitant with the marine record as described above show that the Porcupine Basin record does pick up some changes in the terrestrial realm. This can also be observed in the palaeoenvironmental indices: the W/C index and the S/D correlate show similar trends (Figure 2.12) and a clear lead or lag in either of the records cannot

be observed. Nonetheless, the offshore location of Site U1318 probably biases the terrestrial record. The peaks in angiosperm and bisaccate pollen and the S/D index from ca. 14.2–14 Ma, just before the *Palaeocystodinium* acme, are most noteworthy. A possible explanation could be increased precipitation and enhanced runoff. Similar periods with increased precipitation before Mi-3 have been observed in northern Europe by *Larsson et al.* (2011) and *Utescher et al.* (2012). Whether this increase in precipitation is a single peak or a longer period with higher precipitation will have to be elucidated by analysis of sediments from the Porcupine Basin underneath the samples from this study. For future detailed studies connecting the terrestrial and marine realms a shelf location would be more suited.

4.4. Dinocyst palaeoecology

Of the most common dinocysts in the assemblage five taxa have not been associated with a particular environmental preference: *Batiacasphaera hirsuta, Batiacasphaera* cpx, *Labyrinthodinium truncatum, Paucisphaeridium* sp. A and *Paucisphaeridium* sp. B.

Based on sediments from Baffin Bay and the Iceland Sea as well as additional data from other study sites *Schreck and Matthiessen* (2013) suggest that the species *Batiacasphaera micropapillata* and *Batiacasphaera minuta* may be associated with outer neritic to oceanic conditions, with a broad range of temperatures and possibly a preference with increased nutrient availability. Furthermore, these taxa co-occur with the outer neritic to oceanic species *Impagidinium* spp. *and Nematosphaeropsis* spp. However, such a co-occurrence cannot be observed at the Porcupine Basin. Neither can it be concluded that, based on our data, these species have a clear outer-neritic to oceanic preference. When comparing the abundances of *Batiacasphaera hirsuta* and the *Batiacasphaera* cpx with the palaeoenvironmental indices it can be observed that increased abundances of these taxa, especially *Batiacasphaera hirsuta,* can be correlated with peaks in the N/O index. On the PCA (Figure 2.7) *Batiacasphaera* spp. plots on the lower side of the second axis, but the angle is less steep than the angle of the inner neritic goniodomaceans. In a species specific PCA (data not shown) it can be observed that *Batiacasphaera hirsuta* has a negative loading on the second axis, whereas the *Batiacasphaera* cpx is positive. From the comparison with the N/O index and the PCA it is suggested that both species have a neritic preference, but *Batiacasphaera hirsuta* has a preference for more proximal neritic conditions than the *Batiacasphaera* cpx. The preference for nutrient enriched conditions as suggested by *Schreck and Matthiessen* (2013) is supported by PCA analysis, since the taxa have a positive loading on the first gradient.

The Miocene dinocyst *Labyrinthodinium truncatum* has a less clear association when comparing its abundance with the palaeoenvironmental indices. Peaks in abundance correlate with peaks in the W/C index, as well as with certain peaks in the N/O index. However, when observing the PCA, *Labyrinthodinium truncatum* plots together with some warm species along the second axis. This suggests that the species probably had a preference for warmer, neritic conditions, but the temperature preference will have to be confirmed by independent temperature reconstructions.

The two *Paucisphaeridium* taxa also have an ambiguous correlation: peaks correlate to lows in the N/O index, as well as peaks in the P/G ratio. On the PCA the species plot in the same direction of the goniodomaceans, but with a bigger loading, and they also plot next to some peridinioid species. Based on the association with a more proximal location of the shore as indicated by the lower N/O and the correlation with peridinioid species these two *Paucisphaeridium* species possibly prefer proximal environments with a higher nutrient load.

5. Conclusion

Based on this high-resolution study the hypothesis of *Louwye et al.* (2008), that the environmental change they observed is correlated to the Mi-events, can be confirmed. In our high-resolution record Mi-3a, Mi-3b and Mi-4 have been identified; these events can be associated with cooling of sea surface waters and a possible drop in relative sea-level. Mi-3b has a larger impact than Mi-3a and Mi-4, and during Mi-3b an acme of the peridinioid, low-salinity tolerant dinocyst *Palaeocystodinium golzowense* is recorded. This indicates that the relative sea-level decreased drastically. An additional input of nutrients could have been caused by upwelling, due to possible strengthening of the northerlies. Mi-4 is of a less severe nature. No *Palaeocystodinium* acme and intensified upwelling have been observed at this level. After improvement of the age model, time series analysis could be performed to analyse further differences between the Mi-3b and Mi-4 events.

Furthermore the potential environmental preferences of 5 dinocyst taxa have been deduced, based on correlation to the different dinocyst indices, as well as PCA analysis. *Batiacasphaera hirsuta* and the *Batiacasphaera* cpx have preference for neritic environments with increased nutrient loading, although *Batiacasphaera hirsuta* appears to be more inner neritic than the *Batiacasphaera* cpx. *Labyrinthodinium truncatum* prefers warm, neritic conditions, but the temperature range will have to be confirmed by independent temperature reconstructions. Last, *Paucisphaeridium* sp. A and sp. B occur most in proximal environments with a higher nutrient load.

6. Author contributions

SL and THD designed the research project. DP analysed samples for calcareous nannoplankton. WQ did all the palynological processing, counting and analyses, the interpretation of the data, writing of the paper and the preparation of the figures.

7. Acknowledgements

We would like to thank Sabine Van Cauwenberghe for technical assistance. Alex Wülbers and Walter Hale are acknowledged for their help during sampling at the Bremen Core Repository. Christian Zeeden and Hemmo Abels are kindly thanked for the useful discussions on the timing of the Mi-events and the age model. David van Rooij is acknowledged for his help regarding sedimentological issues. This research was funded by the Research Foundation – Flanders (FWO).

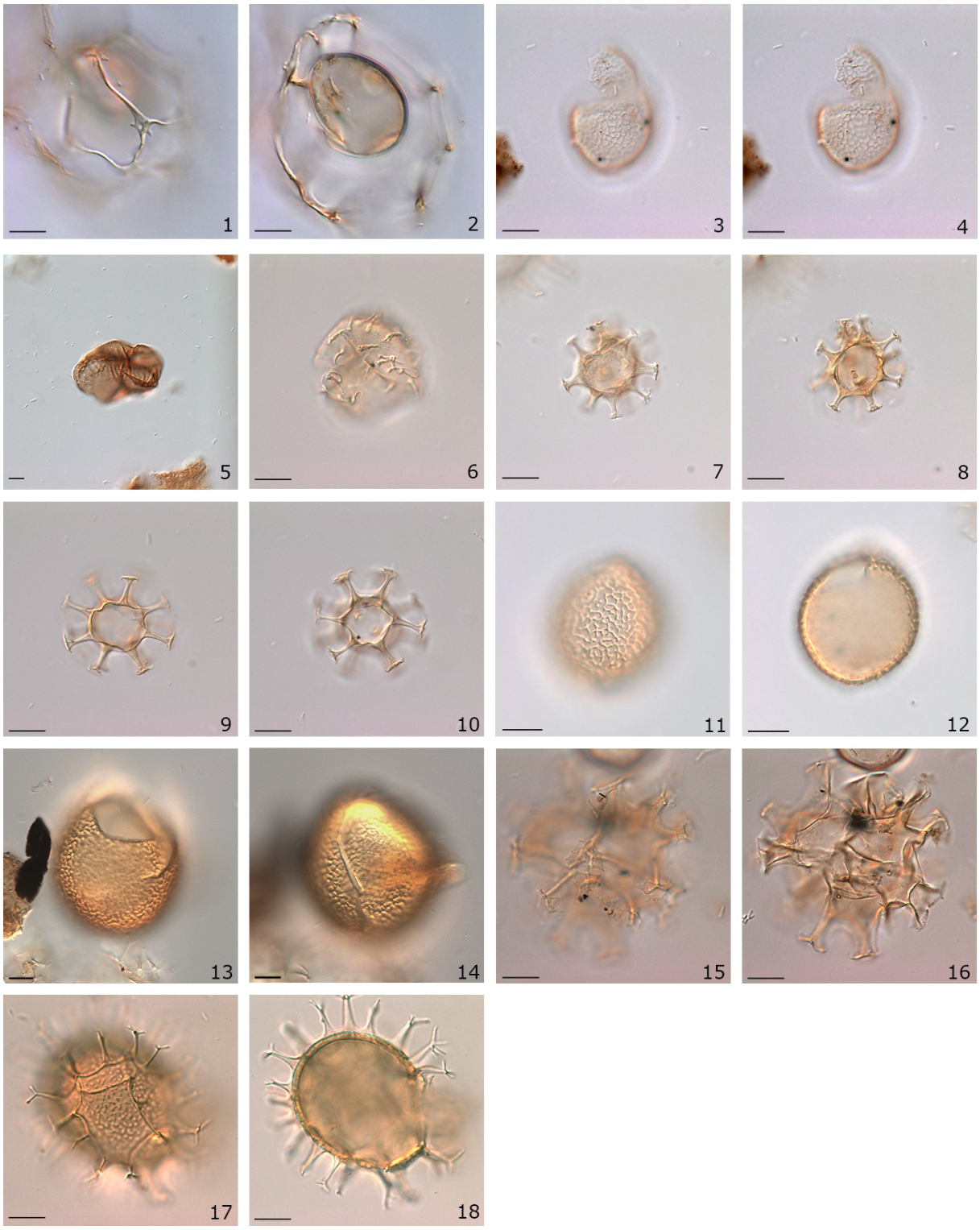

Plate 2.3: Photomicrographs of selected dinoflagellate cyst species. All images taken with interference contrast. Magnification: 1000x unless mentioned. EF: England Finder coordinates. Scale bar: 10 µm. 1–2. *Cannosphaeropsis*? sp. A. Sample 307/1318B/13H1/30–32 cm/506/1, EF: R42-2. 1 high focus on trabeculae tips. 2 mid-focus. 3–4. *Kallosphaeridium* sp. of Head and Westphael (1999). Sample 307/1318B/19X8/30–32 cm/628/1, EF: W30-2. High focus on wall ornamentation. 4 High to mid-focus on the operculum. 5. *Lejeunecysta* cf. *challengerensis*. Sample 307/1318B/12H1/30–32 cm/462/1, EF: V26-2. Magnification 400x. 5 mid-focus on striae. 6. *Operculodinium* sp. 3 of De Verteuil and Norris (1996). Sample 307/1318B/11H4/103–105 cm/454/1, EF: W22. 6 high focus on wall ornamentation and processes. 7–8. *Paucisphaeridium* sp. A. Sample 307/1318B/17X8/13–15 cm/593/1, EF: V28-1. 7 high focus on fibrous processes. 8 mid-focus. 9–10. *Paucisphaeridium* sp. B. Sample 307/1318B/20X1/143-145 cm/630/1, EF E39-1. 9 Mid-focus. 1- high focus on processes. 10 slightly lower focus on smooth processes. 11–12. *Pyxidinopsis* sp. A. Sample 307/1318C/8X4/14–16 cm/673/1, EF: T34-3. 11 high focus on ornamentation. 12 mid-focus. 13–14. *Pyxidinopsis* sp. B. Sample 307/1318C/9X4/80-82 cm/694/1, EF: W27-2. 13 high focus on archaeopyle. 14 low focus. 15–16. *Spiniferites* sp. A. Sample 307/1318B/12H3/133–135 cm/472/1, EF: T40-2. 15 High focus on process tips. 16 high to mid-focus. 17–18. *Spiniferites* sp. C. Sample 307/1318B/11H3/51–53 cm/450/1, EF: Y21-4. 17 high focus on wall ornamentation. 18 mid-focus.

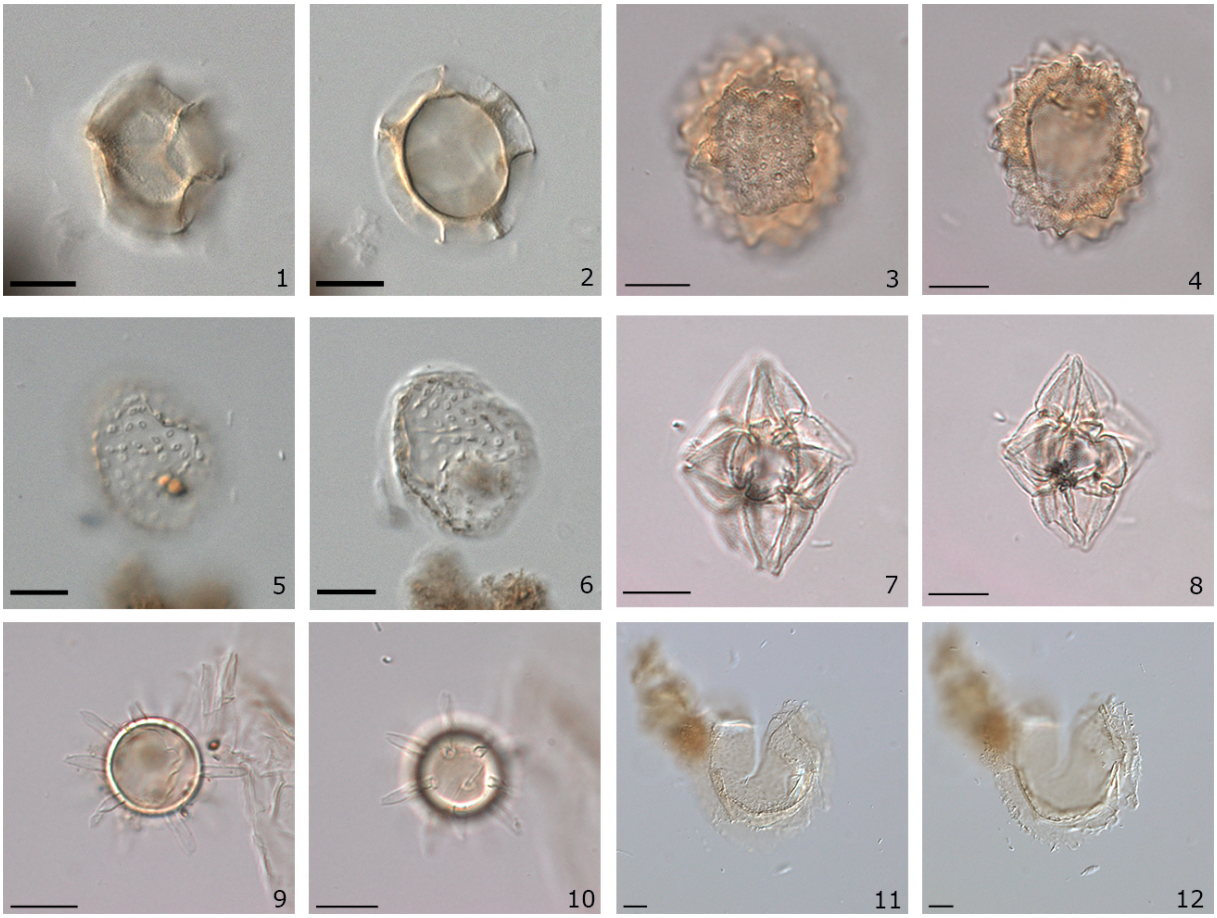

Plate 2.4: Photomicrographs of selected acritarch species. All images taken with interference contrast. Magnification: 1000x unless mentioned. EF: England Finder coordinates. Scale bar: 10 µm. 1–2. Acritarch sp. A. Sample 307/1318B/11H4/3–4 cm/452/1. 1 high focus. 2 mid-focus. 3–4. Acritarch sp. B. Sample 307/1318C/8X6/114–1164 cm/681/1, EF: Y37. 3 High focus. 4 mid-focus. 5–6. Acritarch sp. C. Sample 307/1318B/12H1/133–135 cm/465/1. 5 high focus on ornamentation. 6 low focus. 7–8. Acritarch sp. D. Sample 307/1318C/7H4/70–72 cm/654/1, EF: X28-4. 7 high to mid-focus. 8 mid to low-focus. 9–10. Acritarch sp. E. Sample 307/1318C/8X3/115–117 cm/672/1, EF: V43. 9 mid-focus. 10 high to mid-focus on process base. 11–12. Acritarch sp. G. Sample 307/1318C/8X1/60–62 cm/662/1, EF Q35-4. Magnification 400x. 11 high focus. 12 Mid-focus.

8. References

Abels, H.A., Hilgen, F.J., Krijgsman, W., Kruk, R.W., Raffi, I., Turco, E., Zachariasse, W.J., 2005. Long-period orbital control on middle Miocene global cooling: Integrated stratigraphy and astronomical tuning of the Blue Clay Formation on Malta. Paleoceanography 20, PA4012.

Abrantes, F., 1991. Increased upwelling off Portugal during the last glaciation: Diatom evidence. Marine Micropaleontology 17, 285–310.

Badger, M.P.S., Lear, C.H., Pancost, R.D., Foster, G.L., Bailey, T.R., Leng, M.J., Abels, H.A., 2013. CO_2 drawdown following the middle Miocene expansion of the Antarctic Ice Sheet. Paleoceanography 28, 42–53.

Barton, A.D., Dutkiewicz, S., Flierl, G., Bragg, J., Follows, M.J., 2010. Patterns of Diversity in Marine Phytoplankton. Science 327, 1509 LP-1511.

Bown, P.R. (Ed.), 1998. Calcareous Nannofossil Biostratigraphy. British Micropalaeontological Society Publication Series. Kluwer Academic Publishers, London.

Bradford, M.R., Wall, D.A., 1984. The distribution of Recent organic-walled dinoflagellate cysts in the Persian Gulf, Gulf of Oman, and northwestern Arabian Sea. Palaeontographica Abteilung B 192, 16–84.

Brinkhuis, H., 1994. Late Eocene to Early Oligocene dinoflagellate cysts from the Priabonian type-area (Northeast Italy): biostratigraphy and paleoenvironmental interpretation. Palaeogeography, Palaeoclimatology, Palaeoecology 107, 121–163.

Chen, B., Irwin, A.J., Finkel, Z. V., 2011. Biogeographic distribution of diversity and sizestructure of organic-walled dinoflagellate cysts. Marine Ecology Progress Series 425, 35–45.

Coxall, H.K., Wilson, P. a, Pälike, H., Lear, C.H., Backman, J., 2005. Rapid stepwise onset of Antarctic glaciation and deeper calcite compensation in the Pacific Ocean. Nature 433, 53–57.

Dale, B., 1976. Cyst formation, sedimentation, and preservation: Factors affecting dinoflagellate assemblages in recent sediments from trondheimsfjord, Norway. Review of Palaeobotany and Palynology 22, 39–60.

Dale, B., 1992. Dinoflagellate Contributions to the Open Ocean Sediment Flux, in: Honjo, S. (Ed.), Dinoflagellate Contributions to the Deep Sea. Ocean Biocoenosis Series No. 5. Woods Hole Oceanographic Institution, Woods Hole, pp. 1–32.

Dale, B., 1996. Chapter 31. Dinoflagellate cyst ecology: modelling and geological applications, in: Jansonius, J., McGregor, D.C. (Eds.), Palynology: Principles and Applications. Dallas, Texas, pp. 1249–1276.

De Mol, B., Van Rensbergen, P., Pillen, S., Van Herreweghe, K., Van Rooij, D., McDonnell, A., Huvenne, V., Ivanov, M., Swennen, R., Henriet, J.P., 2002. Large deep-water coral banks in the Porcupine Basin, southwest of Ireland. Marine Geology 188, 193–231.

De Schepper, S., 2006. Plio-Pleistocene dinoflagellate cyst biostratigraphy and palaeoecology of the eastern North Atlantic and southern North Sea Basin. University of Cambridge.

De Schepper, S., Fischer, E.I., Groeneveld, J., Head, M.J., Matthiessen, J., 2011. Deciphering the palaeoecology of Late Pliocene and Early Pleistocene dinoflagellate cysts. Palaeogeography, Palaeoclimatology, Palaeoecology 309, 17–32.

De Cock, K., 2005. 3D-seismiche studie van koralbaanken aan de oostelijke rand van het Porcupine bekken, unpublished M.Sc. thesis, Ghent University, Belgium.

DeConto, R.M., Pollard, D., 2003. Rapid Cenozoic glaciation of Antarctica induced by declining atmospheric CO2. Nature 421, 245–249.

Donders, T.H., Weijers, J.W.H., Munsterman, D.K., Kloosterboer-van Hoeve, M.L., Buckles, L.K., Pancost, R.D., Schouten, S., Sinninghe Damst??, J.S., Brinkhuis, H., 2009. Strong climate coupling of terrestrial and marine environments in the Miocene of northwest Europe. Earth and Planetary Science Letters 281, 215–225.

Dybkjær, K., Piasecki, S., 2010. Neogene dinocyst zonation for the eastern North Sea Basin, Denmark. Review of Palaeobotany and Palynology 161, 1–29.

Eronen, J.T., Fortelius, M., Micheels, A., Portmann, F.T., Puolamäki, K., Janis, C.M., 2012. Neogene aridification of the northern hemisphere. Geology 40, 823–826.

Evitt, W.R., 1985. Sporopollenin Dinoflagellate Cysts. Their Morphology and Interpretation. American Association of Stratigraphic Palynologists Foundation, Dallas, Texas.

Expedition 307 Scientists, 2006. Site U1318, in: Ferdelman, T.G., Kano, A., Williams, T., Henriet, J.-P., the Expedition 307 Scientists (Eds.), Proceedings of the Integrated Ocean Drilling Program. Integrated Ocean Drilling Program Management International, Washington, D.C., pp. 1–57.

Fensome, R.A., MacRae, R.A., Williams, G.L., 2008. DINOFLAJ2, Version 1 [WWW Document]. American Association of Stratigraphic Palynologists, Data Series no. 1.

Flower, B.P., Kennett, J.P., 1994. The middle Miocene climatic transition: East Antarctic ice sheet development, deep ocean circulation and global carbon cycling. Palaeogeography, Palaeoclimatology, Palaeoecology 108, 537–555.

Foubert, A., Beck, T., Wheeler, A.J., Opderbecke, J., Grehan, A., Klages, M., Thiede, J., Henriet, J.-P., the Polarstern ARK-XIX/3a Shipboard party, 2005. New view of the Belgica Mounds, Porcupine Seabight, NE Atlantic: preliminary results from the Polarstern ARK-XIX/3a ROV cruise, in: Freiwald, A., Roberts, J.M. (Eds.), Cold-Water Corals and Ecosystems. Springer Verlag, Berlin, Heidelberg, pp. 403–415.

Foubert, A., Huvenne, V.A.I., Wheeler, A., Kozachenko, M., Opderbecke, J., Henriet, J.-P., 2011, The Moira Mounds, small cold-water coral mounds in the Porcupine Seabight, NE Atlantic: Part B—Evaluating the impact of sediment dynamics through high-resolution ROV-borne bathymetric mapping. Marine Geology 282, 65–78.

González, C., Dupont, L.M., Mertens, K., Wefer, G., 2008. Reconstructing marine productivity of the Cariaco Basin during marine isotope stages 3 and 4 using organic-walled dinoflagellate cysts. Paleoceanography 23, PA3215.

Hardenbol, J., Thierry, J., Farley, M.B., Jacquin, T., De Graciansky, P.C., Vail, P.R., 1998. Cenozoic sequence biochronostratigraphy, in: Mesozoic and Cenozoic Sequence Stratigraphy of European Basins SEPM Special Publication No. 60. Society for Sedimentary Geology, Tulsa, Oklahoma.

Harland, R., 1973. Dinoflagellate cysts and acritarchs from the Bearpaw Formation (upper Campanian) of southern Alberta, Canada. Palaeontology 16, 665–706.

Haywood, A.M., Smellie, J.L., Ashworth, A.C., Cantrill, D.J., Florindo, F., Hambrey, M.J., Hill, D., Hillenbrand, C.D., Hunter, S.J., Larter, R.D., Lear, C.H., Passchier, S., van de Wal, R., 2009. Middle Miocene to Pliocene History of Antarctica and the Southern Ocean, in: Florindo, F., Siegert, M. (Eds.), Developments in Earth and Environmental Sciences. Elsevier, pp. 401–463.

Head, M.J., Riding, J.B., Eidvin, T., Chadwick, R.A., 2004. Palynological and foraminiferal biostratigraphy of (Upper Pliocene) Nordland Group mudstones at Sleipner, northern North Sea. Marine and Petroleum Geology 21, 277–297.

Hilgen, F.J., Lourens, L.J., Van Dam, J.A., Beu, A.G., Boyes, A.F., Cooper, R.A., Krijgsman, W., Ogg, J.G., Piller, W.E., Wilson, D.S., 2012. Chapter 29 - The Neogene Period, in: Gradstein, F.M., Schmitz, J.G.O.D., Ogg, G.M. (Eds.), The Geologic Time Scale. Elsevier, Boston, pp. 923–978.

Huvenne, V.A.I., Croker, P.F., Henriet, J.-P., 2002. A refreshing 3D view of an ancient sediment collapse and slope failure. Terra Nova 14, 33–40.

Huvenne, V.A.I., Bailey, W.R., Shannon, P.M., Naeth, J., di Primio, R., Henriet, J.-P., Horsfield, B., de Haas, H., Wheeler, A., Olu-Le Roi, K., 2007. The Magellan mound province in the Porcupine Basin. International Journal of Earth Sciences 96,

85–101.
Kano, A., Ferdelman, T.G., Williams, T., Henriet, J.P., Ishikawa, T., Kawagoe, N., Takashima, C., Kakizaki, Y., Abe, K., Sakai, S., Browing, E.L., Li, X., Andres, M.S., Bjerager, M., Cragg, B.A., De Mol, B., Dorschel, B., Foubert, A., Frank, T.D., Fuwa, Y., Gaillot, P., Gharib, J.J., Gregg, J.M., Huvenne, V.A.I., Léonide, P., Mangelsdorf, K., Monteys, X., Novosel, I., O'Donnell, R., Rüggeberg, A., Samarkin, V., Sasaki, K., Spivack, A.J., Tanaka, A., Titschack, J., van Rooij, D., Wheeler, A., 2007. Age constraints on the origin and growth history of a deep-water coral mound in the northeast Atlantic drilled during Integrated Ocean Drilling Program Expedition 307. Geology 35, 1051–1054.
Kominz, M.A., Browning, J. V., Miller, K.G., Sugarman, P.J., Mizintseva, S., Scotese, C.R., 2008. Late Cretaceous to Miocene sea-level estimates from the New Jersey and Delaware coastal plain coreholes: An error analysis. Basin Research 20, 211–226.
Krebs, C.J., 1998. Ecological Methodology. Benjamin/Cummings, Menlo Park, California.
Kürschner, W.M., Kvacek, Z., Dilcher, D.L., 2008. The impact of Miocene atmospheric carbon dioxide fluctuations on climate and the evolution of terrestrial ecosystems. Proceedings of the National Academy of Sciences of the United States of America 105, 449–53.
Larsson, L.M., Dybkjær, K., Rasmussen, E.S., Piasecki, S., Utescher, T., Vajda, V., 2011. Miocene climate evolution of northern Europe: A palynological investigation from Denmark. Palaeogeography, Palaeoclimatology, Palaeoecology 309, 161–175.
Laskar, J., Robutel, P., Joutel, F., Gastineau, M., Correia, a. C.M., Levrard, B., 2004. A long-term numerical solution for the insolation quantities of the Earth . Astronomy and Astrophysics 428, 261–285.
Le Danois, E., 1948. Les profundeurs de la mer. Payot, Paris.
Lewis, A.R., Marchant, D.R., Ashworth, A.C., Hemming, S.R., Machlus, M.L., 2007. Major middle Miocene global climate change: Evidence from East Antarctica and the Transantarctic Mountains. Geological Society of America Bulletin 119, 1449–1461.
Louwye, S., Foubert, A., Mertens, K., Van Rooij, D., The IODP Expedition 307 Scientific Party, 2008. Integrated stratigraphy and palaeoecology of the Lower and Middle Miocene of the Porcupine Basin. Geological Magazine 145, 321–344.
Louwye, S., Laga, P., 2008. Dinoflagellate cyst stratigraphy and palaeoenvironment of the marginal marine Middle and Upper Miocene of the eastern Campine area, northern Belgium (southern North Sea Basin). Geological Journal 43, 75–94.
Marret, F., Zonneveld, K.A.F., 2003. Atlas of modern organic-walled dinoflagellate cyst distribution. Review of Palaeobotany and Palynology 125, 1–200.
Matsuoka, K., Head, M.J., 1992. Taxonomic revisions of the Neogene palynomorphs *Cyclopsiella granosa* (Matsuoka) and *Batiacasphaera minuta* (Matsuoka), and a new species of *Pyxidinopsis* Habib (Dinophyceae) from the Miocene of the Labrador Sea, in: Head, M.J., Wrenn, J.H. (Eds.), Neogene and Quaternary Dinoflagellate Cysts and Acritarchs. American Association of Stratigraphic Palynologists Foundation, Dallas, Texas, pp. 165–180.
Mertens, K.N., Ribeiro, S., Bouimetarhan, I., Caner, H., Combourieu Nebout, N., Dale, B., De Vernal, A., Ellegaard, M., Filipova, M., Godhe, A., Goubert, E., Grøsfjeld, K., Holzwarth, U., Kotthoff, U., Leroy, S.A.G., Londeix, L., Marret, F., Matsuoka, K., Mudie, P.J., Naudts, L., Peña-Manjarrez, J.L., Persson, A., Popescu, S.-M., Pospelova, V., Sangiorgi, F., van der Meer, M.T.J., Vink, A., Zonneveld, K.A.F., Vercauteren, D., Vlassenbroeck, J., Louwye, S., 2009a. Process length variation in cysts of a dinoflagellate, *Lingulodinium machaerophorum*, in surface sediments: Investigating its potential as salinity proxy. Marine Micropaleontology 70, 54–69.
Mertens, K.N., Verhoeven, K., Verleye, T., Louwye, S., Amorim, A., Ribeiro, S., Deaf, A.S., Harding, I.C., De Schepper, S., González, C., Kodrans-Nsiah, M., De Vernal, A., Henry, M., Radi, T., Dybkjaer, K., Poulsen, N.E., Feist-Burkhardt, S., Chitolie, J., Heilmann-Clausen, C., Londeix, L., Turon, J.L., Marret, F., Matthiessen, J., McCarthy, F.M.G., Prasad, V., Pospelova, V., Kyffin Hughes, J.E., Riding, J.B., Rochon, A., Sangiorgi, F., Welters, N., Sinclair, N., Thun, C., Soliman, A., Van Nieuwenhove, N., Vink, A., Young, M., 2009b. Determining the absolute abundance of dinoflagellate cysts in recent marine sediments: The *Lycopodium* marker-grain method put to the test. Review of Palaeobotany and Palynology 157, 238–252.
Mertens, K.N., Price, A.M., Pospelova, V., 2012. Determining the absolute abundance of dinoflagellate cysts in recent marine sediments II: Further tests of the *Lycopodium* marker-grain method. Review of Palaeobotany and Palynology 184, 74–81.
Miller, K.G., Wright, J.D., Fairbanks, R.G., 1991. Unlocking the Ice House: Oligocene-Miocene Oxygen Isotopes, Eustasy, and Margin Erosion. Journal of Geophysical Research 96, 6829–6848.
Miller, K.G., Mountain, G.S., the Leg 150 Shipboard Party, Members of the New Jersey Coastal Plain Drilling Project, 1996. Drilling and Dating New Jersey Oligocene-Miocene Sequences: Ice Volume, Global Sea Level, and Exxon Records. Science 271, 1092–1095.
Moran, K., Backman, J., Brinkhuis, H., Clemens, S.C., Cronin, T.M., Dickens, G.R., Eynaud, F., Gattacceca, J., Jakobsson, M., Jordan, R.W., Kaminski, M., King, J., Koc, N., Krylov, A., Martinez, N., Matthiessen, J., McInroy, D., Moore, T.C., Onodera, J., O'Regan, M., Pälike, H., Rea, B., Rio, D., Sakamoto, T., Smith, D.C., Stein, R.R., St. John, K.E.K., Suto, I., Suzuki, N., Takahashi, K., Watanabe, M., Yamamoto, M., Farrell, J., Frank, M., Kubik, P.W., Jokat, W., Kristoffersen, Y., St John, K., Suto, I., Suzuki, N., Takahashi, K., Watanabe, M., Yamamoto, M., Farrell, J., Frank, M., Kubik, P.W., Jokat, W., Kristoffersen, Y., 2006. The Cenozoic palaeoenvironment of the Arctic Ocean. Nature 441, 601–605.
Pagani, M., Zachos, J.C., Freeman, K.H., Tipple, B., Bohaty, S., 2005. Marked decline in atmospheric carbon dioxide concentrations during the Paleogene. Science 309, 600–603.

Patten, B.C., 1962. Species diversity in net phytoplankton of Raritan Bay. Journal of Marine Research 20, 57–75.
Pound, M.J., Haywood, A.M., Salzmann, U., Riding, J.B., 2012. Global vegetation dynamics and latitudinal temperature gradients during the Mid to Late Miocene (15.97–5.33 Ma). Earth-Science Reviews 112, 1–22.
Pross, J., Brinkhuis, H., 2005. Organic-walled dinoflagellate cysts as paleoenvironmental indicators in the Paleogene; a synopsis of concepts. Paläontologische Zeitschrift 79, 53–59.
Reichart, G.J., Brinkhuis, H., 2003. Late Quaternary Protoperidinium cysts as indicators of paleoproductivity in the northern Arabian Sea. Marine Micropaleontology 49, 303–315.
Rochon, A., Marret, F., 2004. Middle latitude dinoflagellates and their cysts: increasing our understanding on their distribution. Review of Palaeobotany and Palynology 128, 1–5.
Roth, J.M., Droxler, A.W., Kameo, K., 2000. The Carribean carbonate crash at the middle to late Miocene transition: linkage to the establishment of the modern global ocean conveyor, in: Leckie, R.M., Sigurdsson, H., Acton, G.D., Draper, G. (Eds.), Proceedings of the Ocean Drilling Program, Scientific Results. Ocean Drilling Program, College Station, Texas, pp. 249–273.
Schreck, M., Matthiessen, J., Head, M.J., 2012. A magnetostratigraphic calibration of Middle Miocene through Pliocene dinoflagellate cyst and acritarch events in the Iceland Sea (Ocean Drilling Program Hole 907A). Review of Palaeobotany and Palynology 187, 66–94.
Schreck, M., Matthiessen, J., 2013. Batiacasphaera micropapillata: Palaeobiogeographic distribution and palaeoecological implications of a critical Neogene species complex, in: Lewis, J.M., Marret, F., Bradley, L. (Eds.), The Micropaleontological Society, Special Publications No. 5. The Geological Society, London, pp. 293–306.
Schreck, M., Meheust, M., Stein, R., Matthiessen, J., 2013. Response of marine palynomorphs to Neogene climate cooling in the Iceland Sea (ODP Hole 907A). Marine Micropaleontology 101, 49–67.
Shevenell, A.E., Kennett, J.P., Lea, D.W., 2004. Middle Miocene Southern Ocean cooling and Antarctic cryosphere expansion. Science 305, 1766–1770.
Shevenell, A.E., Kennett, J.P., Lea, D.W., 2008. Middle Miocene ice sheet dynamics, deep-sea temperatures, and carbon cycling: A Southern Ocean perspective. Geochemistry, Geophysics, Geosystems 9.
Sluijs, A., Pross, J., Brinkhuis, H., 2005. From greenhouse to icehouse; organic-walled dinoflagellate cysts as paleoenvironmental indicators in the Paleogene. Earth-Science Reviews 68, 281–315.
Sluijs, A., Röhl, U., Schouten, S., Brumsack, H.J., Sangiorgi, F., Sinninghe Damsté, J.S., Brinkhuis, H., 2008. Article late Paleocene – Early Eocene paleoenvironments with special emphasis on the Paleocene–Eocene thermal maximum (Lomonosov Ridge, Integrated Ocean Drilling Program Expedition 302). Paleoceanography 23, 1–17.
Taylor, F.J.R. (Ed.), 1987. The biology of dinoflagellates. Botanical Monographs volume 21. Blackwell Scientific Publications, Oxford.
Ter Braak, C.J.., Šmilauer, P., 2002. CANOCO Reference Manual and CanoDraw for Windows User's Guide (version 4.5).
Thomson, C.W., 1873. The depths of the sea. MacMillan and Co, London.
Utescher, T., Ashraf, a R., Dreist, a, Dybkjær, K., Mosbrugger, V., Pross, J., Wilde, V., 2012. Variability of neogene continental climates in Northwest Europe — a detailed study based on microfloras . Turkish Journal of Earth Sciences 21, 289–314.
Van Rooij, D., De Mol, B., Huvenne, V., Ivanov, M., Henriet, J.P., 2003. Seismic evidence of current-controlled sedimentation in the Belgica mound province, upper Porcupine slope, southwest of Ireland. Marine Geology 195, 31–53.
Van Rooij, D., Huvenne, V.A.I., Blamart, D., Henriet, J.-P., Wheeler, A., de Haas, H., 2009. The Enya mounds: a lost mound-drift competition. International Journal of Earth Sciences 98, 849–863.
Verity, P.G., Stoecker, D.K., Sieracki, M.E., Burkill, P.H., Edwards, E.S., Tronzo, C.R., 1993. Abundance, biomass and distribution of heterotrophic dinoflagellates during the North Atlantic spring bloom. Deep Sea Research Part II: Topical Studies in Oceanography 40, 227–244.
Verleye, T.J., Louwye, S., 2010. Recent geographical distribution of organic-walled dinoflagellate cysts in the southeast Pacific (25–53°S) and their relation to the prevailing hydrographical conditions. Palaeogeography, Palaeoclimatology, Palaeoecology 298, 319–340.
Versteegh, G.J.M., 1994. Recognition of cyclic and non-cyclic environmental changes in the Mediterranean Pliocene: A palynological approach. Marine Micropaleontology 23, 147–183.
Westerhold, T., Bickert, T., Röhl, U., 2005. Middle to late Miocene oxygen isotope stratigraphy of ODP site 1085 (SE Atlantic): New constrains on Miocene climate variability and sea-level fluctuations. Palaeogeography, Palaeoclimatology, Palaeoecology 217, 205–222.
Wood, G.D., Gabriel, A.M., Lawson, J.C., 1996. Chapter 3. Palynological techniques — processing and microscopy, in: Jansonius, J., McGregor, D.C. (Eds.), Palynology: Principles and Applications. American Association of Stratigraphic Palynologists Foundation, Dallas, Texas, pp. 29–50.
Woodruff, F., Savin, S.M., 1991. Mid-Miocene isotope stratigraphy in the deep sea: High-resolution correlations, paleoclimatic cycles, and sediment preservation. Paleoceanography 6, 755–806.
Zachos, J., Pagani, M., Sloan, L., Thomas, E., Billups, K., 2001. Trends, Global Rhythms, Aberrations in Global Climate 65Ma to Present. Science 292, 686–693.
Zachos, J.C., Dickens, G.R., Zeebe, R.E., 2008. An early Cenozoic perspective on greenhouse warming and carbon-cycle dynamics. Nature 451, 279–283.
Zevenboom, D., Brinkhuis, H., Visscher, H., 1994. Dinoflagellate cysts palaeoenvironmental analysis of the Oligocene/Miocene transition in northwest and central Italy. Giornale di geologia, serie 3a 56, 155–169.

Zonneveld, K.A.F., Marret, F., Versteegh, G.J.M., Bogus, K., Bonnet, S., Bouimetarhan, I., Crouch, E., de Vernal, A., Elshanawany, R., Edwards, L., Esper, O., Forke, S., Grøsfjeld, K., Henry, M., Holzwarth, U., Kielt, J.-F., Kim, S.-Y., Ladouceur, S., Ledu, D., Chen, L., Limoges, A., Londeix, L., Lu, S.-H., Mahmoud, M.S., Marino, G., Matsouka, K., Matthiessen, J., Mildenhal, D.C., Mudie, P., Neil, H.L., Pospelova, V., Qi, Y., Radi, T., Richerol, T., Rochon, A., Sangiorgi, F., Solignac, S., Turon, J.-L., Verleye, T., Wang, Y., Wang, Z., Young, M., 2013. Atlas of modern dinoflagellate cyst distribution based on 2405 data points. Review of Palaeobotany and Palynology 191, 1–197.

Zonneveld, K.A.F., Versteegh, G., Kodrans-Nsiah, M., 2008. Preservation and organic chemistry of Late Cenozoic organic-walled dinoflagellate cysts: A review. Marine Micropaleontology 68, 179–197.

Chapter 3.

Some new acritarch species from the lower and middle Miocene of the Porcupine Basin, North Atlantic Ocean:

Biostratigraphy and palaeoecology

Willemijn Quaijtaal, Kenneth Neil Mertens, Stephen Louwye

Six new acritarch species were observed during a high-resolution study on the upper Burdigalian to Serravallian (lower and middle Miocene) of the Porcupine Basin (Integrated Ocean Drilling Leg 307, off southwestern Ireland). The stratigraphical ranges and palaeoenvironmental preferences of the six new species were assessed. *Cometesphaera bullatio* gen. et sp. nov. is recorded from the upper Burdigalian to the lower Serravallian, while the range of *Cymatiosphaera*? *deverteuilii* sp. nov. is restricted to the upper Serravallian. *Platycystidia manumii* sp. nov. is recorded from the upper Burdigalian to the upper Langhian. *Porcupinea collaris* gen. et sp. nov. and *Porcupinea indentata* gen. et sp. nov. range from the upper Langhian to the lower Serravallian, and from the uppermost Burdigalian to the upper Serravallian, respectively. *Pusillisphaera solaris* gen. et sp. nov. is recorded from the upper Burdigalian to the upper Serravallian.

Published in: Palynology (2014), vol. 39, 37–55.

Some new acritarch species from the middle Miocene of Porcupine Basin, North Atlantic Ocean: biostratigraphy and palaeoecology

1. Introduction

The middle Miocene was a time of profound climatological change. The warm climate of the mid Miocene Climatic Optimum (MMCO; 16–14.5 Ma; *Abels et al.*, 2005) was terminated by a series of brief cooling events. These cooling events are the so-called Mi-events, and were identified as positive increases in benthic stable oxygen isotopes ($\delta^{18}O$) (*Miller et al.*, 1996, 1991). Mi-events 1 and 2 precede the MMCO; Mi-events 3 to 7 succeeded the MMCO. Of the latter, Mi-3 is thought to have had the most profound effect. It can be associated with an increase in East Antarctic Ice Sheet volume, global cooling, mid-latitude aridification, sea-level change, and biotic turnover (e.g. *Flower and Kennett*, 1994; *Haywood et al.*, 2009; *Lewis*, 2007; *Pound et al.*, 2012; *Shevenell et al.*, 2004). Specific causes are not known yet, but will have to be sought in CO_2 drawdown, changes in palaeoceanography or a favourable orbital configuration (*Abels et al.*, 2005; *Badger et al.*, 2013; *Kürschner et al.*, 2008; *Shevenell et al.*, 2004; *Westerhold et al.*, 2005). New high-resolution records can elucidate the causes and order of changes surrounding the Mi-events.

Integrated Ocean Drilling Program (IODP) Leg 307 drilled the Porcupine Basin, offshore southwestern Ireland, a region that is historically well-known for its deep water-habitats (*Le Danois*, 1948; *Thomson*, 1873). The goal of the expedition was to obtain more information about the initiation of growth of the deep-sea reefs, i.e. coral mounds, which are present in the area (*Expedition 307 Scientists*, 2006). During this expedition, Hole 1318 (Figure 3.1) recovered ~150 m sediments of middle Miocene age (*Louwye et al.*, 2008). *Louwye et al.* (2008) observed pronounced shifts in the organic-walled dinoflagellate cyst (dinocyst) assemblages, which they related to changes in temperature and productivity. *Quaijtaal et al.* (2014) subsequently showed that some of these assemblage shifts could be correlated with Mi-events Mi-3a, Mi-3b and Mi-4, and concluded that these can be associated with sea-surface cooling and sea level changes.

During the palynological study of *Quaijtaal et al.* (2014), dinocysts and acritarchs were analysed. Of the first group the importance for biostratigraphy and palaeoecology is widely recognized (e.g. *Fensome et al.*, 1996). However, Miocene acritarchs are understudied. *De Schepper and Head* (2008, 2014) noted that acritarchs incidentally can outnumber dinocysts in abundance. They also showed the biostratigraphical importance and the palaeoecological application of several acritarchs in the Pliocene. *Verhoeven et al.* (2014) performed a study on acritarchs from the Oligocene to Pliocene sediments; *Manum* (1976) on Eocene to Miocene sediments. Here we describe six new Miocene acritarch species *Cometesphaera bullatio*, *Cymatiosphaera? deverteuilii, Platycystidia manumii, Porcupinea collaris, Porcupinea indentata and Pusillisphaera solaris*. Furthermore, we discuss the importance of these new species for biostratigraphy and palaeoecology.

2. Material and methods

2.1. Material

Site U1318 of IODP Leg 307 was drilled in May 2005 off Southwest Ireland (Figure 3.1). The analysed samples were taken from Holes U1318B (51°26.148'N lat., 11°33.019'W long.) and U1318C (51°26.150.4358'N lat., 11°33.040'W long.). A detailed description of the lithology was provided by *Expedition 307 Scientists* (2006). The sedimentary sequence at Site 1318 could be divided into the lithostratigraphic units 1, 2 and 3, of which the latter is subdivided into subunits 3A, 3B and 3C (Figure 3.2). The analysed interval (subunits 3A and 3B) mainly consisted of silts, silty clays and fine-grained sands with varying carbonate contents (10–50%). A total of 194 samples were analysed palynologically by *Quaijtaal et al.*, (2014; unpublished data) for dinoflagellate cysts, acritarchs and other marine organic-walled palynomorphs at an average sample resolution of ca. 22 ka. The age model used is from *Quaijtaal et al.*, (2014), which provided an update for the age model given by *Louwye et al.* (2008). This age model incorporates a hiatus separating lithostratigraphic units 3A and 3B at ca. 133.2 mcd (~128 ka), and a newly discovered hiatus at 104.31–104.60 mcd (~244 ka). Furthermore, the magnetostratigraphy was shifted by two magnetochrons towards an older age from 122 mcd downwards. Average sedimentation rates were 5.8 cm/ka.

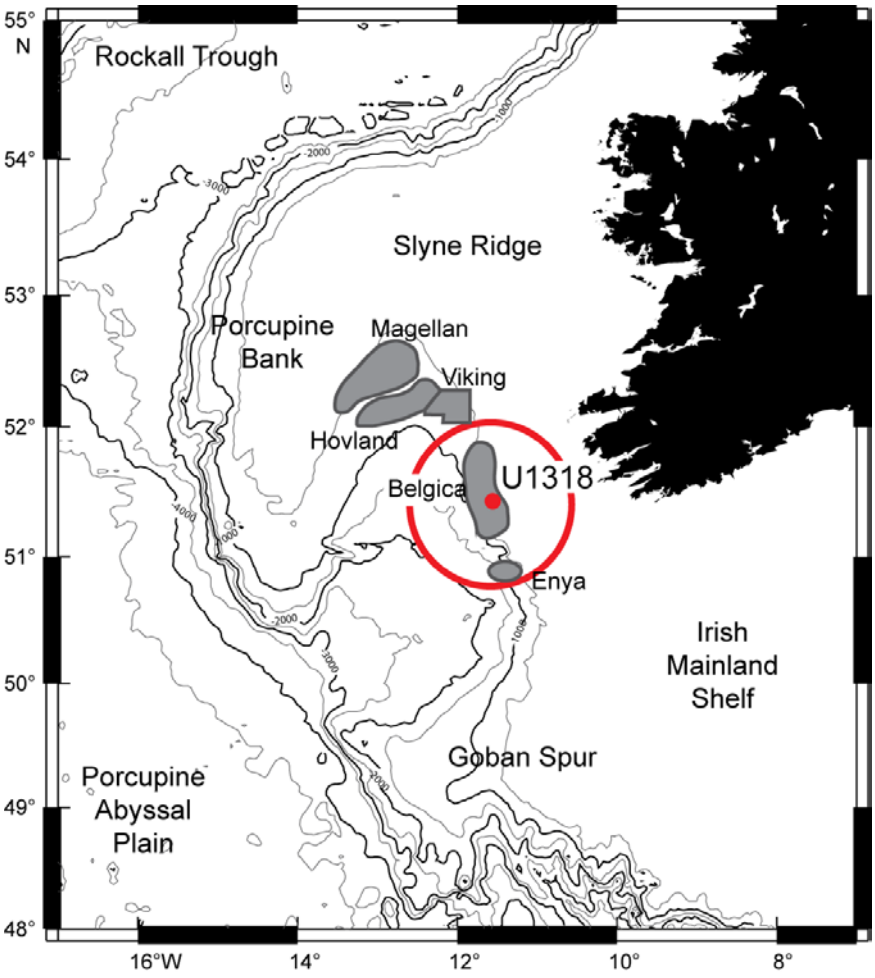

Figure 3.1: Location of the study area in Porcupine Basin, off southwest Ireland. Grey: coral mound provinces after *Foubert et al.* (2011).

2.2. Methods

Standard palynological preparation techniques were applied (*Quaijtaal et al.*, 2014). The samples have been cleaned and oven-dried at 60°C, weighed and rehydrated. About 10 to 15 grams dry sediment were weighed and one or two tablets of the spore *Lycopodium clavatum* (batch no. 177745, X = 18584 ± 829 and batch no. 1031, X = 20848 ± 2186; Supplementary Table 3.1) were added. Chemical treatment includes demineralization with warm hydrochloric acid (2N) and hydrofluoric acid (40%) for the removal of carbonates and silicates, respectively. Residues were placed in an ultrasonic bath for 30 seconds and sieved over a 10 µm nylon mesh screen and transferred into a plastic vial with several drops of $CuSO_4$ solution to prevent fungal growth. Vials were centrifuged at 2000 rpm for 5 min, supernatant water removed and one drop of homogenized residue was mounted on a microscope slide

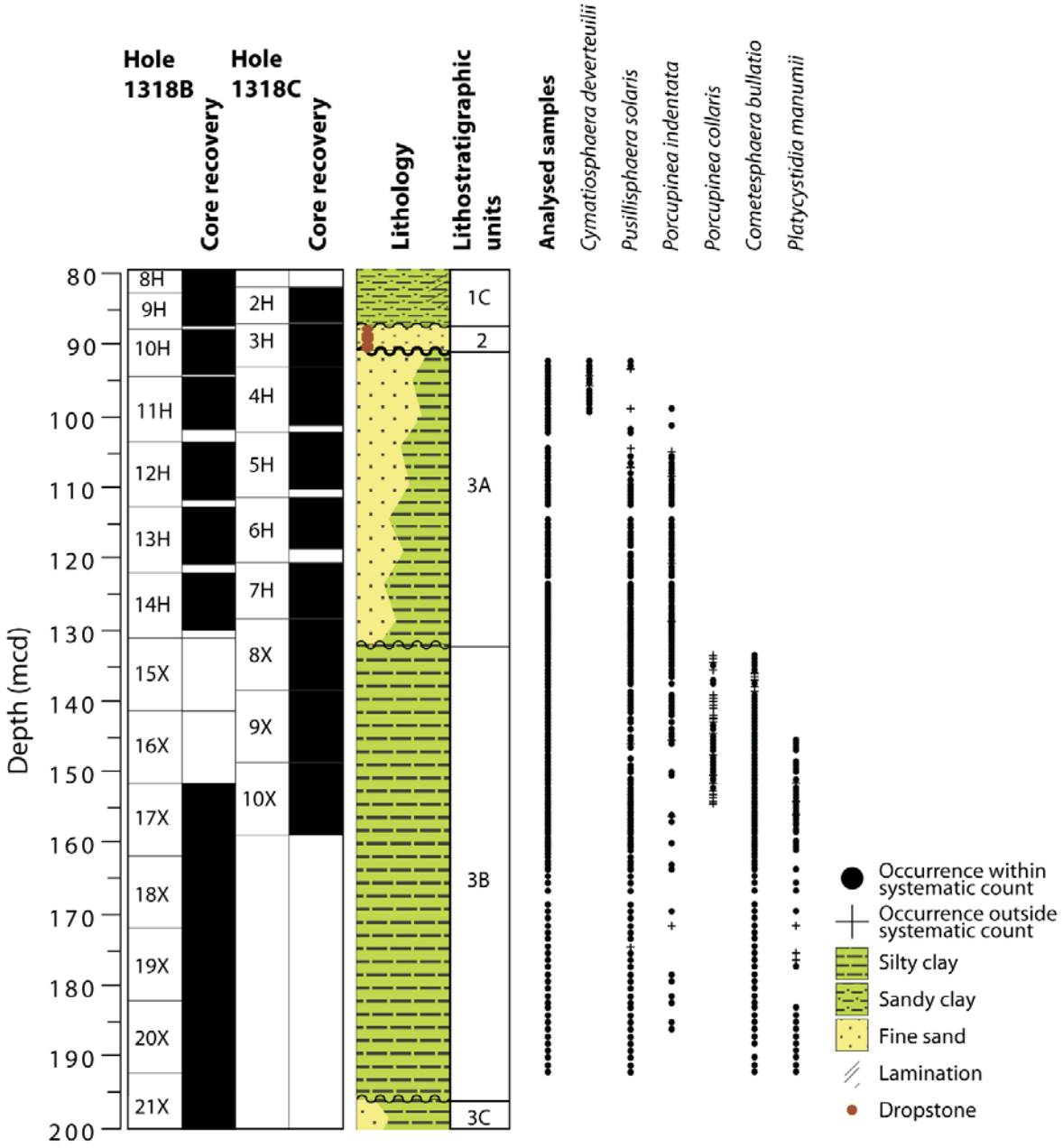

Figure 3.2: Depth (in meters composite depth), core recovery, lithology, lithostratigraphic units and sample positions in the studied sequence in Holes 1318B and 1318C. Wavy lines indicate an unconformity. The ranges of the acritarch species are listed according to their highest occurrence.

in a drop of liquid glycerol gelatine. The slides were then covered with a cover slip and sealed with nail polish. A minimum of 300 dinocysts were systematically counted in non-overlapping traverses; the remainder of the slide was then scanned for rare species and specimens suitable for microphotography. Countings of the new acritarch species can be found in Supplementary Table 3.1. The preservation of palynomorphs was moderate to excellent (*Quaijtaal et al.*, 2014). The slides were counted using a Zeiss AxioImagerA1 transmitted light microscope at 400x magnification equipped with a Zeiss Axiocam MRc5 camera. Several samples were analysed with scanning electron microscopy (SEM). For this purpose a smear slide was made by transferring one drop of palynological residue to a glass microscope slide that was sputter coated with gold. Because of the small size of the new acritarchs two samples were re-sieved over a 37 µm mesh screen and retained on a 10 µm mesh screen to analyse the fraction between 10 µm and 37 µm. The samples were examined using a JEOL6400 SEM at Ghent University.

Taxonomy follows *Fensome et al.* (2008), suprageneric nomenclature follows *Fensome et al.* (1990). The terminology used for describing fossil acritarchs used follows *Williams et al.* (2000). Holotypes are stored in the collection of the Royal Belgian Institute for Natural Science, Brussels, Belgium. Highest and lowest occurrences were defined by the mid-point between a presence and an absence of a species.

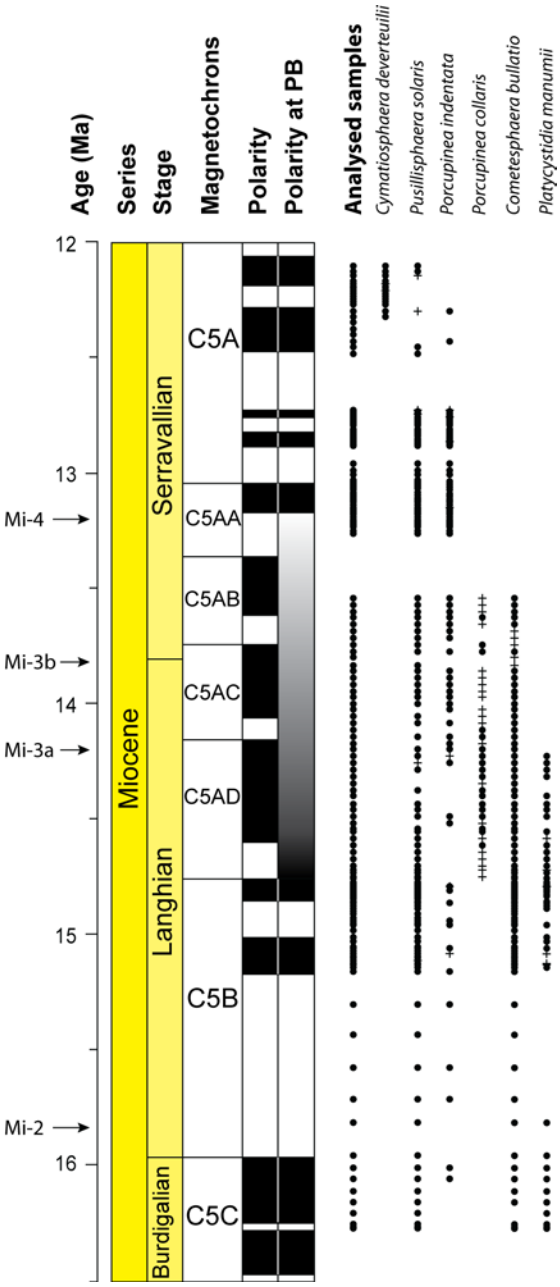

Figure 3.3: Age, stratigraphy and magnetostratigraphy of the studied sequence in Holes 1318B and 1318C. Polarity at PB: polarity present at the Porcupine Basin; magnetostratigraphy from *Louwye et al.* (2008) and *Quaijtaal et al.* (2014). Sample positions are given. The ranges of the acritarch species are listed according to their highest occurrence.

3. Systematic palaeontology

Group ACRITARCHA Evitt 1963

Genus *Cometesphaera* gen. nov.

Type. *Cometesphaera bullatio* gen. et sp. nov.

Etymology. from the Latin word for comet, *cometes*, and the Latin word for ball, *sphaera*, referring to the antapical velum of the genus that looks like the tail of a comet.

Diagnosis. small, subspherical to elliptical, hypocavate acritarchs with an antapical velum that looks like the tail of a comet. The thin outer wall is connected to a thin inner body by several columnar structures that are only visible under the light microscope. The outer wall is appressed to the inner body around a polygonal pylome that sometimes has rounded angles.

Cometesphaera bullatio sp. nov.
Plate 3.1, Figures 1–20

Synonymy. Dinocyst sp. D (pars) in *Quaijtaal et al.* (2014), supplementary table 1.
Holotype. Plate 3.1, Figures 1–5**.** Slide PB666-1, England Finder coordinates W37/1.
Stratigraphical horizon and type locality. Serravallian, Porcupine Basin, offshore southwestern Ireland, IODP Leg 307, 1318C (51°26.150.4358'N lat., 11°33.040'W long.), 8X2, 62–64 cm, 132.78 mcd.
Repository. Royal Belgian Institute for Natural Science, Brussels, Belgium, catalogue number IRSNB b6692.
Etymology. From the Latin word *bullatio*, meaning bubbling or having bulb-like formations.
Diagnosis. A small, subspherical to elliptical, hypocavate acritarch composed of two wall layers. The inner wall is thin (ca. 0.4 µm) and connected to a thin (ca. 0.4 µm), coarsely pitted outer wall through several columnar structures. The distance between the inner and outer wall increases from apex to antapex. A polygonal pylome is present at the apex, the operculum is free.
Description. A small species of *Cometesphaera* with a subspherical to elliptical outline in equatorial view. The cyst is composed of two wall layers. The shagreenate, transparent inner layer forms an inner body with a spherical to subspherical shape. The thickness of this inner layer is circa 0.4 µm. The transparent outer layer is slightly thinner and is loosely appressed to the inner body around the polygonal pylome and to the upper ca. one third to half the inner body. Both layers are separated otherwise, the separation being the greatest at the opposite side of the pylome. On the antapical side the outer layer is supported by several columnar structures, only visible under the light microscope (Plate 3.1, Figures 3, 7). The outer layer is characterized by pitting of varying size and position. A polygonal pylome is present on the apex. The angles of the corners are occasionally rounded. The operculum is simple and free, and sometimes collapsed into the inner body.
Dimensions. Holotype. Maximum diameter inner body: 14.8 µm; average apical separation between inner body and outer wall: 1.3 µm; maximum antapical separation between inner body and outer wall: 8.8 µm; thickness inner wall: 0.4 µm; thickness outer wall: 0.3 µm. Range. Maximum diameter inner body: 13.4(14.7)17.3 µm; average apical separation between inner body and outer wall: 0.5(1.2)2.3 µm; maximum antapical separation between inner body and outer wall: 4.2(8.9)11.4 µm; thickness inner wall: 0.2(0.4)0.7 µm; thickness outer wall: 0.2(0.4)0.6 µm. Number of specimens measured: 8.
Comparison. Because of its distinct morphology, *Cometesphaera bullatio* is easily distinguished from any other palynomorph.
Remarks. Multiple specimens have been observed where the antapical separation between the inner wall and the outer wall is not as large as the specimens illustrated here. Separation in these specimens is either smaller than the holotype, or equal to the degree of separation at the apex.
Geographical and stratigraphical distribution. The species is recorded in low abundances from the upper Burdigalian to the lower Serravallian of the Porcupine Basin (until 133.65 mcd; Figures 3.2–3.3). This highest occurrence correlates to an age of ~13.55 Ma. *Cometesphaera bullatio* sp. nov. has only been recorded in the Porcupine Basin so far.

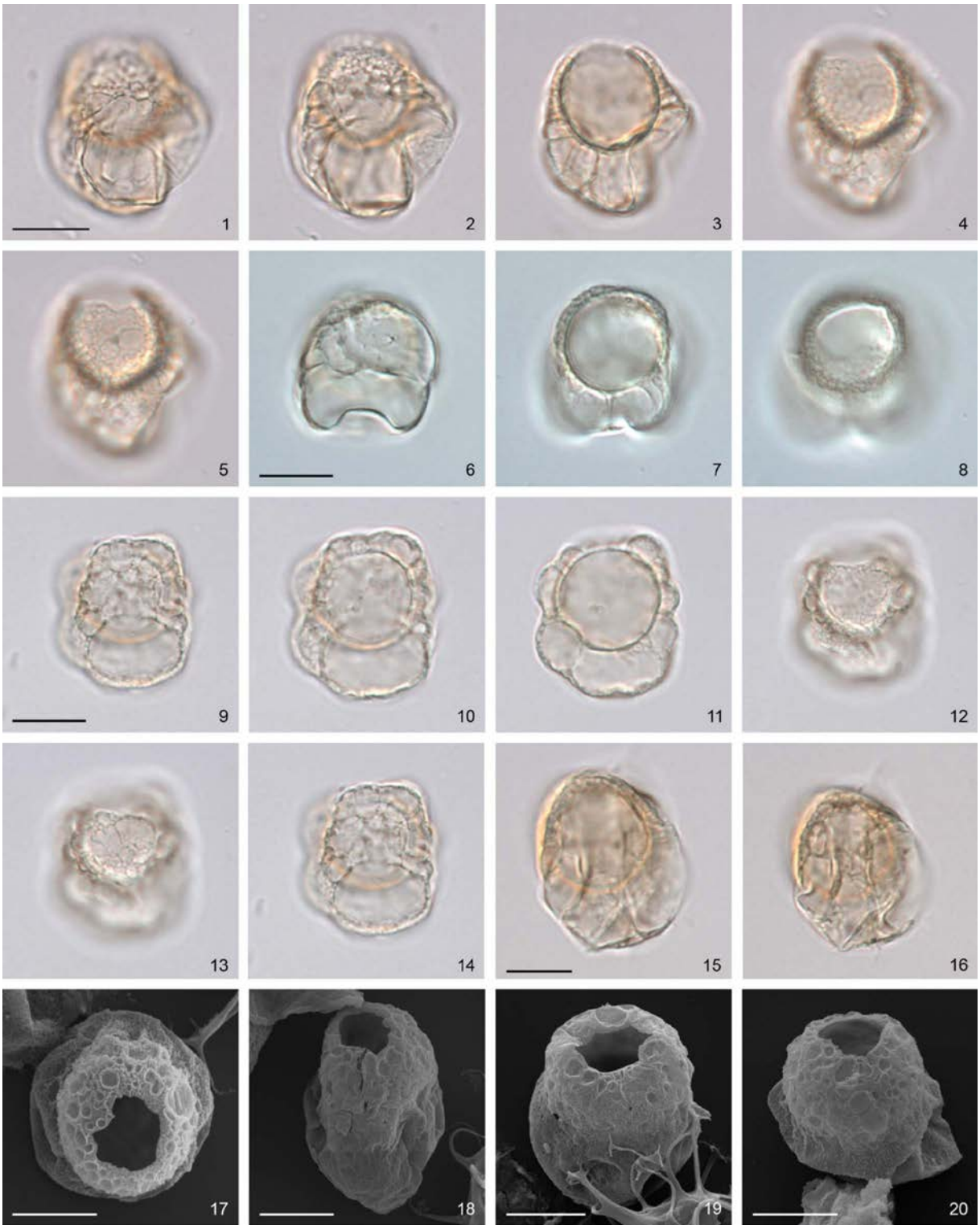

Plate 3.1: Photomicrographs (Figures 1–16) and SEM photographs (Figures 17–20) of *Cometesphaera bullatio* sp. nov. All specimens are from the Miocene of Porcupine Basin, off southwest Ireland. EF: England Finder coordinates. Scale bars represent 10 µm. Figures 1–5. Holotype, slide Slide PB666-1, EF: W37/1, slightly differing foci varying from high focus (Figure 1) to low focus (Figure 4). Figures 6–8. Slide PB674-1, EF: E17/2, high focus (Figure 6), optical section (Figure 7), low focus (Figure 8). Figures 9–14. Slide PB695-1, EF: W17/4, slightly differing foci from high focus (Figure 9) to low focus (Figure 13). Figure 15–16. Slide PB674-1, EF: W20/4, high focus (Figure 15), slightly lower high focus (Figure 16). Figure 17. Stub 666-1. Figure 18. Stub 666-1. Figure 19. Stub 666-1. x1500. Figure 20. Stub 666-1.

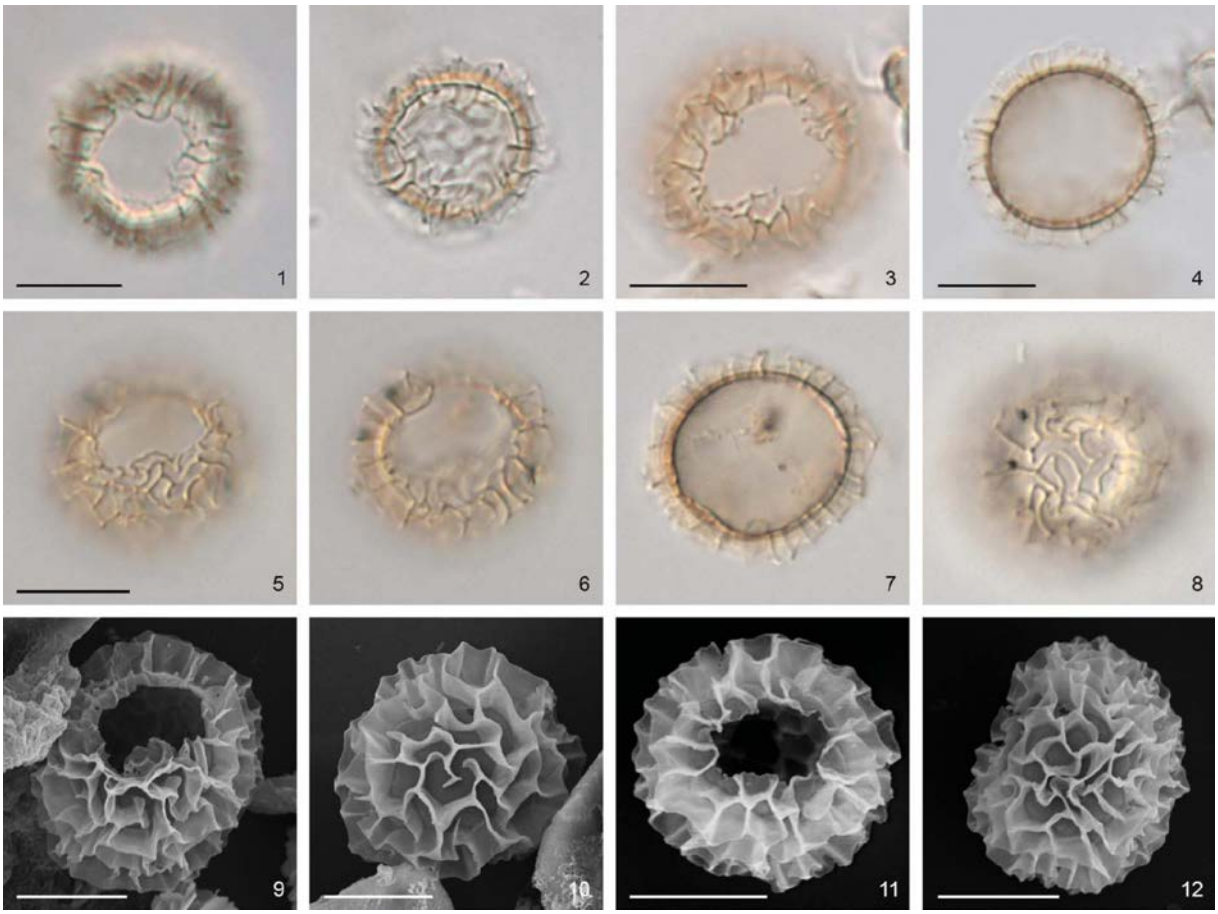

Plate 3.2: Photomicrographs (Figures 1–8) and SEM photographs (Figures 9–12) of *Cymatiosphaera? deverteuilii* sp. nov. All specimens are from the Miocene of Porcupine Basin, off southwest Ireland. EF: England Finder coordinates. Scale bars represent 10 µm. Figures 1–2. Holotype, slide PB453-1, EF: U33/1, high focus on pylome (Figure 1), optical section (Figure 2). Figures 3–4. Slide PB440-1, EF: Y35/2. high focus on pylome (Figure 3), optical section (Figure 4). Figures 5–8. Slide PB451-1, W16/4. Slightly differing foci from high focus on pylome (Figure 5) to low focus (Figure 8). Figure 9. Stub PB453. Figure 10. Stub PB453. Figure 11. Stub PB453. Figure 12. Stub PB453.

Genus *Cymatiosphaera* O. Wetzel 1933, ex Deflandre 1954
Cymatiosphaera? *deverteuilii* sp. nov.
Plate 3.2, Figures 1–12

Synonymy.
Gen. et sp. indet VI in *Engel* (1992), pl. 1, figs. 19–20.
Dinocyst sp. A in *Quaijtaal et al.* (2014), supplementary table 1.
Holotype. Plate 3.2, Figures 1–2, slide PB453-1, England Finder coordinates U33/1.
Stratigraphical horizon and type locality. Serravallian (upper middle Miocene), Porcupine Basin, offshore southwestern Ireland, IODP Leg 307, Hole 1318B (51°26.148'N lat., 11°33.019'W long.), 11H4, 52–54 cm, 99.95 mcd.
Repository. Royal Belgian Institute for Natural Science, Brussels, Belgium, catalogue number IRSNB b6693.
Etymology. Named after the palynologist Laurent de Verteuil, for his significant contribution on the taxonomy of dinocysts from the Miocene of New Jersey and Maryland, US.
Diagnosis. A small, spherical to subspherical acritarch. The body is covered with numerous non-tabular, single-layered septa that are meandering and anastomosing. The septa divide the surface of

the body into irregular polygonal fields. Septa can be recurvate distally. The thin central body wall is psilate to shagreenate. No tabulation has been observed. The pylome is polygonal.

Description. A small, transparent *Cymatiosphaera* species with a spherical to subspherical shape. The body consists of a thin (ca. 0.3 µm), psilate to shagreenate wall ornamented with numerous septa. The septa are mostly continuous and form irregular polygonal fields. Discontinuous septa extending partly into the polygonal fields are present. The septa do not reflect any tabulation and meander and anastomose over the entire cyst surface, creating a labyrinth-like structure. Distally recurvate septa have been observed in several specimens. A pylome is mostly present. The distinct angular edges of the pylome can be observed under light microscopy; the operculum is free. SEM analysis shows that the pylome outlines are not straight but follow the septa, giving the edges an undulating, serrate or denticulate appearance (Plate 3.2, Figures 9, 11).

Dimensions. Holotype. Maximum diameter central body: 14.3 µm; average height of septa: 2.1 µm; thickness wall: 0.2 µm. Range. Maximum diameter central body: 14.3(15.4)16.1 µm; height of septa: 1.5(2.4)3.3 µm; thickness wall central body: 0.1(0.3)0.4 µm. Number of specimens measured: 6.

Comparison. *Cymatiosphaera*? *deverteuilii* sp. nov. is characterized by the small size of the central body, the low height of the crests and the irregular polygonal fields. *Cymatiosphaera latisepta* De Schepper and Head (2008) differs by the characteristic distally expanded crests and the presence of vacuoles within the crests. The margins of the crests of *Cymatiosphaera*? *fensomei* De Schepper and Head (2014) are distally irregular. Furthermore, small supportive features occur at the base of the crests. *Cymatiosphaera*? *baffinensis* Head et al. (1989) and *Cymatiosphaera*? *invaginata* Head et al. (1989) both differ by the presence of a depression or invagination at the interconnections of the crests, and the absence of discontinuous septa.

Remarks. The assignment to the genus *Cymatiosphaera* is provisional because of the specific polygonal pylome, a feature not readily associated with the genus.

Geographical and stratigraphical distribution. The species is recorded continuously in low abundances in the upper Serravallian of the Porcupine Basin with a lowest occurrence in Chron C5An.2n at 12.34 Ma (99.46 mcd; Figures 3.2–3.3). The highest occurrence of this species (as Gen. et sp. indet VI) is in the upper Miocene of the Irminger Basin, off western Iceland (*Engel*, 1992).

Genus *Platycystidia* Cookson and Eisenack 1960

Platycystidia manumii sp. nov.

Plate 3.3, Figures 1–16

Synonymy.

Platycystidia(?) sp. II of *Manum*, (1976), pl. 6 figs. 17–22.

Acritarch sp. F of *Quaijtaal et al.* (2014), supplementary table 1.

Holotype. Plate 3.3, Figures 1–4, Slide PB709, England Finder coordinates X24/2.

Stratigraphical horizon and type locality. Langhian, Porcupine Basin, offshore southwestern Ireland, IODP Leg 307, Hole 1318C (51°26.150.4358'N lat., 11°33.040'W long.), 10X2, 103–132 cm, 153.65 mcd.

Repository. Royal Belgian Institute for Natural Science, Brussels, Belgium, catalogue number IRSNB b6694.

Etymology. In recognition of Svein Manum who recorded this species for the first time in the middle Oligocene to middle Miocene of the Norwegian Sea.

Diagnosis. A small bi-layered acritarch with a subrectangular outline. The outer wall forms wing-like folds around the elongated inner body. The outer wall has a fine mesh-like structure that appears granular under the light microscope.

Description. A small, bi-layered acritarch with an elongated subrectangular outline, the cyst being slightly longer than broad. The outer wall is thin and transparent. Under the light microscope the outer wall appears to be finely granular, but SEM analysis reveals the fine mesh-like structure of the outer wall (Plate 3.3, Figures. 13–16). The inner wall is slightly thicker and forms an elongated inner body. The ambitus of the inner body is subrectangular with rounded angles. A few discrete and low protrusions on the level surface of the inner body are randomly developed. The outer wall does not appear to be in contact with the inner wall, except at the poles, and forms wing-like folds along the longitudinal axis of the inner body. The specimens have often a folded or wrinkled appearance caused by the thin nature of the outer wall. Discretely curved or more or less straight lines are sometimes present on the surface of the outer wall (Plate 3.3, Figure 4). No specific orientation of these lines can be determined. A pylome was not readily observed.

Dimensions. Holotype. Transverse diameter inner body: 9.8 µm; longitudinal diameter inner body: 14.6 µm; transverse diameter outer body: 17.2 µm; longitudinal diameter outer body: 17.3 µm. Range. Transverse diameter inner body: 8.1(9.1)9.1 µm; longitudinal diameter inner body: 13.9(15.4)16.9 µm; transverse diameter outer body: 15.9(17.7)20.5 µm; longitudinal diameter outer body: 17.3(20.0)22.6 µm. Number of specimens measured: 9.

Comparison. *Platycystidia manumii* sp. nov. differs from other *Platycystidia* species by the thin outer wall with the fine mesh-like structure that appears to be granular under the light microscope, the folded appearance, and the small dimensions.

Geographical and stratigraphical distribution. *Platycystidia manumii* is recorded intermittently in low abundances from the upper Burdigalian to the upper Langhian of the Porcupine Basin (until 145.51 mcd; Figures 3.2–3.3). This highest occurrence correlates to an age of ~14.23 Ma. *Manum* (1976) observed this species as *Platycystidia*(?) sp. II in the lower and upper Oligocene and lower and middle Miocene from the Norwegian-Greenland Sea.

Comparison. *Platycystidia manumii* sp. nov. differs from other *Platycystidia* species by the thin outer wall with the fine mesh-like structure that appears to be granular under the light microscope, the folded appearance, and the small dimensions.

Geographical and stratigraphical distribution. *Platycystidia manumii* is recorded intermittently in low abundances from the upper Burdigalian to the upper Langhian of the Porcupine Basin (until 145.51 mcd; Figures 3.2–3.3). This highest occurrence correlates to an age of ~14.23 Ma. *Manum* (1976) observed this species as *Platycystidia*(?) sp. II in the lower and upper Oligocene and lower and middle Miocene from the Norwegian-Greenland Sea.

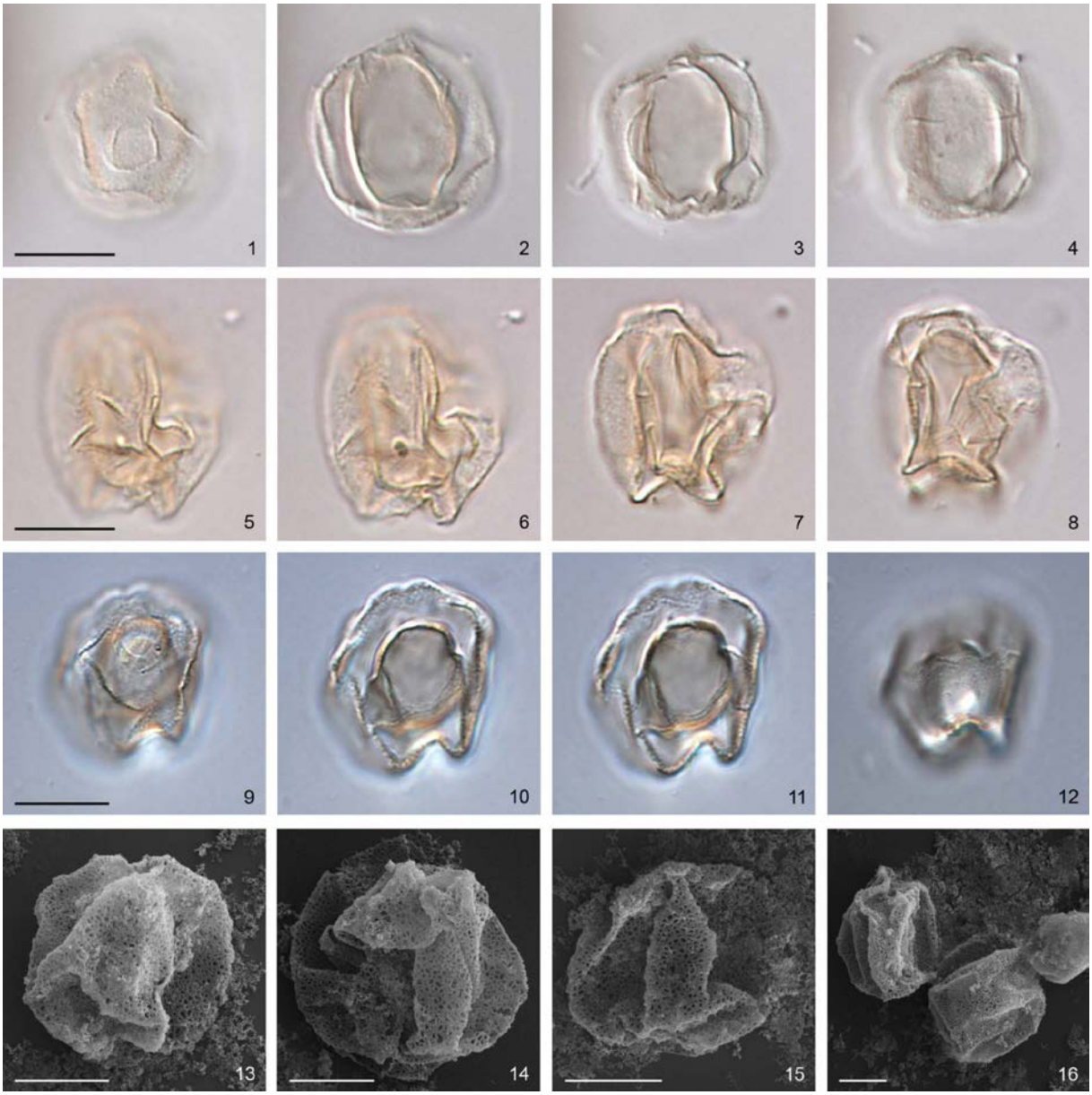

Plate 3.3: Photomicrographs (Figures 1–12) and SEM photographs (Figures 13–16) of Platycystidia manumii sp. nov. All specimens are from the Miocene of Porcupine Basin, off southwest Ireland. EF: England Finder coordinates. Scale bars represent 10 µm. Figures 1–4. Holotype, slide PB709-1, EF: X24/2, slightly differing foci varying from high focus (Figure 1) to low focus (Figure 4). Figures 5–8. Slide PB631-2, EF: O35/3, slightly differing foci varying from high focus (Figure 5) to low focus (Figure 8). Figures 9–12. Slide PB629-1, EF: K34/3, slightly differing foci varying from high focus (Figure 9) to low focus (Figure 12). Figure 13. Stub PB629. Figure 14. Stub PB629. Figure 15. Stub PB629. Figure 16. Stub PB629.

Genus *Porcupinea* gen. nov.

Type. *Porcupinea collaris* gen. et sp. nov. (Plate 3.4, Figures 1–8).
Etymology. named after the Porcupine Basin, offshore southwestern Ireland, where the type species was found.
Diagnosis. Small, spheroidal to subspheroidal acritarchs with a broad equatorial collar or flange with a spongy to cancellous internal structure. The collar is massive or to a certain degree fenestrated. The equatorial collar holds an inner body that is ornamented with a varying number of processes on both sides. The thin outer wall is discretely ornamented with structures of low relief. The pylome has an irregular polygonal shape.

Porcupinea collaris sp. nov.
Plate 3.4, Figures 1–16, Plate 3.5, Figures 1–12

Synonymy.
Dinocyst (precingular archaeopyle?)I in *Manum* (1976), p. 911, pl. 2, figs. 16–18.
Acritarch sp. 2 in *Head et al.* (1989), p. 496, pl. 5, figs. 1–2.
Dinocyst sp. D (pars) in *Quaijtaal et al.* (2014), supplementary table 1.
Holotype. Plate 3.4, Figures 1–8, slide PB692-2, England Finder coordinates F32/1.
Stratigraphical horizon and type locality: Langhian (middle Miocene), Porcupine Basin, offshore southwestern Ireland, IODP Leg 307, 1318C (51°26.150.4358'N lat., 11°33.040'W long.), 9X3, 130–132 cm, 145.51mcd.
Repository. Royal Belgian Institute for Natural Science, Brussels, Belgium, catalogue number IRSNB b6695.
Etymology. From the Latin *collare*, meaning collar, referring to the broad equatorial collar of the species.
Diagnosis. A small acritarch characterized by a broad equatorial collar of varying width and composed of spongy to cancellous material. A spherical body is located in the centre of the collar, and bears discrete processes on both sides. The polygonal pylome in the inner body is irregular, the operculum free.
Description. A small acritarch species with a circular to subcircular outline in polar view. The species is characterized by a broad equatorial, spongiform to cancellous collar. The thickness of the collar is variable in equatorial view, and can constitute up to half of the circular outline. The thin outer wall of the collar is scabrate to granulate, but a slightly pitted outer surface was observed occasionally. The equatorial collar is connected to the inner body. The diameter of the inner body is typically a third to half of the total diameter. The edges of the collar are smooth and slightly undulating on both sides. On both sides of the collar the inner body is ornamented with discrete, hollow processes of equal length but with varying width (Plate 3.5, Figures 1–8, 11). The tapering or near-columnar processes are slender and finely striated. The number of processes on each side varies between three and nine. The processes are closed and possess a thickened rim distally. A pylome is usually observed on one side (the apex?) of the inner body. The operculum is usually free and often collapsed into the central cavity. Three or four processes are usually present on the outer side of the operculum. The outline of the pylome is irregular and often runs along the bases of the remaining processes, when present.

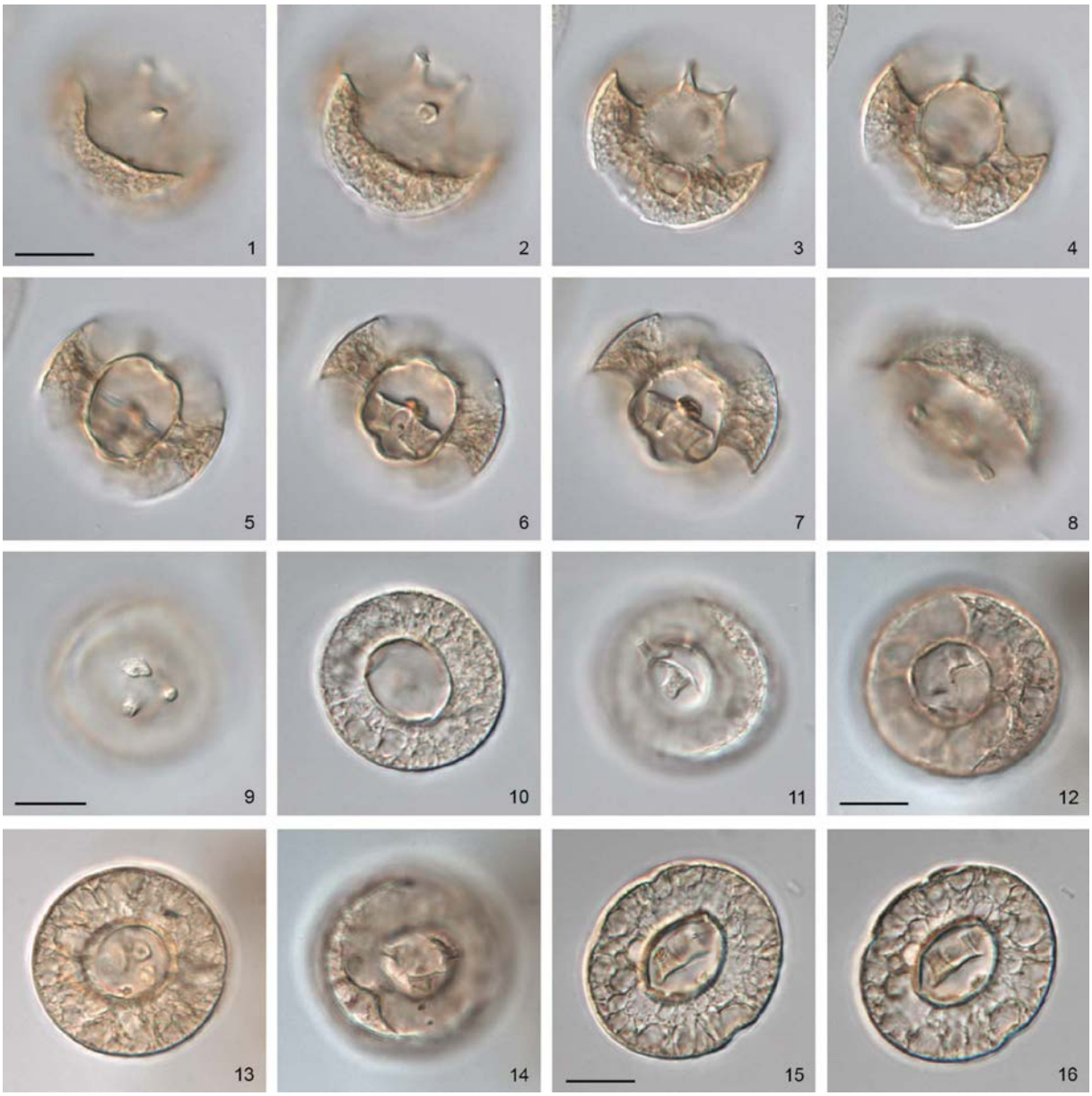

Plate 3.4: Photomicrographs (Figures 1–16) of *Porcupinea collaris* sp. nov. All specimens are from the Miocene of Porcupine Basin, off southwest Ireland. EF: England Finder coordinates. Scale bars represent 10 µm. Figures 1–8. Holotype, slide slide PB692-2, EF: F32/1, slightly differing foci varying from high focus (Figure 1) to low focus (Figure 8). Figures 9–11. Slide PB692–2, EF: J24/4, slightly differing foci varying from high focus (Figure 9), optical section (Figure 10) to low focus (Figure 11). Figures 12–14. Slide PB692-2, EF: B23/4, slightly differing foci varying from high focus (Figure 12), optical section (Figure 13) to low focus (Figure 14). Figures 14–16. Slide PB292-2, EF: P20/1, slightly differing foci on optical section.

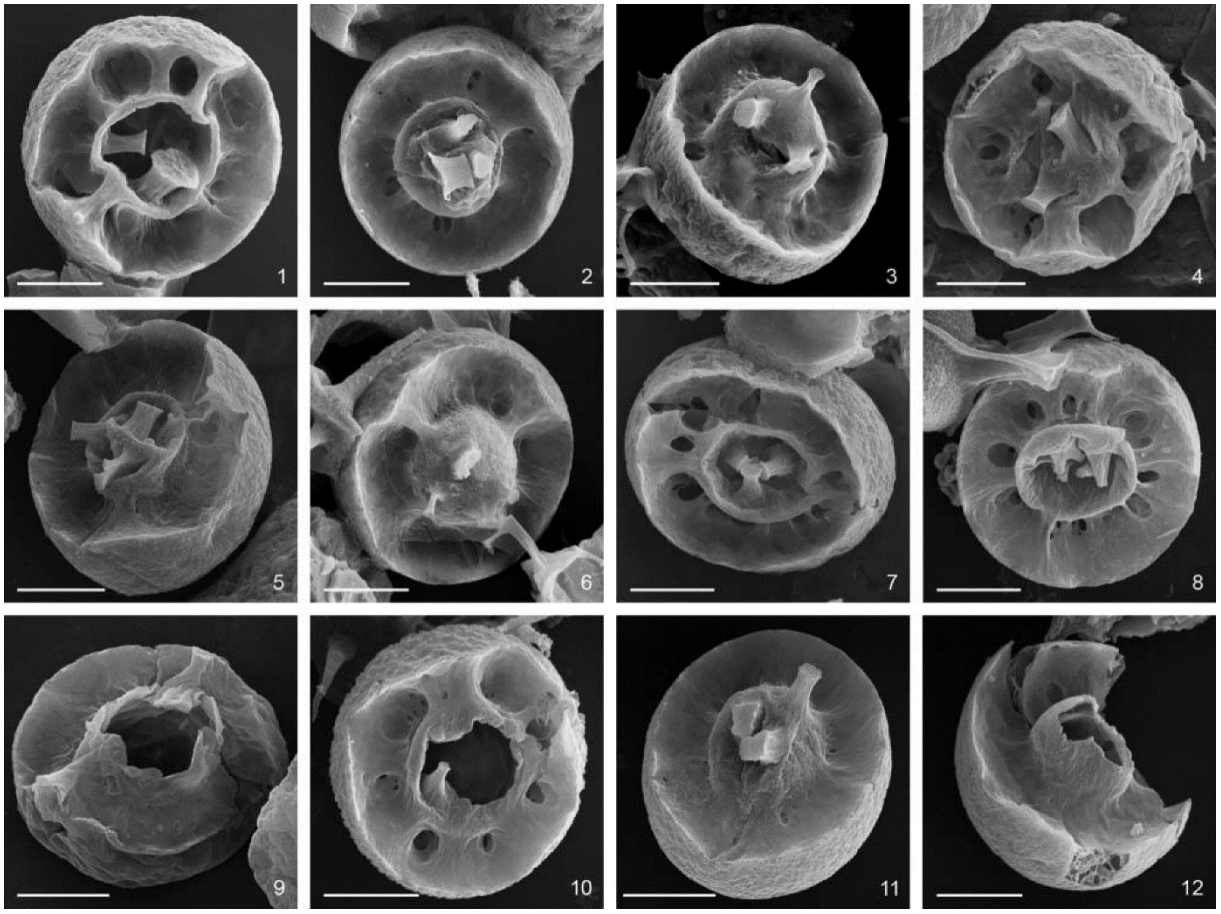

Plate 3.5: SEM photographs (Figures 1–12) of *Porcupinea collaris* sp. nov. All specimens are from the Miocene of Porcupine Basin, off southwest Ireland. Scale bars represent 10 µm. Figure 1. Stub PB504. Figure 2. Stub PB504. Figure 3. Stub PB504. Figure 4. Stub PB504. Figure 5. Stub PB692. Figure 6. Stub PB692. Figure 7. Stub PB692. Figure 8. Stub PB695. Figure 9. Stub PB692. Figure 10. Stub PB692. Figure 11. Stub PB692. Figure 12. Stub PB692.

Dimensions. Holotype. Maximum diameter: 28.0 µm; maximum diameter inner body: 15.2 µm; length processes: 4–4.3 µm. Range: Maximum diameter: 25.6(28.0)30.8 µm; maximum diameter inner body: 11.2(13.2)15.2; length processes: 3.3(4.0)4.5 µm. Number of specimens measured: 13.

Comparison: A comparison with the other *Porcupinea* species is given below. No other acritarch genus possesses similar morphological traits.

Remarks. Large circular to elongate perforations of the internal spongiform or cancellous material of the collar were occasionally observed (Plate 3.4, Figures 3, 10, 16; Plate 3.5, Figure 12). The perforations can consist of small circular holes to elongate cavations stretching from the inner body to the outer wall (Plate 3.5, Figures 1–4, 7–8, 10), giving the species a fenestrate aspect. *Head et al.* (1989) also noted such perforations in some specimens of their Acritarch sp. 2, and assumed that these fenestrate specimens could be considered as intermediate forms between their Acritarch sp. 1 *Head et al.* (1989) which is characterized by a cancellous equatorial collar supported by fibrous radial structures, and their Acritarch sp. 2 *Head et al.* (1989). Acritarch sp. 1 *Head et al.* (1989) was not recorded in our material.

Geographical and stratigraphical distribution. *Porcupinea collaris* sp. nov. is recorded from the upper Langhian to the lower Serravallian of the Porcupine Basin in almost continuous, low abundances. Its lowest occurrence lies just above the top of magnetosubchron C5Bn.1n at 154.52 mcd (~14.76 Ma),

the highest occurrence lies below the bottom of magnetosubchron C5AAn as present in the Porcupine Basin, at 133.65 mcd (Figures 3.2–3.3). *Manum* (1976) observed the species in early to middle Miocene sediments from the Norwegian-Greenland Sea. The species was recorded as Acritarch sp. 2 by *Head et al.* (1989) from the lower and middle Miocene (rare occurrences) of Hole 645E in Baffin Bay. *Head et al.* (1989) also report a questionable rare occurrence of a single specimen in the upper Miocene of the latter area.

Porcupinea indentata sp. nov.
Plate 3.6, Figures 1–16

Synonymy. Dinocyst sp. B in *Quaijtaal et al.* (2014), supplementary table 1.
Holotype. Plate 3.6, Figures 1–5. Slide PB542-1, England finder coordinates X16/1.
Stratigraphical horizon and type locality. Serravallian, Porcupine Basin, offshore southwestern Ireland, IODP Leg 307, 1318B (51°26.148'N lat., 11°33.019'W long.), 13H5, 140–142 cm, 121.76 mcd.
Repository. Royal Belgian Institute for Natural Science, Brussels, Belgium, catalogue number IRSNB b6696.
Etymology. From the Latin *indentare*, in reference to the many indentations in the equatorial collar.
Diagnosis. A small acritarch characterized by a broad equatorial collar, composed of spongy to cancellous material. The collar is typically indented to a varying degree. Within the collar-like structure an inner body is present that bears hollow processes on both sides of the collar. The wall of the inner body and the collar is striate in polar view. Occasionally, an irregular, polygonal pylome is formed in the inner body. The operculum is usually free.
Description. A small *Porcupinea* species with a circular to subcircular ambitus in polar view. The equatorial collar is characterized by shallow to deep indentations. The width of the collar appears constant. In its centre the collar holds a hollow, spherical body with a diameter that is typically half to two-thirds of the total diameter. The inner body bears individually separate, hollow processes on both sides of the collar. The processes are striated and widen proximally. Distally they form slightly expanded platform-like structures with a spiny margin (Plate 3.6, Figure 15). The spines are broad-based. Similar small projections are present at the rim of the collar (Plate 3.6, Figure 15). The wall of the inner body and the collar is distinctly ornamented with coarse striations (Plate 3.6, Figure 16). The striate ornamentation is best observed in polar view. An irregular, polygonal pylome is occasionally formed within the inner body. The operculum is free.
Dimensions. Holotype. Maximum diameter: 24.8 µm; minimum diameter inner body: 12.21 µm; maximum diameter inner body: 15.08 µm; length processes: 4–6.1 µm; thickness wall inner body: 0.2 µm; thickness outer wall: 0.2 µm. Range: Maximum diameter: 18.8(24.6)27.4 µm; minimum diameter inner body: 12.2(13.2)14.6 µm; maximum diameter inner body: 13.1(14.9)15.5; length of processes: 3.0(5.0)7.9 µm; thickness wall inner body: 0.1(0.2)0.3; thickness outer wall: 0.1(0.3)0.4 µm. Number of specimens measured: 7.
Comparison. *Porcupinea indentata* sp. nov. differs from *Porcupinea collaris* sp. nov. by the distinct indentations of the collar-like structure and the characteristic coarse striation of the wall. Furthermore, the collar-like structure is not fenestrated.
Geographic and stratigraphic distribution. The species is recorded in low abundances from the uppermost Burdigalian to upper Serravallian of the Porcupine Basin (Figure 3.3) and even continuously from 146.04 to 105.11 mcd, i.e. the upper Langhian to lower Serravallian (Figures 3.2–3.3). Outside

this depth range the species is recorded sporadically. *Porcupinea indentata* sp. nov has only been recorded in the Porcupine Basin so far.

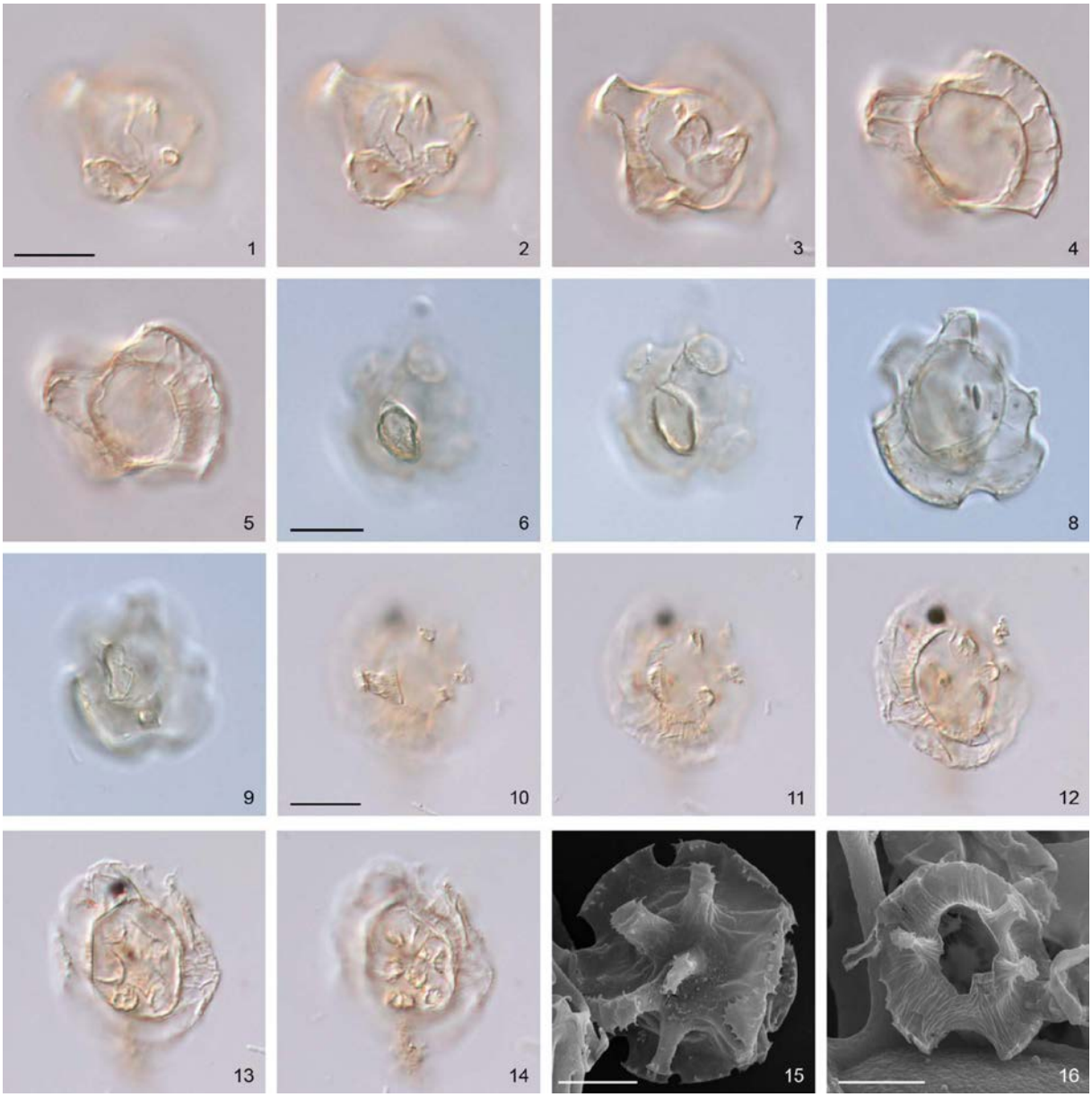

Plate 3.6: Photomicrographs (Figures 1–14) and SEM photographs (Figures 15–16) of *Porcupinea indentata* sp. nov. All specimens are from the Miocene of Porcupine Basin, off southwest Ireland. EF: England Finder coordinates. Scale bars represent 10 µm. Figures 1–5. Holotype, slide PB542-1, EF: X16/1, slightly differing foci varying from high focus (Figure 1) to low focus (Figure 5). Figures 6–9. Slide PB672-1, EF: V16/4, slightly differing foci varying from high focus (Figure 6) to low focus (Figure 9). Figures 10–14. Slide PB716-1, EF: E18/1, slightly differing foci varying from high focus (Figure 10) to low focus (Figure 14). Figure 15. Stub PB504. Figure 16. Stub PB504.

Genus *Pusillisphaera* gen. nov.

Type. *Pusillisphaera* gen. et sp. nov. (Plate 3.7, 1–4).
Etymology. from the Latin word *pusillus*, meaning tiny, and the Latin *sphaera*, meaning ball.
Diagnosis. small, bi-layered spherical to subspherical acritarchs. The thin outer layer is connected to a thin inner body through numerous non-tabular invaginations. A polygonal pylome is usually visible, with a free operculum.

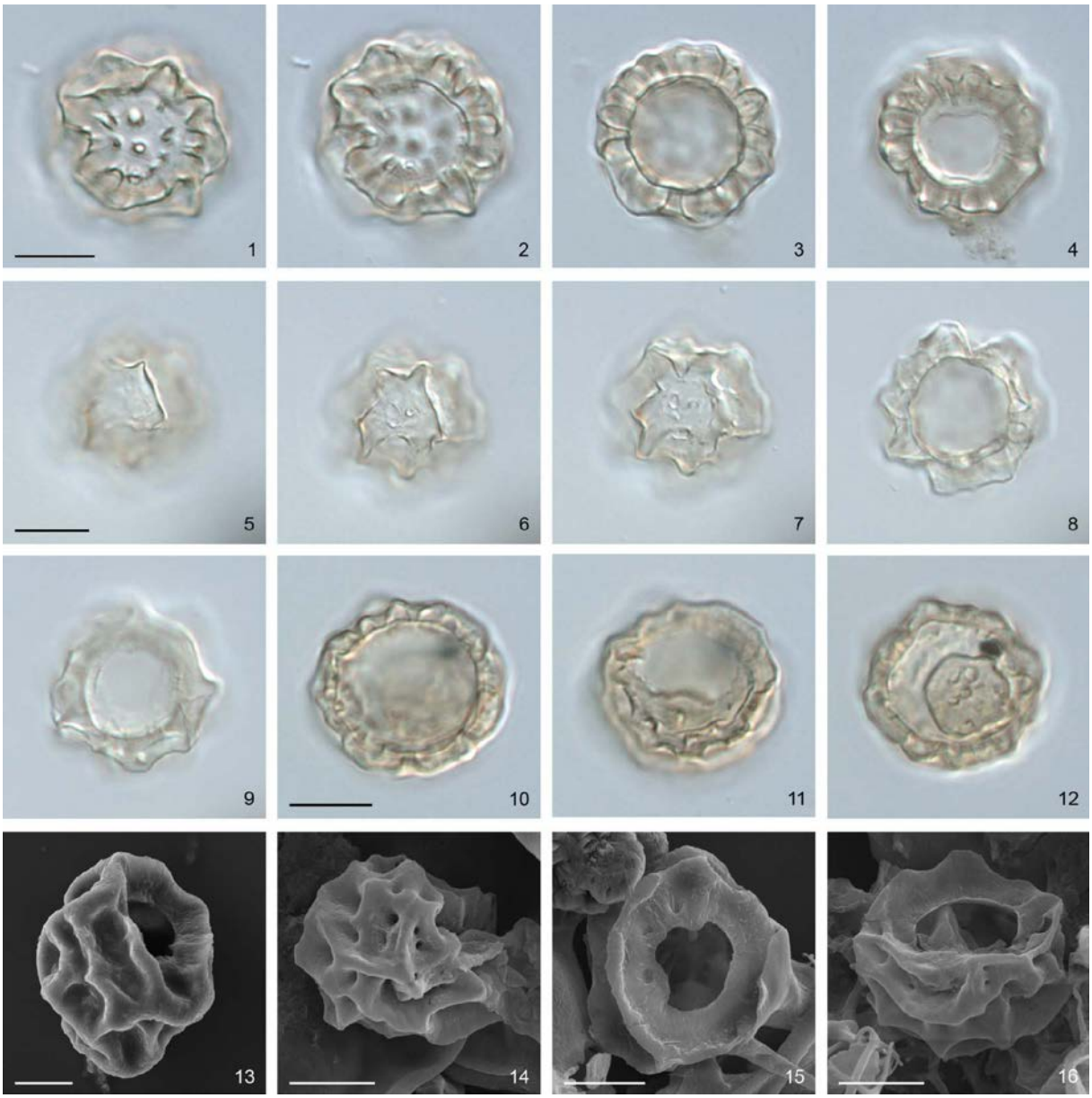

Plate 3.7: Photomicrographs (Figures 1–12) and SEM photographs (Figures 13–16) of *Pusillisphaera solaris* sp. nov. All specimens are from the Miocene of Porcupine Basin, off southwest Ireland. EF: England Finder coordinates. Scale bars represent 10 µm. Figures 1–4. Holotype, slide PB672-1, England Finder coordinates K32/4, slightly differing foci varying from high focus (Figure 1) to low focus (Figure 4). Figures 5–9. Slide PB667-1, EF: W44/3, slightly differing foci varying from high focus (Figure 5) to low focus (Figure 9). Figures 10–12. Slide PB540-1, EF: W23/3, differing foci varying from high focus (Figure 10), slightly lower low focus (Figure 11) to optical section (Figure 12). Figure 13. Stub PB453. Figure 14. Stub PB542. Figure 15. Stub PB542. Figure 16. Stub PB542.

Pusillisphaera solaris sp. nov.
Plate 3.7, Figures 1–16

Synonymy. Dinocyst sp. B in *Quaijtaal et al.* (2014), supplementary table 1.
Holotype. Plate 3.7, Figures 1–4, slide PB672-1, England Finder coordinates K32/4.
Stratigraphical horizon and type locality. Langhian, Porcupine Basin, offshore southwestern Ireland, IODP Leg 307, 1318C (51°26.150.4358'N lat., 11°33.040'W long.), 8X3, 115–117 cm, 135.68 mcd.
Repository. Royal Belgian Institute for Natural Science, Brussels, Belgium, catalogue number IRSNB b6697.
Etymology. From the Latin *sol* meaning 'sun'.
Diagnosis. A small, spherical to subspherical acritarch composed of an inner body with a smooth to scabrate surface, and a psilate to shagreenate outer layer that is attached to the inner body through numerous non-tabular funnel-shaped invaginations. The invaginations of the thin outer layer give it a sun-shaped appearance. A polygonal pylome is usually present, the operculum is free.
Description. The wall of the small acritarch species is bilayered. The inner wall has an average thickness of 0.3 µm and forms a spherical to subspherical inner body with a smooth to scabrate surface. The outer wall is slightly thinner and under light microscopy it appears to be smooth. However, when observed with scanning electron microscopy, the outer wall displays a psilate to shagreenate surface (Plate 3.7, Figures 13–14). The outer wall is separated from the inner body, except where it forms numerous funnel-shaped invaginations that connect the outer wall to the inner body. No invaginations have been observed in the immediate surroundings of the pylome. In some specimens this area is striated (Plate 3.7, Figure 13). Foveolate structures have also been observed on some specimens. A polygonal pylome is usually visible. The operculum is simple, free and was often observed present in the inner body.
Dimensions. Holotype. Maximum diameter inner body: 14.1 µm; separation inner body-outer wall: 4.1 µm; thickness wall inner body: 0.3 µm; thickness outer wall: 0.3 µm. Range. Maximum diameter inner body: 14.1(14.8)16.6 µm; separation inner body-outer wall: 1.8(3.9)5.5 µm; thickness wall inner body: 0.2(0.3)0.6 µm; thickness outer wall: 0.1(0.3)0.5 µm. Number of specimens measured: 8.
Comparison. *Pusillisphaera solaris* is morphologically closest to the dinocyst *Ataxiodinium zevenboomii* Head (1997). However, species of *Ataxiodinium* have a precingular archaeopyle, while *Pusillisphaera solaris* has a polygonal pylome. Furthermore, *Ataxiodinium zevenboomii* Head (1997) is larger in size (range total length: 31–50 µm). The acritarch *Lavradosphaera lucifer* De Schepper and Head (2008) differs from *Pusillisphaera solaris* by being tri-layered and its surface structure is formed by ridges and cones instead of funnel-shaped invaginations.
Geographical and stratigraphical distribution. *Pusillisphaera solaris* sp. nov. is recorded in low abundances from the upper Burdigalian to upper Serravallian of Porcupine Basin (Figure 3.3). Until now this species has not been documented in other locations.

4. Biostratigraphy

Of the six newly described acritarchs, two span the entire record: *Porcupinea indentata* and *Pusillisphaera solaris* (Figures 3.2 and 3.3). However, *Porcupinea indentata* only shows two spot occurrences after the hiatus at 104.31–104.60 mcd that might be considered to be reworked. However, reworking at the Porcupine Basin is generally low (*Quaijtaal et al.*, 2014).

The other 4 species show clearly defined occurrences. The lowest occurrence (LO) of *Platycystidia manumii* cannot be determined exactly since it is already present in the lowest analysed sample at 192.05 mcd (~16.28 Ma; Figures 3.2–3.3). Its highest occurrence (HO) is at 145.26 mcd (Figure 3.2), corresponding to an age of 14.22 Ma (Figure 3.3). Theoretically this should fall within magnetosubchron C5ADn. However, the magnetostratigraphy of this interval is unclear at the Porcupine Basin and this correlation to the magnetostratigraphy should be approached with caution. *Porcupinea collaris* has its LO at 154.59 mcd or ~14.76 Ma (Figures 3.2–3.3) LO. This falls within the theoretical magnetosubchron C5ADr. This assumption can be made with somewhat less caution, since the LO is 26 cm apart from the top of magnetosubchron C5Bn.1n. The species ranges on until at least 133.65 mcd (Figure 3.2). *Cometesphaera bullatio* has an uncertain LO in the lowest analysed sample at 192.05 mcd (~16.28 Ma; Figures 3.2–3.3). Its HO is shared with *Cometesphaera bullatio* at 133.65 mcd. No age determination of these HO's can be made, since they fall within the hiatus that separates lithostratigraphic units 3A and 3B at 133.2 mcd (Figure 3.2). The highest biostratigraphic event is the LO of *Cymatiosphaera? deverteuilii* at 99.71 mcd. The LO corresponds to an age of 12.34 Ma, and is the most reliable marker event, since the magnetostratigraphy of this interval was determined to be magnetosubchron C5An.2n. This species probably ranges further into the Late Miocene, as *Engel* (1992) has observed before.

5. Palaeoecology

As previously remarked by *De Schepper and Head* (2014), acritarchs can make up a significant part of the total palynomorph assemblage, and disregarding acritarchs in a palaeoenvironmental reconstruction can result in a loss of information. However, the biological affinity of most of these acritarchs is unknown, complicating the palaeoecological interpretation of the acritarch assemblage. However, *De Schepper and Head* (2014) also state that the assumption has to made that most acritarchs inhabit surface waters.

At the Porcupine Basin acritarchs are an important part of the palynomorph assemblage as well, 27% on average. Given that most acritarchs probably live in surface waters, a comparison with other surface parameters could provide more information regarding possible environmental preferences of the newly described acritarch species. The only surface parameters available for the Porcupine Basin are the dinocyst indices from *Quaijtaal et al.* (2014), complemented with the data from the newly analysed samples (unpublished data). However, these indices are based on assumptions regarding the palaeoenvironmental preferences of dinocysts as well, and such a comparison has to be interpreted with caution.

A simple way of correlating a set of samples with environmental information is with a Canonical Correspondence Analysis (CCA). The variance in species over two axes can then be explained in terms of environmental parameters. A CCA on untransformed relative abundance data was performed with Canoco 4.5 (*Ter Braak and Šmilauer*, 2002), adding 4 dinocyst indices (Warm/Cold, Neritic/Oceanic, Peridinioid/Gonyaulacoid and Sporomorph/Dinocyst) to the dataset as environmental parameters (Figure 3.4). These dinocyst indices are based upon the assumed palaeoenvironmental preferences

from the dinoflagellates that produced the dinocysts, and express relative changes in sea-surface temperature and -productivity, sea-level and coastal proximity respectively. The data is from *Quaijtaal et al.*, (2014; unpublished data). The first two axes explain 98.7% of the variance of the acritarchs in relation to the dinocyst indices (Table 3.1). The first axis explains 93.6% of the variance and can be assigned to the Warm/Cold (W/C), Neritic/Oceanic (N/O) and Sporomorph/Dinocyst (S/D) indices. These three indices all plot in the same direction. In contrast to shelf settings, the W/C index and the N/O index correlate with each other at the Porcupine Basin due to the influence of transport of palynomorphs (See *Quaijtaal et al.*, 2014, fig. 13). Unfortunately, without additional proxies, it is impossible to separate these factors. The second axis explains an additional 5.1% and can be assigned to the Peridinioid/Gonyaulacoid (P/G) index, a measure for sea surface productivity.

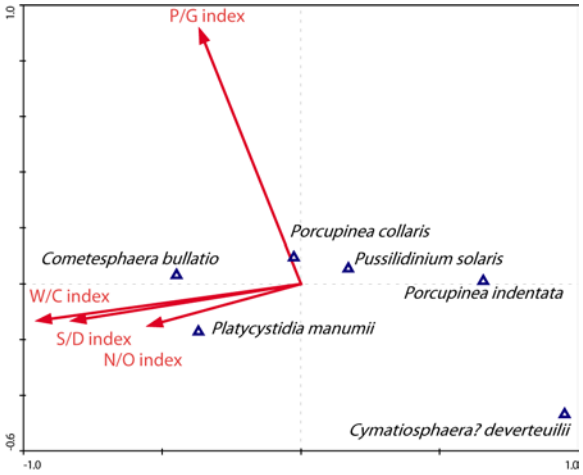

Figure 3.4: CCA (Canonical Correspondence Analysis). The occurrences of the six new acritarch species are plotted against four palaeoenvironmental indices: the Warm/Cold (W/C) index as a measure for sea-surface temperature; the Neritic/Oceanic (N/O) index as a measure for relative sea-level and/or transport from the shelf; the Sporomorph/Dinocyst (S/D) index as a measure for coastal proximity; the Peridinioid/Gonyaulacoid (P/G) ratio as a measure for sea-surface productivity.

From Figure 3.4 it can be observed that there is a clear separation between the new acritarch species. Most of the species plot along the first axis, indicating that they either respond to sea-surface temperature or changes in water depth as a result of sea-level changes. The species that plot strongly on the positive side of the X-axis are *Cymatiosphaera? deverteuilii* and *Porcupinea indentata* (Table 3.2); they possibly have a preference for colder waters or correlate to conditions with less transport from the shelf. The preference for colder water of *Cymatiosphaera? deverteuilii* might be confirmed by the presence of the species in the more northerly Irminger Basin. *Cometesphaera bullatio* and *Platycystidia manumii* plot on the negative side of the x-axis, implying that they might be associated with warmer sea-surface temperatures or conditions with more transport of palynomorphs from the shelf. *Porcupinea collaris* and *Pusillisphaera solaris* do not appear to show a strong correlation to the x-axis, nor the y-axis. The only species that appears to have a clear (negative) correlation on the y-axis is *Cymatiosphaera? deverteuilii*. This could suggest that it also prefers more oligotrophic (i.e. less productive) surface waters.

Table 3.1
Species-environment correlations, and cumulative percentages of variance of species data and of species-environment relation for the first four axes.

Axes	1	2	3	4
Species-environment correlations:	0.805	0.181	0.129	0.026
Cumulative percentage variance				
of species data:	16.4	17.3	17.5	17.5
of species-environment relation:	93.6	98.7	100	100

Table 3.2
Eigenvalues of the six new acritarch species on the first four axes. Positive values on the first axis indicate a preference for either colder sea-surface temperatures, a more distal location from the shore or higher relative sea-level, or a combination of these factors; positive values on axis 2 indicate a preference for a more productive environment.

Species	Axis 1	Axis 2	Axis 3	Axis 4
Cymatiosphaera? deverteuilii	1.4437	-0.7126	0.137	0.0235
Porcupinea indentata	0.999	0.0159	-0.0738	-0.0181
Pusillisphaera solaris	0.2594	0.0832	0.063	0.0098
Porcupinea collaris	-0.0385	0.1446	-0.35	0.0645
Cometesphaera bullatio	-0.6812	0.0477	0.0019	-0.0074
Platycystidia manumii	-0.5611	-0.2609	-0.0381	0.0002

6. Further recommendations

The previous sections show the potential of these small acritarchs in biostratigraphy and palaeoecology. However, a lot of palynological studies use a 15 µm mesh size for sieving, which is about the size of most small acritarchs. Therefore, in order to avoid loss of these species, it is recommended that a 10 µm mesh be used for sieving.

Because of their small size it is also to be recommended that SEM analysis of these acritarchs be performed. SEM analysis often reveals features that cannot be observed under the light microscope, such as the apparently fine mesh-like structure of *Platycystidia manumii* that appears to be granular under light microscopy. SEM analysis might also elucidate the biological affinity of these acritarchs. The polygonal pylome that has been observed in most of the newly described acritarchs is unusual and too irregular to be like the apical archaeopyle of Gonyaulacoid dinocysts. However, there is a certain similarity to the archaeopyle types of calcareous dinocysts summarized by *Streng et al.* (2004). Nonetheless, the morphology of calcareous cysts is notably less complex than the newly described acritarchs.

7. Conclusions

Six previously undescribed acritarch species have been described from the middle Miocene of Porcupine basin, off southwestern Ireland: *Cometesphaera bullatio* gen. et sp. nov., *Cymatiosphaera? deverteuilii* sp. nov., *Platycystidia manumii* sp. nov., *Porcupinea collaris* gen. et sp. nov., *Porcupinea indentata* gen. et sp. nov. and *Pusillisphaera solaris* gen. et sp. nov. These species were all recorded in the upper Burdigalian to Serravallian with their own specific biostratigraphical ranges. Furthermore, the possible palaeoecological preference of these species was determined, where temperature and/or depth habitat proved to be the most important determining factor.

8. Author contributions

SL designed the project. KNM did the scanning electron microscopy (SEM) on selected samples. WQ did the palynological processing, counting and analyses, the interpretation of the data, writing of the paper and the preparation of the figures.

9. Acknowledgements

The samples for this study were provided by the Integrated Ocean Drilling program. Walter Hale en Alex Wülbers kindly supported us during sampling at the Bremen Core Repository. Sabine Van Cauwenberghe and Renaat Dasseville are thanked for their technical assistance. Martin Head (Brock University, Canada) and Lucy Edwards (US Geological Survey) kindly shared some thoughts on the morphology of the genus *Porcupinea*. We would like to thank the two reviewers, Karen Dybkjær (GEUS, Denmark) and Dirk Munsterman (TNO Utrecht, The Netherlands) for the constructive remarks. This work was supported by the Research Foundation-Flanders (FWO) under Grant G017911N. Kenneth Neil Mertens is a postdoctoral researcher of the Research Foundation-Flanders (FWO).

10. References

Abels, H.A., Hilgen, F.J., Krijgsman, W., Kruk, R.W., Raffi, I., Turco, E., Zachariasse, W.J., 2005. Long-period orbital control on middle Miocene global cooling: Integrated stratigraphy and astronomical tuning of the Blue Clay Formation on Malta. Paleoceanography 20, PA4012.

Badger, M.P.S., Lear, C.H., Pancost, R.D., Foster, G.L., Bailey, T.R., Leng, M.J., Abels, H.A., 2013. CO_2 drawdown following the middle Miocene expansion of the Antarctic Ice Sheet. Paleoceanography 28, 42–53.

De Schepper, S., Head, M.J., 2014. New late Cenozoic acritarchs: evolution, palaeoecology and correlation potential in high latitude oceans. Journal of Systematic Palaeontology 12, 493–519.

De Schepper, S., Head, M.J., 2008. New dinoflagellate cyst and acritarch taxa from the Pliocene and Pleistocene of the Eastern North Atlantic (DSDP Site 610). Journal of Systematic Palaeontology 6, 101–117.

Engel, E.R., 1992. Palynologische Evidenz klimarelevanter Ereignisse in miozänen Sedimenten des Nordatlantiks. Schweizerbart Science Publishers, Stuttgart, Germany.

Expedition 307 Scientists, 2006. Site U1318, in: Ferdelman, T.G., Kano, A., Williams, T., Henriet, J.-P., the Expedition 307 Scientists (Eds.), Proceedings of the Integrated Ocean Drilling Program. Integrated Ocean Drilling Program Management International, Washington, D.C., pp. 1–57.

Fensome, R.A., MacRae, R.A., Williams, G.L., 2008. DINOFLAJ2, Version 1 [WWW Document]. American Association of Stratigraphic Palynologists, Data Series no. 1.

Fensome, R.A., Riding, J.B., Taylor, F.J.R., 1996. Chapter 6. Dinoflagellates, in: Jansonius, J., McGregor, D.C. (Eds.), Palynology: Principles and Applications. American Association of Stratigraphic Palynologists Foundation, Dallas, Texas, pp. 107–169.

Fensome, R.A., Williams, G.L., Barss, M.S., Freeman, J.M., Hill, J.M., 1990. Acritarchs and fossil prasinophytes: an index to genera, species and infraspecific taxa. American asociation of Stratigraphic Palynologists Contribution Series 25. American Association of Stratigraphic Palynologists Foundation, Dallas, Texas.

Flower, B.P., Kennett, J.P., 1994. The middle Miocene climatic transition: East Antarctic ice sheet development, deep ocean circulation and global carbon cycling. Palaeogeography, Palaeoclimatology, Palaeoecology 108, 537–555.

Foubert, A., Huvenne, V.A.I., Wheeler, A., Kozachenko, M., Opderbecke, J., Henriet, J.-P., 2011, The Moira Mounds, small cold-water coral mounds in the Porcupine Seabight, NE Atlantic: Part B—Evaluating the impact of sediment dynamics through high-resolution ROV-borne bathymetric mapping. Marine Geology 282, 65–78.

Haywood, A.M., Smellie, J.L., Ashworth, A.C., Cantrill, D.J., Florindo, F., Hambrey, M.J., Hill, D., Hillenbrand, C.D., Hunter, S.J., Larter, R.D., Lear, C.H., Passchier, S., van de Wal, R., 2009. Middle Miocene to Pliocene History of Antarctica and the Southern Ocean, in: Florindo, F., Siegert, M. (Eds.), Developments in Earth and Environmental Sciences. Elsevier, pp. 401–463.

Head, M.J., 1997. Thermophilic Dinoflagellate Assemblages from the Mid Pliocene of Eastern England. Journal of Paleontology 71, 165–193.

Head, M.J., Norris, G., Mudie, P.J., 1989. Palynology and dinocyst stratigraphy of the Miocene in ODP Leg 105, Hole 645E, Baffin Bay, in: Srivastava, S.P., Arthur, M., Clement, B., Al., E. (Eds.), Proceedings of the Ocean Drilling Program, Scientific Results 105. U.S. Government Printing Office, Washington, pp. 467–514.

Kürschner, W.M., Kvacek, Z., Dilcher, D.L., 2008. The impact of Miocene atmospheric carbon dioxide fluctuations on climate and the evolution of terrestrial ecosystems. Proceedings of the National Academy of Sciences of the United States of America 105, 449–53.

Le Danois, E., 1948. Les profondeurs de la mer. Payot, Paris.

Lewis, A.R., Marchant, D.R., Ashworth, A.C., Hemming, S.R., Machlus, M.L., 2007. Major middle Miocene global climate change: Evidence from East Antarctica and the Transantarctic Mountains. Geological Society of America Bulletin 119, 1449–1461.

Louwye, S., Foubert, A., Mertens, K., Van Rooij, D., The IODP Expedition 307 Scientific Party, 2008. Integrated stratigraphy and palaeoecology of the Lower and Middle Miocene of the Porcupine Basin. Geological Magazine 145, 321–344.

Manum, S.B., 1976. Dinocysts in Tertiary Norwegian-Greenland Sea sediments (Deep Sea Drilling Project Leg 38), with observations on palynomorphs and palynodebris in relation to environment, in: Talwani, M., Udintsev, G., Al., E. (Eds.), Initial Reports of the Deep Sea Drilling Project 38. U.S. Government Printing Office, Washington, pp. 897–919.

Miller, K.G., Mountain, G.S., the Leg 150 Shipboard Party, Members of the New Jersey Coastal Plain Drilling Project, 1996. Drilling and Dating New Jersey Oligocene-Miocene Sequences: Ice Volume, Global Sea Level, and Exxon Records. Science 271, 1092–1095.

Miller, K.G., Wright, J.D., Fairbanks, R.G., 1991. Unlocking the Ice House: Oligocene-Miocene Oxygen Isotopes, Eustasy, and Margin Erosion. Journal of Geophysical Research 96, 6829–6848.

Pound, M.J., Haywood, A.M., Salzmann, U., Riding, J.B., 2012. Global vegetation dynamics and latitudinal temperature gradients during the Mid to Late Miocene (15.97–5.33 Ma). Earth-Science Reviews 112, 1–22.

Quaijtaal, W., Donders, T.H., Persico, D., Louwye, S., 2014. Characterising the middle Miocene Mi-events in the Eastern North Atlantic realm: A first high-resolution marine palynological record from the Porcupine Basin. Palaeogeography, Palaeoclimatology, Palaeoecology 399, 140–159.

Shevenell, A.E., Kennett, J.P., Lea, D.W., 2004. Middle Miocene Southern Ocean cooling and Antarctic cryosphere expansion. Science 305, 1766–1770.

Streng, M., Hildebrand-Habel, T., Willems, H., 2004. A proposed classification of archeopyle types in calcareous

dinoflagellate cysts. Journal of Paleontology 78, 456–483.
Ter Braak, C.J.., Šmilauer, P., 2002. CANOCO Reference Manual and CanoDraw for Windows User's Guide (version 4.5).
Thomson, C.W., 1873. The depths of the sea. MacMillan and Co, London.
Verhoeven, K., Louwye, S., Paez-Reyes, M., Mertens, K.N., Vercauteren, D., 2014. New acritarchs from the late Cenozoic of the southern North Sea Basin and the North Atlantic realm. Palynology 38, 38–50.
Westerhold, T., Bickert, T., Röhl, U., 2005. Middle to late Miocene oxygen isotope stratigraphy of ODP site 1085 (SE Atlantic): New constrains on Miocene climate variability and sea-level fluctuations. Palaeogeography, Palaeoclimatology, Palaeoecology 217, 205–222.
Williams, G.L., Fensome, R.A., Miller, M.A., Sarjeant, W.A.S., 2000. A glossary of the terminology applied to dinoflagellates, acritarchs and prasinophytes, with emphasis on fossils. American Association of Stratigraphic Palynologists Contribution Series 37. American Association of Stratigraphic Palynologists Foundation, Dallas, Texas.

Chapter 4.

A revised and improved age model for the middle Miocene part of IODP Site U1318

(Porcupine Basin, offshore southwestern Ireland)

Willemijn Quaijtaal, Steven Tesseur, Timme H. Donders, Philippe Claeys, Stephen Louwye

Integrated Ocean Drilling Program Leg 307 Site U1318 is one of the few relatively complete middle Miocene drillcores from the North Atlantic (Porcupine Basin, offshore southwestern Ireland). Using benthic foraminiferal stable carbon and oxygen isotopes the existing age model for Site U1318 was improved. The stable isotope record displays globally recognized isotope events, used to revise the existing magnetostratigraphy-based age-model. Two intervals contained misidentified magnetochrons which were corrected. The sampled interval now has a refined age between 12.75–16.60 Ma with a temporal resolution of ~29 ka.

Published in: Geological Magazine (2017), doi:10.1017/S0016756816001278.

A revised and improved age model for the middle Miocene part of IODP Site U1318 (Porcupine Basin, offshore southwestern Ireland)

1. Introduction

The middle Miocene was a period of profound climate change (e.g. *Flower and Kennett*, 1994; *Zachos et al.*, 2001). A relatively warm period, the Middle Miocene Climatic Optimum (MMCO; 16–14.5 Ma according to *Abels et al.* (2005); 17–15 Ma according to *Shevenell and Kennett*, 2004) terminated during the Middle Miocene Climate Transition (MMCT; ~14 Ma, Langhian–Serravallian), the second largest glaciation after the Eocene–Oligocene Transition (*Zachos et al.*, 2001). Global comparison between stable isotopic records is essential in understanding the palaeoceanographic and climatic changes during the MMCO and MMCT. Several high-resolution isotope records spanning the MMCO and/or MMCT have become available over the last years, but three large areas remain uncovered: the Indian Ocean, the North Atlantic Ocean and the Arctic Ocean. The Arctic Ocean is extremely difficult to drill, and the few recovered cores have a low recovery (*Moran et al.*, 2006). The North Atlantic Ocean however has numerous drill sites. Nonetheless, the studies from these locations often suffer from hiatuses and generally have a lower resolution than the existing Pacific and Southern Ocean records.

Louwye et al. (2008) and *Quaijtaal et al.* (2014) presented palynological data from the Porcupine Basin in the eastern North Atlantic (Figure 4.1). Sediments from Integrated Ocean Drilling Program (IODP) Site U1318 are of late early Miocene to middle Miocene age and contained well-preserved organic-walled dinoflagellate cysts (dinocysts) and other marine palynomorphs (*Louwye et al.*, 2008). *Louwye et al.* (2008) proposed a first age model for IODP Site U1318 based on magnetostratigraphy, biostratigraphic dinocyst data and the Sr-dating of a mollusc (*Kano et al.*, 2007). As reported by *Expedition 307 Scientists* (2006), the shipboard palaeomagnetic measurements at Site U1318 were affected by magnetic overprint and by noise in the cryogenic magnetometer, rendering the identification of the weak original palaeomagnetic signature difficult. The measured magnetic intensity was considered very low and several measurements have an indistinct inclination between -20° and 20° rather than a distinct value near -90° or 90° (*Louwye et al.*, 2008). To overcome these problems *Louwye et al.* (2008) measured the magnetic signature on several discrete samples since these measurements would not be affected by a magnetic overprint. *Quaijtaal et al.* (2014) updated the age model of *Louwye et al.* (2008) with the aid of additional biostratigraphic dinocyst and calcareous nannoplankton data. However, biostratigraphic tie-points can be diachronic and correlation to global events is necessary to place the 'barcode' of magnetostratigraphy in time correctly.

Here we present new benthic foraminiferal stable carbon and oxygen isotope data from intermediate water depths in the eastern North Atlantic Ocean. These data from a new, relatively complete record fill up one of the data gaps in the North Atlantic Ocean. Additionally, the benthic $\delta^{18}O$ and $\delta^{13}C$ stable isotope records presented in this paper aid in confirming or adapting the magnetostratigraphy of *Quaijtaal et al.* (2014) using magnetostratigraphic tie-points provided by *Miller et al.* (1991, 1996, 1998) and globally recognizable isotope stratigraphic events defined by *Woodruff and Savin* (1991).

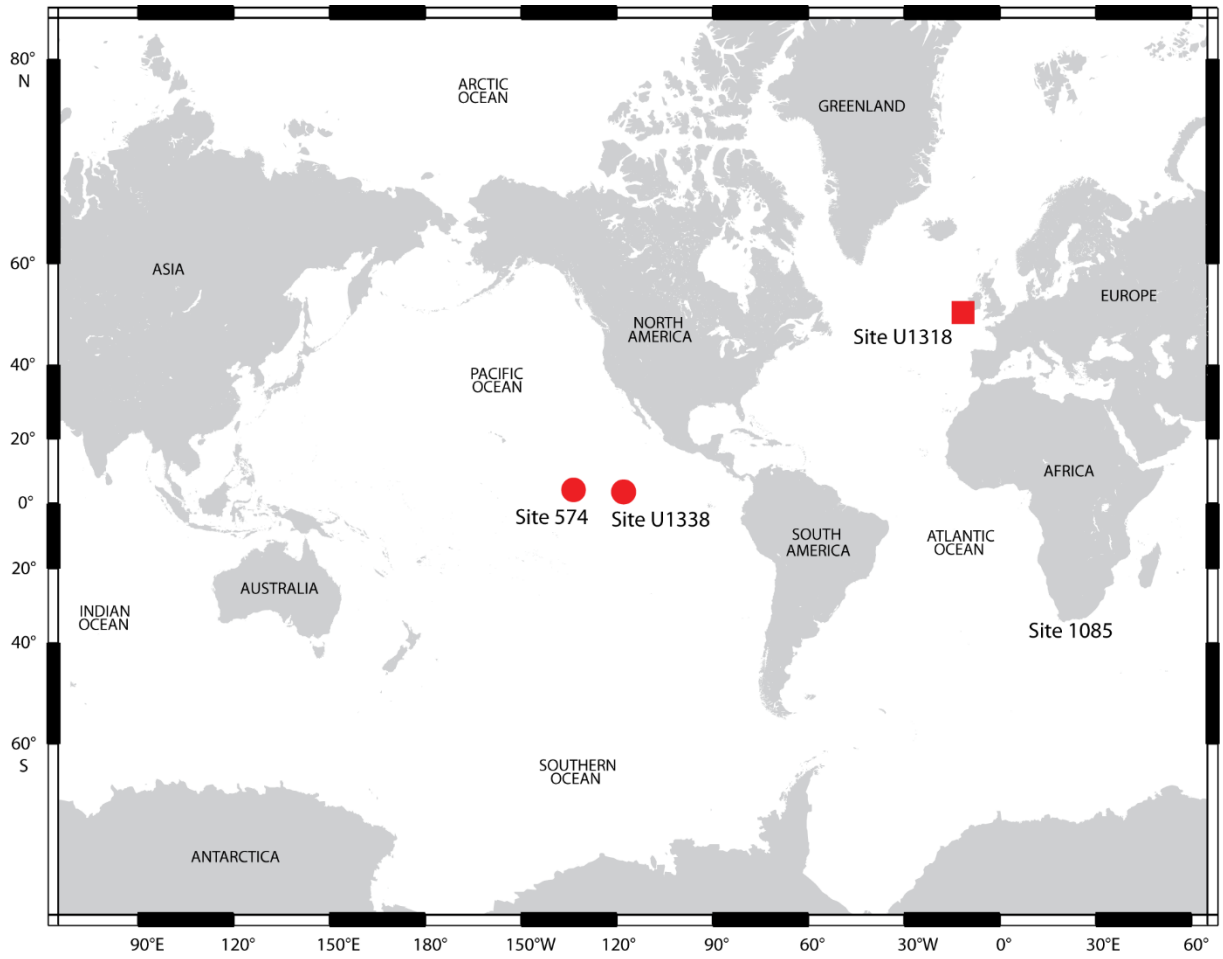

Figure 4.1: Location of Integrated Ocean Drilling Program (IODP) drill Site U1318, as well as the location of DSDP Site 574 and IODP Site U1338. Figure adapted from IODP drill site maps (http://iodp.tamu.edu/scienceops/maps.html).

2. Material

One hundred and forty-five samples from IODP Leg 307, Site U1318 were selected for stable carbon and oxygen isotope measurements on benthic foraminifera (Figure 4.2, Supplementary Table 4.1). Site U1318 (water depth 409 m) was drilled in May 2005 and a composite record was established from Holes U1318B (51°26.148'N lat., 11°33.019'W long.) and U1318C (51°26.150.4358'N lat., 11°33.040'W long.), based on physical properties (*Expedition 307 Scientists*, 2006). The composite record spans seismic units P1, P2 and P3 (*Van Rooij et al.*, 2003) that correspond to (parts of) lithostratigraphic units 1–3. The seismic units and lithostratigraphy are described into more detail in *Expedition 307 Scientists* (2006) and *Quaijtaal et al.* (2014; Figure 4.2). The samples for this study were selected from lithostratigraphic units 3A, 3B and 3C that mainly consist of greenish-grey clay and are divided into subunits based on their calcium carbonate contents. Subunit 3A and 3B correspond to seismic unit P2; subunit 3C corresponds to seismic unit P1 (*Expedition 307 Scientists*, 2006). Sample spacing in the composite record is ~1 m on average.

3. Methodology

3.1. Strategy for isotope analysis

Benthic isotopic records are preferably generated from epifaunal benthic species, since the relative change in $\delta^{13}C$ values of epifaunal foraminifer tests of similar sized specimens from the same species are dominantly influenced by the $\delta^{13}C$ values of seawater (e.g. *Fontanier et al.*, 2008; *Jorissen*, 2003). The most abundant epifaunal species in the record is *Cibicidoides pachyderma*. This species is morphologically similar to the often used *Cibicidoides mundulus* (ex *Cibicidoides kullenbergi*) and is known to occur from the early Oligocene until today (*Holbourn et al.*, 2013a). Unfortunately *Cibicidoides pachyderma* was not present in every sample, and measurements on a mixture of several other epifaunal benthic foraminifera were not justified due to preservational problems. Therefore the infaunal taxon *Uvigerina* sp. (0-3 cm within the sediment) was selected for measurements in addition to *Cibicidoides pachyderma*. *Uvigerina* sp. specimens were present almost consistently from 196.54 mcd upwards (Figure 4.2; Supplementary Table 4.1), with a relatively high abundance and a general good to excellent preservation. The species was absent below 197.59 mcd. The $\delta^{13}C$ value of infaunal species is, unlike for epibenthic species, not only influenced by the $\delta^{13}C$ value of the seawater at a given offset, but is also influenced by the microhabitat. In general a deeper microhabitat results in a more depleted $\delta^{13}C$ signature, which is a potential consequence of the pore water $\delta^{13}C$ dissolved inorganic carbon (DIC) gradient and/or a consequence of microhabitat effects (*Fontanier et al.*, 2008; *McCorkle et al.*, 1985). Despite this drawback, the advantage of measuring the isotopes on the well-preserved *Uvigerina* sp. specimens is to identify and prevent preservation issues that could affect the $\delta^{18}O$ values of less-well preserved *Cibicidoides pachyderma* specimens (*Sexton and Wilson*, 2009) and to prevent having a mixture of epibenthic specimens with possibly different isotope disequilibrium correction factors. Changes in the $\delta^{18}O$ values of *Uvigerina* sp. are, as well as the $\delta^{18}O$ values of *Cibicidoides pachyderma,* expected to reflect changes in the $\delta^{18}O$ value of the seawater (by e.g. glaciation) and the prevailing temperature. There is no known microhabitat influence on the $\delta^{18}O$ isotopes (*Fontanier et al.*, 2008).

For isotope measurements the samples were oven dried at 60°C for 24 hours, weighed and subsequently soaked in a tetra-natriumdiphosphat-decahydrat solution (5 g/L) for at least 24 hours in order to deflocculate the clay (after *Snyder and Waters*, 1984). Afterwards, the samples were washed over a sieve with a 63 µm mesh size. The remaining >63 µm fraction was removed from the sieve with distilled water, oven-dried and weighed. The samples were then dry-sieved into three fractions: the 63–180 µm fraction, the 180–250 µm fraction and the >250 µm fraction. Foraminifera were preferentially picked in the 180–250 µm fraction and complemented with foraminifera from the >250 µm fraction. Two to six specimens (circa 40 to 70 µg) were required for each measurement. The preservation of the picked foraminifera was evaluated relatively to each other with the binocular microscope by breaking the foraminifera, and assessing the transparency or the fading of textures. The preservation was generally good to moderate for the *Cibicidoides pachyderma* specimens. Large secondary crystals were never observed with the binocular microscope, although Scanning Electron Microscopy showed that some specimens had minor secondary crystals on their test walls, which might have influenced the isotopic values (Plate 4.1). However, there are no indications that the isotopes from these specimens deviate from the others. The *Uvigerina* sp. specimens were generally well-preserved.

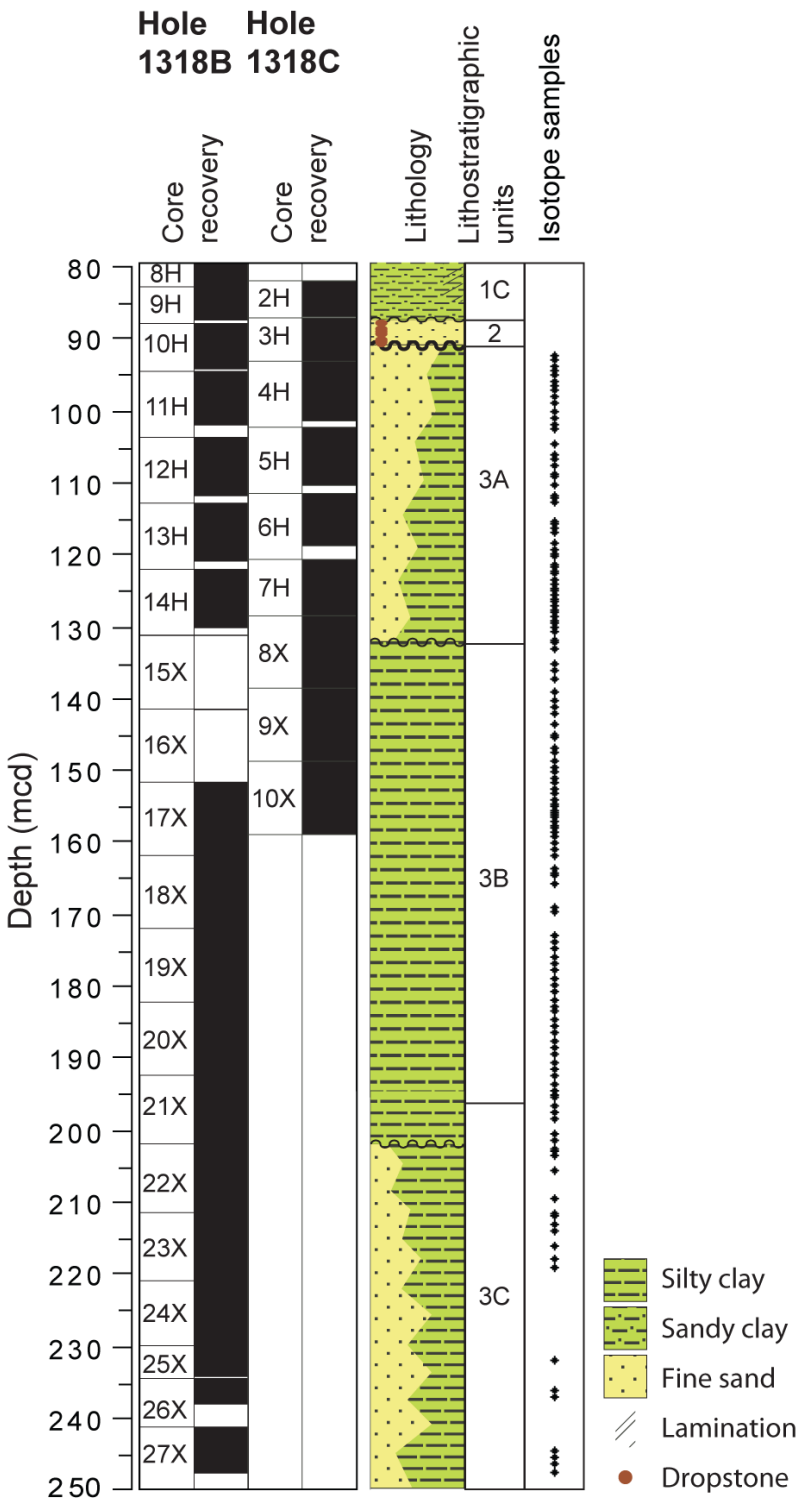

Figure 4.2: Core recovery (in black), lithology, lithostratigraphy of holes U1318B and U1318C and position of samples analyzed for stable isotopes.

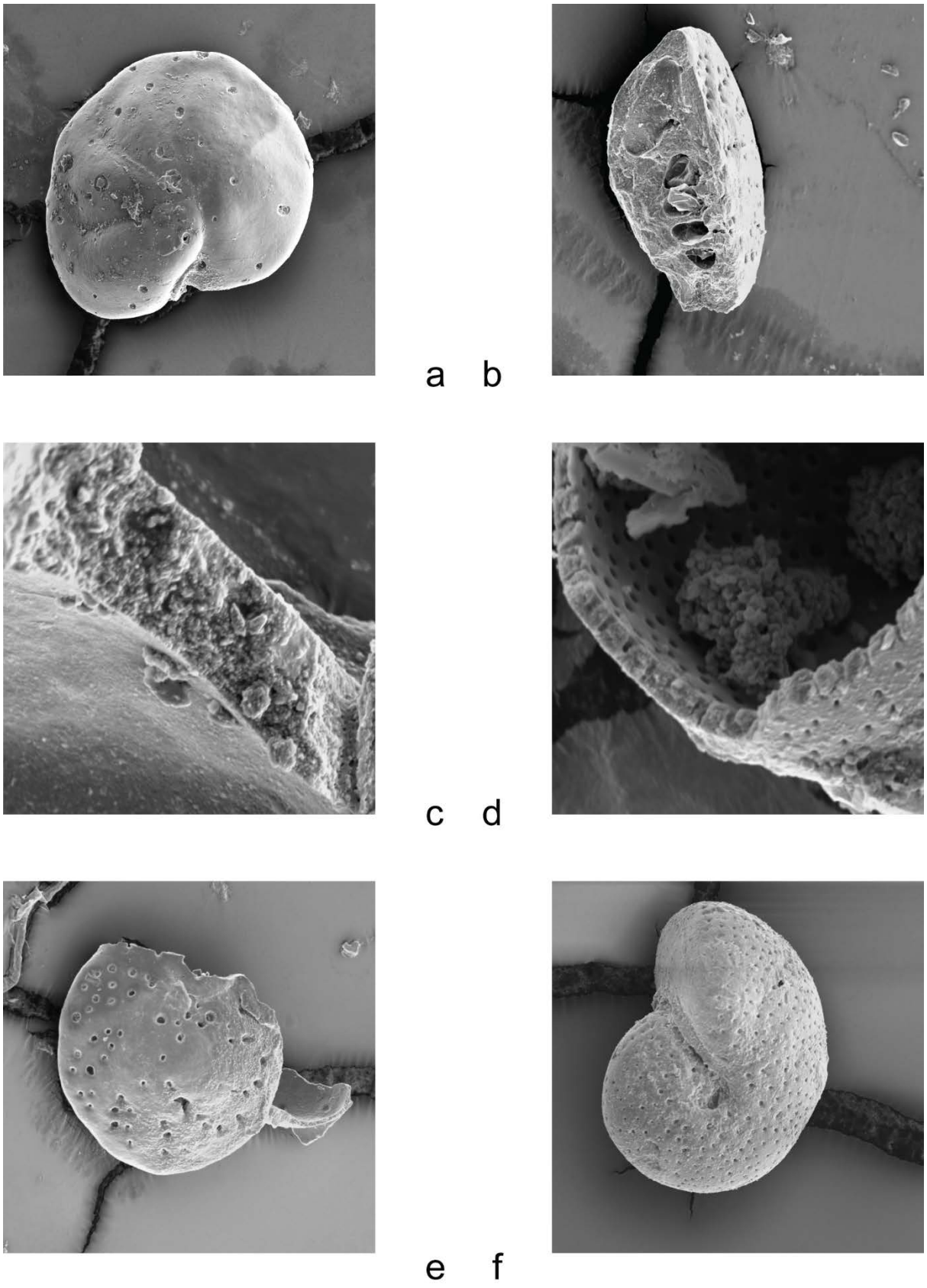

Plate 4.1: (a)-(d). Examples of well-preserved benthic foraminifera. (a) A well-preserved specimen of *Cibicidoides pachyderma*. (b) Lateral view of a broken specimen of *Cibicidoides pachyderma*, showing that the chambers are still open. (c) Detail of a wall of *Cibicidoides*, showing that there is no recrystallization on the walls. (d) Wall detail of a specimen of *Uvigerina* sp. showing open pores (e)-(f). Examples of less-well preserved benthic foraminifera. (e) Specimen of *Cibicidoides pachyderma* showing both good and bad preservation; left side shows no signs of recrystallization, whereas the right side is affected. (f) Specimen of *Cibicidoides pachyderma* that is badly affected by recrystallization.

The $\delta^{18}O$ and the $\delta^{13}C$ stable isotope ratios were measured with a ThermoFinnigan Delta^{plus} XL Mass spectrometer at the Vrije Universiteit Brussel (VUB) in Belgium. This continuous flow isotope ratio mass spectrometer (CF-IRMS) is equipped with an automated ThermoFinnigan Kiel III carbonate preparation line. Accuracy corrections were made with an in-house standard called NCM. The analytical precision averages 0.031‰ (1σ) for $\delta^{13}C$ and 0.080‰ (1σ) for $\delta^{18}O$. All data (Supplementary Table 4.1) are reported against the Vienna Pee Dee Belemnite (VPDB) standard after calibration of the in-house standard with NBS-19. Duplicate measurements were carried out on eight samples. Stable oxygen isotope data are here used for stratigraphic purposes only.

3.3. Correction factors for isotopic measurements

The $\delta^{13}C$ and $\delta^{18}O$ measurements of modern benthic foraminifera often have a consistent offset from calcite precipitated in equilibrium, and between different species. This is considered a consequence of microhabitat preferences and vital effects (e.g. *Katz et al.*, 2003). Despite their different habitat, changes in the $\delta^{18}O$ value of *Cibicidoides pachyderma* and *Uvigerina* sp. are both expected to reflect the prevailing temperature and the $\delta^{18}O$ value of the seawater at the time of test precipitation. The $\delta^{18}O$ values are therefore assumed to correlate linearly. In 59 samples, both *Cibicidoides pachyderma* and *Uvigerina* sp. were analysed for stable isotopes. The $\delta^{18}O$ values of both species show a near 1:1 relation (see Figure 4.3a). The linear regression resulted in the following equation: $\delta^{18}O_{Cibicidoides\ pachyderma} = 0.984 * \delta^{18}O_{Uvigerina\ sp.} - 0.296‰$ with a coefficient of determination (R^2) of 0.94 and a prediction error of 0.096‰ (1σ, root mean square error of prediction). This good correlation confirms that the $\delta^{18}O$ value of *Uvigerina* sp. can predict the $\delta^{18}O$ value of *Cibicidoides pachyderma.* The equation can be simplified with the assumption of a slope of 1, which results in the formula: $\delta^{18}O_{Cibicidoides\ pachyderma} = \delta^{18}O_{Uvigerina\ sp.} - 0.311‰$ with a prediction error of 0.097‰ (1σ, root mean square error of prediction). This prediction error is considered a consequence of the average analytical precision of 0.080‰. The good correlation furthermore suggests that the moderate preservation of some *Cibicidoides pachyderma* specimens only has a minor or an insignificant impact on the measured $\delta^{18}O$ values in this study. On the other hand, there is a weaker correlation for $\delta^{13}C$ between *Cibicidoides pachyderma* and *Uvigerina* sp. (see Figure 4.3b). The linear regression resulted in the equation: $\delta^{13}C_{Cibicidoides\ pachyderma} = 0.692 * \delta^{13}C_{Uvigerina\ sp.} + 1.137‰$ with a coefficient of determination (R^2) of 0.52 and a prediction error of 0.170‰ (1σ, root mean square error of prediction). This lower correlation cannot be considered a consequence of preservation since $\delta^{13}C$ has been demonstrated to be more robust to recrystallization than $\delta^{18}O$ (e.g. *Sexton et al.*, 2006). The $\delta^{13}C$ values of *Uvigerina* sp. are on average 1.076‰ more depleted than the $\delta^{13}C$ values of *Cibicidoides pachyderma*. This is likely the result of the infaunal habitat of *Uvigerina* sp. Similar offsets of ca. 0.9‰ between *Uvigerina* and *Cibicidoides* were found by *Shackleton and Hall* (1984) and *Shackleton et al.* (1984). The lower $\delta^{13}C$ correlation between both taxa is suggested to be a result of the variation of the $\delta^{13}C_{DIC}$ pore water gradient with time and the possible migration of the infaunal species within the sediment. For correlation of globally recognizable $\delta^{13}C$ maxima however this should be of no consequence.

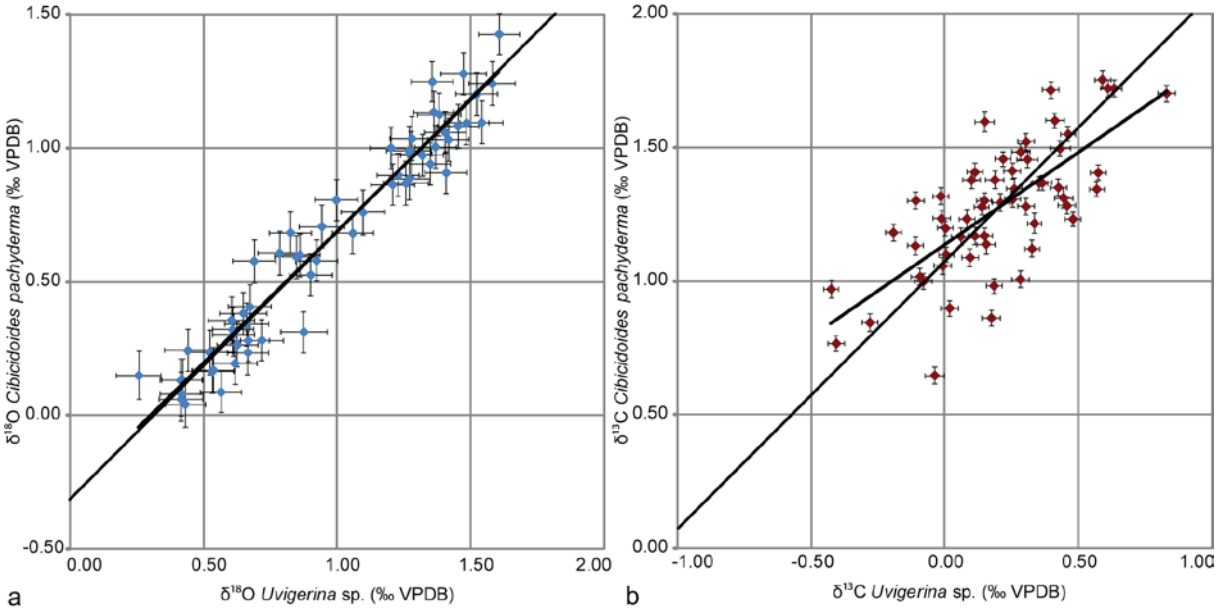

Figure 4.3: Correlation between uncorrected stable isotope measurements of *Cibicidoides pachyderma* and *Uvigerina* sp.. (a) Correlation of $\delta^{18}O$. The correlation between the two species is $\delta^{18}O_{Cibicidoides\ pachyderma} = 0.984*\delta^{18}O_{Uvigerina\ sp.} - 0.296‰$, R^2 is 0.94, prediction error is 0.096‰ (1σ, root mean square error of prediction). (b) Correlation of $\delta^{13}C$. The correlation between the two species is $\delta^{13}C_{Cibicidoides\ pachyderma} = 0.692*\delta^{13}C_{Uvigerina\ sp.} + 1.137‰$, R^2 is 0.5172, prediction error is 0.170‰ (1σ, root mean square error of prediction). Error bars depict 1 standard deviation (1σ).

3.4. Isotope Stratigraphy

Woodruff and Savin (1991) demonstrated that specific events in the benthic $\delta^{18}O$ and $\delta^{13}C$ isotope records from the Antarctic, Atlantic, Indian and Pacific Oceans could be correlated. They defined seven $\delta^{13}C$ maxima (CM 1–7) and positive or negative $\delta^{18}O$ excursions (A–G). They 'relied heavily' (*Woodruff and Savin,* 1991, p. 762) on the high-resolution isotope record of DSDP Site 574 in the Pacific Ocean to define distinct isotope features. Therefore, we correlate our $\delta^{13}C$ and $\delta^{18}O$ records of IODP Site U1318 (Porcupine Basin) with the isotopic records of DSDP Site 574 composed of data of *Pisias et al.* (1985), *Shackleton* (unpublished data, 1985, as tabulated by *Woodruff and Savin* (1989)) and *Woodruff and Savin* (1989, 1991), using the terminology of *Woodruff and Savin* (1991), plotted against depth because the initial data was plotted against depth and to avoid problems with different versions of time scales. Furthermore, we include a correlation with IODP Site U1338 in the eastern equatorial Pacific using a recent high-resolution stable isotope study with an astronomically-tuned time scale by *Holbourn et al.* (2014). However, the isotope stratigraphy of *Woodruff and Savin* (1991) is not calibrated against magnetostratigraphy, a correlative tool that is available in the Porcupine Basin (*Louwye et al.,* 2008). Therefore we have chosen to additionally compare the $\delta^{18}O$ against the Mi-(Miocene isotope) zonation of *Miller et al.* (1991, 1996, 1998) using the updated ages of *Boulila et al.* (2011). The base of these Mi-zones, or Mi-events, is defined by the maximum $\delta^{18}O$ value of one of the originally nine prominent positive $\delta^{18}O$ excursions, possibly related to periods of cryosphere expansion (*Miller et al.,* 1991). By linking the isotope events of *Woodruff and Savin* (1991) to those of *Miller et al.* (1991, 1996, 1998) we can link our isotope stratigraphy to the correct magnetochron.

4. Results

The isotope stratigraphic correlation between the three compared records is straightforward, despite the fact that IODP Site U1338 and DSDP Site 574 are located in the Pacific Ocean and that IODP Site U1318 is located in the North Atlantic (Figure 4.4). If we compare the absolute isotopic $\delta^{18}O$ and $\delta^{13}C$ values between the three records, the $\delta^{18}O$ values from IODP Site U1318 are approximately 1.5‰ lower than the $\delta^{18}O$ values of IODP Site U1338 and DSDP Site 574 (Figure 4.4). It is assumed that the significantly more depleted $\delta^{18}O$ values in the Porcupine Basin record are mainly a reflection of the warmer temperature conditions as a consequence of the shallower water depth. The absolute $\delta^{13}C$ values of IODP Sites U1318, U1338 and DSDP Site 574 are remarkably similar.

4.1. Determination of isotope stratigraphic tie-points

Discussed from major to minor events, the most prominent event in the record is $\delta^{18}O$ event E, which is defined as an abrupt $\delta^{18}O$ increase of approximately 0.5‰. Event E is present in all three records and facilitates further comparison and aids in the recognition of other isotope stratigraphic tie-points (Figure 4.4). At Site U1318 event E can be observed from 143.51–133.17 mcd. This event is immediately followed by CM6, subdivided into CM6a and CM6b, at 131.81 and 126.61 mcd respectively. CM6 is coeval with the base of Mi-zone Mi-3, tied to magnetosubchron C5ABr (*Miller et al.*, 1991). The $\delta^{18}O$ maximum that will be the base of Mi-3, at 128.11 mcd, lies just within an interval of normal polarity. According to the age model of *Quaijtaal et al.* (2014) this is C5AAn (Figure 4.5), but because of the $\delta^{18}O$ maximum corresponding to Mi-3 it is more likely that this normal subchrons represents C5ABn. Chron C5ABr then lies just below Mi-3 in our record, within the undefined polarity interval from 154.85–130.02 mcd.

Working downcore, the next stratigraphic tie-point should be CM5. In our record CM5, at ca. 149.7 mcd, is less pronounced than in the records of DSDP Site 574 and IODP Site U1338 (Figure 4.4). A problem with correlating CM5 is that there appear to be three peaks with increased $\delta^{13}C$ values around the interval that *Woodruff and Savin* (1991) indicated. The middle peak is highest at DSDP Site 574, whereas in IODP Sites U1318 and U1338 the uppermost peak is heaviest. Therefore these peaks are tentatively named 5A, 5B and 5C, respectively (155.05, 148.51 and 145.51 mcd at Site U1318). However, these peaks may also be artefacts of the different resolution between the three records. For depth correlation the average depth/age value of the three peaks was used.

The next carbon isotope maximum at Site U1318 downcore, CM4, is located at 203.55 mcd (Figure 4.4). CM4 appears to be more pronounced at the Porcupine Basin in comparison to the other two records. This $\delta^{13}C$ maximum is higher than CM6, which is not the case in the Pacific records.

The $\delta^{18}O$ event D is less easily characterized. The definition of *Woodruff and Savin* (1991) states that it is a period of low $\delta^{18}O$ between CM4, and CM5 that is longer in duration than events A–C.

Figure 4.4: Stable benthic oxygen ($\delta^{18}O$) and carbon isotopes ($\delta^{13}C$). Oxygen isotopes are represented by blue squares, carbon isotopes by red dots. Oxygen isotope events A-F of *Woodruff and Savin* (1991) are indicated next to the $\delta^{18}O$ curve, carbon maxima of *Woodruff and Savin* (1991) are indicated next to the $\delta^{13}C$ curve. The red dashed line is the CM line of 1.6‰ from *Woodruff and Savin* (1991) as set from Site 574. (a) Isotopes from DSDP Site 574 versus depth (*Pisias et al.*, 1985; Shackleton, unpubliched data tabulated by Woodruff & Savin, 1989; *Woodruff and Savin*, 1989, 1991). $\delta^{13}C$ values were not corrected for vital effects. (b) Isotopes from IODP Site U1318 versus depth. Dark blue squares and dark red dots are uncorrected measurements on *Cibicidoides pachyderma*, light blue crosses and red plusses are corrected measurements on *Uvigerina* sp. using the following formulas: $\delta^{18}O_{Cibicidoides\ pachyderma} = 0.984*\delta^{18}O_{Uvigerina\ sp.} - 0.296‰$; $\delta^{13}C_{Cibicidoides\ pachyderma} = 0.692*\delta^{13}C_{Uvigerina\ sp.} + 1.137‰$. (c) Isotopes from IODP Site U1338 versus age. Data from *Holbourn et al.* (2014). $\delta^{13}C$ values were not corrected for vital effects.

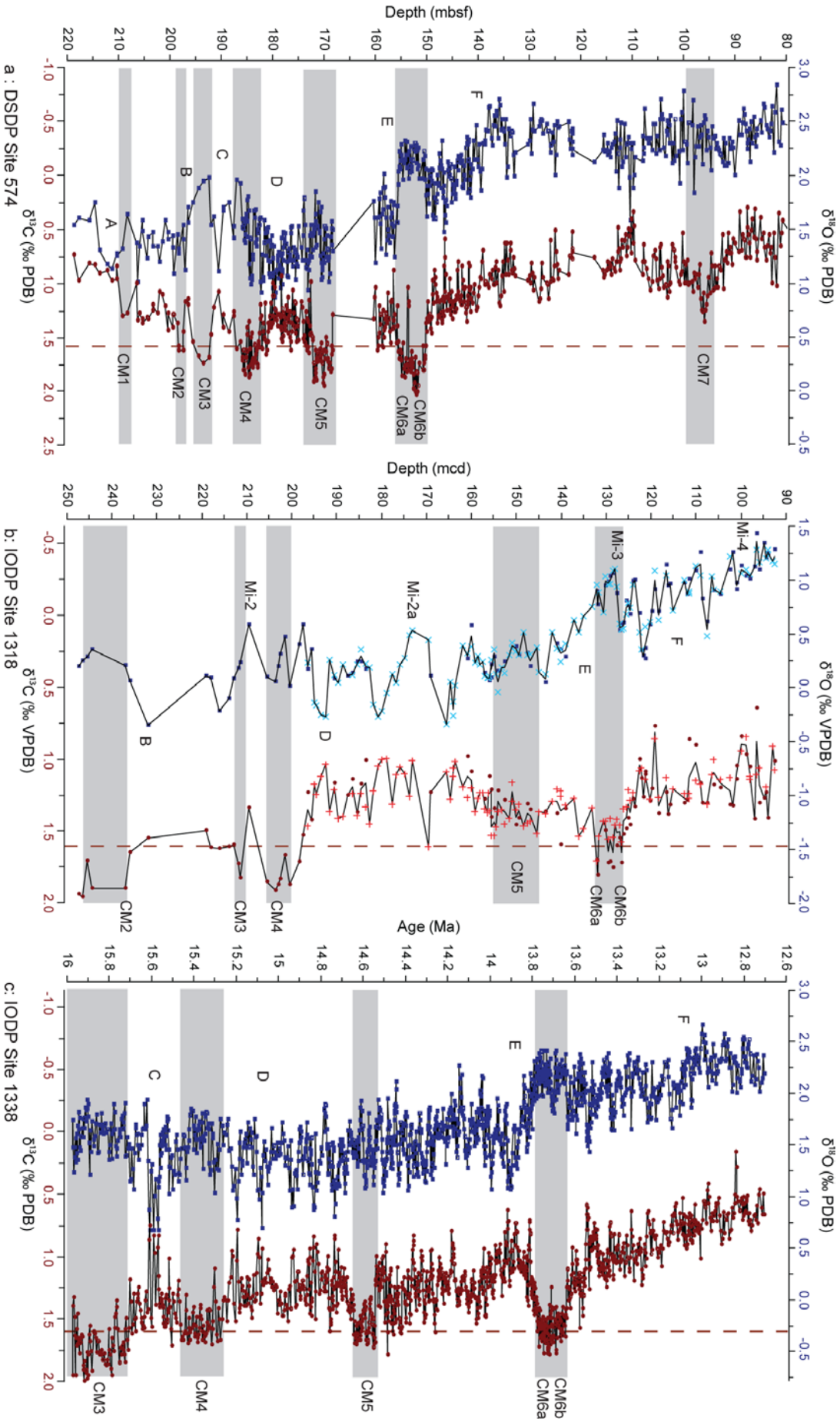
a : DSDP Site 574
Depth (mbsf)
δ13C (‰ PDB)
δ18O (‰ PDB)
A
B
C
D
E
F
CM1
CM2
CM3
CM4
CM5
CM6b
CM6a
CM7
b: IODP Site 1318
Depth (mcd)
δ13C (‰ VPDB)
δ18O (‰ VPDB)
Mi-2
Mi-2a
Mi-3
Mi-4
Age (Ma)
c: IODP Site 1338

However, the interval they appoint to D in their table 11 is rather short. This interval is the first interval of lower $\delta^{18}O$ values, but at both Sites 574 and U1338 five peaks with decreased values follow.
At Site U1318 three intervals with lighter values can be found, of which we defined the first as the D-event at 195.03–192.51 mcd (Figure 4.4). After this lighter interval at Site U1338, at ca. 14.7 Ma, a decrease in the amplitude of the $\delta^{18}O$ cycli can be observed (*Holbourn et al.*, 2014). This tipping point can also be identified at IODP Site U1318, around ~162 mcd, where the $\delta^{18}O$ minima of the $\delta^{18}O$ cycli decrease, from -0.3‰ to 0.0‰, while the $\delta^{18}O$ maxima remain around 0.5‰.

The identification of CM3 is not straightforward. At first the heavy values at around 250–240 mcd were thought to be CM3. However, CM3 is contemporaneous with the base of Mi-zone Mi-2, tied to the base of magnetosubchron C5Br (*Miller et al.*, 1991). According to the age model of *Quaijtaal et al.* (2014) the initial interval for CM3 should correspond to subchron C5Cr.3n, and the base of C5Br should be at 184.15 mcd (Figure 4.5). However, at the latter depth no clear $\delta^{18}O$ maximum and corresponding carbon isotope maximum can be observed. Another carbon isotope maximum can be observed just directly below CM4 at 211.57 mcd. This maximum is close to a $\delta^{18}O$ maximum at 209.55 mcd, and just below an interval of reversed polarity. Although this does not fit the description of Mi-2 entirely, the resolution of the isotope records in this interval is somewhat lower than higher up the composite record and it is to be expected that the highest maxima lie within the non-sampled part. Therefore we tentatively appoint a depth of 211.57 mcd to CM3 and a depth of 209.55 mcd to Mi-2. There are no decreased $\delta^{18}O$ values between CM3 and CM4, implying that isotope event C of *Woodruff and Savin* (1991) is not present in the Porcupine Basin. This event however is 'often exhibited as a single data point' (*Woodruff and Savin*, 1991) and it might therefore be missing due to the lower sampling resolution in this part of the composite.

Due to the successful identification of Mi-zones Mi-2 and Mi-3 zone Mi-2a could also be identified. According to *Miller et al.* (1998) zone Mi-2a is tied to the base of magnetosubchron C5ADr. The fourth reversal above 207.15 mcd (base C5Br according to the location of Mi-2) is at 166.25 mcd (Figure 4.4). There are two $\delta^{18}O$ maxima surrounding this point, at 159.98 mcd and at 173.08 mcd. Both points are located within an interval of normal polarity, contradictory to the indication of *Miller et al.* (1998). We have tentatively placed Mi-2a at 173.08 mcd because of the slightly heavier $\delta^{18}O$ values.

The remaining CM at 237.1 mcd in IODP Site U1318 is CM2 (Figure 4.4). It is plausible that the low $\delta^{18}O$ value at approximately 232.045 mcd then corresponds to $\delta^{18}O$-event B, although this depth should be treated with care since this is a single measurement and the resolution between 220 mcd and 240 mcd is very low.

The remaining $\delta^{18}O$ event of *Woodruff and Savin* (1991) is event F. This event is coeval with the base of Mi-zone Mi-4 at the base of (undivided) C5Ar (*Miller et al.*, 1991). Several $\delta^{18}O$ maxima are present above the base of zone Mi-3 at the Porcupine Basin. The fourth reversal above the top of C5ABr/base of C5ABn (as indicated by the location of Mi-3) should mark the base of C5Ar, the location of Mi-4 according to *Miller et al.* (1991, 1998), and is located at 116.51 mcd (Figure 4.4, 4.5). Around that depth a smaller $\delta^{18}O$ maximum can be observed. However, according to (*Holbourn et al.*, 2005, 2007, 2013b) there is an interval of dominance of the 100 kyr eccentricity cycle between 13.5–13.1 Ma, which at the Porcupine Basin should be between ~128 and 102 mcd (13.1–12.5 Ma according to *Quaijtaal et al.* (2014); A. Holbourn, pers. comm., 2016). The $\delta^{18}O$ maximum at the end of this eccentricity-dominated interval should mark Mi-4, and we place the base of zone Mi-4 at 101.95 mcd. Isotope event F spans 121.76–109.11 mcd. Event F is defined as the start of an episode of maximum mid-Miocene $\delta^{18}O$ values (*Woodruff and Savin*, 1991). It also corresponds to one of the major

incremental steps of increasing $\delta^{18}O$ values and decreasing amplitude in the $\delta^{18}O$ variability recognized by (*Holbourn et al.*, 2007). Furthermore, the relative increase in $\delta^{18}O$ maxima after $\delta^{18}O$ event E and F is approximately 0.3‰ in all three records.

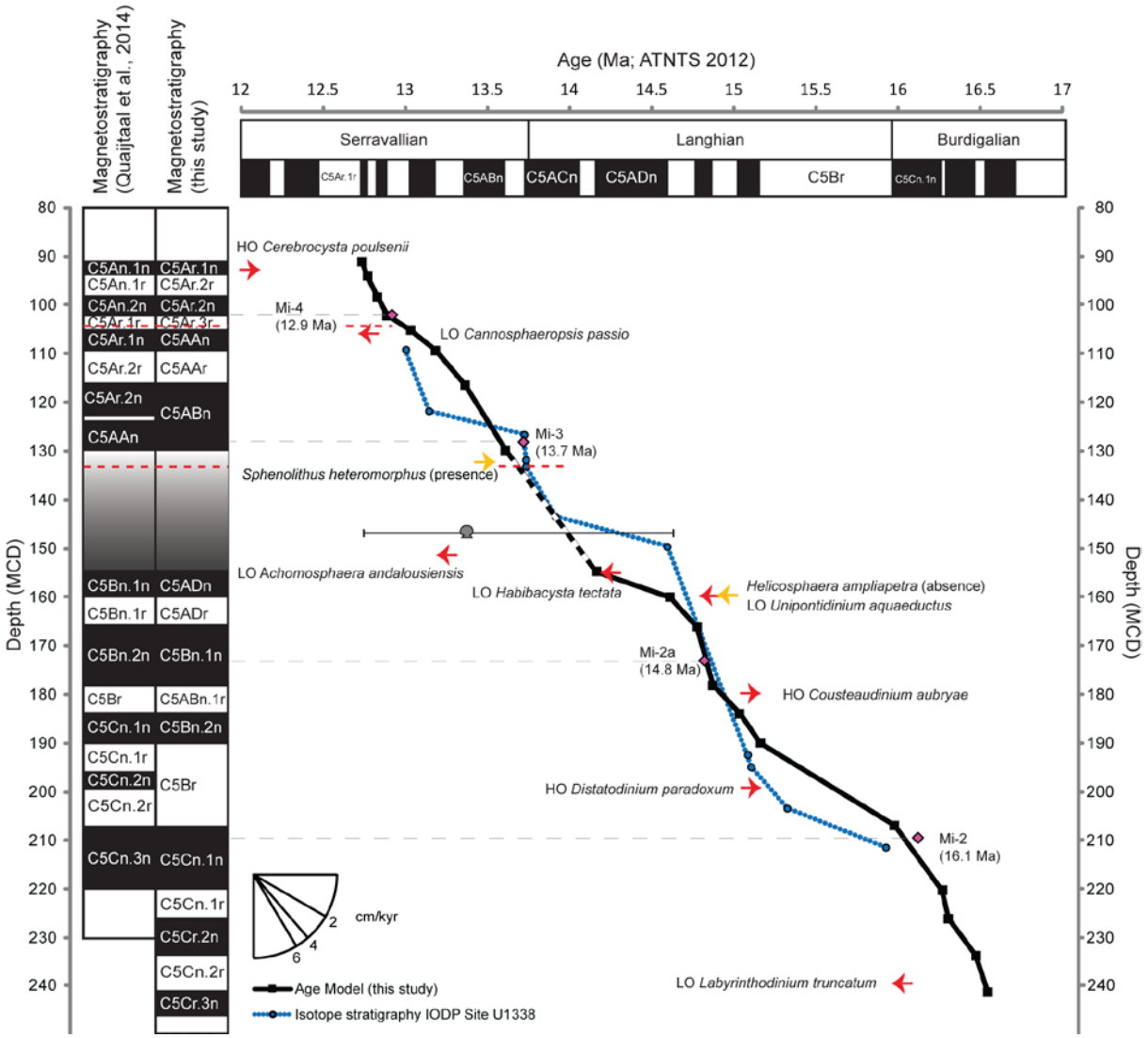

Figure 4.5: Updated age model for IODP Site U1318 (in black). In blue the tie-points based on the isotope stratigraphy of Site 1338. Pink diamonds represent the Mi-events versus depth at Site U1318 and ages from *Boulila et al.* (2011), connected to the magnetostratigraphy at Site U1318 with grey dashed lines. The black dashed line indicates the interval where ages were interpolated because of the uncertainty in the magnetostratigraphy. Black squares are magnetostratigraphic tie-points, red dashed lines indicate hiatuses, red arrows indicate dinocyst biostratigraphic tie-points, yellow arrows indicate nannoplankton presence or absence, grey mollusc indicates Sr-isotopic age from *Kano et al.* (2007).

4.2. Revision of the age model

The astronomically tuned isotopic events recognized at IODP Site 1338 provide a first approximate age for the corresponding events at IODP Site U1318 (see Table 4.1). According to the isotope stratigraphy, the record at IODP site U1318 encompasses a time interval from somewhat older than 16 Ma to somewhat younger than 13 Ma (Figures 4.4, 4.5), in contrast to the age model of *Quaijtaal et al.* (2014) that suggests a time interval from approximately 17.8 Ma to 12.0 Ma. The approximate ages provided

by the isotope stratigraphy correspond better with three biostratigraphic dinocyst ages in the lower part of the record (Figure 4.5). The highest occurrence of *Cousteaudinium aubryae* and *Distatodinium paradoxum* were calibrated against the top of magnetosubchron C5Br (*de Verteuil and Norris*, 1996), now at an age of 15.16 Ma (ATNST 2012). The lowest occurrence of *Labyrinthodinium truncatum* at 237 mcd, in the bottom part of the record, is correlated against the Burdigalian–Langhian boundary according to (*Williams et al.*, 2004). This boundary is currently dated at 15.97 Ma, supported by a Sr-isotope dating of <16.6 Ma by *Dybkjær and Piasecki* (2010).

The first direct tie-points for magnetostratigraphy were provided by the base of Mi-zones (Table 4.2, Figure 4.5). The identification of the base of Mi-2 led to the interpretation of the reversal at 207.15 mcd as the boundary between magnetosubchrons C5Cn.1n and C5Br. Mi-2a provided the identification of the boundary between C5Bn.1n and C5ADr at 166.25 mcd. This indicates that the age model of *Quaijtaal et al.* (2014) is one magnetochron too old during Mi-2a and two magnetochrons too old during Mi-2. Above the undefined polarity interval from 130.02–154.85 mcd we can identify the boundary between C5ABr and C5ABn at 130.02 mcd due to the position of Mi-3 at 128.11 mcd. The boundary between C5Ar.2n and C5Ar.3r could be identified because of Mi-4. The age model of *Quaijtaal et al.* (2014) is one magnetochron too young for the interval spanning Mi-3, and two magnetochrons too young during Mi-4.

Table 4.1
Depths and ages of the isotope stratigraphic events of *Woodruff and Savin* (1991) for DSDP Site 574, IODP Site U1318 and IODP Site 1338.

Selected Isotope Stratigraphy Events (*Woodruff and Savin*, 1991)	**DSDP Site 574**	**IODP Site U1338**		**IODP Site U1318**	
	Depth (mbsf)	Depth (mcd)	Age (Ma)	Depth (mcd)	Age (Ma, ATNTS 2012)
CM1	209.31	N/A	N/A	N/A	N/A
CM2	197.4	N/A	N/A	237.085	16.50
CM3	193.46	433.56	15.92	211.57	16.07
CM4	184.71	414.67	15.32	203.55	15.80
CM5A	172.11	395.63	14.62	155.05	14.18
CM5B	170.01	394.13	14.58	148.51	14.02
CM5C	168.71	392.98	14.55	145.51	13.95
CM5 (average)	170.28	394.25	14.59	149.69	14.05
CM6A	154.31	366.13	13.73	131.81	13.65
CM6B	152.01	365.58	13.72	126.61	13.55
CM7	95.89 (?)	N/A	N/A	N/A	N/A
δ^{18}O Event A	213.71–210.31	N/A	N/A	N/A	N/A
δ^{18}O Event B	196.97	N/A	N/A	232.045	16.43
δ^{18}O Event C	190.55	424.84–423.84	15.61–15.57	N/A	N/A
δ^{18}O Event D	179.91–179.37	409.60–409.00	15.10–15.08	195.03–192.51	15.39–15.27
δ^{18}O Event E	156.31–155.31	373.09–366.33	13.91–13.73	143.51–133.17	13.91–13.68
δ^{18}O Event F	138.43–137.82	345.71–339.58	13.14–13.0	121.76–109.11	13.46–13.17

The combination of offsets between the different magnetochrons and the differential offsets between the Mi-events indicate that a simple shift in magnetochrons would not provide a solution. Therefore we have carefully studied the inclination data of Site U1318. From ca. 160 mcd downwards the divergence between the bio- and isotope stratigraphic tie-points and the age model of *Quaijtaal et al.* (2014) becomes largest. When re-studying the inclination data it appeared that the signal of the discrete samples of *Louwye et al.* (2008) in the interval between 190.15 and 207.15 mcd is quite irregular (see their figure 8). *Louwye et al.* (2008) interpreted this interval as three magnetosubchrons: C5Bn.1r, C5Bn.2n and C5Br. The interpretation of C5Bn.2n is based on two discrete measurements. However, the surrounding measurements are relatively scattered whereas in most subchrons the measurements tend to cluster together. We therefore have reinterpreted this interval as being one magnetosubchron: C5Br. This reinterpretation is compatible with the isotope stratigraphy and the longer duration of magnetosubchron C5Br fits better with the sediment thickness (17 m). Therefore, from the base of the composite record up to 207.15 mcd the magnetostratigraphy was shifted by two chrons toward a younger age; from 190.15 up to 154.85 mcd age was shifted one chron upward.

The interval between 154.85 and 130.02 mcd proves to be more difficult due to the lack of discrete samples, as well as the hiatus at 133.2 mcd. Therefore we have linearly interpolated between the two assigned reversals encompassing this interval.

For the interval from 130.02 mcd to the top of the composite record we used the same approach as in the interval below 154.85 mcd. Re-evaluation of the inclination data showed that the short reversed interval between 124.32–122.81 mcd is misinterpreted. The discrete measurements show no sign of any reversals, and most on-board measurements point towards a normal polarity. Therefore we interpret the interval between 130.02–116.51 mcd as one instead of three magnetosubchrons. Aided by the location of the Mi-events and their corresponding magnetosubchrons, from 130.02–116.51 mcd age was shifted one magnetochron toward older age, and from 116.15 mcd to the top of the composite record age was shifted two magnetochrons toward older age. This implies that the interval between 154.85 and 130.02 mcd contains three magnetosubchrons (Figure 4.5).

An overview of all tie-points can be found in Table 4.3, a visualisation of the new age model is displayed in Figure 4.5.

Table 4.2

Ages, corresponding magnetosubchrons and depths of the Mi-zones of *Miller et al.* (1991, 1998). First ages and magnetosubchrons according to *Boulila et al.* (2011) and *Miller et al.* (1991, 1998), following depths, ages and magnetosubchrons according to this study.

Mi-zone	Age (Ma)	Magnetosubchron	Depth (mcd)	Age (Ma; ATNTS 2012)	Magnetosubchron
	(*Boulila et al.*, 2011)	(*Miller et al.*, 1991, 1998)	(Site U1318)	(Site U1318)	(Site U1318)
Mi-4	12.9	base C5Ar	101.95	12.88	base C5Ar.2n
Mi-3	13.7	C5ABr	128.11	13.57	base C5ABn
Mi-2a	14.8	base C5ADr	173.08	14.83	C5Bn.1n
Mi-2	16.1	base C5Br	209.55	16.03	top C5Cn.1n

5. Discussion and conclusions

With the aid of stable isotope stratigraphy we have been able to refine the age model for IODP Site U1318. The sampled interval now encompasses an age between 12.75–16.60 Ma; the average sampling resolution of our stable isotope record with the new age model is ~29 ka. The estimated duration of the hiatus from 104.31–104.60 mcd is estimated at ca. 32 ka. Due to the uncertainties in the magnetostratigraphy from 154.85 to 130.02 mcd the duration of the hiatus at 133.20 mcd cannot be determined and the model was linearly interpolated up- and downwards.

Sedimentation rates vary between ~1.2–16.9 cm/ka. The record can roughly be divided into five sections. The first section, between 241.45–207.15 mcd, has an average sedimentation rate of 6.03 cm/ka and ends shortly after Mi-2. Sedimentation rates decrease to 2.6 cm/ka on average between 207.5–178.35 mcd. From 178.35–160.15 mcd rates increase to ~6.9 cm/ka. For the fourth section (160.15–130.02 mcd) the average sedimentation of ca. 3 cm/ka is a rough estimate, since the age model was linearly interpolated between two recognizable magnetic reversals. The last section (130.02–91.44 mcd) has relatively constant sedimentation rates of ~4.45 cm/ka.

Table 4.3
Magnetostratigraphic and biostratigraphic tie-points for Site U1318. Tie-points in bold are used to generate the age model.

Bio- /Magnetostratigraphic event	Age (Ma)	Site	Palaeomagnetic interpretation		Reference for age
			Depth (mbsf)	Depth (mcd)	
Top C5An.1n	**12.049**		N/A	N/A	**ATNTS 2012**
HO *Cerebrocysta poulsenii* (*Quaijtaal et al.*, 2014)	12.1	1318B	87.795	92.735	*Schreck et al.*, 2012
Bottom C5An.1n	**12.174**		N/A	N/A	**ATNTS 2012**
Top C5An.2n	**12.272**	**1318B**	N/A	N/A	**ATNTS 2012**
Bottom C5An.2n	**12.474**	**1318B**	N/A	N/A	**ATNTS 2012**
LO *Cannosphaeropsis passio* (*Quaijtaal et al.*, 2014)	12.73	1318B	101.565	105.875	*Hilgen et al.*, 2012
Top C5Ar.1n	**12.735**	**1318B**	**86.2**	**91.14**	**ATNTS 2012**
Bottom C5Ar.1n	**12.77**	**1318B**	**89.1**	**94.04**	**ATNTS 2012**
Top C5Ar.2n	**12.829**	**1318C**	**94**	**98.43**	**ATNTS 2012**
Bottom C5Ar.2n	**12.887**	**1318C**	**97.8**	**102.23**	**ATNTS 2012**
Top Hiatus 1				**104.31**	**Linear interpolation**
Bottom Hiatus 1				**104.60**	**Linear interpolation**
Top C5AAn	**13.032**	**1318C**	**99.1**	**105.2**	**ATNTS 2012**
Bottom C5AAn	**13.183**	**1318B**	**103.3**	**109.4**	**ATNTS 2012**
LO *Achomosphaera andalousiensis* (unpublished)	13.2	1318C	145.5	151.405	*Hilgen et al.*, 2012
Top C5ABn	**13.363**	**1318B**	**110.8**	**116.51**	**ATNTS 2012**
Sr-dated mollusc fragment	(12.74) 13.381 (14.624)	1318C	140.83	146.74	*Kano et al.*, 2007
Presence *Sphenolithus heteromorphus* (*Quaijtaal et al.*, 2014)	>13.52	1318C	127.29	131.81	*Hilgen et al.*, 2012
Bottom C5ABn	**13.608**	**1318B**	**125.5**	**130.02**	**ATNTS 2012**
Top Hiatus 2				**133.20**	
Bottom Hiatus 2				**133.20**	
Top C5ACn	13.739		N/A	N/A	ATNTS 2012
Bottom C5ACn	14.07		N/A	N/A	ATNTS 2012
Top C5ADn	**14.163**	**1318B**	**148.7**	**154.85**	**ATNTS 2012**
LO *Habibacysta tectata* (unpublished)	14.2	1318B	149.05	155.1	*Schreck et al.*, 2012
Bottom C5ADn	**14.609**	**1318B**	**154.2**	**160.15**	**ATNTS 2012**
Top C5Bn.1n	**14.775**	**1318B**	**160.1**	**166.25**	**ATNTS 2012**
LO *Unipontidinium aquaeductus* (unpublished)	14.8	1318C	153.765	159.815	*Dybkjær and Piasecki*, 2010
Bottom C5Bn.1n	**14.87**	**1318B**	**172.2**	**178.35**	**ATNTS 2012**
Absence *Helicosphaera ampliaperta* (Quaijtaal et al., 2014)	<14.91	1318C	153.7	159.65	*Hilgen et al.*, 2012
Top C5Bn.2n	**15.032**	**1318B**	**178**	**184.15**	**ATNTS 2012**
Bottom C5Bn.2n	**15.16**	**1318B**	**184**	**190.15**	**ATNTS 2012**
HO *Cousteaudinium aubryae* (unpublished)	15.16	1318B	173.72	179.87	*de Verteuil and Norris*, 1996
HO *Distatodinium paradoxum* (*Louwye et al.*, 2008)	15.16	1318B	193.155	199.305	*de Verteuil and Norris*, 1996
LO *Labyrinthodinium truncatum* (*Louwye et al.*, 2008)	15.97	1318B	233.415	239.565	*Dybkjær and Piasecki*, 2010
Top C5Cn.1n	**15.974**	**1318B**	**201**	**207.15**	**ATNTS 2012**
Bottom C5Cn.1n	**16.268**	**1318B**	**214.3**	**220.45**	**ATNTS 2012**
Top C5Cn.2n	**16.303**	**1318B**	**220.1**	**226.35**	**ATNTS 2012**
Bottom C5Cn.2n	**16.472**	**1318B**	**227.8**	**233.95**	**ATNTS 2012**
Top C5Cn.3n	**16.543**	**1318B**	**235.3**	**241.45**	**ATNTS 2012**

The Porcupine Basin benthic foraminiferal stable isotope records show clear imprints of globally recognized stable isotope events, have relatively large temporal range and will therefore be significant for further interbasinal comparisons and correlations with surface ocean parameters to elucidate triggers and drivers for Miocene climatic transitions. Some of these stable isotope events were used as guidelines for the correct identification of palaeomagnetic reversals. The other points were compared to the astronomically-tuned high-resolution record from IODP Site 1338 and used to improve the age model for IODP Site U1318 further. Furthermore, the oxygen isotope measurements on benthic foraminifer species *Cibicidoides pachyderma* and *Uvigerina* sp. correlate very well. Measurements on *Uvigerina* sp. can be converted to *Cibicidoides* using the following formula: $\delta^{18}O_{Cibicidoides\ pachyderma} = 0.984*\delta^{18}O_{Uvigerina\ sp.} - 0.296‰$ ($R^2 = 0.94$), prediction error 0.096‰ (1σ, root mean square error of prediction).

6. Author contributions

SL and THD designed the research project. ST prepared samples for benthic foraminiferal analysis, picked foraminifera and prepared the samples for measurements. The samples were analysed at the lab of PC. WQ did all the interpretation of the data, writing of the paper and the preparation of the figures.

7. Acknowledgements

The data used for this study can be found in Supplementary Table 4.1. The samples for this study were provided by the Integrated Ocean Drilling Program. This work was supported by the Research Foundation-Flanders (FWO) under project number G.0179.11N. Ph.C. thanks the Hercules Foundation Flanders for support of the Stable Isotope facility. The advice of dr. An Holbourn on Miocene stable oxygen isotopes was very valuable for the improvement of the age model. Niels de Winter is thanked for his support during the isotopic measurements in Brussels. Walter Hale and Alex Wülbers kindly supported W.Q and S.L. during sampling at the Bremen Core Repository. The authors thank Dirk Munsterman and one anonymous reviewer for their useful comments to improve the manuscript.

8. References

Abels, H.A., Hilgen, F.J., Krijgsman, W., Kruk, R.W., Raffi, I., Turco, E., Zachariasse, W.J., 2005. Long-period orbital control on middle Miocene global cooling: Integrated stratigraphy and astronomical tuning of the Blue Clay Formation on Malta. Paleoceanography 20, PA4012.

Boulila, S., Galbrun, B., Miller, K.G., Pekar, S.F., Browning, J. V., Laskar, J., Wright, J.D., 2011. On the origin of Cenozoic and Mesozoic "third-order" eustatic sequences. Earth-Science Reviews 109, 94–112.

de Verteuil, L., Norris, G., 1996. Miocene dinoflagellate stratigraphy and systematics of Maryland and Virginia. Micropaleontology, supplement 42, 1–172.

Dybkjær, K., Piasecki, S., 2010. Neogene dinocyst zonation for the eastern North Sea Basin, Denmark. Review of Palaeobotany and Palynology 161, 1–29.

Expedition 307 Scientists, 2006. Site U1318, in: Ferdelman, T.G., Kano, A., Williams, T., Henriet, J.-P., the Expedition 307 Scientists (Eds.), Proceedings of the Integrated Ocean Drilling Program. Integrated Ocean Drilling Program Management International, Washington, D.C., pp. 1–57.

Flower, B.P., Kennett, J.P., 1994. The middle Miocene climatic transition: East Antarctic ice sheet development, deep ocean circulation and global carbon cycling. Palaeogeography, Palaeoclimatology, Palaeoecology 108, 537–555.

Fontanier, C., Jorissen, F.J., Michel, E., Cortijo, E., Vidal, L., Anschutz, P., 2008. Stable Oxygen and Carbon Isotopes of Live (Stained) Benthic Foraminifera From Cap-Ferret Canyon (Bay of Biscay). The Journal of Foraminiferal Research 38, 39–51.

Hilgen, F.J., Lourens, L.J., Van Dam, J.A., Beu, A.G., Boyes, A.F., Cooper, R.A., Krijgsman, W., Ogg, J.G., Piller, W.E., Wilson, D.S., 2012. Chapter 29 — The Neogene Period, in: Gradstein, F.M., Schmitz, J.G.O.D., Ogg, G.M. (Eds.), The Geologic Time Scale. Elsevier, Boston, pp. 923–978.

Holbourn, A., Kuhnt, W., Schulz, M., Erlenkeuser, H., 2005. Impacts of orbital forcing and atmospheric carbon dioxide on Miocene ice-sheet expansion. Nature 438, 483–487.

Holbourn, A., Kuhnt, W., Schulz, M., Flores, J.A., Andersen, N., 2007. Orbitally-paced climate evolution during the middle Miocene "Monterey" carbon-isotope excursion. Earth and Planetary Science Letters 261, 534–550.

Holbourn, A., Henderson, A.S., MacLeod, N., 2013a. A to V, in: Atlas of Benthic Foraminifera. Wiley-Blackwell, Oxford, UK, pp. 15–615.

Holbourn, A., Kuhnt, W., Frank, M., Haley, B.A., 2013b. Changes in Pacific Ocean circulation following the Miocene onset of permanent Antarctic ice cover. Earth and Planetary Science Letters 365, 38–50.

Holbourn, A., Kuhnt, W., Lyle, M., Schneider, L., Romero, O., Andersen, N., 2014. Middle Miocene climate cooling linked to intensifi cation of eastern equatorial Pacifi c upwelling. Geology 42, 19–22.

Jorissen, F.J., 2003. Benthic foraminiferal microhabitats below the sediment-water interface, in: Gupta, B.K. Sen (Ed.), Modern Foraminifera. Springer Netherlands, Dordrecht, pp. 161–179.

Kano, A., Ferdelman, T.G., Williams, T., Henriet, J.P., Ishikawa, T., Kawagoe, N., Takashima, C., Kakizaki, Y., Abe, K., Sakai, S., Browing, E.L., Li, X., Andres, M.S., Bjerager, M., Cragg, B.A., De Mol, B., Dorschel, B., Foubert, A., Frank, T.D., Fuwa, Y., Gaillot, P., Gharib, J.J., Gregg, J.M., Huvenne, V.A.I., Léonide, P., Mangelsdorf, K., Monteys, X., Novosel, I., O'Donnell, R., Rüggeberg, A., Samarkin, V., Sasaki, K., Spivack, A.J., Tanaka, A., Titschack, J., van Rooij, D., Wheeler, A., 2007. Age constraints on the origin and growth history of a deep-water coral mound in the northeast Atlantic drilled during Integrated Ocean Drilling Program Expedition 307. Geology 35, 1051–1054.

Katz, M.E., Katz, D.R., Wright, J.D., Miller, K.G., Pak, D.K., Shackleton, N.J., Thomas, E., 2003. Early Cenozoic benthic foraminiferal isotopes: Species reliability and interspecies correction factors. Paleoceanography 18, doi:10.1029/2002PA000798.

Louwye, S., Foubert, A., Mertens, K., Van Rooij, D., The IODP Expedition 307 Scientific Party, 2008. Integrated stratigraphy and palaeoecology of the Lower and Middle Miocene of the Porcupine Basin. Geological Magazine 145, 321–344.

McCorkle, D.C., Emerson, S.R., Quay, P.D., 1985. Stable carbon isotopes in marine porewaters. Earth and Planetary Science Letters 74, 13–26.

Miller, K.G., Wright, J.D., Fairbanks, R.G., 1991. Unlocking the Ice House: Oligocene–Miocene Oxygen Isotopes, Eustasy, and

Margin Erosion. Journal of Geophysical Research 96, 6829–6848.
Miller, K.G., Mountain, G.S., the Leg 150 Shipboard Party, Members of the New Jersey Coastal Plain Drilling Project, 1996. Drilling and Dating New Jersey Oligocene–Miocene Sequences: Ice Volume, Global Sea Level, and Exxon Records. Science 271, 1092–1095.
Miller, K.G., Mountain, G.S., Browning, J. V., Kominz, M., Sugarman, P.J., Christie-Blick, N., Katz, M.E., Wright, J.D., 1998. Cenozoic global sea level, sequences, and the New Jersey Transect: Results From coastal plain and continental slope drilling. Reviews of Geophysics 36, 569–601.
Moran, K., Backman, J., Brinkhuis, H., Clemens, S.C., Cronin, T.M., Dickens, G.R., Eynaud, F., Gattacceca, J., Jakobsson, M., Jordan, R.W., Kaminski, M., King, J., Koc, N., Krylov, A., Martinez, N., Matthiessen, J., McInroy, D., Moore, T.C., Onodera, J., O'Regan, M., Pälike, H., Rea, B., Rio, D., Sakamoto, T., Smith, D.C., Stein, R.R., St. John, K.E.K., Suto, I., Suzuki, N., Takahashi, K., Watanabe, M., Yamamoto, M., Farrell, J., Frank, M., Kubik, P.W., Jokat, W., Kristoffersen, Y., St John, K., Suto, I., Suzuki, N., Takahashi, K., Watanabe, M., Yamamoto, M., Farrell, J., Frank, M., Kubik, P.W., Jokat, W., Kristoffersen, Y., 2006. The Cenozoic palaeoenvironment of the Arctic Ocean. Nature 441, 601–605.
Pisias, N.G., Shackleton, N.J., Hall, M.A., 1985. Stable isotope and calcium carbonate records from hydraulic piston cored hole 574A: High-resolution records from the middle Miocene, in: Mayer, L., F, T. (Eds.), Initial Reports of the Deep Sea Drilling Project Vol. 85. U.S. Government Printing Office, Washington, pp. 735–748.
Quaijtaal, W., Donders, T.H., Persico, D., Louwye, S., 2014. Characterising the middle Miocene Mi-events in the Eastern North Atlantic realm: A first high-resolution marine palynological record from the Porcupine Basin. Palaeogeography, Palaeoclimatology, Palaeoecology 399, 140–159.
Schreck, M., Matthiessen, J., Head, M.J., 2012. A magnetostratigraphic calibration of Middle Miocene through Pliocene dinoflagellate cyst and acritarch events in the Iceland Sea (Ocean Drilling Program Hole 907A). Review of Palaeobotany and Palynology 187, 66–94.
Sexton, P.F., Wilson, P.A., Pearson, P.N., 2006. Microstructural and geochemical perspectives on planktic foraminiferal preservation: "Glassy" versus "Frosty." Geochemistry, Geophysics, Geosystems 7, Q12P19.
Sexton, P.F., Wilson, P.A., 2009. Preservation of benthic foraminifera and reliability of deep-sea temperature records: Importance of sedimentation rates, lithology, and the need to examine test wall structure. Paleoceanography 24, PA2208.
Shackleton, N.J., Hall, M.A., 1984. 16 . Oxygen and Carbon Isotope Stratigraphy of Deep Sea Drilling Project Hole 552a: Plio-Pleistocene Glacial History. Initial Reports of the Deep Sea Drilling Project 81, 599–609.
Shackleton, N.J., Hall, M.A., Boersma, A., 1984. Oxygen and carbon isotope data from Leg 74 foraminifers. Initial Reports of the Deep Sea Drilling Project 74, 599–612.
Shevenell, A.E., Kennett, J.P., 2004. Paleoceanographic change during the Middle Miocene climate revolution: an Antarctic stable isotope perspective. Geophysical Monograph Series 148, 1–18.
Snyder, S.W., Waters, V.J., 1984. Cenozoic Planktonic Foraminiferal Biostratigraphy of the Goban Spur Region, Deep Sea Drilling Project Leg 80, in: Graciansky, P.C. de, Poag, C.W., et al. (Eds.), Initial Reports of the Deep Sea Drilling Project Vol. 80. U.S. Government Printing Office, Washington, D.C., pp. 439–472.
Van Rooij, D., De Mol, B., Huvenne, V., Ivanov, M., Henriet, J.P., 2003. Seismic evidence of current-controlled sedimentation in the Belgica mound province, upper Porcupine slope, southwest of Ireland. Marine Geology 195, 31–53.
Williams, G.L., Brinkhuis, H., Pearce, M.A., Fensome, R.A., Weegink, J.W., 2004. Southern Ocean and global dinflagellate cyst events compared: index events for the Late Cretaceous Neogene, in: Exon, N.F., Kennett, J.P., Malone, M.J. (Eds.), Proceedings of the Ocean Drilling Program, Scientific Results Volume 189. pp. 1–98.
Woodruff, F., Savin, S.M., 1989. Miocene Deepwater Oceanography. Paleoceanography 4, 87–140.
Woodruff, F., Savin, S.M., 1991. Mid-Miocene isotope stratigraphy in the deep sea: High-resolution correlations, paleoclimatic cycles, and sediment preservation. Paleoceanography 6, 755–806.
Zachos, J., Pagani, M., Sloan, L., Thomas, E., Billups, K., 2001. Trends, Global Rhythms, Aberrations in Global Climate 65Ma to Present. Science 292, 686–693.

Chapter 5.

North Atlantic sea surface cooling during Miocene glaciation events in response to insolation and CO_2 change

Willemijn Quaijtaal, Stefan Schouten, Timme H. Donders, Ivo Vandemoortel, Stephen Louwye

During the Middle Miocene Climate Transition (ca. 14 million years ago) global climate transited from a temperature maximum, the Middle Miocene Climatic Optimum, to colder conditions and more extensive glaciations through several stepwise cooling and/or glaciation events. However, not much is known about the rate of change, degree of surface cooling and glaciation extent, particularly of the Northern hemisphere and especially from the North Atlantic Ocean, a key area for the meridional overturning circulation. Here we present the first detailed Atlantic sea surface temperature reconstructions based on marine palynology and organic geochemistry between 16.6 and 12.7 Ma providing multiproxy evidence for significant Northern Hemisphere sea surface temperature decreases during global $\delta^{18}O$ increases. The record reflects cooling and glaciation, in response to insolation and greenhouse gas forcing. Transient cooling of 3–5.5°C occurs until atmospheric CO_2 falls below 280 ppm. Then, in concurrence with minimal long term eccentricity and obliquity amplitude modulation, cooling is of a more permanent nature concurrent with possible bipolar glaciation. The most pronounced cooling in the Porcupine Basin records, of 6°C, can be linked to the Mi-3 $\delta^{18}O$ excursion. Spring and summer sea surface cooling leads subsurface and deep water cooling during the Mi-3 and Mi-4 glaciations, indicating enhanced seasonality and strong circumstantial evidence for bipolar glaciation.

Intended for publication

North Atlantic sea surface cooling during Miocene glaciation events in response to insolation and CO_2 change

1. Introduction

Following the relatively warm Middle Miocene Climatic Optimum (MMCO; 17–14.7 Ma; *Holbourn et al.,* 2015), the global climate cooled during a series of events known as the Middle Miocene Climate Transition (MMCT; ~14 million years ago, Ma; Langhian–Serravallian), the second of three major transitions from the Paleogene Greenhouse world to the modern day Icehouse world (*Zachos et al.*, 2001). The MMCT is characterised by increases in stable oxygen isotope ratios ($\delta^{18}O$) measured on the calcareous shells of benthic foraminifera, a group of unicellular marine zooplankton. Seven positive $\delta^{18}O$ excursions have been reported in the Miocene (*Boulila et al.*, 2011; *Miller et al.*, 1991, 1996, 1998) representing decreasing deep water temperatures and/or cryosphere expansion (Chapter 1, Figure 1.1). These excursions or Mi-events are defined as the maximum $\delta^{18}O$ value within larger $\delta^{18}O$ excursions (*Miller et al.*, 1991). Crucially, the most pronounced $\delta^{18}O$ increase during the MMCT is the Miocene Isotope (Mi)- 3 zone or event, which is commonly associated with East Antarctic Ice Sheet (EAIS) growth (*Haywood et al.*, 2009; *Shevenell and Kennett*, 2004), although Northern Hemisphere (NH) glaciation has also been suggested (*Moran et al.*, 2006). During this period of cryosphere expansion there is evidence for major global climate reorganisation with NH and mid-latitude aridification (*Eronen et al.*, 2012; *Flower and Kennett*, 1994), global scale carbon cycle changes (*Woodruff and Savin*, 1989) and species turnover in both terrestrial and marine biota (*Flower and Kennett*, 1994). Among the most-mentioned causes of the MMCT are a drawdown of atmospheric CO_2, palaeoceanographical changes, and a favourable orbital configuration for cryosphere expansion (*Abels et al.*, 2005; *Badger et al.*, 2013; *Greenop et al.*, 2014; *Kürschner et al.*, 2008; *Levy et al.*, 2016; *Pagani et al.*, 2005; *Shevenell et al.*, 2004; *Westerhold et al.*, 2005). The focus of many recent studies has therefore been the modelling of various palaeoceanographic parameters across the MMCT (*Goldner et al.*, 2014; *Herold et al.*, 2012), cyclicity analysis of high-resolution isotope records to determine possible orbital forcing (*Abels et al.*, 2005; *Holbourn et al.*, 2007; *Westerhold et al.*, 2005) and reconstruction of atmospheric pCO_2 values (*Badger et al.*, 2013; *Foster et al.*, 2012; *Greenop et al.*, 2014; *Pagani et al.*, 1999; *Zhang et al.*, 2013). However, these studies have not been able to pinpoint the exact cause of the MMCT, not in the least due to a lack of detailed surface temperature data, particularly in the North Atlantic where any developing NH ice sheets would have strengthened the regional cooling signature.

The period of sustained global warmth (MMCO) preceding the MMCT cannot, based on current understanding of climate feedbacks (*Goldner et al.*, 2014) , be explained by the available Miocene atmospheric CO_2 estimates that are near modern levels. Climate simulations of the MMCO underestimate mean annual temperature and deep water temperature by regionally up to 4°C in comparison with proxy data (*Goldner et al.*, 2014; *Herold et al.*, 2012), with a total offset of equator to pole temperature gradients up to 10°C (*Goldner et al.*, 2014). This suggests that the presence or absence of icecaps partly determines climate sensitivity to a given CO_2 forcing (*DeConto and Pollard*, 2003). A CO_2 forcing without a NH ice cap would thus result in a warmer mean state compared to similar forcing starting from a bipolar glaciated condition as seen in the Quaternary. Vapour and vegetation feedbacks (*Knorr et al.*, 2011), as well as deep thermocline configuration (*LaRiviere et al.*, 2012), can additionally explain part of this hysteresis behaviour of the climate. Reduced sea ice and

permanent El Nino (El Padre) conditions, as suggested for the Pliocene warm period, only explain a small portion of the proxy-data – model mismatch (*Goldner et al.*, 2014; *Herold et al.*, 2012). Consequently, at current estimates of Miocene palaeo-CO_2, the MMCO and subsequent MMCT imply threshold climate conditions that, once crossed, do not return to warm conditions under similar forcing.

A major complicating factor for understanding the Miocene climate is that the temperature and cryosphere components in benthic oxygen isotope signals are difficult to separate. Independent temperature reconstructions are imperative to separate these components for the middle Miocene increases in $\delta^{18}O$. However, essentially no NH palaeotemperature records across both the MMCO and MMCT that document the temperature component during the $\delta^{18}O$ increases exist. Those records available have a short time span (*Badger et al.*, 2013) or a low resolution (*Donders et al.*, 2009; *Schreck et al.*, 2013).

Here we present the first detailed North Atlantic sea-surface temperature (SST) records across the MMCO and the MMCT from the Porcupine Basin (Integrated Ocean Drilling Program Leg 307, Site U1318). A recently generated benthic foraminiferal stable carbon- and oxygen isotope record was used for isotope stratigraphy and improvement of the existing age model for Site U1318 (*Quaijtaal et al.*, 2017). We generated independent SST records based on membrane lipids (glycerol dialkyl glycerol tetraethers, GDGT's) produced by Thaumarchaeota, the so-called TetraEther indeX of 86 carbon atoms TEX_{86} (*Schouten et al.*, 2002), and the alkenone unsaturation index $U^{K'}_{37}$ (*Brassell et al.*, 1986; *Müller et al.*, 1998), based on alkenones produced by haptophyte algae. In addition, we have determined independent relative sea-surface temperatures based on assemblages of organic-walled dinoflagellate cysts (dinocysts). Dinocysts are produced as a part of the life cycle of dinoflagellates, unicellular algae that are sensitive indicators of different environmental parameters, e.g. temperature (*De Schepper et al.*, 2011; *Head*, 1997; *Versteegh*, 1994) (See Supplementary Note 1). By combining our temperature records with benthic $\delta^{18}O$ we can consistently compare the temperature change of four Mi-events across a background of declining CO_2 and changing orbital parameters and assess tipping points leading to the MMCT.

2. Methods

2.1. Organic geochemistry TEX_{86}

Ca. 5 grams of freeze-dried sediment was ground and extracted using accelerated solvent extraction (ASE 350 system, Dionex) using dichloromethane (DCM)/methanol (MeOH) (9:1, v/v). Extracts were separated in apolar, ketone and polar fractions over an activated Al_2O_3 column using hexane/DCM (9:1, v/v), hexane/DCM (1:1, v/v) and DCM/MeOH (1:1, v/v) respectively.

For TEX_{86} the dried polar fraction, containing tetraether lipids, was dissolved in hexane/isopropanol (99:1, v/v), filtered over a 0.45µm polytetrafluorethylene (PTFE) filter (⌀ 4mm), and analysed by high performance liquid chromatography/ atmospheric pressure positive ion chemical ionization mass spectrometry (HPLC/ APCI-MS), following the methodology of *Schouten et al.* (2007). Analyses were performed on an Agilent 1100 series LC/MSD SL and separation and a Prevail Cyano column (2.1 x 150mm, 3µm; Alltech), maintained at 30°C. The GDGTs were eluted isocratically using a changing mixture of hexane and propanol. The first 5 minutes proportions were 99% hexane: 1% propanol, then increasing linearly toward 1.8% in 45 minutes. Flow rate was 0.2 mL per minute. Single ion monitoring was set to scan the 5 $[M+H]^+$ ions of the GDGTs (dwell time 237 ms for each ion). TEX_{86} values were calculated after *Schouten et al.* (2007). No data points had to be excluded because of

fluvial input of soil organic matter as the branched isoprenoid tetraether (BIT) index was <0.1 on average (n=245, min=0.04, max=0.23), below the threshold of 0.3 (*Hopmans et al.*, 2004). The values for the Methane Index (*Zhang et al.*, 2011) (n = 245, average = 0.20, min = 0.17, max = 0.28) and ratios of GDGT-0 and crenarchaeol (*Weijers et al.*, 2011) (n = 45, average = 0.57, min = 0.37, max = 0.84) also indicate that there was no substantial input of methanotrophic or methanogenic archaea. The good correlation between TEX_{86} and the Ring Index (*Zhang et al.*, 2016) (RI= 2.73* TEX_{86} + 0.86, R^2= 0.72) shows that the TEX_{86} is primarily derived from marine Thaumarchaeota. To calculate SST the following equation was used: SST^H= 68.4*TEX_{86}^H + 38.6, where TEX_{86}^H=log(TEX_{86}) (*Kim et al.*, 2010). Standard error on TEX_{86}^H reconstructed temperatures is 2.5°C. Alternative calibrations, such as the Bayesian (*Tierney and Tingley*, 2014, 2015) show a similar SST pattern, but with different absolute temperatures.

2.2. Organic geochemistry $U^{K'}_{37}$

For $U^{K'}_{37}$ the ketone fraction, containing alkenones, was dissolved in hexane, and injected for gas chromatography using a Hewlett Packard 6890N Network GC system equipped with a 50 m long– 0.32 mm diameter silica column coated with CP Sil-5 (thickness 0.12 µm). The carrier gas used was helium. Oven temperature was programmed at 70°C for injection and increased by 20°C min^{-1} up to 200°C, then increased by 3°C min^{-1} until 320°C. This final temperature was maintained for 30 min. The $U^{K'}_{37}$ was calculated after *Prahl and Wakeham* (1987), i.e. $U^{K'}_{37}$ = [37:2] / [37:2 + 37:3], SST was calculated after *Müller et al.* (1998): SST = ($U^{K'}_{37}$ – 0.044) / 0.033. Calibration error on $U^{K'}_{37}$ reconstructed temperatures is 1.5°C.

2.3. Palynology

In addition to the 123 palynological data points of *Quaijtaal et al.* (2014), 99 additional downcore samples were processed and counted. Seventy-five samples were taken from Hole 1318B, 24 samples were taken from Hole 1318C (See Supplementary Table 5.1). The samples were processed according to *Quaijtaal et al.* (2014). Two tablets of the exotic spore *Lycopodium clavatum* were added to calculate absolute dinocyst abundances. Slides were counted in non-overlapping traverses using a Zeiss AxioImager A1 light microscope at 400x magnification until a minimum of 300 dinocysts was counted. The use of SST_{dino} or the Warm/Cold dinocyst index, as well as the species used in the index, is explained in Supplementary Note 5.1 and *Quaijtaal et al.* (2014).

2.4. Data

All data can be found in Supplementary Table 5.1.

3. Results

Our Porcupine Basin TEX_{86}^H Sea Surface Temperature (SST_{TEX86H}) record shows changes of 2–4°C superimposed on a gradual cooling from maxima of 27°C around 16.4 Ma to minima of 18°C around 12.8 Ma (Figure 5.1). In contrast, $U^{K'}_{37}$ SST ($SST_{UK'37}$) is substantially higher and relatively constant, with temperatures between 25.8 and 29°C (See Figure 5.1 and 5.2). The $U^{K'}_{37}$ is well above 0.9 in all samples except two (Supplementary Table 5.1), hence approaching maximum detectable temperatures and therefore likely not able to record fluctuations in SST >28°C (*Müller et al.,* 1998). Our relative sea surface temperature index based on dinocyst assemblages (SST_{dino}; 0 (cold) to 1 (warm))(*Quaijtaal et al.*, 2014), follows both the long-term cooling trend as well as the transient SST decreases during the $\delta^{18}O$ increases.

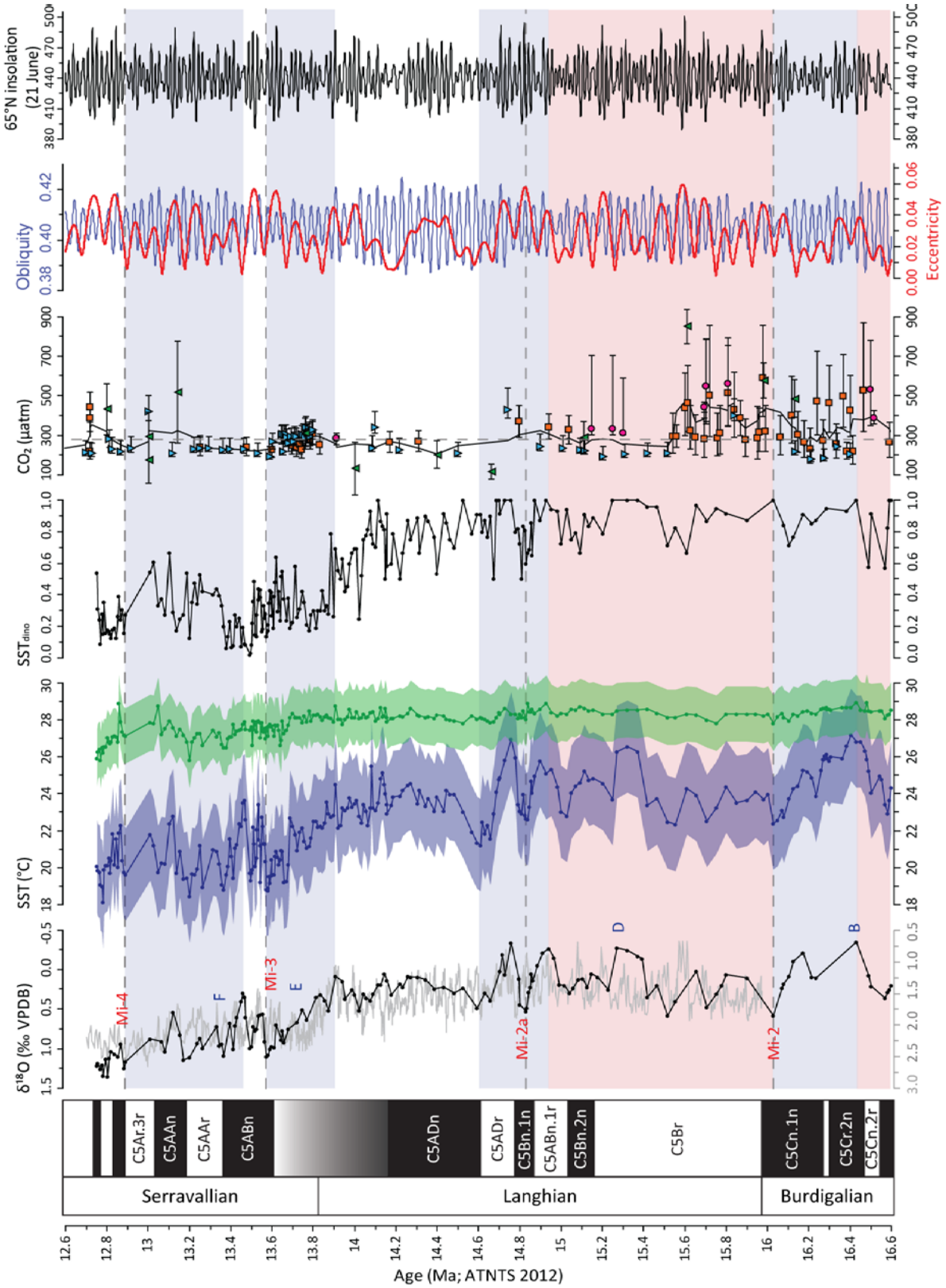

Figure 5.1 Stratigraphy, magnetostratigraphy, benthic $\delta^{18}O$ from Site U1318 (*Quaijtaal et al.,* 2017) (black) and Site U1338 *(Holbourn et al.,* 2014) (grey), SST_{TEX86H} (blue) with 2.5°C standard error envelope, $SST_{UK'37}$ (green) with 1.5°C standard error envelope, SST_{dino}, atmospheric CO_2, obliquity, eccentricity and 65°N solar insolation (21 June) versus age. Atmospheric CO_2 was compiled from boron isotopes (orange squares) (*Badger et al.,* 2013; *Foster et al.,* 2012; *Greenop et al.,* 2014), phyto-alkenones (blue downward triangles) (*Badger et al.,* 2013; *Freeman and Hayes,* 1992; *Pagani et al.,* 2005; *Zhang et al.,* 2013), stomata (pink circles) (*Kürschner et al.,* 2008; *Royer et al.,* 2001) and paleosols (green upward triangles) (*Cerling,* 1991; *Ekart et al.,* 1999; *Retallack,* 2009); solid line is a 5-point running average through all data points; dashed line marks 280 ppmv pre-industrial atmospheric CO_2.CO_2 data from before 2012 were collected from *Honisch et al.* (2012). Red bar indicates the MMCO (*Holbourn et al.,*2017), blue bars represent cold intervals surrounding the Mi-events. Grey dashed lines and red text indicate the position of the Mi-events; blue letters represent the oxygen isotope events of *Woodruff and Savin* (1991).

The Site U1318 SST_{TEX86H} record shows a surprisingly strong correlation with the benthic $\delta^{18}O$ record (R^2 = 0.88; p<0.0001) (See Figure 5.3). Correlation of SST_{TEX86H} to $SST_{UK'37}$ is lower, but still highly significant (R^2=0.66; p<0.0001), likely due to the fact that the $U^{K'}_{37}$ is at its maximum value and thus is less variable and more susceptible to noise in the record. The correlation between SST_{TEX86H} and SST_{dino} (R^2=0.54; p<0.0001) is lower than the correlation between SST_{TEX86H} and $\delta^{18}O$ as the SST_{dino} shows more high-order variability. One explanation might be the different growth seasons of the organisms on which the temperature proxies are based. Dinoflagellates generally bloom during late spring or summer (*Barton et al.*, 2015), whereas thaumarchaeotal-based SST may represent winter temperatures (*Lopes Dos Santos et al.*, 2013). Alternatively, the better correlation between SST_{TEX86H} and benthic foraminiferal $\delta^{18}O$ in comparison to the strictly SST_{dino} and $SST_{UK'37}$ might be because SST_{TEX86H} reflects more of a subsurface (0–200 m) signal compared to the algal-based proxies (*Huguet et al.*, 2007). The first option is unlikely due to the very high temperatures, and it is more likely that changes in TEX_{86}^{H} represent changes in subsurface temperature. This possibly explains the offset between the lower SST_{TEX86H} relative to the proxies based on strictly surface dwelling algae. Because we calculate our SST_{TEX86H} record using a formula calibrated to SST, however, it is still likely that TEX_{86}^{H} represents SST. An alternative TEX_{86} calibration for subsurface (0–200 m) temperatures (*Kim et al.*, 2008) has been plotted in Figure 5.4. Modern annual SST (0–10 m) at Site U1318 is 12.6°C (*Locarnini et al.*, 2013), indicating that SSTs during the MMCO and MMCT were substantially higher than at present, and comparable to regional terrestrial temperature estimates (*Donders et al.*, 2009). With these new temperature records we are able to determine the magnitude and timing of the four main cooling events identified at the Porcupine Basin. The majority of the cooling events (blue bars in Figure 5.1) is mirrored by increases in benthic $\delta^{18}O$.

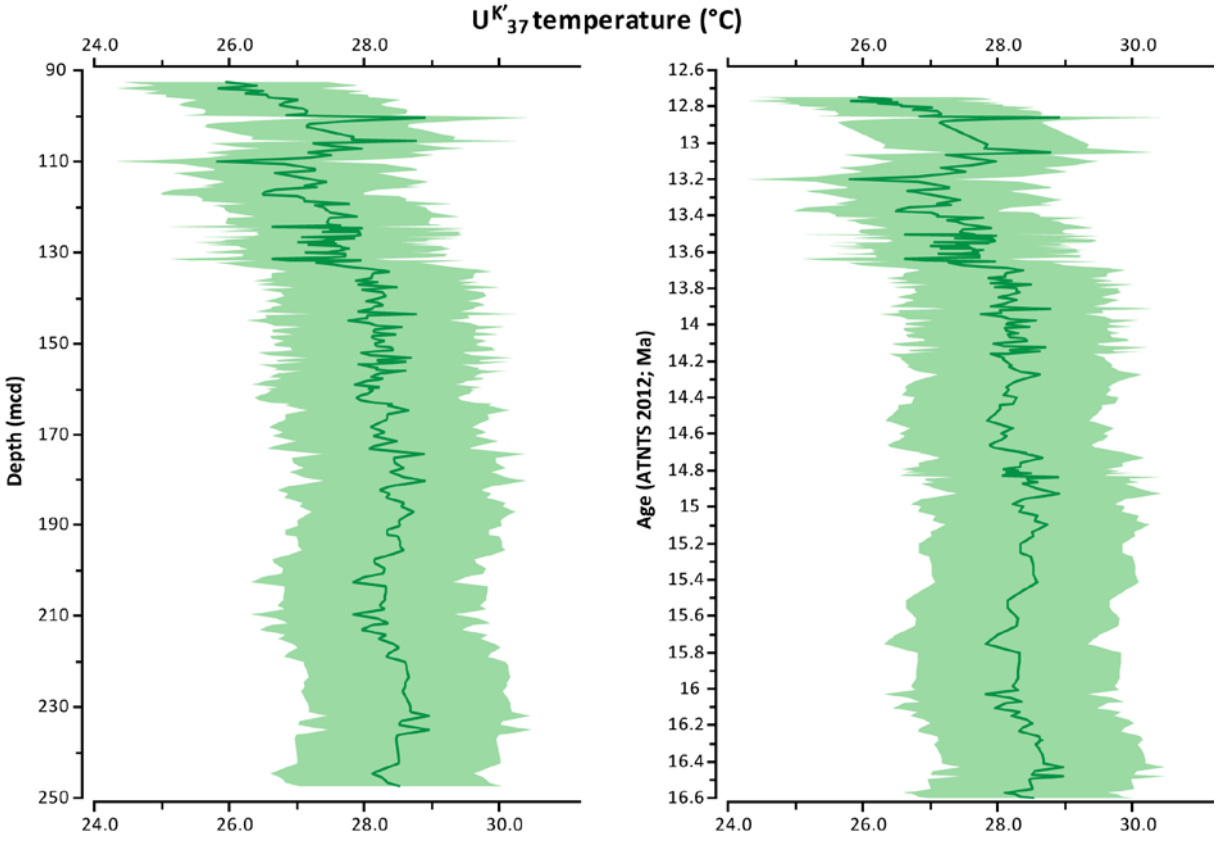

Figure 5.2: $SST_{UK'37}$ with 1.5°C standard error envelope versus depth and age.

The similarity of the U1318 benthic $\delta^{18}O$ to that of deep water site U1338 (Figure 5.1) suggests that, because of the good correlation between benthic $\delta^{18}O$ and SST_{TEX86H}, there is a major temperature component in the global $\delta^{18}O$ signal. The $SST_{UK'37}$ does not show these large decreases in SST due to the near-maximum values of the $U^{K'}_{37}$ index throughout the record, and will only be discussed below when showing larger (>1.5°C) fluctuations.

The first, transient cooling can be correlated to Mi-2 (16.03 Ma; Figure 5.1). The $\delta^{18}O$ excursion of 0.93‰ lasts ca. 400 ka and is accompanied by a SST_{TEX86H} cooling of ~5°C. The dinocyst assemblage response is moderate, shown by a decrease in SST_{dino}. The second sea-surface cooling, corresponding to Mi-2a (~14.8 Ma), is of a two-step nature. A first, moderate SST cooling of ~3°C (SST_{TEX86H}) is coeval with a positive $\delta^{18}O$ excursion of 0.8‰ (Figure 5.1), followed by a decrease in SST_{dino}. All three proxies then rapidly (within ~80 ka) recover towards warmer temperatures, followed by a second relatively rapid (150 ka), non-transient cooling of ~5.5°C. The response in the dinocyst assemblage is even faster, ca. 10 ka.

The most prominent feature in our SST records is a gradual cooling of ca. 6°C from ~13.9 to 13.6 Ma (Figure 5.1) that encompasses several correlative events: CM5, isotope event E, CM6 (*Woodruff and Savin*, 1991), and Mi-3 (*Boulila et al.*, 2011). This cooling is accompanied by a positive $\delta^{18}O$ excursion of 1.02‰ (Mi-3/ isotope event E). SST_{dino} cooling starts prior to the gradual changes in SST_{TEX86H} and $\delta^{18}O$ as a ~200 ka period where the index shows rapid (~10 ka) high amplitude (>0.6) variability and subsequently attains more stable, lower values, pointing towards a large transition towards a dinocyst assemblage indicative of much colder water masses, including species that nowadays inhabit temperate, subpolar and polar regions (*Zonneveld et al.*, 2013). During Mi-3, $SST_{UK'37}$ shows a small decrease of ~1.7°C (See Figure 5.1 and 5.2). After this decrease $SST_{UK'37}$ drops below 28°C and fluctuates more, indicating increasing sensitivity to temperature fluctuations. A short recovery follows after Mi-3, quickly followed by two minor rapid cooling events of ca. 4°C and 5°C, also visible in $SST_{UK'37}$ and SST_{dino}. Interestingly, SST_{dino} does indicate an increase in SST during the last of these rapid cooling events following Mi-3, starting from minimum values (<0.1).

Mi-4 (12.9 Ma) is of a smaller magnitude than Mi-3, both in $\delta^{18}O$ (0.71‰) and SST_{TEX86H} cooling (ca. 3°C; Figure 5.1). $SST_{UK'37}$ indicates a small temperature decrease of ~1.6° and a decrease in SST_{dino}. However, there is a small hiatus prior to the Mi-4 maximal $\delta^{18}O$ (104.31–104.60 mcd; *Quaijtaal et al.*, 2014), possibly causing the Mi-4 cooling not to be fully captured at the Porcupine Basin. With Mi-4 a general cooling trend commences that can be observed in the $\delta^{18}O$, SST_{TEX86H}, $SST_{UK'37}$ and SST_{dino}.

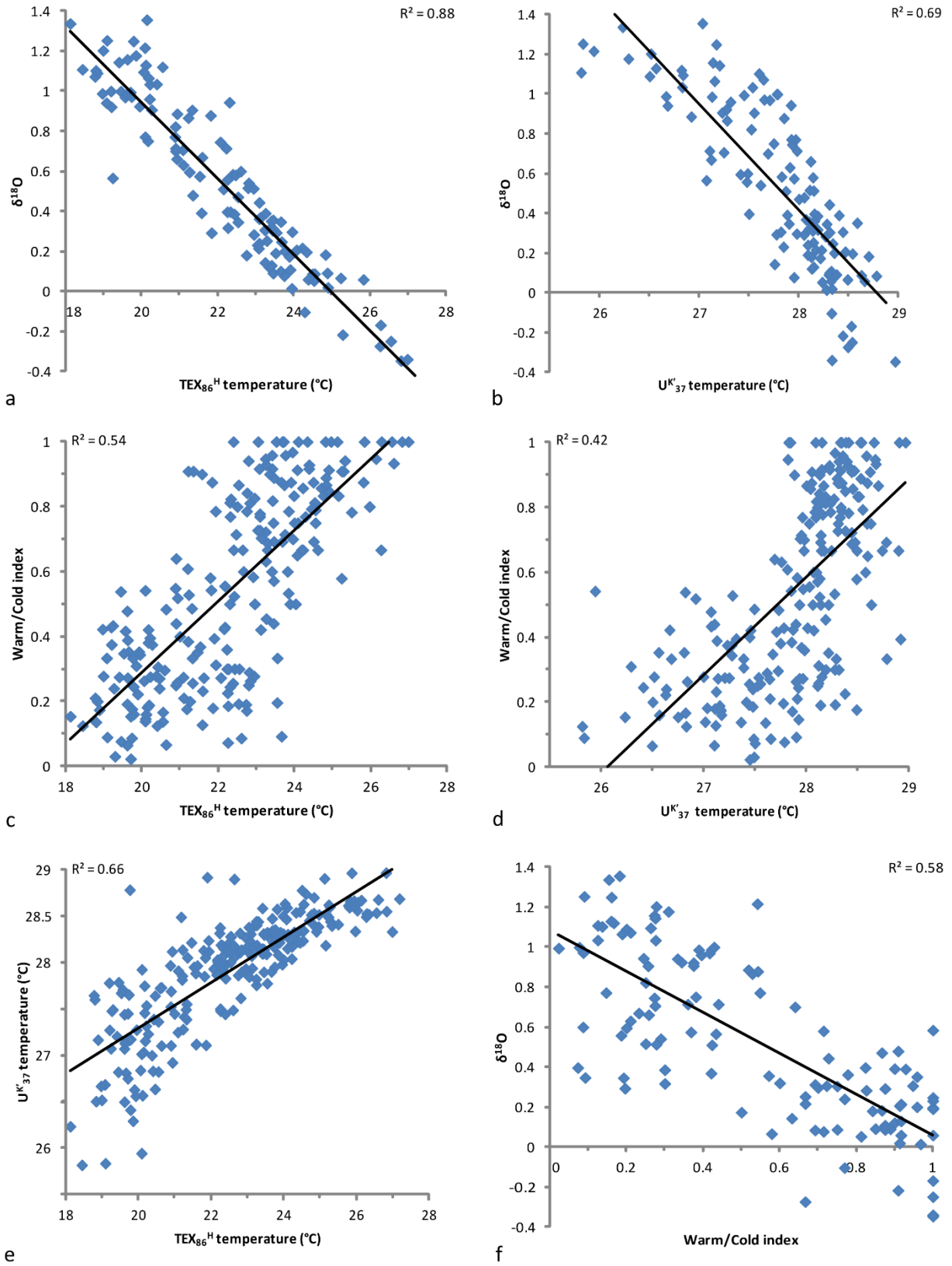

Figure 5.3: correlation between a) SST_{TEX86H} and benthic $\delta^{18}O$ (*Quaijtaal et al.*, 2017) b) $SST_{UK'37}$ and benthic $\delta^{18}O$ (*Quaijtaal et al.*, 2017) c) SST_{TEX86H} and SST_{dino} d) $SST_{UK'37}$ and SST_{dino} e) SST_{TEX86H} and $SST_{UK'37}$ f) SST_{dino} and benthic $\delta^{18}O$ (*Quaijtaal et al.*, 2017).

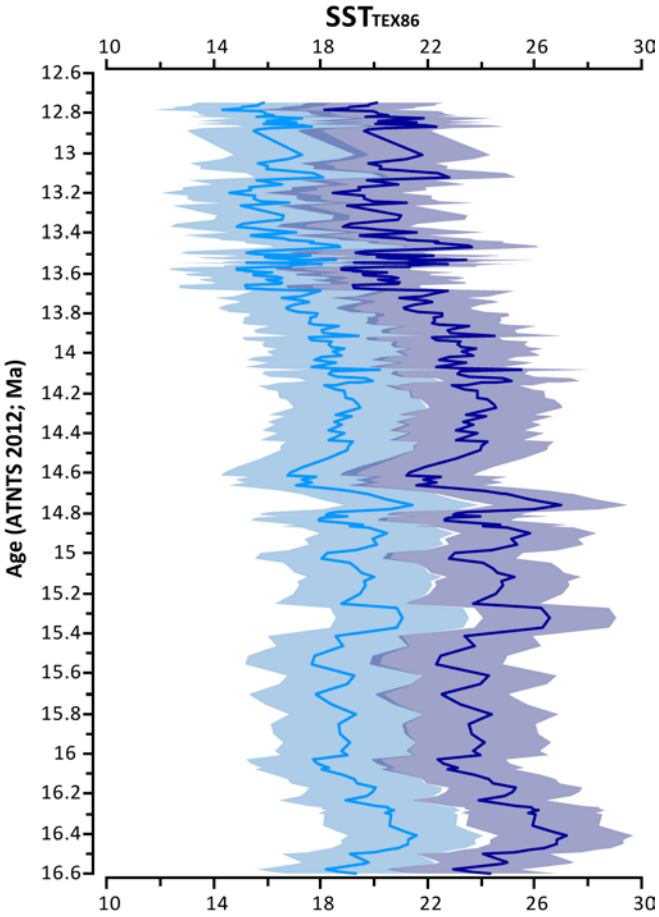

Figure 5.4: SST_{TEX86H} (dark blue) and alternative subsurface calibration $SST_{TEX86200m}$ (light blue) with 2.5°C standard error envelope versus age.

4. Discussion

Our results clearly show a strong cooling of the North Atlantic Ocean during all Mi-events. The benthic $\delta^{18}O$ record of the Porcupine Basin is similar to that of Pacific Site U1338 (*Holbourn et al.*, 2014; Figure 5.3). Since there is a good correlation of the Site U1318 benthic $\delta^{18}O$ with the SST_{TEX86} record implying that temperature is the biggest influence on the Site U1318 benthic $\delta^{18}O$ record, the similarity between the Site U1318 and Site U1338 benthic $\delta^{18}O$ records suggests that there is a major NH temperature component in $\delta^{18}O$. The reconstructed temperature records indicate a strong systematic relation between the glaciations during the MMCT and surface water cooling. Crucially, post-event SSTs during Mi-3 and Mi-4 are lower than prior to the event, indicative of a climate system transition, possibly involving NH glaciations. Compared to Mi-2 and Mi-2a, timing of the cooling during Mi-3 and Mi-4 is structured somewhat differently between SST_{dino} and SST_{TEX86H}. Both reveal surface cooling at the Porcupine Basin, but SST_{dino} minima lead the SST_{TEX86} signal, indicating an initially seasonal rather than mean annual cooling. Conversely, at the end of Mi-3 and Mi-4, warming in the SST_{dino} leads SST_{TEX86}. An SST_{dino} increase typically represents summer season warming, consistent with a scenario of summer melt of a continental NH ice sheet, after which mean annual temperatures increased again. This suggests that seasonal surface cooling (warming) precedes bottom water cooling (warming) and/or cryosphere expansion (contraction). Before discussing the possible forcing of this transition, we consider the global pattern of the temperature changes.

While no broad set of temperature records are available to obtain a global view of the stepwise transition from MMCO and across the MMCT, some data is available that allows comparison of developing gradients (Table 5.1; Figure 5.5). Bottom water temperature (BWT) change towards Mi-2 shows a pole to equator gradient with 1°C towards the equator and 3°C towards the poles (*Cooke et al.*, 2008; *Lear et al.*, 2010; *Shevenell et al.*, 2008). During Mi-2, Southern Hemisphere (SH) SST decreases with 3–4°C (*Shevenell et al.*, 2004), somewhat less than the 5°C at the Porcupine Basin. Continental north-western European Mean Annual Air Temperature (MAT) and palaeobotanical records indicate a cooling of 3–4°C (*Donders et al.*, 2009; *Utescher et al.*, 2012). Remarkably, the peak warmth following Mi-2 at ca. 15.6 Ma found in Pacific sites (*Holbourn et al.*, 2013, 2014, 2015) cannot be observed at the Porcupine Basin. This could indicate that either the resolution of Site U1318 is insufficient to capture this peak warmth, or that the MMCO peak warmth is a strictly Pacific phenomenon. The Mi-2a cooling is somewhat less strong than Mi-2, but similarly structured (Table 5.1). Interestingly, the rapid cooling following Mi-2a (~14.6 Ma) that we observe has only been reported in the subtropical northwestern Pacific (*Holbourn et al.*, 2010). The cooling associated with Mi-3 can be observed in most other Miocene temperature records from pole to equator. SH BWT decreases 1.5–2°C (*Cooke et al.*, 2008; *Lear et al.*, 2010; *Shevenell et al.*, 2008), where Southern Ocean SST decreases 6–7°C (*Kuhnert et al.*, 2009; *Shevenell et al.*, 2004). For the NH only SST and continental records are available. SST cools from 2°C at Pacific low latitudes (*Holbourn et al.*, 2010) to 6°C at the Porcupine Basin. MAT shows ca. 7°C cooling, but palaeobotanical records hardly show any floristic change (*Donders et al.*, 2009; *Utescher et al.*, 2012). The slightly stronger cooling at higher latitudes indicates that the equator–pole temperature gradient became steeper during Mi-3, and remained so after. Further steepening of this gradient can be observed during Mi-4. Significantly, a high-latitude record from the Iceland Sea shows a large SST decrease of ca. 6.5°C, larger than at the Porcupine Basin (~3°C). Although the low resolution Icelandic record only has 2 data points in this interval (*Schreck et al.*, 2013), this developing strong latitudinal gradient is a possible indication of a transient NH ice sheet during Mi-4. Southern Ocean SST records show hiatuses at this time (*Shevenell et al.*, 2004, 2008) or do not cover this period (*Kuhnert et al.*, 2009; *Shevenell et al.*, 2008), complicating comparison of cooling at both poles. A BWT record from the Tasman Sea indicates a cooling of only ca. 1°C (*Lear et al.*, 2010) when a significant Antarctic ice sheet had already formed. The SST_{dino} increase at Porcupine at the end of Mi-4 could indicate stronger seasonality at that time with annual SST staying low while spring/summer temperatures increased, melting any NH ice. This agrees with Central European continental records where significant cooling and floristic change starts around Mi-4 and not during Mi-3 (*Donders et al.*, 2009; *Utescher et al.*, 2012).

Our new independent temperature record now allows constraining the impact of orbital forcing and CO_2 on SST in the North Atlantic Ocean and comparing this to their impact on global ice volume for the first time. Existing reconstructions and modelling of Antarctic ice sheet extension imply high sensitivity to atmospheric CO_2 with expansion at or below 280 ppm and ice sheet minima at ~500 ppm with expansion generally coinciding with eccentricity minima (*Levy et al.*, 2016). Indeed, comparison of timing of the Porcupine Basin cooling events with the calculated obliquity and eccentricity cycles as well as 21 June 65°N insolation (*Laskar et al.*, 2004) shows most major (Mi-2, the cooling following Mi-2a, Mi-3, Mi-4) and some smaller temperature decreases to coincide with eccentricity minimum nodes and minima in insolation (Figure 5.3), whereas only the four Mi-events coincide with minimum nodes in 1.2 Ma obliquity amplitude modulation. Two surface coolings in our organic geochemical and dinocyst records, coincident with Mi-2 and Mi-3, occur simultaneously with 21 June 65°N insolation minima and minimum nodes in both 1.2 Ma obliquity amplitude modulation

and 2.4 Ma long-term eccentricity (Figure 5.3). Such a specific orbital configuration creates favourable conditions for expansion of the cryosphere (*Zachos et al.*, 2001). Nevertheless, a notably strong expansion of the Antarctic ice sheet as during Mi-3 has not been observed at Mi-2 (*Levy et al.*, 2016). The Mi-2 cooling observed at the Porcupine Basin, as well as the response in the dinocyst assemblages, is of a less strong and non-permanent nature. This is consistent with atmospheric CO_2 values between ca. 300–500 ppm at which NH glaciation is highly unlikely (Figure 5.3). At ca. 14.6 Ma atmospheric CO_2 falls below ca. 280 ppm, coincident with the rapid cooling following Mi-2a. Combined with the minima in eccentricity and obliquity amplitude modulation the threshold for bipolar glaciation (*DeConto et al.*, 2008) is crossed, as is shown by irreversible SST decrease at Porcupine from ~14.2 Ma. The amplified variability and long-term SST decrease following Mi-2a are consistent with a scenario of NH glaciation as a result of combined CO_2 and insolation forcing. Indeed, *Knies and Gaina* (2008) find peak occurrences of ice rafted debris in the Barents Sea from ~15 Ma onwards. The cooling seen in the SST_{dino}, as well as prominent minima in 21 June 65°N insolation during the early phase of the Mi-events points to importance of summer temperature decrease for the development of NH glaciation. This implies that the combination of low atmospheric CO_2 and minima in both long-term eccentricity and obliquity amplitude modulation were imperative for the onset of the MMCT starting at Mi-3. Once established, temperatures did not fully recover, possibly due to presence of Arctic sea ice and transient ice sheets (*DeConto et al.*, 2008).

Table 5.1
A global overview of the temperature decreases across the four Mi-events covering the MMCO and MMCT

Mi-event	Hemisphere	Latitude	Region	Reference	Sea Surface Temperature	Bottom Water Temperature	Continental temperature
Mi-4	NH	69°14'N	Iceland Sea	*Schreck et al.*, 2013	6.5		
(12.9Ma)	NH	51°26'N	Porcupine Basin	This study	3		
	NH	19°27'N	South China Sea	*Holbourn et al.*, 2010	1		
	SH	16°44'S	Wombat Plateau	*Lear et al.*, 2010		1	
	SH	40°30'S	southern Tasman Sea	*Cooke et al.*, 2008		1.5	
Mi-3	NH	ca. 51°40'N	Roer Valley Graben	*Donders et al.*, 2009			7
(13.7 Ma)	NH	51°26'N	Porcupine Basin	This study	6		
	NH	ca. 50°90'N	Lower Rhine Basin	*Utescher et al.*, 2012			1.5
	NH	35°54'N	Mediterranean	*Badger et al.*, 2013	min. 4.5		
	NH	19°27'N	South China Sea	*Holbourn et al.*, 2010	2		
	SH	16°44'S	Wombat Plateau	*Lear et al.*, 2010		1.5	
	SH	40°30'S	southern Tasman Sea	*Cooke et al.*, 2008		min. 2	
	SH	46°4'S	Southern Ocean	*Kuhnert et al.*, 2009	6		
	SH	48°30'S	south Tasman Rise	*Shevenell et al.*, 2004, 2008	6–7	2	
Mi-2 a	NH	51°26'N	Porcupine Basin	This study	3–5.5		
(14.8 Ma)	NH	ca. 50°90'N	Lower Rhine Basin	*Utescher et al.*, 2012			3
	NH	19°27'N	South China Sea	*Holbourn et al.*, 2010	1–3		
	SH	16°44'S	Wombat Plateau	*Lear et al.*, 2010		1	
	SH	48°30'S	south Tasman Rise	*Shevenell et al.*, 2004, 2008	4	3	
Mi-2	NH	ca. 51°40'N	Roer Valley Graben	*Donders et al.*, 2009			4
(16.1 Ma)	NH	51°26'N	Porcupine Basin	This study	5		
	NH	ca. 50°90'N	Lower Rhine Basin	*Utescher et al.*, 2012			2–4
	SH	16°44'S	Wombat Plateau	*Lear et al.*, 2010		1	
	SH	40°30'S	southern Tasman Sea	*Cooke et al.*, 2008		2	
	SH	48°30'S	south Tasman Rise	*Shevenell et al.*, 2004, 2008	3–4	3	

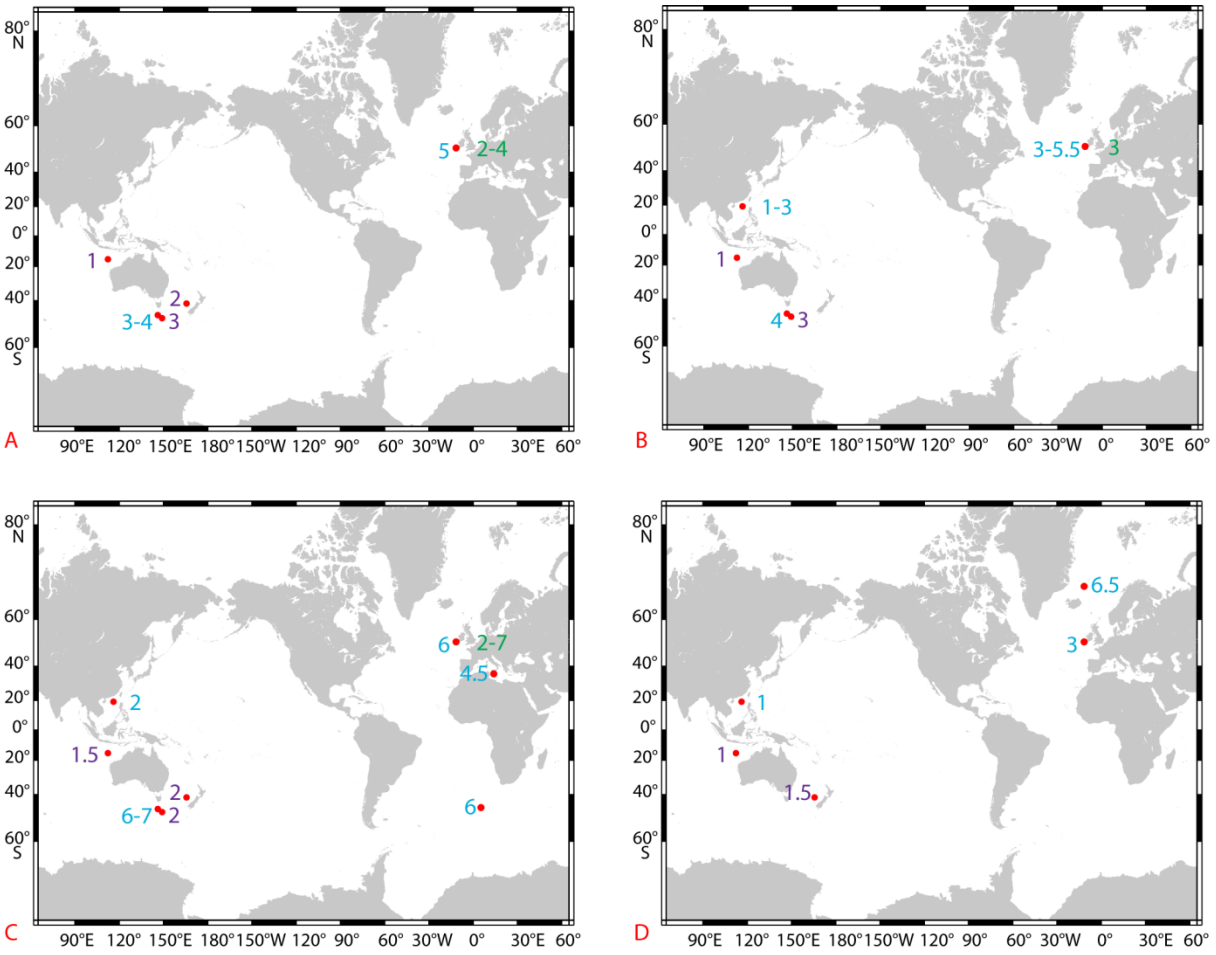

Figure 5.5: graphic view of Table 5.1. Degree of temperature change across the different Mi-events. Sea-surface temperature in blue, bottom water temperature in dark purple, continental temperature in green. A: Mi2; B: Mi-2a; C: Mi-3; D: Mi-4.

5. Author contributions

SL and THD designed the research project. This study has been established thanks to collaboration with and support of SS. IV did the preparations for, and performed the measurements on 51 samples for organic geochemistry. WQ did the preparation of, and geochemical measurements of the remaining majority of the samples. She also did the chemical maceration, counting and analyses for the palynology. Furthermore she interpreted all combined data, wrote the paper and prepared the figures.

6. Acknowledgements

The samples for this study were provided by the Integrated Ocean Drilling Program. This work was supported by the Research Foundation-Flanders (FWO) under project number G.0179.11N. SS was supported by the Netherlands Earth Science Center, funded by the Ministry of Education, Culture and Science (OCW). Anchelique Mets, Jort Ossebaar, Monique Verweij (NIOZ) and Sabine Van Cauwenberghe (UGent) are thanked for their technical assistance (technical assistance). Walter Hale and Alex Wülbers kindly supported WQ and SL during sampling at the Bremen Core Repository.

7. References

Abels, H.A., Hilgen, F.J., Krijgsman, W., Kruk, R.W., Raffi, I., Turco, E., Zachariasse, W.J., 2005. Long-period orbital control on middle Miocene global cooling: Integrated stratigraphy and astronomical tuning of the Blue Clay Formation on Malta. Paleoceanography 20, PA4012.

Badger, M.P.S., Lear, C.H., Pancost, R.D., Foster, G.L., Bailey, T.R., Leng, M.J., Abels, H.A., 2013. CO_2 drawdown following the middle Miocene expansion of the Antarctic Ice Sheet. Paleoceanography 28, 42–53.

Barton, A.D., Lozier, M.S., Williams, R.G., 2015. Physical controls of variability in North Atlantic phytoplankton communities. Limnology and Oceanography 60, 181–197.

Boulila, S., Galbrun, B., Miller, K.G., Pekar, S.F., Browning, J. V., Laskar, J., Wright, J.D., 2011. On the origin of Cenozoic and Mesozoic "third-order" eustatic sequences. Earth-Science Reviews 109, 94–112.

Brassell, S.C., Eglinton, G., Marlowe, I.T., Pflaumann, U., Sarnthein, M., 1986. Molecular stratigraphy: a new tool for climatic assessment. Nature 320, 129–133.

Cerling, T.E., 1991. Carbon dioxide in the atmosphere; evidence from Cenozoic and Mesozoic Paleosols. American Journal of Science 291, 377–400.

Cooke, P.J., Nelson, C.S., Crundwell, M.P., 2008. Miocene isotope zones, paleotemperatures, and carbon maxima events at intermediate water-depth, Site 593, Southwest Pacific. New Zealand Journal of Geology and Geophysics 51, 1–22.

De Schepper, S., Fischer, E.I., Groeneveld, J., Head, M.J., Matthiessen, J., 2011. Deciphering the palaeoecology of Late Pliocene and Early Pleistocene dinoflagellate cysts. Palaeogeography, Palaeoclimatology, Palaeoecology 309, 17–32.

DeConto, R.M., Pollard, D., 2003. A coupled climate-ice sheet modeling approach to the Early Cenozoic history of the Antarctic ice sheet. Palaeogeography, Palaeoclimatology, Palaeoecology 198, 39–52.

DeConto, R.M., Pollard, D., Wilson, P. a, Pälike, H., Lear, C.H., Pagani, M., 2008. Thresholds for Cenozoic bipolar glaciation. Nature 455, 652–656.

Donders, T.H., Weijers, J.W.H., Munsterman, D.K., Kloosterboer-van Hoeve, M.L., Buckles, L.K., Pancost, R.D., Schouten, S., Sinninghe Damsté, J.S., Brinkhuis, H., 2009. Strong climate coupling of terrestrial and marine environments in the Miocene of northwest Europe. Earth and Planetary Science Letters 281, 215–225.

Ekart, D.D., Cerling, T.E., Montanez, I.P., Tabor, N.J., 1999. A 400 million year carbon isotope record of pedogenic carbonate; implications for paleoatomospheric carbon dioxide. American Journal of Science 299, 805–827.

Eronen, J.T., Fortelius, M., Micheels, A., Portmann, F.T., Puolamäki, K., Janis, C.M., 2012. Neogene aridification of the northern hemisphere. Geology 40, 823–826.

Flower, B.P., Kennett, J.P., 1994. The middle Miocene climatic transition: East Antarctic ice sheet development, deep ocean circulation and global carbon cycling. Palaeogeography, Palaeoclimatology, Palaeoecology 108, 537–555.

Foster, G.L., Lear, C.H., Rae, J.W.B., 2012. The evolution of pCO 2, ice volume and climate during the middle Miocene. Earth and Planetary Science Letters 341–344, 243–254.

Freeman, K.H., Hayes, J.M., 1992. Fractionation of carbon isotopes by phytoplankton and estimates of ancient CO2 levels. Global Biogeochemical Cycles 6, 185–198.

Goldner, A., Herold, N., Huber, M., 2014. The challenge of simulating the warmth of the mid-Miocene climatic optimum in CESM1. Climate of the Past 10, 523–536.

Greenop, R., Foster, G.L., Wilson, P.A., Lear, C.H., 2014. Middle Miocene climate instability associated with high-amplitude CO2 variability. Paleoceanography 29, 845–853.

Haywood, A.M., Smellie, J.L., Ashworth, A.C., Cantrill, D.J., Florindo, F., Hambrey, M.J., Hill, D., Hillenbrand, C.D., Hunter, S.J., Larter, R.D., Lear, C.H., Passchier, S., van de Wal, R., 2009. Middle Miocene to Pliocene History of Antarctica and the Southern Ocean, in: Florindo, F., Siegert, M. (Eds.), Developments in Earth and Environmental Sciences. Elsevier, pp. 401–463.

Head, M.J., 1997. Thermophilic Dinoflagellate Assemblages from the Mid Pliocene of Eastern England. Journal of Paleontology 71, 165–193.

Herold, N., Huber, M., Müller, R.D., Seton, M., 2012. Modeling the Miocene climatic optimum: Ocean circulation. Paleoceanography 27, PA1209.

Holbourn, A., Kuhnt, W., Schulz, M., Flores, J.A., Andersen, N., 2007. Orbitally-paced climate evolution during the middle Miocene "Monterey" carbon-isotope excursion. Earth and Planetary Science Letters 261, 534–550.

Holbourn, A., Kuhnt, W., Regenberg, M., Schulz, M., Mix, A., Andersen, N., 2010. Does Antarctic glaciation force migration of the tropical rain belt? Geology 38, 783–786.

Holbourn, A., Kuhnt, W., Clemens, S., Prell, W., Andersen, N., 2013. Middle to late Miocene stepwise climate cooling: Evidence from a high-resolution deep water isotope curve spanning 8 million years. Paleoceanography 28, 688–699.

Holbourn, A., Kuhnt, W., Lyle, M., Schneider, L., Romero, O., Andersen, N., 2014. Middle Miocene climate cooling linked to intensification of eastern equatorial Pacific upwelling. Geology 42, 19–22.

Holbourn, A., Kuhnt, W., Kochhann, K.G.D., Andersen, N., Meier, K.J.S., 2015. Global perturbation of the carbon cycle at the onset of the Miocene Climatic Optimum. Geology 43, 123–126.

Honisch, B., Ridgwell, A., Schmidt, D.N., Thomas, E., Gibbs, S.J., Sluijs, A., Zeebe, R., Kump, L., Martindale, R.C., Greene, S.E., Kiessling, W., Ries, J., Zachos, J.C., Royer, D.L., Barker, S., Marchitto, T.M., Moyer, R., Pelejero, C., Ziveri, P., Foster, G.L., Williams, B., 2012. The Geological Record of Ocean Acidification. Science 335, 1058–1063.

Hopmans, E.C., Weijers, J.W.H., Schefuß, E., Herfort, L., Sinninghe Damsté, J.S., Schouten, S., 2004. A novel proxy for terrestrial organic matter in sediments based on branched and isoprenoid tetraether lipids. Earth and Planetary

Science Letters 224, 107–116.
Huguet, C., Schimmelmann, A., Thunell, R., Lourens, L.J., Damsté, J.S.S., Schouten, S., 2007. A study of the TEX86 paleothermometer in the water column and sediments of the Santa Barbara Basin, California. Paleoceanography 22, 1–9.
Kim, J.H., Schouten, S., Hopmans, E.C., Donner, B., Sinninghe Damsté, J.S., 2008. Global sediment core-top calibration of the TEX_{86} paleothermometer in the ocean. Geochimica et Cosmochimica Acta 72, 1154–1173.
Kim, J.H., van der Meer, J., Schouten, S., Helmke, P., Willmott, V., Sangiorgi, F., Koç, N., Hopmans, E.C., Damsté, J.S.S., 2010. New indices and calibrations derived from the distribution of crenarchaeal isoprenoid tetraether lipids: Implications for past sea surface temperature reconstructions. Geochimica et Cosmochimica Acta 74, 4639–4654.
Knorr, G., Butzin, M., Micheels, A., Lohmann, G., 2011. A warm Miocene climate at low atmospheric CO2 levels. Geophysical Research Letters 38, 1–5.
Kuhnert, H., Bickert, T., Paulsen, H., 2009. Southern Ocean frontal system changes precede Antarctic ice sheet growth during the middle Miocene. Earth and Planetary Science Letters 284, 630–638.
Kürschner, W.M., Kvacek, Z., Dilcher, D.L., 2008. The impact of Miocene atmospheric carbon dioxide fluctuations on climate and the evolution of terrestrial ecosystems. Proceedings of the National Academy of Sciences of the United States of America 105, 449–53.
LaRiviere, J.P., Ravelo, A.C., Crimmins, A., Dekens, P.S., Ford, H.L., Lyle, M., Wara, M.W., 2012. Late Miocene decoupling of oceanic warmth and atmospheric carbon dioxide forcing. Nature 486, 97–100.
Laskar, J., Robutel, P., Joutel, F., Gastineau, M., Correia, a. C.M., Levrard, B., 2004. A long-term numerical solution for the insolation quantities of the Earth . Astronomy and Astrophysics 428, 261–285.
Lear, C.H., Mawbey, E.M., Rosenthal, Y., 2010. Cenozoic benthic foraminiferal Mg/Ca and Li/Ca records: Toward unlocking temperatures and saturation states. Paleoceanography 25, 1–11.
Levy, R., Harwood, D., Florindo, F., Sangiorgi, F., Tripati, R., von Eynatten, H., Gasson, E., Kuhn, G., Tripati, A., DeConto, R., Fielding, C., Field, B., Golledge, N., McKay, R., Naish, T., Olney, M., Pollard, D., Schouten, S., Talarico, F., Warny, S., Willmott, V., Acton, G., Panter, K., Paulsen, T., Taviani, M., 2016. Antarctic ice sheet sensitivity to atmospheric CO 2 variations in the early to mid-Miocene. Proceedings of the National Academy of Sciences 113, 3453–3458.
Locarnini, R.A., Mishonov, A.V., Antonov, J.I., Boyer, T.P., Garcia, H.E., Baranova, O.K., Zweng, M.M., Paver, C.R., Reagan, J.R., Johnson, D.R., Hamilton, M., Seidov, D., 2013. World Ocean Atlas 2013, Volume 1: Temperature.
Lopes Dos Santos, R. a., Spooner, M.I., Barrows, T.T., De Deckker, P., Sinninghe Damsté, J.S., Schouten, S., 2013. Comparison of organic ($U^{K'}_{37}$, TEX_{86}^{H}, LDI) and faunal proxies (foraminiferal assemblages) for reconstruction of late Quaternary sea surface temperature variability from offshore southeastern Australia. Paleoceanography 28, 377–387.
Miller, K.G., Wright, J.D., Fairbanks, R.G., 1991. Unlocking the Ice House: Oligocene–Miocene Oxygen Isotopes, Eustasy, and Margin Erosion. Journal of Geophysical Research 96, 6829–6848.
Miller, K.G., Mountain, G.S., the Leg 150 Shipboard Party, Members of the New Jersey Coastal Plain Drilling Project, 1996. Drilling and Dating New Jersey Oligocene–Miocene Sequences: Ice Volume, Global Sea Level, and Exxon Records. Science 271, 1092–1095.
Miller, K.G., Mountain, G.S., Browning, J. V., Kominz, M., Sugarman, P.J., Christie-Blick, N., Katz, M.E., Wright, J.D., 1998. Cenozoic global sea level, sequences, and the New Jersey Transect: Results from coastal plain and continental slope drilling. Reviews of Geophysics 36, 569–601.
Moran, K., Backman, J., Brinkhuis, H., Clemens, S.C., Cronin, T.M., Dickens, G.R., Eynaud, F., Gattacceca, J., Jakobsson, M., Jordan, R.W., Kaminski, M., King, J., Koc, N., Krylov, A., Martinez, N., Matthiessen, J., McInroy, D., Moore, T.C., Onodera, J., O'Regan, M., Pälike, H., Rea, B., Rio, D., Sakamoto, T., Smith, D.C., Stein, R.R., St. John, K.E.K., Suto, I., Suzuki, N., Takahashi, K., Watanabe, M., Yamamoto, M., Farrell, J., Frank, M., Kubik, P.W., Jokat, W., Kristoffersen, Y., St John, K., Suto, I., Suzuki, N., Takahashi, K., Watanabe, M., Yamamoto, M., Farrell, J., Frank, M., Kubik, P.W., Jokat, W., Kristoffersen, Y., 2006. The Cenozoic palaeoenvironment of the Arctic Ocean. Nature 441, 601–605.
Müller, P.J., Kirst, G., Ruhland, G., von Storch, I., Rosell-Melé, A., 1998. Calibration of the alkenone paleotemperature index $U^{K'}_{37}$ based on core-tops from the eastern South Atlantic and the global ocean (60°N–60°S). Geochimica et Cosmochimica Acta 62, 1757–1772.
Pagani, M., Arthur, M.A., Freeman, K.H., 1999. Miocene evolution of atmospheric carbon dioxide. Paleoceanography 14, 273–292.
Pagani, M., Zachos, J.C., Freeman, K.H., Tipple, B., Bohaty, S., 2005. Marked decline in atmospheric carbon dioxide concentrations during the Paleogene. Science 309, 600–603.
Prahl, F.G., Wakeham, S.G., 1987. Calibration of unsaturation patterns in long-chain ketone compositions for palaeotemperature assessment. Nature 330, 367–369.
Quaijtaal, W., Donders, T.H., Persico, D., Louwye, S., 2014. Characterising the middle Miocene Mi-events in the Eastern North Atlantic realm: A first high-resolution marine palynological record from the Porcupine Basin. Palaeogeography, Palaeoclimatology, Palaeoecology 399, 140–159.
Quaijtaal, W., Tesseur, S., Donders, T.H., Claeys, P., Louwye, S., 2017. A revised and improved age model for the middle Miocene part of IODP Site U1318 (Porcupine Basin, offshore southwestern Ireland). Geological Magazine.
Retallack, G.J., 2009. Refining a pedogenic-carbonate CO2 paleobarometer to quantify a middle Miocene greenhouse spike. Palaeogeography, Palaeoclimatology, Palaeoecology 281, 57–65.
Royer, D.L., Wing, S.L., Beerling, D.J., Jolley, D.W., Koch, P.L., Hickey, L.J., Berner, R.A., 2001. Paleobotanical Evidence for Near Present-Day Levels of Atmospheric CO2 During Part of the Tertiary. Science 292, 2310 LP-2313.

Schouten, S., Hopmans, E.C., Schefuß, E., Sinninghe Damsté, J.S., 2002. Distributional veriations in marine crenarchaeol membrane lipids: a new tool for reconstructing ancient sea water temperatures? Earth and Planetary Science Letters 204, 265–274.

Schouten, S., Huguet, C., Hopmans, E.C., Kienhuis, M.V.M., Damste, J.S.S., 2007. Analytical Methodology for TEX 86 Paleothermometry by High-Performance Liquid Chromatography / Atmospheric Pressure Chemical Ionization-Mass Spectrometry. Analytical chemistry 79, 2940–2944.

Schreck, M., Meheust, M., Stein, R., Matthiessen, J., 2013. Response of marine palynomorphs to Neogene climate cooling in the Iceland Sea (ODP Hole 907A). Marine Micropaleontology 101, 49–67.

Shevenell, A., Kennett, J., 2004. Paleoceanographic change during the Middle Miocene climate revolution: an Antarctic stable isotope perspective, in: Exon, N.F., Kennett, J.P., Malone, M.J. (Eds.), The Cenozoic Southern Ocean: Tectonics, Sedimentation, and Climate Change Between Australia ad Antarctica, American Geophysical Union. Washington, D.C., 235–251.

Shevenell, A.E., Kennett, J.P., Lea, D.W., 2004. Middle Miocene Southern Ocean cooling and Antarctic cryosphere expansion. Science 305, 1766–1770.

Shevenell, A.E., Kennett, J.P., Lea, D.W., 2008. Middle Miocene ice sheet dynamics, deep-sea temperatures, and carbon cycling: A Southern Ocean perspective. Geochemistry, Geophysics, Geosystems 9, 1–14.

Tierney, J.E., Tingley, M.P., 2014. A Bayesian, spatially-varying calibration model for the TEX86 proxy. Geochimica et Cosmochimica Acta 127, 83–106.

Tierney, J.E., Tingley, M.P., 2015. A TEX86 surface sediment database and extended Bayesian calibration. Scientific Data 2, 150029.

Utescher, T., Ashraf, a R., Dreist, a, Dybkjær, K., Mosbrugger, V., Pross, J., Wilde, V., 2012. Variability of neogene continental climates in Northwest Europe — a detailed study based on microfloras . Turkish Journal of Earth Sciences 21, 289–314.

Versteegh, G.J.M., 1994. Recognition of cyclic and non-cyclic environmental changes in the Mediterranean Pliocene: A palynological approach. Marine Micropaleontology 23, 147–183.

Weijers, J.W.H., Lim, K.L.H., Aquilina, A., Damsté, J.S.S., Pancost, R.D., 2011. Biogeochemical controls on glycerol dialkyl glycerol tetraether lipid distributions in sediments characterized by diffusive methane flux. Geochemistry, Geophysics, Geosystems 12, 1–15.

Westerhold, T., Bickert, T., Röhl, U., 2005. Middle to late Miocene oxygen isotope stratigraphy of ODP site 1085 (SE Atlantic): New constrains on Miocene climate variability and sea-level fluctuations. Palaeogeography, Palaeoclimatology, Palaeoecology 217, 205–222.

Woodruff, F., Savin, S.M., 1989. Miocene Deepwater Oceanography. Paleoceanography 4, 87–140.

Woodruff, F., Savin, S.M., 1991. Mid-Miocene isotope stratigraphy in the deep sea: High-resolution correlations, paleoclimatic cycles, and sediment preservation. Paleoceanography 6, 755–806.

Zachos, J., Pagani, M., Sloan, L., Thomas, E., Billups, K., 2001. Trends, rhythms, and aberrations in global climate 65 Ma to present. Science 292, 686–693.

Zhang, Y.G., Zhang, C.L., Liu, X.L., Li, L., Hinrichs, K.U., Noakes, J.E., 2011. Methane Index: A tetraether archaeal lipid biomarker indicator for detecting the instability of marine gas hydrates. Earth and Planetary Science Letters 307, 525–534.

Zhang, Y.G., Pagani, M., Liu, Z., Bohaty, S.M., DeConto, R., 2013. A 40-million-year history of atmospheric CO 2 A 40-million-year history of atmospheric CO 2. Philosophical transactions of The Royal Society.

Zhang, Y.G., Pagani, M., Wang, Z., 2016. Ring Index : A new strategy to evaluate the integrity of TEX_{86} paleothermometry. Paleoceanography 31, 220–232.

Zonneveld, K.A.F., Marret, F., Versteegh, G.J.M., Bogus, K., Bonnet, S., Bouimetarhan, I., Crouch, E., de Vernal, A., Elshanawany, R., Edwards, L., Esper, O., Forke, S., Grøsfjeld, K., Henry, M., Holzwarth, U., Kielt, J.-F., Kim, S.-Y., Ladouceur, S., Ledu, D., Chen, L., Limoges, A., Londeix, L., Lu, S.-H., Mahmoud, M.S., Marino, G., Matsouka, K., Matthiessen, J., Mildenhal, D.C., Mudie, P., Neil, H.L., Pospelova, V., Qi, Y., Radi, T., Richerol, T., Rochon, A., Sangiorgi, F., Solignac, S., Turon, J.-L., Verleye, T., Wang, Y., Wang, Z., Young, M., 2013. Atlas of modern dinoflagellate cyst distribution based on 2405 data points. Review of Palaeobotany and Palynology 191, 1–197.

Chapter 6.
Conclusions

Willemijn Quaijtaal

Unpublished

Conclusions

The middle Miocene of the Porcupine Basin (IODP Site U1318) was studied palynologically at a high resolution (~20 ka sample spacing). These data were combined with benthic stable carbon and oxygen isotopes and organic geochemical temperature reconstructions and led to the precise determination of the ages and the duration of the Mi-events in the in eastern North Atlantic realm for the first time. We have been able to compare these cooling events in terms of magnitude using the organic geochemical temperature signal and biotic responses as inferred from the organic-walled dinoflagellate cyst record. By applying stable isotope stratigraphy the scale and timing of changes at Site U1318 could be compared to the global record.

1. Revising the Site U1318 age model

An initial age-depth model for Site U1318, based on magnetostratigraphy and dinocyst biostratigraphy, was constructed by *Louwye et al.* (2008). However, this model was presented in meters below seafloor (mbsf) instead of meters composite depth (mcd), a prerequisite when working with parallel cores. Therefore, stratigraphic tie-points were converted to mcd and adapted to the 2012 time scale (*Gradstein et al.*, 2012). In addition, the shipboard palaeomagnetic measurements suffered from magnetic overprint and noise from the cryogenic magnetometer. This led to a very low magnetic intensity signal, leading to difficulties reading the signal. The measurement of discrete samples to avoid magnetic overprint by *Louwye et al.* (2008) improved the interpretation of the magnetostratigraphy. Nonetheless, measurements were only performed on samples from Hole U1318B, leaving the core gap covered by Hole U1381C uncovered. This could eventually lead to problems in global correlations, especially since biostratigraphy as a guide to magnetostratigraphy is prone to diachroneity. Therefore magnetostratigraphic tie-points from Hole U1318C were removed due to the lack of discrete measurements.

Through adding additional biostratigraphic tie-points from organic-walled dinoflagellate cysts and calcareous nannoplankton, the age-depth model could be significantly improved. It then became apparent that there were notable differences between the dinocyst and calcareous nannoplankton biostratigraphy and magnetostratigraphy. However, biostratigraphic tie-points can be rather diachronous, so other globally correlatable points were needed to confidentially place the magnetostratigraphy.

Benthic foraminiferal carbon- and oxygen isotope stratigraphy provides an accurate tool for global correlation between records. Two correlational tools are available: the isotope stratigraphy of *Woodruff and Savin* (1991) and the Miocene oxygen isotope zones of *Miller et al.* (1991) that are also linked to magnetostratigraphy. Therefore, a benthic foraminiferal stable carbon ($\delta^{13}C$) and oxygen ($\delta^{18}O$) isotope record was produced. A total of 145 samples from IODP Site U1318 was taken and analysed. The epifaunal species *Cibicidoides pachyderma* and the infaunal species *Uvigerina* sp. were chosen for stable isotope measurements. The latter species was used since *C. pachyderma* was not present in every analyzed sample. Differences between the records of both species due to vital and environmental effects were corrected to values of *Cibicidoides pachyderma* using the following equations: $\delta^{18}O_{C.\ pachyderma} = 0.984 * \delta^{18}O_{Uvigerina\ sp.} - 0.296‰$ ($R^2 = 0.94$) and $\delta^{13}C_{C.\ pachyderma} = 0.692 * \delta^{13}C_{Uvigerina\ sp.} + 1.137‰$ ($R^2 = 0.52$).

The benthic $\delta^{13}C$ and $\delta^{18}O$ records were first compared to two deep sea Pacific stable carbon and oxygen isotope records: Deep Sea Drilling Project Site 574 (*Woodruff and Savin*, 1991) and IODP Site U1338 (*Holbourn et al.*, 2014). The first record was used to define the original isotope stratigraphy of *Woodruff and Savin* (1991); the second record is a high-resolution record with an orbitally tuned age model. Combining both records led to the identification of carbon isotope maxima CM2 through CM6b and isotope minima and maxima B through F. By comparing the isotope stratigraphy of *Woodruff and Savin* (1991) to the ages of the events at Site U1338 it was also possible to correlate the $\delta^{18}O$ zonation and Miocene isotope (Mi-)events of *Miller et al.* (1991) using the ages of *Boulila et al.* (2011). This way Mi-events Mi-2a, Mi-2, Mi-3 and Mi-4 could be identified unequivocally. Since these are linked to the magnetostratigraphic record potential issues with the magnetostratigraphic record of Site U1318 could be resolved.

A first age indication could be given by linking the isotope stratigraphy of *Woodruff and Savin* (1991) at Site U1318 to the ages of Site U1338. These indicate an age of the record from somewhat older than 16 Ma to somewhat younger than 13 Ma, in contrast to the age model of *Quaijtaal et al.* (2014) that indicates an age of ca 17.8 to 12 Ma. The ages based on isotope stratigraphy also matched better with the biostratigraphic tie-points. The magnetostratigraphic tie-points provided by correlation to the Mi-zones of *Miller et al.* (1991) showed that the magnetostratigraphy was two chrons too old around Mi-2 and one chron too old at Mi-2 relative to the tie-points of *Miller et al.* (1991). On the other hand, at Mi-3 the magnetostratigraphy was one chron too young and at Mi-4 two chrons too young. Due to this non-linear offset the magnetostratigraphic signal was studied again. Previous subchrons C5Bn.1r, C5Bn.2n and C5Br were reinterpreted as one subchron: C5Br. Subchrons C5Ar.2n, C5Ar.3r and C5AAn were reinterpreted as C5ABn.

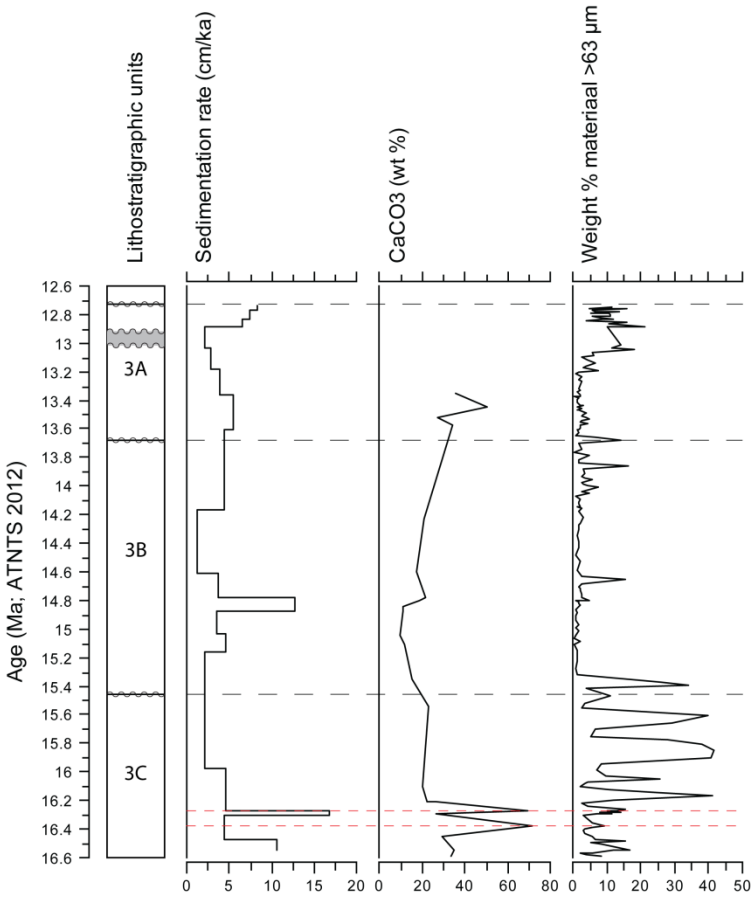

Figure 6.1: Lithostratigraphic units, sedimentation speeds, $CaCO_3$ content (from *Expedition 307 Scientists* (2006)) and weight % material >63 µm against the age model from *Quaijtaal et al.* (2017).

The new age model for Site U1318 encompasses an age of 12.75–16.60 Ma for the sampled interval with an average sampling resolution of ~29 ka. Sedimentation rates with the improved age model vary between ~1.2 to 16.9 cm/ka (See Figure 6.1). The unconformity separating lithostratigraphic units 3C and 3B is dated at ~15.5 Ma. Unit 3C is characterized by high weight percentages of the fraction material >63 µm. Sedimentation speeds decrease as the wt% >63 µm increases. This can be indicative of faster flowing bottom water currents. Two dolomitized intervals are present in this unit (Figure 6.1). This could indicate that

sedimentation came to a complete halt allowing for lithification but based on the current age model this process cannot be linked to any of the environmental processes assessed in this thesis.

Palaeoceanographical rearrangements are a more likely option. *Woodruff and Savin* (1989) and *Wright et al.* (1992) suggest that before the RD2 reflector that separates units 3C and 3B prevalent deep and intermediate waters were most likely dominated by Southern Component Water (SCW; an analogue of the modern Antarctic Bottom Water; AABW) or Southern Component Intermediate Water (SCIW) respectively, supplemented by two warmer water masses with higher salinity: Northern Component Water (NCW), though in very small volumes, and Tethyan Outflow Water (*Woodruff and Savin*, 1989; *Wright et al.,* 1992). *Van Rooij et al.* (2003) suggest that the RD2 reflector and concomitant unconformity is caused by *'vigorous bottom currents due to the introduction of Norwegian Sea Water in the North Atlantic Ocean'*, as previously suggested by *Thiede* (1980). The latter author suggests that during the middle Miocene the Iceland-Faeroe Ridge started to subside, allowing water from the Norwegian-Greenland Seas to flow into the North Atlantic Ocean. However, *Thiede* (1980) also states that full submergence was not reached until the Pliocene. This change from prevalence of SCW or SCIW to NCW could have affected bottom water currents. If this were the case, the start of NCW flowing into the North Atlantic can now be dated at ~15.5 Ma.

The unconformity separating lithostratigraphic units 3B and 3A is dated at ~13.7 Ma. This date is coeval with the maximum extent of the Mi-3 event. Since Mi-3 is generally associated with cryosphere extension it is likely that this unconformity is the result of glacioeustatic sea-level lowering. It is remarkable that no distinct hiatus is present, confirming the uniqueness of the Porcupine Basin sediments.

The hiatus that follows from ~13.0–12.9 Ma is coeval with the climatological Mi-4 event. However, this event is not as severe as Mi-3 (see below). After this hiatus percentages of the fraction material >63 μm increase, as well as sedimentation speeds. This indicates that bottom water current speed increases again. Therefore, the hiatus might also be related to palaeoceanographical changes.

Which water masses were prevalent at the Porcupine Basin during the middle Miocene is still uncertain, but it appears that there were two distinct bottom water regimes: one with stronger bottom currents during lithostratigraphic unit 3C and the end of 3A, and a calmer environment during the deposition of unit 3B and the beginning of unit 3A.

2. Middle Miocene palynology

A first preliminary low-resolution palynological study on the Porcupine Basin by *Louwye et al.* (2008) indicated a clear response of the dinocyst assemblage in response to the transition from the Middle Miocene Climatic Optimum (MMCO) to the Middle Miocene Climatic Transition (MMCT).

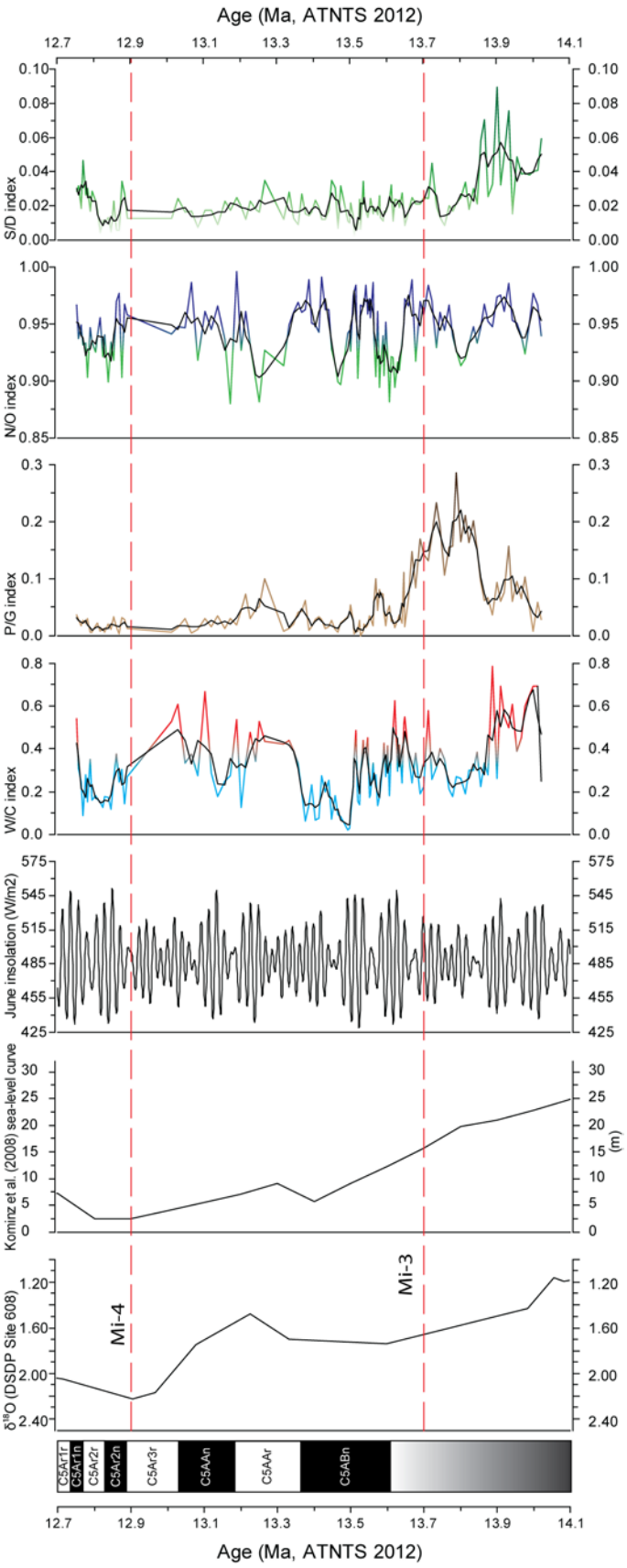

In the study of *Quaijtaal et al.* (2014) a high-resolution palynological analysis was carried out with a ~22 ka (50 cm) sample spacing. Since publication of this study the age model for Site U1318 was updated in *Quaijtaal et al.* (2017) and implications of the new age model will be discussed here. The studied interval still encompasses the majority of the MMCT (~14.0–12.75 Ma) with an average sample spacing of now ~20 ka. The analyzed interval is limited relative to the old model that encompassed a longer interval (14.4–12 Ma; See Figure 6.2) and Mi-3a is lost within the terminology used by *Quaijtaal et al.* (2017). This Mi-3a event is also not present in the most recent definitions and age-determinations by *Boulila et al.* (2011) which will be used subsequently.
Four qualitative environmental dinocyst indices were used to assess the palaeoenvironment: the warm/cold (W/C) index for relative sea-surface temperature (SST), the Peridinioid/Gonyaulacoid (P/G) index for sea-surface productivity and the neritic/oceanic (N/O) and sporomorph/dinocyst (S/D) indices for relative sea level. In addition, dinocyst diversity was calculated using three methods: richness (number of species), Shannon-Wiener index, and evenness.

Two Mi-events were identified in the record: Mi-3 and Mi-4 (in contrast to the ages and definitions provided by *Miller et al.*, 1996, Figure 12 of Chapter 2). Mi-3 is the largest event in the studied interval of *Quaijtaal et al.* (2014). It is accompanied by a prominent stepwise decrease in SST, a sea level lowering and an increase in

Figure 6.2: Magnetostratigraphy, $\delta^{18}O$ of DSDP Site 608, *Kominz et al.* (2008) sea-level curve, June insolation at the Porcupine Basin and palaeoecological indices versus age (Ma; ATNTS 2012; newest age model). Isotope data and positioning of the Mi-zones from *Miller et al.* (1991) and *Abels et al.* (2005), insolation data from *Laskar et al.* (2004). Red lines indicate the position of the Mi-zones. Thick black line is a 3-point running average of the indices.

productivity and dinocyst diversity, as inferred from the W/C, P/G, N/O and S/D indices. During Mi-4 decreases in SST, sea level and dinocyst diversity can also be observed but there is no increased productivity. The event is also shorter in duration than Mi-3. Minima and maxima in SST correlate to June insolation minima and maxima and indicate a significant role for orbital forcing of the Mi-events and the marine biotic response. Palynomorph-derived sea-level based on the S/D index correlates to the western North Atlantic backstripped sea-level record of *Kominz et al.* (2008), but the response of the N/O index after updating the age model was less clear, most likely because of the relatively offshore position of Site U1318. The N/O index shows a cyclic behaviour, with cycles of approximately 200 ka.

Typical of Mi-3 is the acme of the dinocyst species *Palaeocystodinium golzowense*, peaking at ~13.8 Ma. This acme could point towards lower sea-surface salinity and/or higher primary productivity since *Palaeocystodinium golzowense* has a supposed heterotrophic feeding habit, but could also be tolerant to low-salinity environments. Strengthened northerlies could have enhanced upwelling, providing the extra nutrients into the environment. However, since with the current data it is not possible to separate both factors, additional data on either *Palaeocystodinium golzowense* from other locations, sea-surface salinity and –productivity is essential to elucidate the acme.

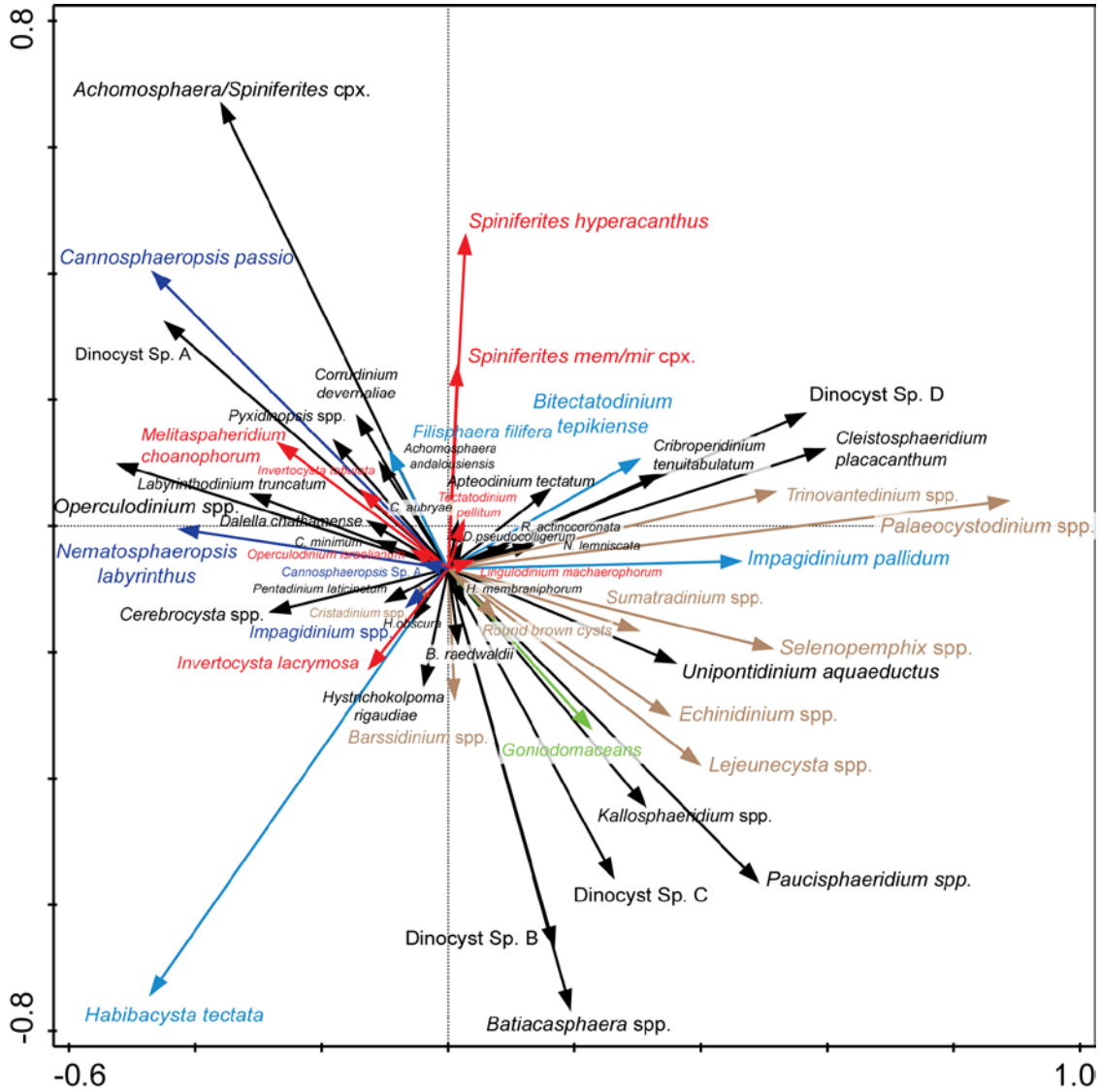

Figure 6.3: PCA bi-plot of the first and second PCA axes. Species abundance data were transformed using a Hellinger transformation. Warm-water species indicated in red, cold-water species indicated in light blue, inner neritic species in green, outer neritic and oceanic species in dark blue, peridinioid species in brown.

Using multivariate statistics tentative palaeoecological preferences of five dinocyst species was derived. The initial PCA by *Quaijtaal et al.* (2014) was heavily skewed by the large influence of three taxa: *Habibacysta tectata, Palaeocystodinium golzowense* and the *Spiniferites/Achomosphaera* complex. Therefore, a Hellinger transformation was performed on the data prior to performing the PCA (Figure 6.3). This method gives low weight to rare species and obtains a more equal spread in a PCA (*Legendre and Gallagher,* 2001). In the PCA with untransformed data the variance explained by the first two axes was 72.3%, where the first axis represented a combination of sea-surface productivity and -temperature, and the second axis represented relative sea-level. In the PCA with the transformed data the first two axes only explain 36.44% of the data variance (first axis 20.57%, second axis 15.87%). The only axis that can be explained by known environmental parameters is the first PCA axis. On the right side most heterotrophic species, cold-water species and inshore species plot, whereas warm-water and offshore species plot on the left side. These are variables that co-vary during global cooling, i.e. cooling and/or glaciation lead to a sea-level lowering, and enhanced input of nutrients due to either enhanced upwelling or input from the continent.
This change in species distribution could also alter the inferred environmental preferences of five dinocyst taxa *Batiacasphaera hirsuta* and the *Batiacasphaera* complex still have a neritic preference in environments enriched in nutrients based on the new PCA. *Batiacasphaera hirsuta* furthermore has a more proximal neritic preference than the *Batiacasphaera* complex based on the N/O index. *Labyrinthodinium truncatum* still prefers warmer conditions, but the neritic association is doubtful based on the new PCA. *Paucisphaeridium* sp. A and *Paucisphaeridium* sp. B likely still prefer proximal, eutrophic environments.

3. Early to middle Miocene acritarch biostratigraphy

During the palynological study mentioned above special interest was given to acritarchs. Most marine palynological preparation methods use a sieve with a 15 µm mesh rather than a 10 µm mesh, resulting in a loss of small (>15 µm) palynomorphs such as dinocysts, acritarchs and pollen. However, acritarchs can significantly outnumber dinocysts in abundance and they are of biostratigraphical and palaeoecological importance (*De Schepper and Head*, 2008, 2014). Therefore, the small palynomorphs were specially noted. This resulted in the discovery of six new species of acritarchs: *Cometesphaera bullatio* gen. nov. et sp. nov., *Cymatiosphaera*? *deverteuilii* sp. nov., *Platycystidia manumii* sp. nov., *Porcupinea collaris* gen. nov et sp. nov., *Porcupinea indentata* gen. nov. et sp. nov. and *Pusillisphaera solaris* gen. nov. et sp. nov. were all described from the Porcupine Basin. Their stratigraphic ranges were determined and their palaeoecological preferences assessed using multivariate statistics.

Cometesphaera bullatio is a small acritarch with a round central body and a membrane on the lower half that resembles the tail of a comet, hence the name. The membrane is pitted and several columnar structures connect the outer membrane — or velum — to the inner body. The pylome is located at the apex (the top) of the acritarch and is polygonal. The operculum is free. The average inner body of a specimen is ~14.7 µm in diameter, and 0.4 µm thick. The outer wall is 0.3 µm thick, with a maximal separation between the inner and outer body of 8.8 µm. The species occurs from the upper Burdigalian (or older) up to the lower Serravallian where it goes extinct in magnetosubchron C5ABr. The species is most likely associated with warmer sea-surface conditions or conditions with more transport from the shelf.

Cymatiosphaera? *deverteuilii* is a small spherical to subspherical acritarch that is covered with meandering septa that form a labyrinth-like structure with irregular polygonal fields on the acritarch.

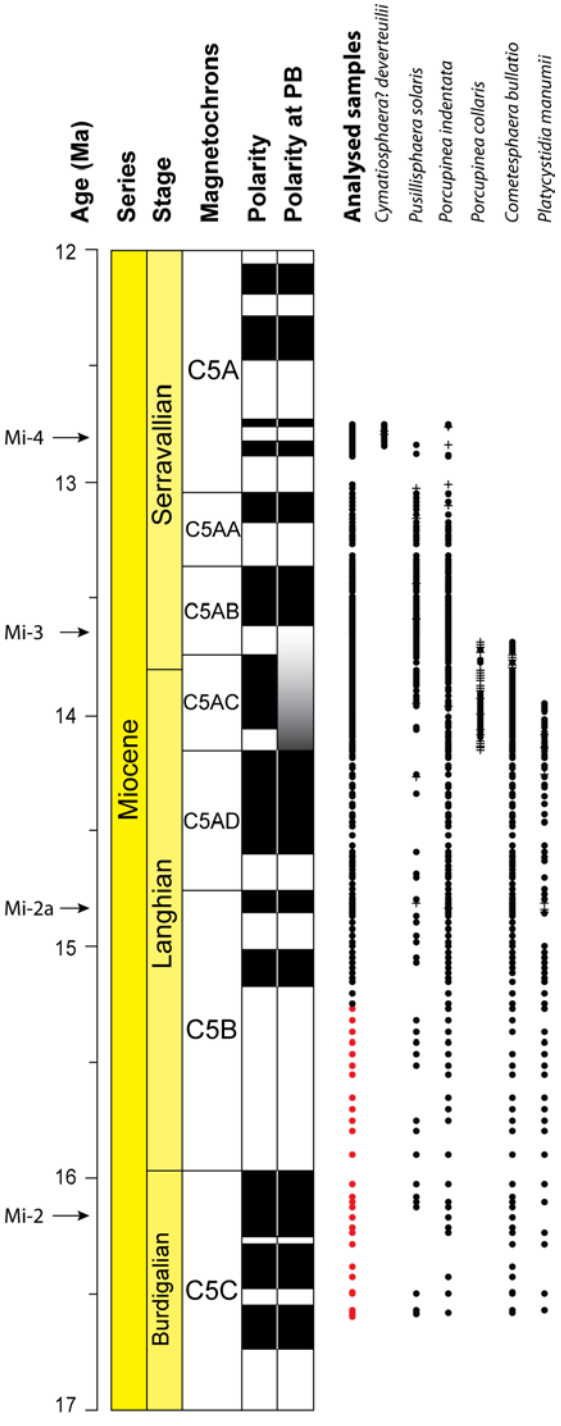

Figure 6.4: Revised age, stratigraphy and magnetostratigraphy of the sequence studied in Holes U1318B and U1318C. Polarity at PB: polarity at the Porcupine Basin. Sample positions are given, red circles represent 28 additional (unpublished) samples. The ranges of the acritarch species are listed according to their highest occurrence (HO).

The pylome is located at the apex and is polygonal with distinct angular edges. The operculum is free. The average diameter of the inner body is ~14.3 µm and the thickness is 0.2 µm. The septa are ~2.1 µm high. It first appears in the Serravallian in magnetosubchron C5Ar.2n (updated against the newest age-model, see below) and disappears in the upper Miocene of the Irminger Basin as Gen. et sp indet VI (*Engel*, 1992). The species likely has a preference for colder surface waters in an oligotrophic setting.

Platycystidia manumii is a small elongate subrectangluar acritarch that consists of two layers. The outer wall is mesh-like but appears granular under the light microscope. It forms wing-like folds around the inner body. The slightly thicker inner body is elongate. No pylome could be observed. The inner body is ~9.1 µm wide and ~15.4 µm long and the outer body is ~17.7 µm wide and 20.0 µm long. The species occurs from the upper Burdigalian and disappears in the upper Langhian in magnetosubchron C5ACn (updated against the newest age-model, see below). Based on multivariate statistics this species probably has a preference for warm surface waters or conditions with more transport from the shelf.

Porcupinea collaris is a small spheroidal to subsphaeroidal acritarch that has a broad equatorial spongy collar or flange around the inner body. The smooth-edged collar can take up to half of the circular outline. There is a varying number (3–9) of slender, hollow and striated processes on both sides of the collar. The irregular pylome is probably at the apex of the acritarch and the operculum, bearing three to four processes, is often collapsed into the inner body. The average diameter of the species is 28.0 µm, the inner body measures ~13.2 µm and the processes are ~4.0 µm on average. *Porcupinea collaris* first appears during the upper Langhian (just above magnetosubchron C5ADn) and ranges to the lower Serravallian (Base C5ABr). No clear palaeoenvironmental association could be determined based on the multivariate statistics.

Porcupinea indentata is similar to *P. collaris*, but it has shallow to deep indentations in the collar. Its processes widen proximally, and distally they form platform-like structures with spiny margins. These spines are also projected across the collar. The pylome is irregular polygonal, with a free operculum. The average maximum diameter is 24.6 µm, the inner body is on average 13.2–14.9 µm in diameter and the processes measure ~5.0 µm. *Porcupinea indentata* appears from the uppermost Burdigalian to the upper Serravallian. It shows a preference for colder waters or conditions with less transport from the shelf.

Pusillisphaera solaris is a subspherical to spherical acritarch consisting of two layers. The outer layer is connected to the inner body through numerous non-tabular invaginations. These funnel-shaped invaginations give the acritarch a sun-shaped appearance under the microscope. There are no invaginations close to the pylome that is polygonal with a simple, free operculum. The inner body is ~14.8 µm on average, the distance between the inner body and outer wall is 3.9 µm on average. It occurs from the upper Burdigalian throughout the Langhian into the lower Serravallian. Multivariate statistics showed no clear environmental preferences.

After publication of the paper by *Quaijtaal et al.* (2015) the age model and magnetostratigraphy have been revised. Therefore, the ranges of the six acritarch species were plotted against the most recent age-model in Figure 6.4. Additionally, data points from 28 samples that were analysed after publication of the study (unpublished data) were added to this figure. The new age-model has no stratigraphic implications for *Porcupinea indentata* and *Pusillisphaera solaris* since they are long-ranging species that occur throughout the record. According to the new age model they would only range from the Langhian, but with the newly analysed samples the lowest occurrences (LO) remain within the Burdigalian. The LO of *Cymatiosphaera*? *deverteuilii* is now within magnetosubchron C5Ar.2n rather than C5An.2n and therefore somewhat older. The highest occurrences (HO) of *Cometesphaera bullatio* and *Porcupinea collaris* are still within the uncertain part of the magnetostratigraphy, possibly within C5ABr rather than C5ABn. The LO of *Porcupinea collaris* has shifted from C5Bn.1n to the older C5ACn, still within the uncertain part of the magnetostratigraphy. The HO of *Platycystidia manumii* has become somewhat younger at C5ACn instead of C5ADn. It is also possible to place the LOs and HOs of the species in an environmental context because of the temperature reconstructions in Chapter 5. The LO of *Porcupinea collaris* is at ~14.16 Ma, and its LO at ~13.69 Ma. This interval is coeval with the interval where the largest change in SST_{dino} can be observed. According to the CCA *P. collaris* does not have a clear environmental preference, but it is possible that the species is tolerant to the quickly changing conditions occurring at the start of the MMCT. The HO of *Platycystidia manumii* at ~13.95 is contemporaneous with the initiation of the Mi-3 cooling as can be observed in the benthic $\delta^{18}O$ and SST_{TEX86H}, as well as the point where the SST_{dino} permanently indicates cooler temperatures. It is likely that this species was intolerant to colder surface waters, especially since the CCA indicates the species to have a preference for warmer sea-surface waters. The HO of *Cometesphaera bullatio* at 13.69 Ma, coeval with that of *Porcupinea collaris,* was already noted to fall within the hiatus that separates lithostratigraphic units 3a and 3B. Around that time SST_{TEX86H} decreases ca. 3.5°C. *Boulila et al.* (2011) have dated Mi-3 at 13.7 Ma, and although maximum benthic $\delta^{18}O$ is somewhat younger at the Porcupine Basin, it is very likely that the HOs of *Cometesphaera bullatio* and *Porcupinea collaris* can be associated with Mi-3 and the concomitant decrease in SST. The LO of *Cymatiosphaera*? *deverteuilii* at 12.84 Ma follows shortly after Mi-4. Temperatures were low, confirming the colder preferences as indicated by the CCA.

4. Temperature change across the MMCO and MMCT

A yet unattended question is what processes exactly are responsible for the change from the MMCO into the MMCT. Modelling studies often suffer from mismatches between modelled and proxy data (e.g. *Goldner et al.*, 2014; *Herold et al.*, 2012). This is caused by a severe lack of numerical (temperature) data that can be used as model input, especially in the North Atlantic Ocean. There are more high-resolution stable benthic oxygen isotope records available (e.g. *Holbourn et al.*, 2014; *Shevenell et al.*, 2004; *Westerhold et al.*, 2005), but not all of them span the entire MMCO and MMCT, or they suffer from significant hiatuses. None of these high-resolution records is available in the North Atlantic Ocean. An additional problem is that the temperature signal in benthic $\delta^{18}O$ records cannot be separated from the cryosphere component. This stresses the need for North Atlantic temperature records.

Therefore three sea-surface temperature records were generated from IODP Site U1318: one based on the TEX_{86} proxy, one based on the $U^{K'}_{37}$ proxy and a qualitative relative sea-surface temperature proxy based on dinocyst assemblages. These were compared to the Site U1318 benthic $\delta^{18}O$ record that was created for isotope stratigraphy, a compilation of CO_2 records and the orbital parameters obliquity and eccentricity, as well June insolation for 65°N.

TEX_{86}-temperatures (SST_{TEX86}) during the MMCO and MMCT show a gradual cooling from 27°C from the late Burdigalian to 16.4°C in the early Serravallian and were significantly higher than nowadays (12.6°C annually, 0–10 m water depth at Site U1318; *Locarnini et al.*, 2013). Superimposed on the gradual cooling trend there are near-cyclic changes of 2–4°C. Furthermore there is a strong correlation to the benthic $\delta^{18}O$ record ($R^2 = 0.88$). SST_{TEX86} also is very similar to the benthic $\delta^{18}O$ record of Pacific Ocean Site U1338, implicating that there is a major northern hemisphere temperature component in the global $\delta^{18}O$ signal. $U^{K'}_{37}$ temperatures ($SST_{Uk'37}$) are even higher (25.8–29°C), but the $U^{K'}_{37}$ approaches its maximum and thus maximum detectable temperatures. There is a less strong correlation to SST_{TEX86} ($R^2 = 0.66$). The substantial difference between SST_{TEX86} and $SST_{Uk'37}$ and the stronger correlation of SST_{TEX86} to benthic $\delta^{18}O$ than to $SST_{Uk'37}$ led us to believe that the SST_{TEX86} represents subsurface rather surface temperatures. Relative sea-surface temperatures based on dinocyst assemblages (SST_{dino}) follow both short-term transient coolings and the long-term cooling trend.

All four Mi-events are represented in the SST_{TEX86} and SST_{dino} record. Remarkable is the two-step nature of Mi-2a. Mi-3 is the most prominent of all four Mi-events, with a decrease in SST_{TEX86} of ca. 6°C. From Mi-3 onwards $SST_{Uk'3}$ starts showing small temperature fluctuations in the order of ~1.5°C. SST_{dino} and $SST_{Uk'37}$, derived from organisms that bloom during spring and summer, lead the annual SST_{TEX86} signal from Mi-3 onwards, indicating that seasonal cooling and warming occur prior to mean annual cooling and warming, probably in response to summer melt of a continental northern hemisphere ice sheet. Global comparison also indicates a stronger pole to equator gradient during Mi-3 and Mi-4, indicative of stronger seasonality.

Comparison with eccentricity, obliquity and insolation shows that some smaller and the most important decreases in temperature coincide with minima in eccentricity and insolation. However, the larger temperature decreases during Mi-2 and Mi-3 additionally require a minimum in obliquity amplitude modulation. Permanent cooling only occurs after atmospheric CO_2 drops below 280 ppm, the limit for bipolar glaciation (*DeConto et al.*, 2008), implying that this threshold, in combination with minima in eccentricity and obliquity amplitude modulation are prerequisite for the onset of the MMCT.

5. Limitations on the assessment of the palaeoecology of dinocysts using organic chemistry

The subsequent step would be to correlate the organic geochemical TEX_{86} and $U^{K'}_{37}$ temperature records to organic-walled dinocyst and acritarch abundances in order to quantitatively determine early to middle Miocene temperature ranges of dinocysts and acritarchs. This is an interesting train of thought since most evidence on palaeoecological preferences of extinct dinocysts and acritarchs is indirect evidence, e.g. comparison with other species with known ecological affinities (e.g. *de Verteuil and Norris*, 1996; *Louwye et al.*, 2007), multivariate statistics (*Quaijtaal et al.*, 2014) or geographic distribution (e.g. *Head et al.*, 1989).

A first attempt to provide quantitative sea surface temperature ranges for extinct dinoflagellate cysts was made by De Schepper et al. (2011) who correlated relative abundances of extant and extinct dinocysts from the late Pliocene to early Pleistocene North Atlantic to planktonic foraminiferal Mg/Ca temperatures and compared temperature ranges of Pliocene–Pleistocene extant species to present ranges. A one-on-one comparison using split samples (one part palynology, one part organic geochemistry) from the Miocene of the Porcupine Basin would provide a good extension of De Schepper et al. (2011).

Such a study nonetheless proved problematic. On the one hand, problems were caused by the limitations of the study itself, such as the single study site and working with fossils in general (closed-sum effect, overrepresentation of certain species, taphonomical processes and transport). On the other hand the organic geochemical temperature proxies caused severe limitations

The first proxy, $U^{K'}_{37}$, would be the most ideal option for comparison with the dinocyst record, since the molecules used in this proxy are produced by haptophyte algae, primary producers among which coccolithophorids also belong. These algae share their photosynthetic habit and sea-surface habitat with most dinoflagellates, making it very likely that they live in the same water depths. Unfortunately, the $U^{K'}_{37}$ proxy proved unsuitable for this type of research since most values exceed a $U^{K'}_{37}$ of 0.9 and approach the maximum of 1, limiting the temperature range between 26–29°C (Chapter 5).

Temperatures reconstructed with TEX_{86} showed a much larger range (18–27°C) than $U^{K'}_{37}$ temperatures and would therefore be more suitable to study extinct dinocyst temperature ranges. However, the ecology of the producers of the molecules (GDGTs) used for the TEX_{86}, Thaumarchaeota, is complex. There is a wide diversity among the Thaumarchaeota and pure cultures are hardly available. They are chemoautotrophs and oxidize ammonia as a main nutrient source. Marine Thaumarchaeota are widespread throughout the water column, but predominantly below the upper photic zone <200m. Generally, Cenozoic temperatures reconstructed with TEX_{86} correlates well with SST reconstructed using $U^{K'}_{37}$ and planktonic foraminiferal $\delta^{18}O$ and Mg/Ca, and despite that Thaumarchaeota do not live in the photic zone, like dinoflagellates, TEX_{86} temperatures reflect annual mean SST in most cases (*Schouten et al.*, 2013, and references therein). Nonetheless, it is possible that Thaumarchaeota migrate to deeper water layers under influence of nutrient (ammonia) availability. In this case it is likely that TEX_{86} temperatures represent subsurface rather than surface temperatures. Furthermore, upwelling of cold waters towards the photic zone could influence SST_{TEX86} (*Schouten et al.*, 2013, and references therein).

In Chapter 5 it was concluded that there is a very likely possibility that TEX_{86} represents subsurface rather than surface temperatures, because of the difference in temperatures reconstructed by $U^{K'}_{37}$ and TEX_{86} and the good correlation with benthic foraminiferal stable oxygen isotopes.

However, with the currently available data from the Porcupine Basin it is impossible to assess temperatures of which depth are depicted. Additionally it is possible that, due to climatological changes, the ecology of the Thaumarchaeota has changed temporarily, like during Eocene Thermal Maximum 2 where they migrated towards deeper waters (*Sluijs et al.*, 2009). Due to these uncertainties the TEX_{86} temperature proxy cannot be used to assess extinct dinocyst temperature ranges.

Hence, in order to analyse temperature ranges of extinct dinocyst species either sites have to be found where 1) the $U^{K'}_{37}$ does not approach maxima, 2) the TEX_{86} has a confirmed surface signal or 3) there are other surface temperature proxies, such as the Mg/Ca ratio inferred from surface-dwelling planktonic foraminifera.

6. Future perspectives

As stated above, there is much uncertainty regarding the depth habitat of the Thaumarchaeota during the early to middle Miocene of the Porcupine Basin. One possibility to resolve this issue is to reconstruct the water column structure over time using planktonic foraminifera. This group of zooplankton can be subdivided in planktonic foraminifera with three different depth habitats: surface mixed layer; thermocline; sub-thermocline. Stable isotopes are a very suitable tool to assess water column structure (*Birch et al.*, 2013), but more ideally, temperature reconstructions using clumped isotopes or the Mg/Ca proxy would be required. By comparing the TEX_{86} temperature record to the individual planktonic Mg/Ca temperature records it is possible to disentangle the depth habitat of Thaumarchaeota, but also to constrain probable changes of habitat of Thaumarchaeota due to e.g. changes in the chemocline.

Another advantage of collecting planktonic stable isotopes is that by comparison of stable carbon and oxygen isotopes throughout the water column (including benthic foraminiferal isotopes) information can be obtained on stratification, seasonality and export productivity. The latter results can then be compared to the qualitative productivity record as inferred from dinocysts.

Even though the $U^{K'}_{37}$ temperature has severe limitations for the studied time interval at the Porcupine Basin, the alkenones on which the $U^{K'}_{37}$ proxy is based have a twofold use. The first use is, as previously mentioned, as temperature proxy. The second use is as CO_2 proxy. By measuring stable carbon isotopes ($\delta^{13}C$) on the $C_{37:2}$ alkenone and then combining these with planktonic foraminiferal $\delta^{13}C$ and TEX_{86} or Mg/Ca temperatures, past atmospheric CO_2 can be reconstructed. The principle behind this method is the isotopic fractionating between algal biomass and dissolved inorganic carbon that occurs during photosynthesis. This process is mainly controlled by [$CO_{2(aq)}$] (*Hollander and McKenzie*, 1991; *Pagani et al.*, 1999).

The palynological record can be expanded into the MMCO as well. Several samples were already analyzed for Chapter 5, but no detailed palynological and palaeoecological study was performed for the MMCO. A special interest could be paid to the occurrences of toxic dinocyst species such as *Polysphaeridium zoharyi* (cyst of *Pyrodinium bahamense*) in relationship to the warming that occurred during the MMCO. This interval also has higher percentages pollen, allowing for analysis of the continental response to middle Miocene climate change. In addition, there are several dinocyst taxa that are still under open nomenclature (Chapter 2) that can be described in a taxonomical paper. Some of these taxa might also have biostratigraphical importance and a new middle Miocene biostratigraphy for the eastern North Atlantic could be defined. The age model of *Quaijtaal et al.* (2017) will provide a solid base for this stratigraphy.

Additional improvement can be achieved by increasing the temporal resolution of the record, especially for the MMCO. The maximal possible resolution is one sample per ca. 12 ka, equalling one sample every 50 cm. This allows for detailed statistical correlation methods and time series analysis of the records, examining leads and lags between the different proxies and their causes.

Globally, more effort can be made to generate a global isotope stratigraphy on a higher resolution, rather than one high-resolution stable carbon and oxygen isotope stratigraphy that uses other definitions than the other lower-resolution stable benthic oxygen isotope zonation. Most Pacific and Southern Ocean stable carbon- and oxygen isotope records have a very high resolution allowing for astronomically-tuned age models. Stacking these records could lead to a stratigraphy based on specific peaks in the orbital parameters of the Earth, e.g. the 405 ka eccentricity cycle or a terminology similar to the *Lisiecki and Raymo* (2005) benthic stable oxygen isotope stack that covers 5.5 Ma until now. However, more globally distributed high-resolution benthic stable oxygen records are needed to achieve this goal, especially in the Arctic, Atlantic and Indian Oceans. Additional focus could lie on the opening of oceanic gateways, especially the Greenland-Scotland ridge, a key player in the formation of Northern Component Water (proto-North Atlantic Deep Water) and therefore meridional overturning circulation.

7. References

Birch, H., Coxall, H.K., Pearson, P.N., Kroon, D., O'Regan, M., 2013. Planktonic foraminifera stable isotopes and water column structure: Disentangling ecological signals. Marine Micropaleontology 101, 127–145.

Boulila, S., Galbrun, B., Miller, K.G., Pekar, S.F., Browning, J. V., Laskar, J., Wright, J.D., 2011. On the origin of Cenozoic and Mesozoic "third-order" eustatic sequences. Earth-Science Reviews 109, 94–112.

De Schepper, S., Fischer, E.I., Groeneveld, J., Head, M.J., Matthiessen, J., 2011. Deciphering the palaeoecology of Late Pliocene and Early Pleistocene dinoflagellate cysts. Palaeogeography, Palaeoclimatology, Palaeoecology 309, 17–32.

De Schepper, S., Head, M.J., 2014. New late Cenozoic acritarchs: evolution, palaeoecology and correlation potential in high latitude oceans. Journal of Systematic Palaeontology 12, 493–519.

De Schepper, S., Head, M.J., 2008. New dinoflagellate cyst and acritarch taxa from the Pliocene and Pleistocene of the Eastern North Atlantic (DSDP Site 610). Journal of Systematic Palaeontology 6, 101–117.

de Verteuil, L., Norris, G., 1996. Miocene dinoflagellate stratigraphy and systematics of Maryland and Virginia. Micropaleontology, supplement 42, 1–172.

DeConto, R.M., Pollard, D., Wilson, P.A, Pälike, H., Lear, C.H., Pagani, M., 2008. Thresholds for Cenozoic bipolar glaciation. Nature 455, 652–656.

Engel, E.R., 1992. Palynologische Evidenz klimarelevanter Ereignisse in miozänen Sedimenten des Nordatlantiks. Schweizerbart Science Publishers, Stuttgart, Germany.

Goldner, A., Herold, N., Huber, M., 2014. The challenge of simulating the warmth of the mid-Miocene climatic optimum in CESM1. Climate of the Past 10, 523–536.

Gradstein, F.M., Ogg, J.G., Schmitz, M.D., Ogg, G.M., Agterberg, F.P., Anthonissen, D.E., Becker, T.R., Catt, J.A., Cooper, R.A., Davydov, V.I., Gradstein, S.R., Grossman, E.L., Henderson, C.M., Hilgen, F.J., Hinnov, L.A., McArthur, J.M., Melchin, M.J., Narbonne, G.M., Paytan, A., Peng, S., Peucker-Ehrenbrink, B., Pillans, B., Saltzman, M.R., Simmons, M.D., Shields, G.A., Tanaka, K.L., Vandenberghe, N., Van Kranendonk, M.J., Zalasiewicz, J., Altermann, W., Babcock, L.E., Beard, B.L., Beu, A.G., Boyes, A.F., Cramer, B.D., Crutzen, P.J., van Dam, J.A., Gehling, J.G., Gibbard, P.L., Gray, E.T., Hammer, Ø., Hartmann, W.K., Hill, A.C., Hoffman, P.F., Hollis, C.J., Hooker, J.J., Howarth, R.J., Huang, C., Johnson, C.M., Kasting, J.F., Kerp, H., Korn, D., Krijgsman, W., Lourens, L.J., MacGabhann, B.A., Maslin, M.A., Melezhik, V.A., Nutman, A.P., Papineau, D., Piller, W.E., Pirajno, F., Ravizza, G.E., Sadler, P.M., Speijer, R.P., Steffen, W., Thomas, E., Wardlaw, B.R., Wilson, D.S., Xiao, S., 2012. The Geologic Time Scale. Elsevier, Boston.

Head, M.J., Norris, G., Mudie, P.J., 1989. Palynology and dinocyst stratigraphy of the Upper Miocene and lowermost Pliocene, ODP Leg 105, Site 646, Labrador Sea., in: Srivastava, S.P., Arthur, M., Clement, B., et al. (Eds.), Proceedings of the Ocean Drilling Program, Scientific Results Volume 105. Ocean Drilling Program, College Station, Texas, pp. 423–451.

Herold, N., Huber, M., Müller, R.D., Seton, M., 2012. Modeling the Miocene climatic optimum: Ocean circulation. Paleoceanography 27, PA1209.

Holbourn, A., Kuhnt, W., Lyle, M., Schneider, L., Romero, O., Andersen, N., 2014. Middle Miocene climate cooling linked to intensification of eastern equatorial Pacific upwelling. Geology 42, 19–22.

Hollander, D.J., McKenzie, J.A., 1991. CO2 control on carbon-isotope fractionation during aqueous photosynthesis: A paleo-pCO_2 barometer. Geology 19, 929–932.

Kominz, M.A., Browning, J. V., Miller, K.G., Sugarman, P.J., Mizintseva, S., Scotese, C.R., 2008. Late Cretaceous to Miocene sea-level estimates from the New Jersey and Delaware coastal plain coreholes: An error analysis. Basin Research 20, 211–226.

Legendre, P., Gallagher, E.D., 2001. Ecologically meaningful transformations for ordination of species data. Oecologia129, 271–280.

Lisiecki, L.E., Raymo, M.E., 2005. A Pliocene –Pleistocene stack of 57 globally distributed benthic $\delta^{18}O$ records. Paleoceanography 20, PA1003.

Locarnini, R.A., Mishonov, A. V., Antonov, J.I., Boyer, T.P., Garcia, H.E., Baranova, O.K., Zweng, M.M., Paver, C.R., Reagan, J.R., Johnson, D.R., Hamilton, M., Seidov, D., 2013. World Ocean Atlas 2013. Vol. 1: Temperature. S. Levitus, Ed.; A. Mishonov, Technical Ed.; NOAA Atlas NESDIS 73, 40.

Louwye, S., De Schepper, S., Laga, P., Vandenberghe, N., 2007. The Upper Miocene of the southern North Sea Basin (northern Belgium): a palaeoenvironmental and stratigraphical reconstruction using dinoflagellate cysts. Geological Magazine 144, 33–52.

Louwye, S., Foubert, A., Mertens, K., Van Rooij, D., The IODP Expedition 307 Scientific Party, 2008. Integrated stratigraphy and palaeoecology of the Lower and Middle Miocene of the Porcupine Basin. Geological Magazine 145, 321–344.

Miller, K.G., Mountain, G.S., the Leg 150 Shipboard Party, Members of the New Jersey Coastal Plain Drilling Project, 1996. Drilling and Dating New Jersey Oligocene–Miocene Sequences: Ice Volume, Global Sea Level, and Exxon Records. Science 271, 1092–1095.

Miller, K.G., Wright, J.D., Fairbanks, R.G., 1991. Unlocking the Ice House: Oligocene–Miocene Oxygen Isotopes, Eustasy, and Margin Erosion. Journal of Geophysical Research 96, 6829–6848.

Pagani, M., Arthur, M.A., Freeman, K.H., 1999. Miocene evolution of atmospheric carbon dioxide. Paleoceanography 14, 273–292.

Quaijtaal, W., Donders, T.H., Persico, D., Louwye, S., 2014. Characterising the middle Miocene Mi-events in the Eastern North Atlantic realm: A first high-resolution marine palynological record from the Porcupine Basin. Palaeogeography, Palaeoclimatology, Palaeoecology 399, 140–159.

Quaijtaal, W. Mertens, K.N., Louwye, S., 2015. Some new acritarchs from the lower and middle Miocene of the Porcupine Basin, North Atlantic Ocean: biostratigraphy and palaeoecology. Palynology 39(1), 37–55.

Quaijtaal, W., Tesseur, S., Donders, T.H., Claeys, P., Louwye, S., 2017. A revised and improved age model for the middle Miocene part of IODP Site U1318 (Porcupine Basin, offshore southwestern Ireland). Geological Magazine, DOI: https://doi.org/10.1017/S0016756816001278.

Thiede, J., 1980. Palaeo-oceanography, margin stratigraphy and palaeophysiography of the tertiary North Atlantic and Norwegian-Greenland Seas. Philosophical Transactions of the Royal Society of London A, 294, 177–185.

Schouten, S., Hopmans, E.C., Sinninghe Damsté, J.S., 2013. The organic geochemistry of glycerol dialkyl glycerol tetraether lipids: A review. Organic Geochemistry 54, 19–61.

Shevenell, A.E., Kennett, J.P., Lea, D.W., 2004. Middle Miocene Southern Ocean cooling and Antarctic cryosphere expansion. Science 305, 1766–1770.

Sluijs, A., Schouten, S., Donders, T.H., Schoon, P.L., Rohl, U., Reichart, G.-J., Sangiorgi, F., Kim, J.-H., Sinninghe Damste, J.S., Brinkhuis, H., 2009. Warm and wet conditions in the Arctic region during Eocene Thermal Maximum 2. Nature Geoscience 2, 777–780.

Van Rooij, D., De Mol, B., Huvenne, V., Ivanov, M., Henriet, J.P., 2003. Seismic evidence of current-controlled sedimentation in the Belgica mound province, upper Porcupine slope, southwest of Ireland. Marine Geology 195, 31–53.

Westerhold, T., Bickert, T., Röhl, U., 2005. Middle to late Miocene oxygen isotope stratigraphy of ODP site 1085 (SE Atlantic): New constrains on Miocene climate variability and sea-level fluctuations. Palaeogeography, Palaeoclimatology, Palaeoecology 217, 205–222.

Woodruff, F., Savin, S.M., 1989. Miocene Deepwater Oceanography. Paleoceanography, 4(1), 87–140.

Woodruff, F., Savin, S.M., 1991. Mid-Miocene isotope stratigraphy in the deep sea: High-resolution correlations, paleoclimatic cycles, and sediment preservation. Paleoceanography 6, 755–806.

Wright, J.D., K.G. Miller, Fairbanks, R.G., 1992. Early and middle Miocene stable isotopes: implications for deepwater circulation and climate. Paleoceanography, 7, 357–389.

Supplementary materials.

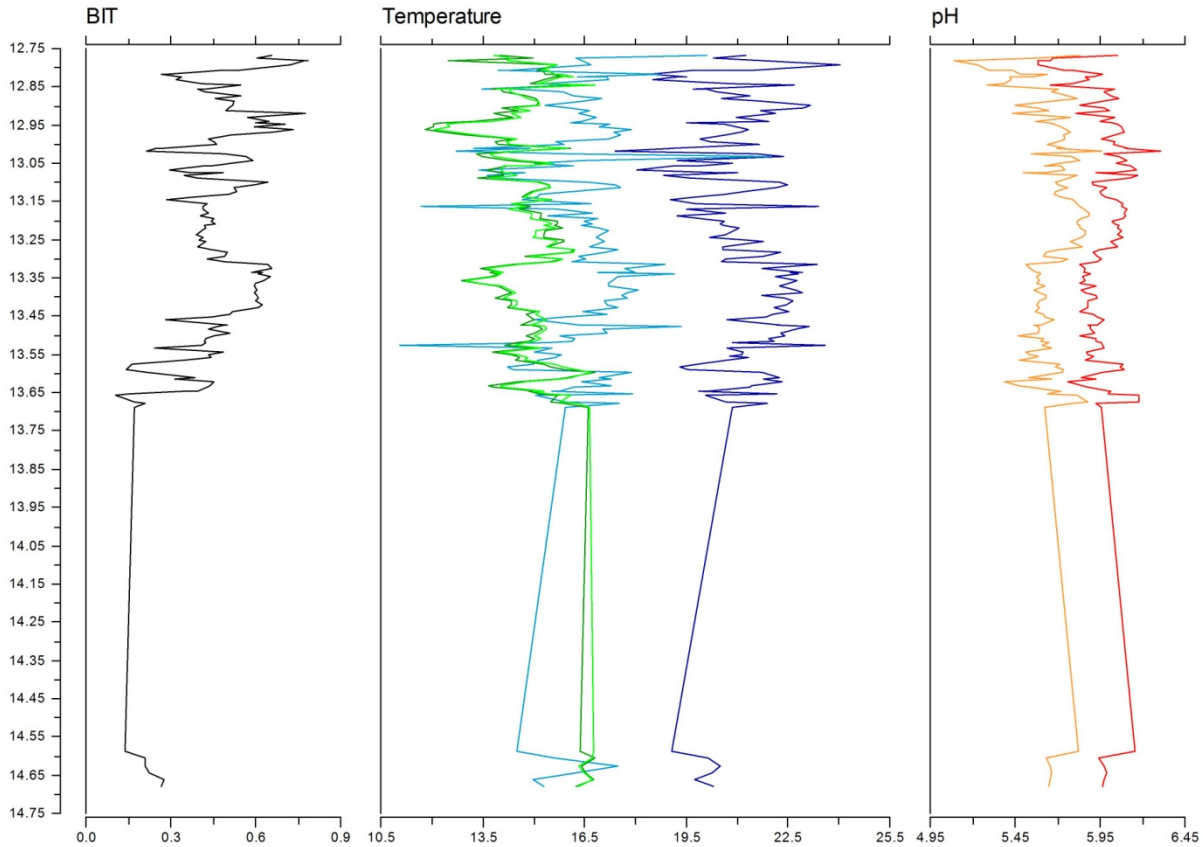

Supplementary Figure 1.1: BIT-index, temperature and soil pH of IODP Site M29A versus age in Ma. Temperature: dark green line represents Mean Annual Ttemperature $(MAT)_{mrs}$ (limited amount of GDGT's), light green line represents MAT_{mr}; light blue line represents TEX_{86}^{L} temperatures, dark blue line represents TEX_{86}^{H} temperatures. Soil pH: orange line represents pH_{mr}, red line represents soil pH_{mrs} (limited amount of GDGT's).

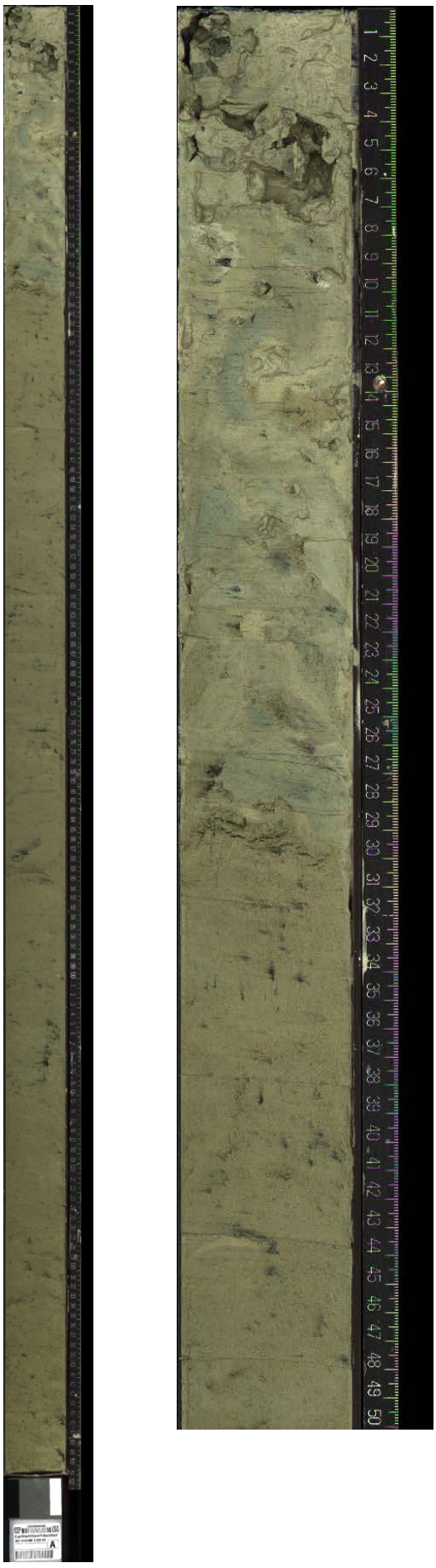

Supplementary Figure 2.1: Core photograph and a close-up of Core 12H1 of IODP Leg 307, Hole U1318B, showing an irregularity within the first 30 cm of the core.

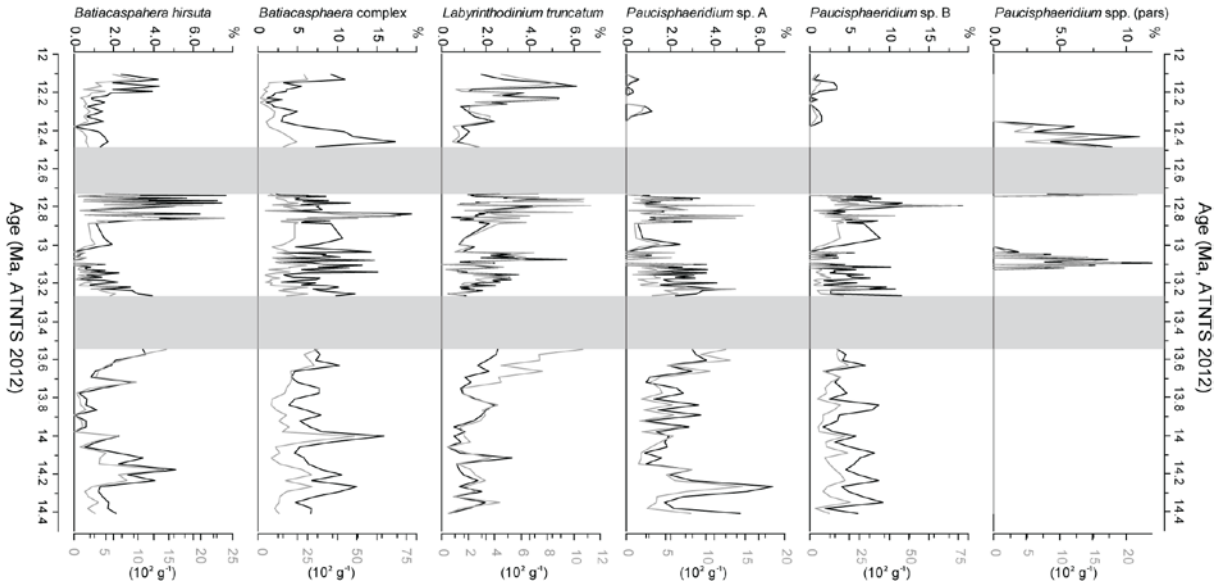

Supplementary Figure 2.2: Abundances of commonly occurring dinocyst taxa not included in the palaeoenvironmental indices versus age (Ma). Black solid lines indicate percentages of the total dinocyst assemblage, grey solid lines represent number of specimens per gram dry sediment. Grey area indicates the hiatus in the record.

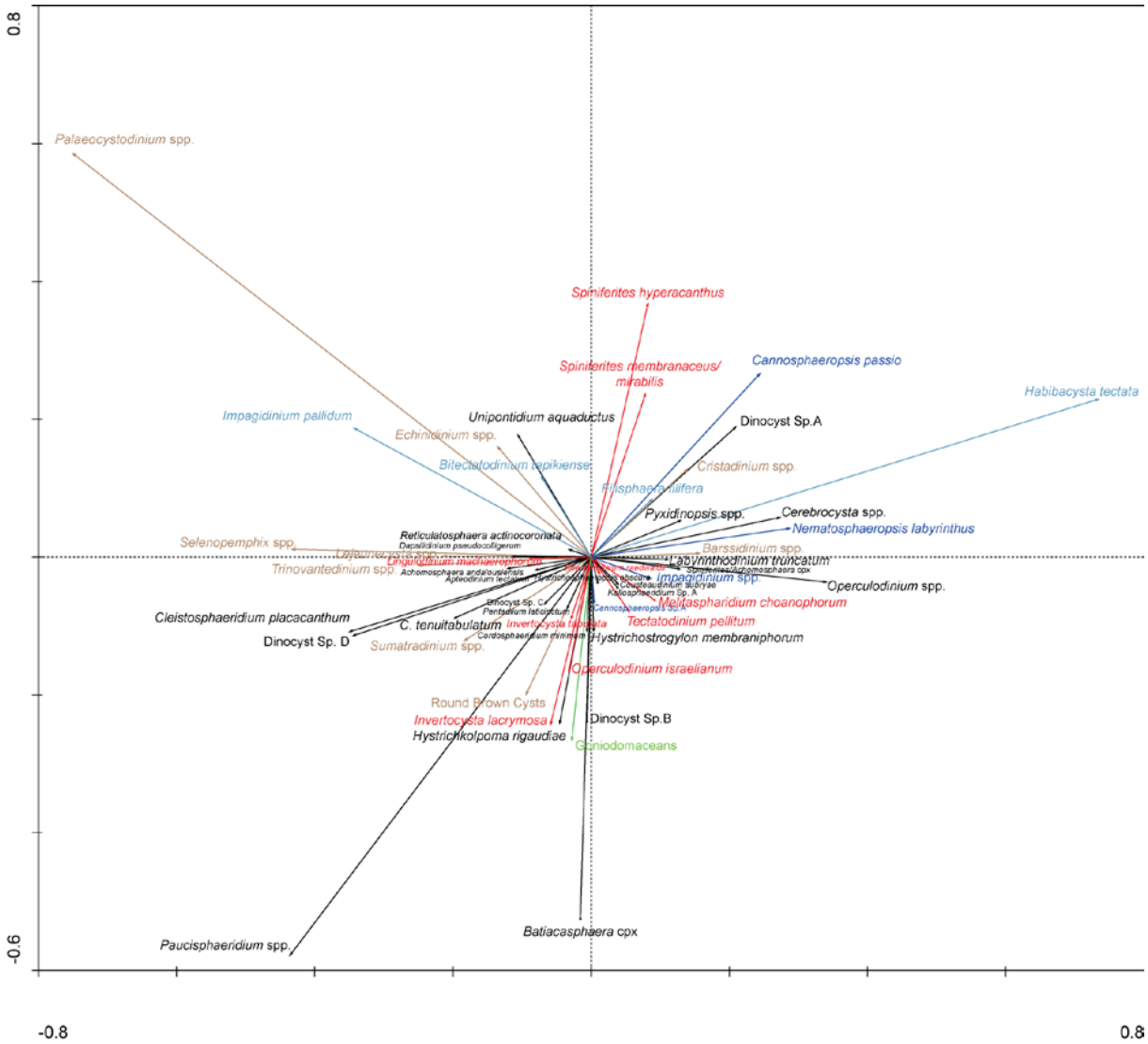

Supplementary Figure 2.3: PCA bi-plot of the second and third PCA axes. Warm-water species indicated in red, cold-water species indicated in light blue, inner neritic species in green, outer neritic and oceanic species in dark blue, peridinioid species in brown. Variation explained by axis 2 19.1%, variation explained by axis 3 10.3%.

On the following pages 138 – 152:

Supplementary Table 2.1: distribution of dinocysts and other organic-walled palynomorphs in Holes 1318B and 1318C

.

Leg	Site	Hole	Core	Type	Section	Top sample interval (cm)	Bottom sample interval (cm)	Core depth(mbsf)	Composite depth (mcd)	Age (Ma)	Batchnumber *Lycopodium* tables	Number of spores per tablet	Number of tablets	Dinoflagellate cysts	*Achomosphaera andalousiensis*	*Apteodinium tectatum*	*Barssidinium graminosum*	*Barssidinium pliocenicum*	*Barssidinium* spp. (pars)	*Batiacaspahera hirsuta*	*Batiacasphaera edwardsiae*	*Batiacasphaera* complex	*Bitektatodinium raedwaldii*	*Bitectatodinium tepikiense*	*Cannosphaeropsis passio*	*Cannosphaeropsis*? sp. A
307	1318	B	10	H	5	50	52	87.50	92.44	12.11	1031	20848	2		x	0	0	x	0	8	0	31	0	0	1	0
307	1318	B	10	H	5	109	111	88.09	93.03	12.13	1031	20848	2		0	0	1	x	0	15	0	39	0	0	0	0
307	1318	B	10	H	6	2	4	88.52	93.46	12.15	1031	20848	2		2	0	0	0	0	9	0	15	0	0	x	0
307	1318	B	10	H	6	50	52	89.00	93.94	12.17	1031	20848	2		x	0	0	0	0	14	1	18	0	0	x	0
307	1318	B	10	H	6	106	108	89.56	94.5	12.18	1031	20848	2		1	0	0	x	0	7	1	13	0	0	6	0
307	1318	B	10	H	7	17	19	90.03	94.97	12.19	1031	20848	2		1	0	0	1	0	13	2	12	0	1	9	0
307	1318	B	11	H	1	47	49	90.97	95.4	12.20	1031	20848	2		x	0	0	0	0	6	2	7	0	0	4	0
307	1318	B	11	H	1	97	99	91.47	95.9	12.22	1031	20848	2		1	0	0	x	0	6	x	7	0	0	6	0
307	1318	B	11	H	2	5	7	92.05	96.48	12.23	1031	20848	2		1	0	0	x	0	3	1	4	0	0	2	0
307	1318	B	11	H	2	55	57	92.55	96.98	12.24	1031	20848	2		1	0	0	x	0	3	1	10	0	0	3	0
307	1318	B	11	H	2	105	107	93.05	97.48	12.25	1031	20848	2		2	0	0	0	0	6	x	4	0	1	7	0
307	1318	B	11	H	3	1	3	93.51	97.94	12.26	1031	20848	2		x	0	0	0	0	4	x	5	0	0	5	0
307	1318	B	11	H	3	51	53	94.01	98.44	12.27	1031	20848	2		1	0	0	0	0	3	1	9	0	1	5	0
307	1318	B	11	H	3	105	107	94.55	98.98	12.30	1031	20848	2		x	0	0	1	0	5	x	17	0	x	6	0
307	1318	B	11	H	4	3	4	95.03	99.46	12.33	177745	18584	2		x	0	0	0	0	3	2	15	0	1	2	0
307	1318	B	11	H	4	52	54	95.52	99.95	12.35	177745	18584	2		1	0	0	0	0	5	1	10	0	2	5	0
307	1318	B	11	H	4	103	105	96.03	100.46	12.38	177745	18584	2		1	0	0	0	0	x	0	19	0	0	x	0
307	1318	B	11	H	5	2	4	96.52	100.95	12.41	177745	18584	2		1	0	0	0	0	4	x	35	0	0	1	0
307	1318	B	11	H	5	52	54	97.02	101.45	12.43	177745	18584	2		2	0	0	0	x	6	x	47	0	0	1	0
307	1318	B	11	H	6	2	4	97.52	101.95	12.46	177745	18584	2		6	0	1	2	0	7	x	72	0	0	x	0
307	1318	B	11	H	6	52	54	98.02	102.45	12.49	177745	18584	2		2	0	0	x	0	4	0	22	0	0	0	0
307	1318	B	12	H	1	30	32	100.30	104.61	12.73	177745	18584	2		6	0	0	0	0	6	0	8	0	0	0	0
307	1318	B	12	H	1	80	82	100.80	105.11	12.73	177745	18584	2		x	0	0	0	0	10	x	9	0	0	0	0
307	1318	B	12	H	1	133	135	101.33	105.64	12.74	177745	18584	2		x	0	0	0	0	30	1	25	0	0	x	0
307	1318	B	12	H	2	30	32	101.80	106.11	12.74	177745	18584	2		1	0	x	x	0	5	1	10	0	0	0	0
307	1318	B	12	H	2	80	82	102.30	106.61	12.75	177745	18584	2		1	0	x	x	0	1	x	38	0	0	0	0
307	1318	B	12	H	2	133	135	102.83	107.14	12.75	177745	18584	2		2	0	1	x	0	6	x	14	0	0	0	0
307	1318	B	12	H	3	30	32	103.30	107.61	12.76	177745	18584	1		X	0	0	X	0	22	0	20	0	x	0	0
307	1318	B	12	H	3	80	82	103.80	108.11	12.76	177745	18584	2		x	0	x	1	0	15	x	20	0	0	0	0
307	1318	B	12	H	3	133	135	104.33	108.64	12.76	177745	18584	1		1	0	0	x	0	2	x	16	0	1	0	0
307	1318	B	12	H	4	30	32	104.80	109.11	12.77	177745	18584	1		1	0	0	x	0	26	x	32	0	0	0	0
307	1318	B	12	H	4	80	82	105.30	109.61	12.77	177745	18584	2		2	0	0	x	0	2	0	21	0	0	0	0
307	1318	B	12	H	4	133	135	105.83	110.14	12.78	177745	18584	1		x	0	x	0	0	9	x	30	0	0	0	0
307	1318	B	12	H	5	30	32	106.30	110.61	12.78	177745	18584	2		0	0	1	1	0	32	x	50	0	0	0	0
307	1318	B	12	H	5	80	82	106.80	111.11	12.78	177745	18584	2		1	0	1	x	0	19	x	31	0	x	0	0
307	1318	B	12	H	5	133	135	107.33	111.64	12.79	177745	18584	2		x	0	0	1	0	12	x	19	0	0	0	0
307	1318	B	12	H	6	30	32	107.80	112.11	12.79	177745	18584	2		3	0	0	1	0	25	1	37	0	0	0	0
307	1318	B	12	H	6	80	82	108.30	112.61	12.80	177745	18584	2		x	0	0	1	0	24	x	36	0	0	0	0
307	1318	B	13	H	1	30	32	109.80	114.66	12.81	177745	18584	2		x	0	0	0	0	4	x	41	0	0	0	4
307	1318	B	13	H	1	90	92	110.40	115.26	12.82	177745	18584	2		1	0	x	0	x	3	x	13	0	0	0	0
307	1318	B	13	H	1	140	142	110.90	115.76	12.82	177745	18584	2		1	0	0	x	0	9	x	39	0	0	0	0
307	1318	B	13	H	2	43	45	111.43	116.29	12.83	177745	18584	2		0	0	0	x	0	10	0	35	0	0	0	0
307	1318	B	13	H	2	90	92	111.90	116.76	12.83	177745	18584	2		0	0	x	1	0	16	1	58	0	0	0	0
307	1318	B	13	H	2	140	142	112.40	117.26	12.84	177745	18584	2		x	0	0	x	0	23	x	70	0	0	0	0
307	1318	B	13	H	3	43	45	112.93	117.79	12.84	177745	18584	2		1	0	1	0	0	2	x	55	0	0	0	0
307	1318	B	13	H	3	90	92	113.40	118.26	12.85	177745	18584	2		x	0	x	1	0	8	x	54	0	0	0	0
307	1318	B	13	H	3	140	142	113.90	118.76	12.85	177745	18584	2		1	0	x	x	0	10	x	62	0	0	0	0
307	1318	B	13	H	4	43	45	114.43	119.29	12.85	177745	18584	2		1	0	x	1	0	21	0	33	0	0	0	0
307	1318	B	13	H	4	90	92	114.90	119.76	12.86	177745	18584	2		1	0	1	x	0	24	0	51	0	0	0	0
307	1318	B	13	H	4	140	142	115.40	120.26	12.86	177745	18584	2		x	0	0	x	0	34	x	26	0	x	0	0
307	1318	B	13	H	5	43	45	115.93	120.79	12.87	177745	18584	2		1	0	1	x	0	17	x	37	0	x	0	0
307	1318	B	13	H	5	90	92	116.40	121.26	12.87	177745	18584	2		x	0	0	x	0	11	x	37	0	x	0	0
307	1318	B	13	H	5	140	142	116.90	121.76	12.88	177745	18584	2		x	0	x	x	0	8	x	22	0	x	0	0
307	1318	B	13	H	6	33	35	117.33	122.19	12.88	177745	18584	2		1	0	0	1	0	5	x	19	0	0	0	0
307	1318	B	13	H	7	18	20	117.65	122.51	12.88	177745	18584	2		0	0	0	x	0	4	x	34	1	0	0	0
307	1318	C	7	H	1	20	22	117.70	123.61	12.96	177745	18584	1		0	0	x	3	0	6	1	42	0	1	0	0
307	1318	B	14	H	1	43	45	119.43	123.95	13.00	177745	18584	2		x	0	0	2	0	7	x	28	0	1	0	0
307	1318	C	7	H	1	70	72	118.20	124.11	13.01	177745	18584	1		x	0	0	x	0	4	0	16	0	0	0	0
307	1318	B	14	H	1	90	92	119.90	124.42	13.03	177745	18584	2		0	0	0	1	0	x	0	45	0	0	0	0
307	1318	C	7	H	1	120	122	118.70	124.61	13.04	177745	18584	1		x	0	0	1	0	2	x	11	0	0	0	0
307	1318	B	14	H	1	140	142	120.40	124.92	13.05	177745	18584	2		x	0	0	x	0	1	x	30	0	0	0	0
307	1318	C	7	H	2	20	22	119.20	125.11	13.05	177745	18584	1		1	0	0	x	0	1	x	29	0	0	0	0
307	1318	B	14	H	2	43	45	120.93	125.45	13.06	177745	18584	2		x	0	0	0	0	0	x	35	0	0	0	0
307	1318	C	7	H	2	70	72	119.70	125.61	13.07	177745	18584	1		0	0	0	x	0	2	0	8	0	x	0	0
307	1318	B	14	H	2	90	92	121.40	125.92	13.07	177745	18584	2		1	0	x	x	0	1	x	37	0	0	0	0

Cannosphaeopsis spp. (pars)	*Capisocysta lata/lyelli*	*Cerebrocysta irregulare*	*Cerebrocysta lagae*	*Cerebrocysta poulsenii*	*Cleistosphaeridium placacanthum*	*Cordosphaeridium minimum*	*Corrudinium devernalieae*	*Cousteaudinium aubryae*	*Cribroperidinium tenuitabulatum*	*Cristadinium cristatoserratum*	*Cristadinium diminutivum*	*Dalella chathamensis*	*Dapsilidinium pseudocolligerum*	*Dinopterigium cladoides* sensu Morgenroth 1966	*Echinidinium aculeatum*	*Echinidinium euaxum*	*Echinidinium nordlandensis*	*Echinidinium sleipnerensis*	*Echinidinium transparantum*	*Echinidinium* sp. A	*Echinidinium* cf. sp A	*Echinidinium* spp. (pars)	*Edwarsiella sexispinosa*	*Filisphaera filifera*	*Geonettia clineae*	*Habibacysta tectata*	*Homotryblium pallidum*	*Homotryblium tenuispinosum*
0	0	2	0	0	0	0	0	0	0	0	0	0	6	0	0	1	x	x	0	0	0	0	x	x	0	10	0	0
0	0	2	0	x	1	0	x	0	0	0	0	0	7	x	0	0	x	1	1	x	0	0	0	3	0	26	0	0
0	0	1	0	0	x	0	0	0	0	0	0	1	16	0	0	0	0	x	0	0	0	0	0	0	0	40	0	0
0	0	5	1	0	x	0	0	0	0	0	0	0	11	0	0	0	x	0	0	0	x	0	0	x	0	71	0	0
0	0	3	0	x	x	0	0	0	0	0	0	0	5	0	0	0	0	1	0	0	0	0	0	4	0	33	0	0
0	0	5	0	0	1	0	0	0	0	0	0	0	8	0	0	0	x	0	0	0	0	0	0	1	0	29	0	0
0	0	2	0	x	x	0	0	0	0	0	0	0	6	0	0	0	0	0	0	0	0	0	0	x	0	10	0	0
0	0	x	0	1	x	0	0	0	0	0	0	0	4	x	0	0	0	0	0	0	0	0	0	x	0	18	0	0
0	0	1	0	x	x	0	0	0	0	0	0	0	4	0	0	0	0	0	0	0	0	0	0	1	0	14	0	0
0	0	x	0	3	1	0	0	0	0	0	0	0	7	0	0	0	0	0	0	0	0	0	0	2	0	18	0	0
0	0	2	0	2	0	0	0	0	0	0	0	0	20	0	0	0	0	0	0	0	0	0	0	1	0	20	0	0
0	0	x	0	x	0	0	1	0	0	0	0	0	6	0	0	x	0	x	0	0	0	0	0	1	0	6	0	0
0	0	1	0	1	x	0	0	0	0	0	0	0	12	0	x	0	0	0	0	0	0	0	0	x	0	29	0	0
0	1	1	0	2	0	0	0	0	0	0	0	0	6	x	0	0	0	x	0	0	0	0	0	1	0	40	0	0
0	1	0	0	x	x	0	0	0	0	0	0	0	10	3	0	0	0	0	0	0	0	0	0	4	0	65	0	0
0	x	x	0	0	0	0	0	0	0	0	0	0	7	3	0	1	0	0	0	0	0	0	0	3	0	19	0	0
0	0	0	0	x	0	1	0	0	x	0	0	0	2	1	0	0	0	0	0	0	0	0	0	0	x	20	0	0
0	0	0	0	x	0	0	0	0	0	0	0	0	x	0	0	0	0	0	0	0	0	0	0	0	0	34	1	0
0	0	0	0	0	0	3	0	0	0	0	0	0	5	0	0	0	0	0	0	0	0	0	0	0	1	33	0	0
0	0	0	0	1	0	2	0	0	0	0	0	0	6	x	0	0	0	0	x	0	0	0	0	0	0	45	1	0
0	0	0	0	x	0	0	0	0	0	0	0	0	7	0	0	0	0	0	0	0	0	0	0	0	0	14	1	0
0	0	0	0	1	x	7	0	0	0	0	0	0	6	0	0	0	0	0	0	0	0	x	0	0	0	4	0	0
0	0	0	0	x	0	3	0	0	0	0	0	0	12	0	0	0	0	0	0	0	0	0	0	0	0	x	0	0
0	0	0	0	1	x	0	0	0	0	0	0	0	9	0	0	0	0	0	0	0	0	0	0	0	0	16	x	0
0	0	0	0	1	2	0	0	0	0	0	0	0	3	0	0	0	x	0	0	0	0	0	0	0	0	9	1	0
0	0	0	0	x	x	0	0	0	0	0	0	0	8	0	x	x	0	x	0	0	0	0	0	0	0	19	0	0
0	x	0	0	x	1	0	0	0	0	0	0	0	5	0	0	0	0	1	0	0	0	0	0	0	0	2	0	0
0	7	0	0	x	x	0	0	0	0	0	0	0	2	0	0	0	0	0	0	0	0	0	0	0	0	25	0	0
0	0	0	0	x	0	0	0	0	0	0	0	0	5	0	0	0	0	1	0	0	0	0	0	0	0	14	0	0
0	4	0	0	x	x	0	0	0	0	0	0	0	8	0	0	1	0	0	0	0	0	0	0	0	0	17	0	x
0	3	0	0	x	x	0	0	0	0	0	0	0	3	0	0	0	0	x	0	0	0	0	0	2	0	18	0	0
0	x	0	0	1	0	0	0	1	0	0	0	0	7	0	0	x	0	1	0	0	0	0	0	0	0	6	1	0
0	3	0	0	2	x	0	0	0	0	0	0	0	7	0	0	x	1	0	0	0	0	0	0	1	0	40	0	0
0	4	0	0	2	1	0	0	0	1	0	0	0	7	0	0	2	1	1	0	1	0	0	0	0	0	21	0	0
0	2	0	0	1	1	0	0	0	0	0	0	0	19	0	0	x	0	x	2	0	0	0	0	1	1	9	0	0
0	3	0	0	3	x	0	0	0	0	0	0	0	3	0	0	0	1	0	0	x	0	0	0	0	0	17	0	0
0	7	0	0	1	x	0	0	0	x	0	0	0	10	0	0	0	0	0	0	1	0	0	0	0	0	17	0	0
0	7	0	0	2	x	0	0	0	0	0	0	0	9	0	0	x	0	1	1	1	0	2	0	0	x	23	0	0
0	2	0	0	1	1	0	0	0	0	0	0	0	21	0	0	0	0	0	0	1	0	0	0	0	0	12	0	0
0	2	0	0	x	0	0	0	0	0	0	0	0	9	0	0	0	x	0	0	0	0	0	0	0	0	13	0	0
0	9	0	0	3	1	0	0	0	0	0	0	0	32	0	0	x	0	x	1	x	0	0	0	0	0	19	0	0
0	3	0	0	x	x	0	0	0	0	0	0	0	22	0	0	1	0	x	0	x	0	0	0	0	0	11	0	0
0	4	0	0	1	x	0	0	0	0	0	0	0	13	0	0	x	0	x	0	x	0	0	0	0	0	39	0	0
0	4	0	0	2	0	0	0	0	0	0	0	0	11	0	0	0	0	1	1	x	0	0	0	0	0	70	0	0
0	1	0	0	1	x	0	0	0	0	0	0	0	19	0	0	x	0	x	0	x	0	0	0	0	0	31	0	0
0	4	0	0	2	x	0	0	0	0	0	0	0	11	0	0	0	0	x	0	0	0	0	0	0	0	40	0	0
0	2	0	0	2	1	0	0	0	0	0	0	0	5	0	0	0	0	x	1	x	0	0	0	0	0	81	0	0
0	0	0	0	1	x	0	0	x	0	0	0	0	5	0	0	0	0	1	x	2	0	0	0	0	0	80	0	1
0	9	0	0	3	x	0	0	0	0	0	0	0	19	0	0	0	0	x	1	1	0	0	0	0	0	36	0	0
0	5	0	0	1	2	0	0	0	0	0	0	0	12	1	0	0	0	x	x	x	0	0	0	0	0	44	0	x
0	4	0	0	2	x	0	x	0	0	0	0	0	11	0	0	1	0	x	x	x	0	0	0	0	0	27	0	0
0	2	0	1	2	x	0	x	0	x	0	0	0	10	0	0	3	0	1	0	0	0	0	0	x	0	82	0	0
0	2	0	0	x	x	0	0	0	x	0	0	0	4	0	0	0	0	0	0	0	0	0	0	x	x	38	0	0
0	1	0	0	1	x	0	0	0	0	0	0	0	11	0	0	x	0	0	0	0	0	0	0	0	0	67	0	x
0	2	0	0	x	x	0	0	0	0	0	0	0	5	0	0	0	0	0	0	0	0	0	0	0	0	91	0	0
0	1	0	0	1	x	0	0	0	0	0	0	0	2	0	2	x	0	2	0	0	0	0	0	0	0	122	0	0
0	2	0	0	x	1	0	0	0	0	0	0	0	6	0	0	1	0	x	1	x	0	0	0	x	0	126	0	0
0	1	0	0	1	x	0	0	0	0	0	3	0	4	0	0	3	0	x	0	0	0	0	0	1	0	59	0	0
0	0	0	0	1	2	1	0	2	0	0	0	0	9	0	0	x	0	x	0	0	0	0	0	0	0	13	0	0
0	14	0	0	x	2	0	0	0	0	0	0	0	17	0	x	x	0	0	0	0	0	0	0	0	0	31	0	0
0	0	0	0	x	3	1	0	2	0	0	0	0	22	0	0	x	0	0	0	0	0	0	0	0	0	19	0	0
0	10	0	0	x	1	0	0	0	0	0	0	0	12	0	0	x	0	0	0	0	0	0	0	1	0	58	0	0
0	0	0	0	1	0	0	0	0	0	0	0	0	7	0	0	2	0	x	0	0	0	0	0	0	0	24	0	0
0	3	0	0	x	1	0	0	0	0	0	x	0	8	0	0	x	0	0	0	0	0	0	0	0	0	18	0	x
0	0	0	0	1	1	3	0	0	0	0	0	0	24	0	0	0	0	0	0	0	0	0	0	0	0	11	0	0

Composite depth (mcd)	Age (Ma)	*Hystrichokolpoma rigaudiae*	*Hystrichosphaeropsis obscura*	*Hystrichostrogylon membraniphorum*	*Impagidinium aculeatum*	*Impagidium arachnion*	*Impagidinium pallidum*	*Impagidinium paradoxum*	*Impagidinium patulum*	*Impagidinium plicatum*	*Impagidinium striialatum*	*Impagidinium sphaericum*	*Impagidinium velorum*	*Impagidinium* spp. (pars)	*Invertocysta lacrymosa*	*Invertocysta tabulata*	*Kallosphaeridium* sp. of Head and Westphal, 1999	*Labyrinthodinium truncatum*	*Lejeunecysta convexa*	*Lejeunecysta challengerensis*	*Lejeunecysta* cf. *challengerensis*	*Lejeunecysta hatterasensis*	*Lejeunecysta marieae*	*Lejeunecysta* spp. (pars)	*Lingulodinium machaerophorum*	*Melitasphaeridium choanophorum*	*Nematosphaeropsis labyrinthus*
92.44	12.11	x	x	0	x	0	1	x	x	0	0	0	0	0	x	x	x	6	0	2	0	0	x	0	5	8	6
93.03	12.13	x	x	0	0	0	0	2	0	0	0	0	0	0	x	1	2	10	0	1	0	0	x	1	2	6	12
93.46	12.15	1	1	0	0	0	x	x	0	0	0	0	0	0	x	0	x	23	0	x	0	0	0	1	4	8	16
93.94	12.17	x	x	0	0	0	x	2	0	0	0	0	0	0	x	1	0	20	0	1	0	0	x	1	3	1	9
94.5	12.18	0	0	0	0	0	2	3	0	0	0	0	0	0	x	1	0	5	0	1	0	0	1	x	9	1	6
94.97	12.19	x	x	0	0	0	2	1	0	0	0	0	0	0	0	x	0	4	0	0	0	0	0	0	4	1	11
95.4	12.20	0	x	0	0	0	1	1	0	0	0	0	0	0	0	0	0	12	0	1	0	0	x	0	5	x	8
95.9	12.22	0	x	0	0	0	3	2	0	0	0	0	0	0	0	0	0	10	0	0	0	0	1	0	1	x	9
96.48	12.23	x	x	0	x	0	3	2	x	0	0	0	0	0	0	1	1	18	0	x	0	0	0	x	1	x	14
96.98	12.24	0	0	0	x	0	x	1	0	0	0	0	0	0	x	1	2	17	0	0	0	0	0	0	2	x	11
97.48	12.25	0	1	0	x	0	0	0	0	0	0	0	0	0	1	x	x	9	0	x	0	0	0	x	1	1	8
97.94	12.26	x	x	0	x	0	x	0	0	0	0	0	0	0	1	x	0	9	0	x	0	0	0	0	x	x	16
98.44	12.27	2	0	1	0	0	2	1	x	0	0	0	0	0	x	0	x	4	0	x	0	0	x	1	3	3	14
98.98	12.30	0	x	2	0	0	2	1	1	0	0	0	0	0	0	0	0	4	0	1	0	0	0	x	2	3	14
99.46	12.33	x	1	0	0	0	5	x	1	0	0	0	0	0	0	x	x	7	0	0	0	0	1	x	7	2	15
99.95	12.35	0	1	x	0	0	4	x	0	1	0	0	0	0	1	1	0	8	0	0	0	0	0	1	4	2	11
100.46	12.38	x	x	x	x	0	x	x	1	0	0	x	0	0	5	0	0	3	0	0	0	x	0	0	1	2	6
100.95	12.41	0	3	0	0	0	0	1	x	0	0	0	0	0	3	0	0	4	0	0	0	0	0	0	2	2	3
101.45	12.43	0	x	0	x	0	1	1	0	0	0	0	0	0	7	0	0	4	0	0	0	0	0	0	2	1	18
101.95	12.46	x	1	x	0	0	2	2	1	0	0	0	0	0	1	0	x	3	0	x	0	0	x	0	3	x	3
102.45	12.49	0	1	x	0	0	2	1	0	0	0	0	0	0	0	0	0	5	0	0	0	x	1	0	1	0	6
104.61	12.73	x	x	x	0	0	12	x	1	0	0	0	0	0	x	0	x	9	0	0	x	x	x	0	3	1	4
105.11	12.73	0	1	x	0	0	9	1	x	0	0	0	0	0	x	0	0	4	0	0	x	x	x	0	1	3	4
105.64	12.74	x	2	x	0	0	4	0	0	0	0	0	0	0	0	0	0	8	0	x	0	0	2	0	3	x	9
106.11	12.74	x	x	x	0	0	1	0	0	0	0	0	0	0	0	0	0	5	0	x	x	0	0	0	2	2	3
106.61	12.75	1	1	2	0	0	2	x	0	0	0	0	0	0	0	0	x	7	0	1	x	0	x	0	1	x	24
107.14	12.75	2	x	x	0	2	2	1	x	0	0	0	x	0	0	0	x	11	0	x	0	0	x	0	2	3	4
107.61	12.76	x	1	0	0	0	2	1	x	0	0	0	1	0	0	0	2	11	0	0	0	0	1	0	1	1	9
108.11	12.76	x	1	0	0	0	x	0	x	0	0	0	0	0	0	0	x	21	0	1	0	1	0	0	3	x	9
108.64	12.76	1	x	3	0	0	6	1	x	0	0	0	0	0	0	0	5	13	0	x	0	0	0	0	1	0	8
109.11	12.77	x	x	1	0	0	9	2	x	0	0	0	x	0	0	1	3	12	0	x	0	2	x	0	4	x	14
109.61	12.77	6	1	x	0	0	x	0	x	0	0	0	0	0	0	0	2	15	0	0	0	1	x	0	3	0	1
110.14	12.78	2	x	0	0	0	1	0	0	0	0	0	x	0	0	x	1	6	0	x	0	0	0	1	3	0	16
110.61	12.78	3	1	x	0	0	1	x	1	0	0	0	0	0	0	0	3	9	0	7	x	1	4	0	7	x	6
111.11	12.78	8	x	0	0	x	2	1	x	0	0	0	x	1	0	0	2	4	0	1	0	x	1	0	7	x	17
111.64	12.79	5	1	2	2	0	4	1	x	0	0	0	0	0	2	0	1	3	0	x	0	1	1	0	3	x	14
112.11	12.79	x	x	4	x	0	8	1	x	0	0	0	1	0	13	0	3	14	0	x	0	1	1	0	6	x	14
112.61	12.80	1	x	1	1	0	3	x	x	0	0	0	0	0	8	x	6	20	0	4	0	x	4	2	2	x	13
114.66	12.81	1	x	x	0	0	3	2	x	0	0	0	0	0	1	0	x	10	0	0	0	x	0	0	2	2	23
115.26	12.82	x	0	x	0	0	1	3	x	0	0	0	0	0	0	0	x	6	0	x	0	0	x	0	3	1	9
115.76	12.82	1	x	1	x	0	7	1	x	0	0	0	0	0	x	0	1	12	0	x	0	x	1	0	3	2	9
116.29	12.83	x	0	0	0	0	3	x	0	0	0	0	0	0	0	0	2	14	0	x	0	0	x	0	2	x	7
116.76	12.83	x	x	x	0	x	5	x	x	0	0	0	0	0	x	0	4	6	0	1	0	1	1	0	5	1	3
117.26	12.84	x	0	0	0	0	2	0	x	0	0	0	1	0	0	x	1	7	0	2	0	0	4	0	1	0	2
117.79	12.84	3	1	x	0	0	0	1	x	0	0	0	x	0	x	0	1	5	0	x	0	0	x	x	1	0	1
118.26	12.85	5	1	0	0	0	3	x	x	0	0	0	0	2	0	x	1	5	0	x	0	x	0	1	3	3	2
118.76	12.85	x	x	x	0	0	3	x	x	0	0	0	0	0	x	0	2	6	0	1	0	1	x	0	3	1	5
119.29	12.85	0	1	0	0	0	4	0	0	0	0	0	x	0	0	x	1	2	0	5	0	0	0	0	4	1	10
119.76	12.86	1	x	x	0	0	1	x	x	0	x	0	x	0	0	x	3	6	0	1	0	1	x	0	4	x	2
120.26	12.86	x	1	x	0	0	4	1	x	0	x	0	0	0	0	x	4	8	0	0	0	x	0	0	3	1	9
120.79	12.87	1	1	x	0	0	5	2	x	0	0	0	0	0	0	x	1	4	0	0	0	x	x	0	4	1	6
121.26	12.87	x	x	x	0	0	7	1	x	0	0	0	0	0	1	x	3	6	0	x	0	2	2	0	2	x	4
121.76	12.88	2	x	0	0	0	3	3	1	0	0	0	1	0	1	x	8	7	0	0	0	0	x	0	2	x	9
122.19	12.88	x	1	x	0	0	2	2	0	0	0	0	x	0	1	0	2	6	0	0	0	0	0	0	1	x	17
122.51	12.88	1	0	1	0	0	4	3	x	0	0	0	0	0	0	0	2	8	0	0	0	0	0	1	1	x	11
123.61	12.96	1	x	0	0	0	5	x	x	0	0	0	0	0	0	x	3	4	0	1	0	0	x	0	2	x	3
123.95	13.00	x	x	0	0	0	x	1	x	0	0	0	0	0	0	0	x	3	0	x	0	2	3	0	1	0	7
124.11	13.01	x	x	0	0	0	3	1	0	0	0	0	0	0	x	0	2	5	0	0	0	0	1	0	4	x	11
124.42	13.03	2	x	0	0	0	1	x	0	0	0	0	0	0	1	0	0	3	0	x	0	x	0	0	3	x	4
124.61	13.04	3	x	0	0	0	1	x	0	0	0	0	0	0	x	1	0	8	0	0	0	x	0	0	1	1	5
124.92	13.05	3	x	0	0	0	x	1	x	0	0	0	0	0	0	0	0	11	0	0	0	0	0	0	4	3	3
125.11	13.05	1	x	0	0	0	5	1	0	0	0	0	1	0	x	x	0	8	0	0	0	1	1	0	1	0	15
125.45	13.06	3	1	0	0	0	1	x	0	0	0	0	0	0	x	0	0	11	0	0	0	0	3	x	x	2	11
125.61	13.07	1	x	0	0	0	6	1	0	0	0	0	0	0	x	0	x	6	0	0	0	0	x	0	2	2	2
125.92	13.07	1	x	1	0	0	3	2	0	0	0	0	0	0	0	0	0	21	0	x	0	0	1	0	2	4	3

Nematosphaeropsis lemniscata	*Operculodinium? borgerholtense*	*Operculodinium centrocarpum*	*Operculodinium? eirikianum*	*Operculodinium giganteum*	*Operculodinium israelianum*	*Operculodinium janduchenei*	*Operculodinium longispinigerum*	*Operculodinium piaseckii*	*Operculodinium* cf. *piaseckii*	*Operculodinium* sp. 3 of De Verteuil and Norris, 1996	*Palaeocystodinium golzowense*	*Palaeocystodinium minor*	*Palaeocystodinium miocaenicum*	*Palaeocystodinium powellense*	*Paucisphaeridium cylindratum*	*Paucisphaeridium* sp. A	*Paucisphaeridium* sp. B	*Paucisphaeridium* spp. (pars)	*Pentadinium laticinctum*	cyst of *Polykrikos kofoidii/schwartzii* sensu Matsuoka et al. 2009	*Polysphaeridium zoharyi*	*Pyxidinopsis fairhavenensis*	*Pyxidinopsis psilata*	*Pyxidinopsis tuberculata*	*Pyxidinopsis vesiculata*	*Pyxidinopsis* sp. A	*Pyxidinopsis* sp. B	*Pyxidinopsis* spp. (pars)
0	0	7	3	0	0	x	0	2	x	0	x	0	0	0	0	x	4	0	x	0	0	1	4	1	x	0	0	0
0	0	4	4	0	1	0	x	1	0	0	x	0	0	0	0	2	2	0	0	0	0	0	x	x	2	0	0	0
0	0	14	18	x	x	0	0	2	0	0	1	0	0	0	0	1	14	0	x	0	0	x	6	x	0	0	0	0
0	0	14	5	x	0	0	0	1	0	0	x	0	0	0	0	0	11	0	x	0	0	2	0	0	0	0	0	0
0	0	38	8	x	1	0	0	1	x	0	2	0	0	0	0	1	12	0	1	0	0	4	x	1	0	0	0	0
0	1	9	3	x	0	0	0	1	0	0	0	0	x	0	0	1	4	0	1	0	0	1	x	1	0	0	0	0
0	1	6	17	x	0	0	0	1	0	0	x	0	0	0	0	1	3	0	0	0	0	x	3	x	0	0	0	0
0	0	4	2	x	0	0	1	2	0	0	1	0	0	0	0	0	0	0	0	0	0	x	2	0	1	0	0	0
0	0	4	2	1	0	0	0	1	0	0	1	0	0	0	0	0	1	0	0	0	0	0	2	0	1	0	0	0
0	0	3	2	0	0	0	0	x	0	0	2	0	0	0	0	0	3	0	1	0	0	1	x	0	0	0	0	0
0	1	11	3	0	0	0	0	x	x	0	1	0	0	0	0	0	0	0	x	0	0	0	x	0	0	0	0	0
0	1	5	2	0	x	x	0	x	0	0	x	0	0	0	0	0	x	0	0	0	0	0	1	x	0	0	0	0
0	x	16	5	0	x	x	1	x	0	2	x	x	0	0	0	4	2	0	x	0	0	x	3	x	x	0	0	0
0	0	7	x	1	1	0	1	1	0	0	1	0	0	0	0	4	4	0	0	0	0	x	1	0	0	0	0	0
0	0	6	16	x	0	0	x	1	0	0	2	0	0	0	0	1	7	0	x	0	0	0	3	0	0	0	0	0
0	0	12	4	2	0	0	0	x	0	0	1	0	0	1	0	0	5	0	0	0	0	0	x	0	0	0	0	0
0	0	4	2	0	2	0	2	x	0	8	1	1	0	x	1	0	0	20	0	0	0	2	2	1	0	0	0	0
0	0	4	x	0	1	0	1	x	0	0	x	x	0	1	1	0	0	10	x	0	0	3	0	x	0	0	0	0
0	0	3	x	0	1	0	0	x	0	2	1	x	0	2	0	0	0	43	0	0	0	3	1	x	0	0	0	0
0	0	12	2	0	2	5	0	0	0	1	1	x	0	1	0	0	0	18	0	0	0	1	1	x	0	0	0	0
0	0	5	7	0	2	1	0	2	0	1	x	0	0	0	0	0	0	27	0	0	0	1	0	2	0	0	0	0
0	0	7	3	0	10	1	0	1	0	x	x	0	0	1	0	0	0	14	1	0	0	1	3	1	0	0	0	0
0	0	16	14	0	8	0	0	x	0	0	x	x	0	x	0	0	0	26	x	0	0	2	1	x	0	0	0	0
0	0	18	2	0	5	1	0	x	0	0	x	0	0	0	0	3	0	24	1	0	0	x	0	0	0	0	0	0
0	0	16	3	0	2	0	0	x	0	0	x	0	0	0	0	4	0	25	4	0	0	1	1	0	0	0	0	0
0	0	15	x	0	6	0	0	2	0	0	x	0	0	x	0	3	35	0	x	0	0	x	x	x	x	x	0	0
0	0	9	3	0	1	0	0	x	0	0	x	0	0	0	0	5	14	0	x	0	0	x	1	x	0	x	0	0
0	1	10	x	0	x	0	0	2	0	0	x	0	0	0	0	13	34	0	x	0	0	0	0	0	x	0	0	0
0	0	8	7	0	x	0	1	x	0	0	0	x	0	x	0	2	36	0	x	0	0	x	0	x	x	0	0	0
0	x	5	2	x	x	x	x	x	0	0	x	0	0	0	0	10	13	0	0	0	0	x	1	x	x	x	0	0
0	1	5	1	0	1	0	0	1	0	0	x	0	0	0	0	4	26	0	x	0	0	0	0	x	2	0	0	0
0	0	11	1	0	3	x	0	1	0	0	x	0	0	0	0	3	28	0	0	0	0	x	0	0	x	1	0	0
0	0	5	0	0	0	1	0	x	0	0	3	0	0	x	0	6	29	0	1	0	0	0	0	0	2	0	0	0
0	0	8	x	0	x	x	0	x	0	0	1	0	0	1	0	2	50	0	1	x	0	x	0	x	3	0	0	0
0	0	9	1	0	1	0	0	x	0	0	x	x	0	x	0	5	51	0	1	0	0	x	0	0	x	1	0	0
0	0	6	x	0	x	0	0	1	0	0	1	x	0	x	0	6	32	0	x	0	0	0	0	0	1	0	0	0
0	0	4	x	0	1	0	0	x	0	0	3	1	0	x	0	20	92	0	x	0	0	0	x	x	x	x	0	0
0	0	4	x	0	1	0	0	1	0	0	6	x	0	x	0	7	57	0	x	0	0	0	0	1	1	0	0	0
0	0	12	3	0	2	0	0	1	0	0	1	0	0	x	0	14	23	0	1	0	0	0	x	0	1	0	0	0
0	0	24	1	0	x	0	0	2	0	0	1	0	0	1	0	1	7	0	x	0	0	0	1	1	1	x	0	0
0	0	25	x	0	1	0	0	x	0	0	x	0	0	x	0	10	26	0	x	0	0	1	0	1	1	0	0	0
0	0	23	0	0	x	0	0	0	0	0	1	0	0	1	0	5	16	0	x	0	0	0	0	0	x	1	0	0
0	0	13	1	0	0	x	0	x	0	0	3	0	0	x	0	3	8	0	1	0	0	0	0	0	x	0	0	0
0	0	4	3	0	0	x	0	x	0	0	4	0	0	x	0	4	13	0	x	0	0	1	0	0	1	0	0	0
0	0	14	4	0	x	0	0	x	0	0	x	0	0	x	0	7	13	0	x	0	0	0	0	0	0	0	0	0
0	x	4	3	0	x	0	0	0	0	0	x	0	0	x	0	11	32	0	0	0	0	0	0	1	x	0	0	0
0	0	11	1	0	x	0	0	x	0	0	1	0	0	x	0	7	9	0	0	0	0	0	x	0	0	0	x	1
0	0	18	1	0	0	0	0	x	0	0	1	0	0	0	0	5	19	0	0	x	0	0	x	0	0	0	0	0
0	0	28	3	0	x	0	0	x	0	1	2	x	0	1	0	14	25	0	x	0	0	0	x	x	1	x	0	0
0	0	19	8	0	x	0	x	1	0	0	x	1	0	0	0	7	29	0	2	0	0	0	0	0	1	0	0	0
0	0	8	4	0	x	0	0	2	0	0	1	x	0	0	0	5	20	0	0	0	0	0	x	0	1	x	0	0
0	0	4	4	0	x	0	0	1	x	0	1	x	0	0	0	6	35	0	x	0	x	0	2	x	1	x	0	0
0	0	3	7	0	x	0	0	2	0	0	2	1	0	0	0	11	29	0	x	0	x	0	2	x	2	x	0	0
0	0	11	2	0	1	0	0	x	1	0	1	0	x	x	0	5	16	0	x	0	0	0	x	x	0	x	0	0
0	0	6	2	0	x	0	0	0	0	0	5	0	0	0	0	2	25	0	x	0	0	0	x	x	x	0	0	0
0	1	3	3	0	0	0	1	0	0	0	x	0	0	0	0	3	35	0	1	0	0	0	0	0	0	0	0	0
0	1	6	x	0	0	0	0	x	0	0	1	0	0	0	0	9	18	0	x	0	0	0	0	x	x	0	0	0
0	x	9	x	0	0	0	0	x	x	0	2	0	0	0	0	4	9	0	0	x	0	x	0	x	0	0	0	0
0	0	7	x	0	x	0	0	x	0	1	2	x	0	2	0	0	0	6	0	0	0	x	0	0	0	0	0	0
0	x	11	2	0	0	0	0	1	0	0	x	0	0	0	0	7	21	0	0	0	0	0	0	0	0	0	0	0
0	0	3	1	0	7	0	1	x	0	2	x	x	0	1	0	0	0	15	x	0	0	4	0	x	0	0	0	0
0	0	10	3	0	x	0	0	x	1	0	0	x	0	x	0	4	12	0	0	0	0	0	x	0	0	0	0	0
0	0	2	1	0	1	0	0	x	0	0	0	x	0	0	0	0	0	24	x	0	0	x	0	1	0	0	0	0
0	x	3	2	0	1	0	1	x	0	0	0	x	0	0	0	6	12	0	x	0	0	0	x	x	0	0	0	0
0	0	2	x	0	2	0	1	2	0	3	x	0	0	1	0	0	0	32	x	0	0	x	x	2	0	0	0	0

Composite depth (mcd)	Age (Ma)	*Reticulatosphaera actinocoronata*	Round brown cysts	*Selenopemphix brevispinosa*	*Selenopemphix dionaeacysta*	*Selenopemphix nephroides*	*Selenopemphix porcupensis*	*Selenopemphix quanta*	*Selenopemphix* spp. (pars)	*Spiniferites hyperacanthus*	*Spiniferites mirabilis/membranaceus*	*Spiniferites solidago*	*Spiniferites/Achomosphaera* complex	*Spiniferites* sp. A	*Spiniferites* sp. B	*Spiniferites* sp. C	*Sumatradinium? delectabilis*	*Sumatradinium hamulatum*	*Sumatradinium soucouyantiae*	*Sumatradinium* spp. (pars)	*Tectatodinium pellitum*	*Trinovantedinium glorianum*	*Trinovantedinium ferugnomatum*	*Trinovantedinium harpagonium*	*Trinovantedinium henrietti*	*Tuberculodinium vancampoe*	*Unipontidinium aquaeductus*	Dinocyst sp. A
92.44	12.11	3	2	x	x	x	0	x	1	5	6	0	184	11	1	0	x	x	4	0	x	0	0	0	0	x	x	3
93.03	12.13	5	1	1	x	x	0	0	0	10	5	0	166	8	x	0	1	0	2	0	0	0	0	x	0	1	0	2
93.46	12.15	5	0	x	0	x	0	x	0	16	3	0	207	10	7	x	x	0	6	0	0	0	0	x	0	1	x	5
93.94	12.17	5	0	2	x	0	x	0	0	x	1	x	103	11	1	x	0	0	2	0	0	0	0	0	0	x	0	1
94.5	12.18	5	0	x	0	x	0	0	0	1	2	x	166	4	1	0	x	x	2	0	0	x	1	x	0	x	0	x
94.97	12.19	2	0	1	1	1	0	0	0	5	6	0	165	9	1	x	1	0	2	0	x	x	0	1	0	x	0	1
95.4	12.20	2	0	x	x	x	0	0	0	9	6	0	186	11	3	0	0	0	1	0	x	0	0	0	0	x	x	3
95.9	12.22	4	0	0	x	0	0	0	0	37	3	0	220	5	2	0	0	0	x	0	0	x	0	0	0	1	x	x
96.48	12.23	x	0	0	0	1	0	0	0	30	4	0	204	5	2	x	0	0	4	0	x	0	0	0	0	x	0	1
96.98	12.24	1	0	1	0	x	0	0	0	17	8	1	189	2	1	x	0	2	1	0	x	0	0	0	0	0	0	4
97.48	12.25	x	0	x	0	x	0	0	0	34	5	0	228	4	4	7	0	x	2	0	1	0	0	0	0	x	0	2
97.94	12.26	2	0	x	0	1	0	0	0	32	3	x	185	5	2	4	0	0	x	0	0	0	0	0	0	x	1	1
98.44	12.27	1	0	2	x	x	0	0	0	16	1	2	269	3	4	15	0	x	x	0	x	0	0	0	0	x	x	10
98.98	12.30	4	0	0	0	x	0	0	0	10	3	0	170	5	5	0	3	1	x	0	0	0	0	0	0	1	0	8
99.46	12.33	x	0	x	0	1	0	x	0	0	5	1	260	10	5	0	x	x	x	0	x	x	0	0	0	x	x	2
99.95	12.35	x	0	2	0	2	0	0	0	5	1	1	186	8	1	0	0	x	2	0	1	0	0	0	0	1	0	9
100.46	12.38	x	1	0	0	x	0	0	0	0	0	0	201	0	0	0	x	0	0	0	2	0	0	0	0	x	0	0
100.95	12.41	0	0	x	0	0	x	0	0	0	0	0	197	0	0	0	0	0	x	0	1	0	0	0	0	1	2	0
101.45	12.43	0	2	1	0	0	0	0	0	0	0	0	177	0	0	0	1	0	3	0	2	0	0	0	0	1	0	0
101.95	12.46	1	0	0	2	1	0	x	0	0	0	0	198	0	0	0	0	0	2	0	0	0	0	x	0	0	0	0
102.45	12.49	1	0	x	0	x	0	0	0	0	0	0	175	0	0	0	x	0	3	0	2	0	0	0	0	x	0	0
104.61	12.73	x	0	x	0	x	0	x	0	0	0	0	232	0	0	0	0	x	1	0	2	0	0	0	0	2	x	0
105.11	12.73	1	0	x	0	x	0	x	0	0	0	0	202	0	0	0	0	2	3	0	x	0	0	0	0	1	x	0
105.64	12.74	1	0	x	0	x	0	0	0	0	0	0	193	0	0	0	0	9	1	0	x	0	0	0	0	2	x	0
106.11	12.74	0	x	1	0	x	0	0	0	0	0	0	264	0	0	0	x	x	1	0	x	0	0	0	0	x	1	0
106.61	12.75	2	1	2	x	x	x	x	0	0	0	0	257	0	0	0	0	x	1	0	x	0	0	x	x	1	11	0
107.14	12.75	1	x	2	0	0	x	0	0	0	0	0	199	0	0	0	1	2	1	0	1	0	0	0	0	x	x	0
107.61	12.76	4	0	0	0	1	0	x	0	4	4	x	184	9	1	0	0	2	0	0	1	0	0	0	x	x	2	0
108.11	12.76	1	1	0	0	1	0	1	0	0	0	0	228	0	0	0	0	2	1	0	x	0	0	x	0	x	5	0
108.64	12.76	4	0	1	0	1	0	0	0	3	3	2	169	20	x	0	0	1	x	0	1	x	0	x	x	1	4	0
109.11	12.77	5	1	1	0	1	0	0	0	7	5	3	138	8	2	0	0	6	x	0	0	0	0	0	x	x	2	0
109.61	12.77	1	0	x	0	x	0	0	0	0	0	0	228	0	0	0	0	2	x	0	x	0	0	0	0	1	2	0
110.14	12.78	x	2	2	0	5	0	1	0	7	1	6	169	7	6	0	0	2	x	0	0	0	0	0	x	x	3	0
110.61	12.78	1	1	x	0	3	0	1	0	0	0	0	172	0	0	0	0	2	1	x	x	x	0	0	0	x	x	0
111.11	12.78	2	x	x	0	3	0	1	0	0	0	0	246	0	0	0	0	1	1	0	x	x	0	0	x	0	4	0
111.64	12.79	2	x	0	0	3	0	0	0	0	0	0	177	0	0	0	0	3	1	0	x	0	0	0	0	x	x	0
112.11	12.79	3	x	x	0	2	x	0	0	0	0	0	148	0	0	0	0	11	1	0	x	x	0	0	0	x	x	0
112.61	12.80	1	3	2	0	11	x	2	0	0	0	0	191	0	0	0	0	3	2	0	1	x	0	0	1	x	3	0
114.66	12.81	x	0	x	0	1	0	x	0	0	0	0	294	0	0	0	0	x	1	0	0	0	0	0	0	x	2	0
115.26	12.82	0	0	0	0	2	0	0	0	0	0	0	198	0	0	0	0	x	x	0	1	0	0	0	0	1	1	0
115.76	12.82	3	0	2	1	2	x	1	0	0	0	0	339	0	0	0	0	3	1	0	x	0	0	x	x	1	2	0
116.29	12.83	1	2	x	0	3	x	x	0	0	0	0	262	0	0	0	0	5	4	0	2	0	0	1	x	x	2	0
116.76	12.83	0	x	x	0	1	0	x	0	0	0	0	158	0	0	0	0	4	3	0	x	0	0	x	x	1	0	0
117.26	12.84	1	0	2	0	1	x	0	0	0	0	0	107	0	0	0	0	1	2	0	x	1	0	x	1	x	x	0
117.79	12.84	1	0	x	0	1	0	0	0	0	0	0	136	0	0	0	0	1	x	0	0	0	0	0	x	2	2	0
118.26	12.85	4	0	1	0	0	0	1	0	0	0	0	107	0	0	0	0	x	1	0	1	x	0	0	x	2	x	0
118.76	12.85	5	0	1	0	0	0	0	0	0	0	0	126	0	0	0	0	2	2	0	x	x	0	0	x	x	1	0
119.29	12.85	1	x	x	0	x	0	x	0	0	0	0	199	0	0	0	0	1	1	0	0	0	0	0	x	2	19	0
119.76	12.86	2	2	2	0	2	0	x	0	0	0	0	289	0	0	0	0	1	1	0	0	0	0	0	0	1	x	0
120.26	12.86	3	1	0	0	x	0	x	0	0	0	0	308	0	0	0	0	x	4	0	x	0	0	x	0	2	1	0
120.79	12.87	2	0	1	0	0	0	x	0	0	0	0	299	0	0	0	0	x	2	0	x	0	0	0	1	x	2	0
121.26	12.87	x	x	x	0	x	0	1	0	0	0	0	130	0	0	0	0	x	1	0	x	0	0	0	0	1	2	0
121.76	12.88	1	1	x	0	0	0	0	0	0	0	0	163	0	0	0	0	x	x	0	1	0	0	0	0	x	1	0
122.19	12.88	3	0	x	0	x	0	0	0	0	0	0	157	0	0	0	0	x	x	0	x	0	0	0	0	1	x	0
122.51	12.88	3	0	0	0	x	1	0	0	2	1	x	129	4	2	0	0	1	0	0	x	0	0	0	x	2	1	0
123.61	12.96	x	0	1	0	x	0	0	0	3	3	2	107	2	1	0	0	2	1	0	0	1	0	0	0	x	6	0
123.95	13.00	x	0	x	0	1	x	0	0	6	5	1	102	5	x	0	0	2	2	0	x	0	0	0	x	x	5	0
124.11	13.01	x	0	1	0	1	1	0	0	10	8	3	138	9	2	0	0	2	1	0	0	0	0	0	x	0	7	0
124.42	13.03	1	0	0	0	0	0	0	0	0	0	0	171	0	0	0	0	0	1	0	0	x	0	0	0	x	19	0
124.61	13.04	x	0	x	0	x	x	0	0	7	7	1	191	18	2	0	0	x	x	0	1	0	0	0	0	x	3	0
124.92	13.05	1	x	0	0	0	0	0	0	0	0	0	201	0	0	0	0	x	2	0	x	0	0	0	0	3	x	0
125.11	13.05	1	0	1	0	x	0	0	0	5	1	x	151	7	x	0	0	x	0	0	0	0	0	0	0	x	1	0
125.45	13.06	1	1	2	0	x	0	0	0	0	0	0	179	0	0	0	0	0	x	0	x	0	0	0	0	1	3	0
125.61	13.07	2	0	0	0	x	0	0	0	5	6	1	197	23	5	0	0	x	x	0	0	0	0	0	x	x	1	0
125.92	13.07	2	0	1	0	x	0	0	0	0	0	0	180	0	0	0	0	0	x	0	x	0	0	0	0	1	1	0

Dinocyst sp. B	Dinocyst sp. C	Dinocyst sp. D	Dinocyst indet.	P-cyst indet.	Reworked dinocysts	Total in situ dinocysts	Acritarchs	*Cyclopsiella elliptica / granosa*	*Nannobarbophora gedlii*	*Nannobarbophora walldalei*	*Palambages*	*Paralecaniella indentata*	*Quadrina? condita*	Skolochorate acritarchs	Acritrach sp. A	Acritarch sp. B	Acritarch sp. C	Acritarch sp. D	Acritarch sp. E	Acritarch sp. F	Acritarch sp. G	Green algae	*Botryococcus*	*Cymatiosphaera baffinensis*	*Cymatiosphaera* spp. (pars)	*Leiosphaeridia rockhallensis*	Other prasinophyte algae	*Pediastrum*	*Pterospermella*	*Tasmanites*	Other marine acritarchs
0	2	0	2	2	7	335		x	31	0	0	0	0	136	4	0	0	0	0	0	0		0	0	11	81	x	0	0	0	
0	1	0	3	0	12	355		1	42	0	0	0	0	117	3	0	0	0	0	0	0		0	0	2	25	0	0	0	0	
0	x	0	4	0	6	458		1	86	0	0	0	0	134	3	0	0	0	0	0	0		0	0	9	66	0	0	0	0	
0	0	0	6	3	5	327		3	54	0	0	0	0	76	2	0	0	0	0	0	0		0	0	16	79	0	0	0	1	
0	0	0	4	0	12	358		0	79	0	0	0	0	99	3	0	0	0	0	0	0		0	0	16	100	0	0	0	1	
0	0	0	3	2	10	329		x	21	0	0	0	0	45	1	0	0	0	0	0	0		0	0	7	50	0	0	0	0	
0	0	0	4	0	4	322		0	37	0	0	0	0	96	4	0	0	0	0	0	0		0	0	14	99	0	0	0	0	
0	0	0	6	0	1	360		0	29	0	0	0	0	38	2	0	0	0	0	0	0		0	0	9	57	x	0	0	0	
0	0	0	3	0	3	338		0	19	0	0	0	0	68	0	0	0	0	0	0	0		0	0	10	67	x	0	0	0	
0	0	0	1	1	2	324		0	18	0	0	0	0	101	3	0	0	0	0	0	0		0	0	17	140	0	0	0	0	
0	0	0	4	0	2	393		0	18	0	0	0	0	73	0	0	0	0	0	0	0		0	0	7	56	0	0	0	0	
0	0	0	1	3	2	303		0	2	0	0	0	0	36	1	0	0	0	0	0	0		0	0	5	29	0	0	0	0	
0	0	0	0	0	3	450		0	31	0	0	0	0	93	7	0	0	0	x	0	0		0	0	5	70	2	0	0	0	
1	x	0	2	0	9	344		0	32	0	0	0	0	70	1	0	1	0	0	0	0		0	0	7	64	0	0	0	0	
0	0	0	7	1	6	473		1	53	0	0	0	0	87	22	0	1	0	0	0	0		0	0	7	100	0	0	0	x	
0	0	0	0	1	4	336		0	24	0	0	0	0	59	9	0	0	0	0	0	0		0	0	16	97	0	0	0	0	
0	0	0	14	2	2	328		0	33	0	0	0	0	169	16	0	0	0	0	0	0		0	0	9	131	0	0	0	0	
0	0	0	6	0	3	322		0	38	0	0	0	0	120	20	0	0	0	0	0	0		0	0	21	3	0	0	0	0	
6	0	0	6	2	6	389		3	40	0	0	0	0	87	7	0	0	0	0	0	0		0	0	34	45	0	0	0	0	
0	1	0	5	2	6	415		7	39	0	0	x	x	65	2	0	0	0	0	0	0		2	0	37	34	0	0	0	0	
0	1	0	5	0	2	302		0	40	0	0	0	0	42	1	0	0	0	0	0	0		0	0	41	19	0	0	0	0	
0	x	0	6	x	5	344		2	11	0	0	x	0	28	1	0	0	0	0	0	0		0	0	8	82	0	0	0	x	
x	0	0	7	0	5	340		2	27	0	0	1	0	28	0	0	0	0	0	0	0		0	0	10	4	0	0	0	0	
4	4	0	13	0	8	391		1	61	0	0	x	0	77	0	0	3	0	0	0	0		0	0	24	7	0	0	0	0	
1	0	0	1	0	7	371		1	25	0	0	0	0	55	0	0	0	0	0	0	0		0	0	28	3	0	0	0	1	
3	1	0	0	0	3	446		0	37	x	0	0	0	44	0	0	0	0	0	0	0		0	0	34	0	0	0	0	0	
1	x	0	2	1	4	303		1	35	8	0	2	0	46	0	1	x	0	0	0	0		0	0	14	2	0	0	0	0	
7	0	0	2	2	5	389		x	82	0	0	0	0	137	0	0	0	0	0	0	0		0	0	9	2	0	0	0	0	
2	4	0	6	4	3	402		x	52	6	0	x	0	83	0	0	1	0	0	0	0		0	0	15	4	0	0	0	0	
x	0	0	4	0	4	333		x	75	2	0	1	0	65	3	0	0	0	0	0	0		0	2	17	8	0	0	0	0	
5	2	0	0	0	5	360		2	67	0	x	1	1	182	0	0	1	0	0	0	0		0	0	10	2	x	0	0	0	
2	5	0	6	3	4	369		x	33	3	0	1	0	90	0	0	x	0	0	0	0		0	1	13	0	0	0	1	0	
3	1	0	2	0	11	387		0	71	0	0	0	x	82	0	0	0	0	0	0	0		0	0	8	0	0	0	0	0	
2	7	0	4	2	2	430		x	74	7	0	0	1	121	0	x	0	0	0	0	0		0	0	18	0	0	0	0	0	
1	4	0	3	3	8	470		1	61	6	0	1	0	90	1	0	1	0	0	0	0		0	0	21	1	0	0	0	0	
7	3	0	9	4	4	355		2	76	2	0	1	0	53	2	0	0	0	0	0	0		0	0	4	1	0	0	0	0	
14	4	0	2	2	0	477		x	99	6	0	0	0	67	2	0	4	0	0	0	0		0	0	39	4	0	0	0	0	
4	4	0	6	2	3	486		0	90	3	0	1	x	61	0	1	0	0	0	0	0		0	0	20	1	0	0	0	0	
4	6	0	5	0	2	502		0	99	6	0	0	0	114	1	0	2	0	0	0	0		0	1	4	x	0	0	0	0	
6	5	0	10	0	9	328		1	16	0	0	1	0	66	1	0	0	0	0	0	0		0	1	2	x	0	0	0	0	
4	6	0	2	0	6	584		0	120	5	0	x	0	236	2	1	2	0	0	0	0		0	1	10	2	0	0	0	0	
1	2	0	1	0	3	443		x	175	2	0	x	x	133	0	0	0	0	0	0	0		0	x	3	0	x	0	0	0	
1	2	0	0	0	3	359		1	51	2	0	0	x	78	0	0	0	0	0	0	0		0	1	13	1	x	0	0	0	
4	7	0	1	2	0	362		1	120	3	0	x	2	75	0	3	0	0	0	0	0		0	2	16	1	1	0	0	x	
2	3	0	4	0	7	314		0	32	0	0	0	0	67	0	0	0	0	0	0	0		0	x	3	1	0	0	x	0	
3	2	0	10	0	5	329		0	56	1	0	1	0	91	1	0	1	1	0	0	0		0	x	6	1	x	0	0	0	
1	0	0	3	1	3	359		0	58	0	0	0	x	78	x	1	0	1	0	0	0		0	x	3	1	0	0	x	x	
4	1	0	3	3	5	452		0	65	1	0	0	2	29	0	1	1	0	0	0	0		1	5	13	2	x	0	0	0	
12	2	0	2	0	4	556		0	19	0	0	x	0	69	1	0	0	0	0	0	0		0	x	6	2	0	0	0	0	
1	4	0	3	1	7	552		x	19	0	0	x	0	65	3	1	0	0	0	0	0		0	x	2	1	0	0	0	0	
x	3	0	7	1	8	485		1	21	2	0	x	0	42	1	x	0	0	0	0	0		0	1	4	1	0	0	0	0	
10	20	0	11	0	7	407		0	39	0	0	2	0	92	1	4	0	0	0	0	0		0	1	13	8	x	0	0	1	
16	13	0	3	0	6	369		1	59	1	0	x	0	70	1	x	0	0	0	0	0		0	0	11	3	0	0	0	0	
3	5	0	3	x	6	347		0	29	0	0	0	0	54	2	0	0	0	0	0	0		0	x	2	2	0	0	0	1	
2	9	0	4	0	3	370		0	14	0	0	0	0	60	1	0	1	0	0	0	0		0	2	4	1	0	0	0	0	
7	4	0	4	x	3	393		0	41	0	0	0	1	88	0	1	2	1	0	0	0		0	0	13	0	0	0	0	0	
4	4	0	6	0	5	370		2	41	0	0	x	0	68	1	0	2	0	0	0	0		0	x	14	1	3	0	0	0	
2	2	0	4	3	6	337		0	31	0	0	0	0	125	2	0	2	0	0	0	0		0	2	8	4	0	0	0	0	
0	9	0	7	2	4	316		0	11	0	0	0	0	86	2	0	0	0	0	0	0		0	0	1	0	0	0	0	1	
3	1	0	1	0	4	375		1	40	0	0	x	1	64	0	1	x	0	0	0	0		0	0	4	x	0	0	0	0	
0	1	0	5	0	4	350		1	11	0	0	x	0	40	0	0	0	0	0	0	0		0	0	5	1	0	0	0	0	
2	4	0	5	0	1	355		0	30	0	0	0	0	81	0	1	1	0	0	0	0		0	x	8	1	0	0	0	0	
0	11	0	8	1	6	337		0	22	0	0	2	0	71	0	0	0	0	0	0	0		0	0	14	0	0	0	0	0	
2	4	0	3	0	4	334		0	37	0	0	1	0	84	0	x	2	0	0	0	0		0	x	6	1	0	0	0	0	
0	6	0	17	0	4	370		0	30	x	0	1	0	95	3	0	0	0	0	0	0		0	0	17	0	0	0	0	1	

Composite depth (mcd)	Age (Ma)	Crustacean egg	Foraminiferal lining > 4 chambers	Pyritised diatoms	Terrestrial palynomorphs	Bisaccate pollen	Angiosperm pollen	Spores	Reworked spores	Reworked pollen	Fungal threads	Fungal spores	Palynomorph indet.
92.44	12.11	0	12	0		4	9	2	0	0	0	0	6
93.03	12.13	0	4	0		12	5	0	0	0	3	0	6
93.46	12.15	0	7	0		6	6	1	0	0	0	0	6
93.94	12.17	0	9	0		15	8	0	x	0	2	0	3
94.5	12.18	0	14	0		7	5	3	0	0	0	0	3
94.97	12.19	0	21	0		10	2	1	0	0	8	0	4
95.4	12.20	0	4	0		1	7	0	0	0	0	0	4
95.9	12.22	0	11	0		7	6	0	0	0	0	0	3
96.48	12.23	0	8	0		6	3	1	0	0	2	0	5
96.98	12.24	0	10	0		3	5	0	0	0	1	1	1
97.48	12.25	0	1	0		1	1	0	0	0	0	0	x
97.94	12.26	x	2	0		4	0	0	0	0	11	0	1
98.44	12.27	0	10	0		3	3	0	0	0	0	0	1
98.98	12.30	0	3	0		1	4	1	0	0	0	1	4
99.46	12.33	0	4	0		0	3	0	0	0	8	0	9
99.95	12.35	0	11	0		5	5	0	0	0	5	1	3
100.46	12.38	0	7	0		2	1	0	0	0	4	1	12
100.95	12.41	0	12	0		2	1	0	0	0	2	0	7
101.45	12.43	0	16	0		8	8	3	0	0	6	0	14
101.95	12.46	0	12	0		7	3	5	0	0	14	0	5
102.45	12.49	0	5	0		3	2	0	0	0	3	0	2
104.61	12.73	0	5	0		4	1	0	0	0	x	0	5
105.11	12.73	0	3	0		7	3	0	0	0	1	0	3
105.64	12.74	0	10	0		2	5	2	0	0	14	0	7
106.11	12.74	0	6	0		7	1	x	0	0	2	0	2
106.61	12.75	0	10	0		2	2	x	0	0	3	0	4
107.14	12.75	0	6	0		4	1	2	0	0	2	0	4
107.61	12.76	0	12	0		8	3	0	0	0	1	0	4
108.11	12.76	0	6	0		4	1	0	0	0	0	0	3
108.64	12.76	0	1	0		7	2	2	0	0	1	0	4
109.11	12.77	0	12	0		8	2	1	0	0	0	0	3
109.61	12.77	0	13	0		6	7	0	0	0	2	0	2
110.14	12.78	0	7	0		6	5	0	0	0	0	0	1
110.61	12.78	0	17	0		3	5	0	0	0	4	1	5
111.11	12.78	0	11	0		8	7	0	0	0	0	1	5
111.64	12.79	0	7	0		5	4	x	0	0	3	1	3
112.11	12.79	0	13	0		11	0	0	0	0	1	0	0
112.61	12.80	0	19	0		15	8	1	0	0	0	0	5
114.66	12.81	0	10	0		5	4	0	0	0	x	0	1
115.26	12.82	0	5	0		9	2	1	0	0	2	x	2
115.76	12.82	0	6	0		11	x	1	0	0	1	1	0
116.29	12.83	0	8	0		1	4	2	0	0	5	1	2
116.76	12.83	0	9	0		8	6	0	0	0	1	0	2
117.26	12.84	0	15	0		3	2	4	0	0	1	1	1
117.79	12.84	0	6	0		5	1	0	0	0	2	x	0
118.26	12.85	0	6	0		6	2	0	0	0	0	0	6
118.76	12.85	0	6	0		11	1	x	0	0	7	2	1
119.29	12.85	0	12	0		7	4	0	0	0	2	2	4
119.76	12.86	0	12	x		6	1	1	0	0	2	1	4
120.26	12.86	0	4	0		7	1	0	0	0	0	0	1
120.79	12.87	0	7	0		7	2	1	0	0	x	1	1
121.26	12.87	0	17	0		12	6	2	0	0	1	1	4
121.76	12.88	0	8	0		12	2	2	0	0	0	0	0
122.19	12.88	0	1	0		1	0	2	0	0	x	0	1
122.51	12.88	0	10	0		9	3	3	0	0	8	0	1
123.61	12.96	0	15	0		5	1	0	0	0	0	0	0
123.95	13.00	0	18	0		2	2	1	0	0	2	1	0
124.11	13.01	0	9	0		10	1	0	0	0	3	0	0
124.42	13.03	0	16	0		1	3	2	0	0	0	0	2
124.61	13.04	0	5	0		1	0	0	0	0	0	0	0
124.92	13.05	0	5	0		1	2	1	0	0	0	0	10
125.11	13.05	0	12	0		2	0	1	0	0	2	0	3
125.45	13.06	0	16	0		5	5	1	0	0	3	2	10
125.61	13.07	0	2	0		2	0	1	0	x	0	0	0
125.92	13.07	0	6	0		5	7	6	0	0	0	0	6

Leg	Site	Hole	Core	Type	Section	Top sample interval (cm)	Bottom sample interval (cm)	Core depth(mbsf)	Composite depth (mcd)	Age (Ma)	Batchnumber *Lycopodium* tables	Number of spores per tablet	Number of tablets	Dinoflagellate cysts	*Achomosphaera andalousiensis*	*Apteodinium tectatum*	*Barssidinium graminosum*	*Barssidinium pliocenicum*	*Barssidinium* spp. (pars)	*Batiacaspahera hirsuta*	*Batiacasphaera edwardsiae*	*Batiacasphaera* complex	*Bitektatodinium raedwaldii*	*Bitectatodinium tepikiense*	*Cannosphaeropsis passio*	*Cannosphaeropsis?* sp. A
307	1318	B	14	H	2	140	142	121.90	126.42	13.09	177745	18584	2		x	0	2	1	0	0	x	12	0	0	0	0
307	1318	C	7	H	3	20	22	120.70	126.61	13.09	177745	18584	2		x	0	1	0	0	0	x	26	0	x	0	0
307	1318	B	14	H	3	43	45	122.43	126.95	13.10	1031	20848	2		x	0	0	x	0	6	0	32	0	x	0	0
307	1318	C	7	H	3	70	72	121.20	127.11	13.11	177745	18584	2		1	0	0	x	0	0	x	53	0	0	0	0
307	1318	B	14	H	3	90	92	122.90	127.42	13.11	1031	20848	2		x	0	0	0	0	3	x	27	0	2	0	0
307	1318	C	7	H	3	120	122	121.70	127.61	13.12	177745	18584	2		0	0	1	2	0	2	1	41	0	0	0	0
307	1318	B	14	H	3	140	142	123.40	127.92	13.13	177745	18584	2		0	0	0	x	0	2	x	18	0	0	0	0
307	1318	C	7	H	4	20	22	122.20	128.11	13.13	177745	18584	1		0	0	0	x	0	5	x	22	0	0	0	0
307	1318	B	14	H	4	43	45	123.93	128.45	13.14	1031	20848	2		0	0	0	0	0	3	0	53	0	x	0	0
307	1318	C	7	H	4	70	72	122.70	128.61	13.15	177745	18584	1		x	0	0	0	0	8	0	21	0	0	0	0
307	1318	B	14	H	4	90	92	124.40	128.92	13.15	1031	20848	2		x	0	1	1	0	5	x	13	0	0	0	0
307	1318	C	7	H	4	120	122	123.20	129.11	13.16	177745	18584	1		x	0	0	0	0	2	x	11	0	0	0	0
307	1318	B	14	H	4	140	142	124.90	129.42	13.17	177745	18584	2		x	0	0	0	0	5	1	16	0	1	0	0
307	1318	C	7	H	5	20	22	123.70	129.61	13.17	1031	20848	2		x	0	0	x	0	2	x	30	0	x	0	0
307	1318	B	14	H	5	43	45	125.43	129.95	13.18	177745	18584	2		x	0	0	x	0	1	x	26	0	0	0	0
307	1318	C	7	H	5	70	72	124.20	130.11	13.19	1031	20848	2		2	0	0	x	0	6	0	21	0	x	0	0
307	1318	B	14	H	5	90	92	125.90	130.42	13.19	1031	20848	2		1	0	0	1	0	9	x	12	0	0	0	0
307	1318	C	7	H	5	120	122	124.70	130.61	13.20	1031	20848	2		1	0	0	x	0	6	0	25	0	0	0	0
307	1318	B	14	H	6	13	15	126.46	130.98	13.21	1031	20848	2		1	0	0	1	0	3	0	21	0	0	0	0
307	1318	C	7	H	6	19	21	125.19	131.1	13.21	1031	20848	2		1	0	0	x	0	3	0	32	2	0	0	0
307	1318	B	14	H	6	60	62	126.93	131.45	13.22	1031	20848	2		x	0	0	x	0	10	0	36	0	x	0	0
307	1318	C	8	X	1	14	16	125.84	131.75	13.23	1031	20848	2		2	0	0	0	0	6	0	29	1	1	0	0
307	1318	B	14	H	7	2	5	127.29	131.81	13.23	1031	20848	2		3	0	0	x	0	6	x	31	0	1	0	0
307	1318	C	8	X	1	60	62	126.30	132.21	13.24	1031	20848	2		x	0	0	x	0	11	0	29	x	x	0	0
307	1318	C	8	X	1	114	116	126.84	132.75	13.26	1031	20848	2		x	0	0	1	0	11	x	42	0	1	0	0
307	1318	C	8	X	2	14	16	127.26	133.17	13.27	1031	20848	2		x	0	0	1	0	14	0	35	x	x	0	0
307	1318	C	8	X	2	62	64	127.74	133.65	13.55	1031	20848	2		1	0	0	1	0	15	x	31	0	1	0	0
307	1318	C	8	X	2	114	116	128.26	134.17	13.58	1031	20848	2		1	0	0	0	0	16	x	35	0	x	0	0
307	1318	C	8	X	3	14	16	128.76	134.67	13.60	1031	20848	2		x	0	0	x	0	9	x	32	0	1	0	0
307	1318	C	8	X	3	60	62	129.22	135.13	13.63	1031	20848	2		x	0	0	0	0	8	1	44	0	1	0	0
307	1318	C	8	X	3	115	117	129.77	135.68	13.66	1031	20848	2		x	0	0	0	0	5	1	22	0	2	0	0
307	1318	C	8	X	4	14	16	130.26	136.17	13.69	1031	20848	2		1	0	0	x	0	4	1	20	x	x	0	0
307	1318	C	8	X	4	60	62	130.72	136.63	13.72	1031	20848	2		1	0	0	x	0	13	x	22	0	x	0	0
307	1318	C	8	X	4	115	117	131.27	137.18	13.75	1031	20848	2		3	0	0	1	0	5	x	27	0	1	0	0
307	1318	C	8	X	5	14	16	131.76	137.67	13.78	1031	20848	2		x	0	0	2	0	1	2	33	0	0	0	0
307	1318	C	8	X	5	60	62	132.22	138.13	13.81	1031	20848	2		2	0	0	0	0	2	x	15	0	x	0	0
307	1318	C	8	X	5	116	118	132.78	138.69	13.84	1031	20848	2		1	0	0	x	0	2	1	13	0	x	0	0
307	1318	C	8	X	6	14	16	133.26	139.17	13.87	1031	20848	2		1	0	0	x	0	4	2	21	0	1	0	0
307	1318	C	8	X	6	60	62	133.72	139.63	13.89	1031	20848	2		x	0	0	x	0	x	2	26	0	x	0	0
307	1318	C	8	X	6	114	116	134.26	140.17	13.92	1031	20848	2		1	0	0	x	0	2	2	18	0	2	0	0
307	1318	C	8	X	7	14	16	134.76	140.67	13.95	1031	20848	2		2	0	0	0	0	2	2	23	0	1	0	0
307	1318	C	8	X	8	13	15	135.19	141.1	13.98	1031	20848	2		1	0	0	x	0	x	2	30	x	1	0	0
307	1318	C	9	X	1	33	35	135.63	141.54	14.00	1031	20848	2		1	0	0	1	0	8	2	57	0	x	0	0
307	1318	C	9	X	1	80	82	136.10	142.01	14.03	1031	20848	2		x	0	0	2	0	4	x	32	0	1	0	0
307	1318	C	9	X	1	130	132	136.60	142.51	14.06	177745	18584	2		x	0	0	0	0	2	1	20	0	0	0	0
307	1318	C	9	X	2	34	36	137.14	143.05	14.09	1031	20848	2		0	0	0	0	0	8	x	17	0	0	0	0
307	1318	C	9	X	2	80	82	137.60	143.51	14.12	177745	18584	2		0	0	0	x	0	13	x	22	0	0	0	0
307	1318	C	9	X	2	130	132	138.10	144.01	14.15	1031	20848	2		1	3	0	x	0	10	x	28	0	2	0	0
307	1318	C	9	X	3	34	36	138.64	144.55	14.18	177745	18584	2		0	0	0	x	0	19	x	30	0	0	0	0
307	1318	C	9	X	3	80	82	139.10	145.01	14.20	1031	20848	2		x	1	0	x	0	11	x	43	0	1	0	0
307	1318	C	9	X	3	130	132	139.60	145.51	14.23	1031	20848	2		x	0	0	2	0	15	x	25	0	0	0	0
307	1318	C	9	X	4	33	35	140.13	146.04	14.26	1031	20848	2		0	x	0	x	0	5	0	47	0	1	0	0
307	1318	C	9	X	4	80	82	140.60	146.51	14.29	1031	20848	2		0	0	0	x	0	4	x	34	0	1	0	0
307	1318	C	9	X	4	130	132	141.10	147.01	14.32	177745	18584	2		0	0	0	x	0	5	0	25	0	0	0	0
307	1318	C	9	X	5	33	35	141.63	147.54	14.35	1031	20848	2		x	1	0	0	0	7	x	19	0	1	0	0
307	1318	C	9	X	5	84	86	142.14	148.05	14.38	177745	18584	2		0	1	0	4	0	7	x	28	0	2	0	0
307	1318	C	9	X	5	130	132	142.60	148.51	14.41	1031	20848	2		0	x	0	1	0	7	x	22	0	0	0	0

Cannosphaeopsis spp. (pars)	*Capisocysta lata/lyelli*	*Cerebrocysta irregulare*	*Cerebrocysta lagae*	*Cerebrocysta poulsenii*	*Cleistosphaeridium placacanthum*	*Cordosphaeridium minimum*	*Corrudinium devernalieae*	*Cousteaudinium aubryae*	*Cribroperidinium tenuitabulatum*	*Cristadinium cristatoserratum*	*Cristadinium diminutivum*	*Dalella chathamensis*	*Dapsilidinium pseudocolligerum*	*Dinopterigium cladoides* sensu Morgenroth 1966	*Echinidinium aculeatum*	*Echinidinium euaxum*	*Echinidinium nordlandensis*	*Echinidinium sleipnerensis*	*Echinidinium transparantum*	*Echinidinium* sp. A	*Echinidinium* cf. sp A	*Echinidinium* spp. (pars)	*Edwarsiella sexispinosa*	*Filisphaera filifera*	*Geonettia clineae*	*Habibacysta tectata*	*Homotryblium pallidum*	*Homotryblium tenuispinosum*
0	0	0	0	x	2	0	0	0	0	0	0	0	21	0	0	0	0	0	0	0	0	0	0	0	0	7	0	0
0	1	0	0	x	2	2	0	0	0	0	0	0	20	0	0	1	0	0	1	0	0	0	0	0	0	14	0	0
0	3	0	0	x	3	0	0	0	x	0	0	0	17	0	0	1	0	0	0	0	0	0	0	2	0	26	0	x
0	0	0	0	x	7	1	0	x	0	0	0	0	19	0	0	0	0	0	0	0	0	2	0	x	0	33	0	0
0	4	0	0	3	2	0	0	0	0	0	0	0	10	0	0	0	0	0	0	0	0	x	0	x	0	14	0	0
0	1	0	0	x	3	0	0	0	0	0	0	0	11	0	0	0	0	x	0	0	0	0	0	0	0	25	0	0
0	2	0	0	0	4	1	0	0	0	0	0	0	12	0	0	2	0	0	0	0	0	0	0	x	0	23	0	1
0	3	0	0	x	2	0	0	0	0	0	0	0	8	0	x	1	0	0	0	0	0	0	0	0	0	36	0	0
0	2	0	0	x	x	0	0	0	0	0	0	0	5	0	0	3	x	0	1	1	0	0	0	2	0	32	x	0
0	7	0	0	1	1	0	0	x	0	0	0	0	7	0	0	x	0	0	0	0	0	0	0	1	0	35	0	0
0	2	0	0	0	x	0	0	0	0	0	x	0	2	0	x	3	0	0	2	0	0	0	0	0	x	8	0	0
0	13	0	0	x	x	0	0	0	0	0	0	0	5	0	0	x	0	x	x	0	0	0	0	1	0	13	0	0
0	7	0	0	0	x	0	0	0	0	0	0	0	3	0	0	x	0	0	0	0	0	0	0	1	0	31	0	0
x	15	0	0	x	x	0	0	x	0	0	0	0	4	0	x	2	0	x	0	0	0	0	0	1	0	22	0	0
0	5	0	0	0	x	0	0	0	0	0	0	0	2	0	0	0	0	1	0	0	0	0	0	x	0	53	0	0
0	2	0	0	2	2	0	0	0	0	0	0	0	9	0	0	1	0	1	0	0	0	0	0	1	0	16	0	0
0	3	0	0	x	x	0	0	0	0	0	0	0	6	0	1	x	0	x	1	0	0	0	0	0	0	8	0	0
0	3	0	0	0	x	0	0	0	0	0	0	0	5	0	0	x	0	0	0	0	0	0	0	0	0	7	0	0
0	0	0	0	x	x	0	0	0	0	0	0	0	3	0	0	x	0	1	x	0	0	0	0	0	0	13	0	0
0	4	0	0	x	1	0	0	0	0	0	1	0	5	0	0	1	0	x	0	0	0	0	0	0	0	19	0	0
0	3	0	0	x	2	0	0	0	0	0	0	0	5	0	0	x	0	0	0	0	0	0	0	0	0	14	0	0
0	7	0	0	1	0	0	0	0	0	0	0	0	11	0	0	5	0	x	0	0	0	0	0	0	0	9	0	0
0	5	0	0	1	3	0	0	0	0	0	0	0	13	0	0	0	0	0	0	0	0	0	0	0	0	9	0	1
0	6	0	0	2	3	0	0	0	0	0	0	0	21	0	1	x	0	0	0	1	1	0	0	0	0	18	0	0
0	4	0	0	1	4	0	0	0	0	0	0	0	2	0	0	1	0	1	0	0	0	0	0	1	0	16	0	0
0	2	0	0	0	2	0	0	0	0	0	x	0	20	x	0	0	0	1	x	0	0	1	0	x	1	9	0	0
0	x	0	0	x	2	0	0	0	0	x	0	0	10	0	0	0	0	0	0	0	1	0	0	0	0	10	0	0
0	1	0	0	x	2	0	0	0	0	0	0	0	9	0	0	0	0	x	0	0	0	0	0	0	0	17	0	0
0	6	0	0	1	1	0	0	x	x	0	0	0	9	0	0	x	0	x	0	0	0	0	0	0	0	10	0	0
0	2	0	0	1	10	0	0	x	0	0	0	0	4	1	0	x	0	x	0	0	0	0	0	3	0	17	0	0
0	2	0	0	x	2	0	0	0	0	0	0	0	19	x	0	1	0	x	0	0	0	0	0	0	0	8	0	0
0	1	0	0	1	4	0	0	0	x	0	0	0	23	0	0	0	1	0	3	0	x	0	0	0	0	8	0	0
0	1	0	0	x	1	0	0	x	0	0	0	0	11	0	x	x	x	x	0	0	0	0	0	2	0	25	0	0
0	1	0	0	x	4	0	0	0	0	0	0	0	19	0	0	2	x	x	0	0	0	0	0	1	0	9	0	0
0	0	0	0	3	1	0	0	0	0	0	x	0	10	x	0	x	x	x	x	0	0	0	0	x	0	18	0	0
0	0	0	0	x	x	0	0	0	0	0	0	0	10	0	0	2	0	0	0	0	0	1	0	0	0	7	0	0
0	1	0	0	x	3	0	0	0	x	0	x	0	7	0	x	1	0	1	0	0	0	0	0	x	0	5	0	0
0	x	0	0	x	4	0	0	0	0	x	0	0	7	0	0	1	0	1	0	0	0	0	0	x	0	14	0	0
0	x	0	0	1	1	0	0	1	x	0	0	0	2	0	0	0	x	0	0	0	0	0	0	x	0	7	0	0
0	x	0	0	1	1	0	0	0	x	0	0	0	9	0	x	1	0	1	3	0	0	0	0	0	0	6	0	0
0	0	0	0	1	2	0	0	0	x	0	0	0	4	1	0	0	0	x	0	0	0	0	0	x	0	11	0	x
0	2	0	0	1	4	0	0	0	x	0	0	0	19	0	0	x	0	0	0	0	0	0	0	x	0	8	0	0
0	x	0	0	0	4	0	0	0	2	0	0	0	6	x	x	0	1	0	0	0	0	0	0	x	0	8	0	x
0	1	0	0	1	13	0	0	0	4	0	0	0	6	x	0	x	x	0	0	0	0	0	0	0	0	6	0	0
0	3	0	0	x	12	0	0	0	6	0	0	0	13	x	0	0	0	1	0	0	0	0	0	0	0	4	0	0
0	1	0	0	0	8	0	0	x	5	0	0	0	7	1	0	1	0	2	0	0	0	0	0	0	0	10	0	x
0	7	0	0	0	6	0	0	0	7	0	0	0	8	x	0	1	0	x	0	0	0	0	0	0	1	3	0	0
0	12	0	0	0	7	0	0	0	5	0	x	0	5	0	0	0	0	1	0	0	0	0	0	0	0	5	0	0
0	8	0	0	0	16	0	0	0	5	0	0	0	10	0	1	x	x	x	0	0	0	0	0	0	0	6	0	0
0	4	0	0	0	9	0	0	x	x	0	0	0	4	x	0	x	0	x	0	0	0	0	0	2	0	4	0	0
0	2	0	0	x	5	0	0	0	5	0	x	0	5	0	0	x	0	1	0	0	0	0	0	1	0	6	0	0
0	3	0	0	0	5	0	0	0	x	0	0	0	5	0	0	0	0	1	0	0	0	0	0	1	0	4	0	0
0	x	0	0	0	1	0	0	0	x	0	0	0	5	0	0	0	0	1	0	0	0	0	0	0	0	1	0	x
0	5	1	0	0	7	0	0	x	1	0	0	0	4	0	0	0	2	1	0	0	0	0	0	x	0	x	0	x
0	1	0	0	0	17	0	0	0	x	0	0	0	5	0	0	x	0	0	0	0	0	0	0	x	0	4	0	x
0	2	x	0	1	3	0	0	1	0	0	0	0	5	1	0	0	0	1	0	0	0	0	0	0	1	x	0	0
0	0	0	0	0	1	0	0	0	1	0	0	0	4	8	0	x	0	x	0	x	0	0	0	1	0	1	0	1

Composite depth (mcd)	Age (Ma)	*Hystrichokolpoma rigaudiae*	*Hystrichosphaeropsis obscura*	*Hystrichostrogylon membraniphorum*	*Impagginium aculeatum*	*Impagidium arachnion*	*Impagidinium pallidum*	*Impagidinium paradoxum*	*Impagidinium patulum*	*Impagidinium plicatum*	*Impagidinium striolatum*	*Impagidinium sphaericum*	*Impagidinium velorum*	*Impagidinium* spp. (pars)	*Invertocysta lacrymosa*	*Invertocysta tabulata*	*Kallosphaeridium* sp. of Head and Westphal, 1999	*Labyrinthodinium truncatum*	*Lejeunecysta convexa*	*Lejeunecysta challengerensis*	*Lejeunecysta* cf. *challengerensis*	*Lejeunecysta hatterasensis*	*Lejeunecysta marieae*	*Lejeunecysta* spp. (pars)	*Lingulodinium machaerophorum*	*Melitasphaeridium choanophorum*	*Nematosphaeropsis labyrinthus*
126.42	13.09	1	x	0	0	0	1	x	x	0	0	0	0	0	x	0	0	3	0	0	0	0	1	0	1	2	4
126.61	13.09	1	x	x	x	x	3	2	x	0	0	0	0	0	0	0	0	9	0	0	0	0	x	0	1	6	5
126.95	13.10	2	x	x	0	0	1	1	x	0	0	0	0	0	0	x	3	x	0	0	0	0	0	x	1	x	5
127.11	13.11	5	x	0	0	0	2	3	0	0	0	0	0	0	0	0	0	6	0	0	0	x	x	0	x	1	6
127.42	13.11	0	x	x	0	0	x	x	x	0	0	0	0	0	0	0	3	8	0	x	0	0	x	2	2	1	3
127.61	13.12	0	x	0	0	0	4	4	x	0	0	0	0	0	0	1	0	9	0	x	0	x	2	0	3	x	5
127.92	13.13	x	1	0	0	0	3	3	0	0	0	0	0	0	1	x	3	1	0	0	0	x	1	x	3	x	12
128.11	13.13	1	1	0	1	0	2	1	x	0	0	0	0	0	0	0	1	2	0	x	0	0	3	0	1	x	4
128.45	13.14	x	0	0	0	0	4	4	0	0	0	0	0	0	0	x	2	4	0	0	0	0	1	x	1	x	12
128.61	13.15	x	0	1	x	0	9	2	x	0	x	x	0	0	0	0	3	3	0	x	0	0	2	0	1	1	8
128.92	13.15	x	3	0	1	0	7	2	x	0	0	0	0	0	0	0	1	14	1	0	0	0	2	3	1	1	7
129.11	13.16	x	2	0	0	0	10	3	0	0	0	0	0	0	0	0	2	7	0	0	0	0	2	0	x	x	9
129.42	13.17	1	1	1	0	0	2	1	x	0	x	0	0	0	0	0	3	11	0	0	0	x	3	0	3	1	8
129.61	13.17	x	x	x	0	0	5	2	x	0	x	0	0	0	x	0	4	9	x	1	0	0	2	0	2	x	11
129.95	13.18	1	1	0	0	0	6	4	x	0	2	0	0	0	0	x	2	11	0	1	0	1	3	2	0	x	11
130.11	13.19	x	x	0	0	0	5	6	x	0	1	0	0	0	x	x	1	9	x	1	0	0	1	0	2	x	10
130.42	13.19	x	x	1	x	0	8	8	0	0	0	0	0	0	x	2	2	11	0	0	0	0	0	2	2	x	8
130.61	13.20	x	x	0	1	0	2	5	1	0	0	1	0	0	0	3	3	6	0	0	0	0	x	0	1	x	14
130.98	13.21	x	0	0	2	0	6	5	x	0	0	0	0	0	0	1	5	5	0	0	0	0	1	2	x	x	10
131.1	13.21	2	2	0	1	0	3	5	0	0	0	0	1	0	0	1	1	9	0	0	0	0	1	x	x	1	11
131.45	13.22	x	x	x	0	0	5	1	x	0	x	0	0	0	0	0	1	3	0	0	0	0	3	0	2	x	8
131.75	13.23	2	x	0	0	0	3	2	x	0	0	0	2	0	0	1	1	5	1	0	0	2	3	1	1	1	2
131.81	13.23	1	x	x	0	0	4	x	x	0	0	0	0	0	x	x	0	4	0	0	0	0	2	1	5	4	4
132.21	13.24	2	1	0	0	0	2	1	0	0	0	0	0	0	0	x	2	7	0	0	0	0	x	0	2	1	5
132.75	13.26	1	3	0	0	0	1	x	x	0	0	0	0	0	0	0	1	1	0	1	0	0	4	2	x	x	1
133.17	13.27	2	1	0	0	0	4	x	0	0	0	0	0	0	0	x	1	4	0	2	0	0	x	x	3	1	11
133.65	13.55	x	1	0	0	0	6	x	0	0	0	0	0	0	0	x	2	11	0	1	0	0	1	5	2	x	1
134.17	13.58	1	0	x	0	0	7	1	0	0	0	0	x	0	0	0	1	11	x	x	0	1	0	0	2	x	2
134.67	13.60	0	x	1	0	0	2	x	x	0	0	0	0	0	0	0	5	9	0	0	0	0	1	x	10	x	2
135.13	13.63	x	1	0	0	0	2	x	0	0	0	0	0	0	0	0	6	7	x	2	0	x	1	0	4	x	4
135.68	13.66	0	x	1	0	0	12	x	x	0	1	0	0	0	0	x	2	10	0	0	0	0	1	1	4	1	6
136.17	13.69	x	x	0	0	0	7	1	1	0	0	x	x	0	0	x	1	5	0	1	0	0	x	1	7	x	3
136.63	13.72	x	x	1	x	0	8	1	x	0	0	0	0	0	0	1	3	6	0	1	0	0	1	2	7	1	7
137.18	13.75	0	0	0	0	0	4	1	x	0	0	0	0	0	0	x	1	3	1	1	0	0	2	0	1	x	2
137.67	13.78	x	x	0	0	0	10	2	x	0	0	0	0	0	0	0	1	4	0	3	0	0	2	2	4	x	3
138.13	13.81	x	0	0	0	0	9	x	x	0	0	0	0	0	0	0	1	5	2	x	0	0	x	4	4	1	4
138.69	13.84	x	x	0	0	0	9	0	1	0	0	0	1	0	0	0	x	8	0	x	0	0	1	1	1	1	6
139.17	13.87	x	0	0	0	0	6	1	x	0	0	0	0	0	0	x	2	7	0	1	0	0	2	1	2	x	6
139.63	13.89	1	x	0	0	0	7	1	x	0	0	0	0	0	0	x	x	6	0	1	0	0	2	2	3	1	5
140.17	13.92	2	0	0	0	0	6	x	x	0	0	0	0	0	0	x	2	5	0	x	0	0	0	x	3	2	4
140.67	13.95	x	0	1	0	0	4	2	2	0	0	0	0	0	0	0	0	2	0	1	0	0	0	0	7	0	6
141.1	13.98	1	x	1	0	0	5	x	2	0	0	0	0	0	x	0	1	4	0	x	0	0	x	0	1	x	6
141.54	14.00	x	0	0	0	0	4	2	0	0	0	0	x	0	0	0	3	2	0	0	0	0	0	4	4	x	1
142.01	14.03	x	1	0	0	0	6	x	x	0	0	0	0	0	0	x	x	3	0	0	0	0	0	x	x	x	5
142.51	14.06	1	x	0	0	0	2	6	x	0	0	0	0	0	0	0	1	1	1	0	0	0	x	0	1	x	7
143.05	14.09	2	x	0	1	0	4	x	x	0	0	0	0	0	x	x	x	3	1	x	0	0	1	2	x	x	1
143.51	14.12	1	1	0	0	0	1	x	x	0	0	0	0	0	0	x	2	12	0	x	0	0	0	x	x	x	5
144.01	14.15	x	x	x	0	0	5	x	x	0	0	0	0	0	x	x	1	3	1	x	0	0	0	1	3	x	5
144.55	14.18	x	x	0	0	0	3	0	0	0	0	0	0	0	x	x	1	3	x	1	0	1	2	0	1	x	0
145.01	14.20	x	x	0	0	0	x	2	1	0	0	0	0	0	0	x	1	4	x	x	0	0	0	2	1	1	9
145.51	14.23	x	x	0	0	0	4	2	1	0	0	0	0	0	0	0	0	6	1	0	0	0	1	2	2	x	3
146.04	14.26	0	0	x	0	0	6	0	0	0	0	0	0	0	0	x	2	3	0	0	0	0	1	0	5	2	7
146.51	14.29	x	1	0	0	0	6	1	0	0	0	0	0	0	0	0	1	6	0	0	0	0	x	2	7	3	7
147.01	14.32	1	1	0	0	0	7	x	1	0	0	0	0	0	0	1	0	2	1	x	0	0	0	x	2	x	4
147.54	14.35	x	2	0	0	0	3	2	0	0	0	0	0	0	0	0	x	8	0	0	0	0	0	0	6	1	2
148.05	14.38	2	0	0	0	0	2	0	0	0	0	0	0	0	0	x	x	5	1	1	0	0	0	1	5	x	8
148.51	14.41	x	1	0	0	0	7	0	0	0	0	0	0	0	0	0	1	1	2	0	0	0	0	x	1	1	7

Nematosphaeropsis lemniscata	*Operculodinium? borgerholtense*	*Operculodinium centrocarpum*	*Operculodinium? eirikianum*	*Operculodinium giganteum*	*Operculodinium israelianum*	*Operculodinium janduchenei*	*Operculodinium longispinigerum*	*Operculodinium piaseckii*	*Operculodinium* cf. *piaseckii*	*Operculodinium* sp. 3 of De Verteuil and Norris, 1996	*Palaeocystodinium golzowense*	*Palaeocystodinium minor*	*Palaeocystodinium miocaenicum*	*Palaeocystodinium powellense*	*Paucisphaeridium cylindratum*	*Paucisphaeridium* sp. A	*Paucisphaeridium* sp. B	*Paucisphaeridium* spp. (pars)	*Pentadinium laticinctum*	cyst of *Polykrikos kofoidii/schwartzii* sensu Matsuoka et al. 2009	*Polysphaeridium zoharyi*	*Pyxidinopsis fairhavenensis*	*Pyxidinopsis psilata*	*Pyxidinopsis tuberculata*	*Pyxidinopsis vesiculata*	*Pyxidinopsis* sp. A	*Pyxidinopsis* sp. B	*Pyxidinopsis* spp. (pars)
0	0	12	3	0	1	0	0	2	0	1	1	x	0	x	0	0	0	14	x	0	0	x	x	x	0	0	0	0
0	0	4	5	0	3	0	0	x	0	0	2	1	0	x	0	0	0	45	x	0	0	0	2	x	x	0	0	0
0	0	8	1	0	x	0	4	x	0	0	4	1	2	0	0	14	17	0	x	0	0	0	x	1	0	0	0	0
0	0	3	3	0	2	0	0	x	0	0	3	2	0	1	0	0	0	31	x	0	0	1	2	1	0	0	0	0
0	0	4	2	0	x	0	3	3	1	0	1	x	0	1	0	9	36	0	1	0	0	0	x	0	x	x	0	0
0	0	1	3	0	x	0	0	1	0	0	8	2	0	0	0	5	0	19	x	0	0	4	0	x	0	0	0	0
0	1	2	3	0	0	0	0	1	x	0	11	11	x	1	0	12	19	0	1	0	1	0	0	1	x	0	0	0
0	0	4	x	0	0	0	1	x	0	0	5	0	1	0	0	7	10	0	x	0	0	0	0	x	x	0	0	0
0	0	3	0	0	0	0	2	1	0	0	7	1	1	0	x	5	11	0	1	0	0	0	0	0	0	0	0	0
0	0	2	1	0	1	0	1	0	0	0	11	2	1	x	0	13	9	0	0	0	0	0	x	x	0	0	0	0
0	0	3	x	0	0	0	8	x	0	0	5	3	x	0	1	3	27	0	0	0	0	0	0	0	x	1	0	0
0	0	6	0	0	0	0	x	x	0	0	2	0	2	x	0	10	15	0	0	0	0	0	0	x	0	0	0	0
0	x	1	1	0	x	0	3	1	1	0	2	0	0	0	0	8	19	0	0	0	0	0	x	1	0	0	0	0
0	0	2	1	0	x	0	4	x	x	0	1	0	2	1	0	12	29	0	x	0	x	0	x	0	0	0	0	0
0	0	4	2	0	x	0	2	0	1	0	1	0	0	0	0	6	16	0	x	0	2	0	0	0	0	0	0	0
0	x	9	2	0	0	x	2	x	1	0	3	x	x	0	0	7	7	0	1	0	0	0	x	x	0	0	0	0
0	x	3	5	0	x	0	7	2	0	0	2	0	0	0	1	9	15	0	x	0	0	0	0	0	0	0	0	0
0	0	3	2	0	0	0	5	3	0	0	1	x	0	0	0	14	20	0	2	0	x	0	1	x	0	0	0	0
0	x	4	6	0	0	0	7	1	x	0	2	0	1	0	3	6	7	0	x	0	0	0	0	0	0	0	0	0
0	0	1	9	0	0	0	1	1	1	0	1	0	0	x	0	7	11	0	0	0	0	0	0	0	0	0	0	0
0	1	9	5	0	x	0	3	x	0	0	x	1	x	0	0	11	34	0	x	0	0	0	x	0	0	0	0	0
0	0	6	1	0	0	0	2	x	0	0	8	0	0	0	0	14	24	0	0	0	0	0	0	1	0	0	0	0
0	x	3	6	0	x	0	1	x	x	0	1	0	0	0	0	22	48	0	x	0	0	0	x	x	0	0	0	0
0	0	6	0	0	0	0	2	x	0	0	11	2	0	x	0	13	10	0	x	0	0	0	x	x	0	0	0	0
0	0	6	1	0	2	0	1	0	0	0	25	3	1	0	0	11	9	0	1	0	0	0	0	0	0	0	0	0
0	0	8	3	0	2	0	5	x	0	0	19	0	1	0	1	8	41	0	x	0	0	0	x	x	0	0	0	0
0	1	5	x	0	2	0	1	x	0	0	55	1	1	0	x	13	15	0	0	0	0	0	2	x	x	0	0	0
0	x	5	x	x	2	0	1	1	0	0	55	x	1	0	2	14	20	0	0	0	0	0	1	0	x	0	0	0
0	0	2	1	0	2	0	0	1	x	0	43	4	0	0	0	16	18	0	0	0	0	x	2	x	1	0	0	0
0	0	x	1	0	x	0	1	1	0	0	51	5	1	0	1	8	30	0	x	0	0	0	1	0	0	0	0	0
0	x	6	x	0	1	0	0	1	0	0	90	4	2	0	1	14	9	0	0	0	0	0	1	1	1	1	0	0
0	x	17	1	0	1	0	1	x	x	0	64	7	0	0	1	5	18	0	x	0	0	0	x	x	0	x	0	0
0	0	7	1	0	4	0	0	x	0	0	28	2	1	0	1	4	14	0	0	0	0	0	0	0	0	0	0	0
0	0	3	x	0	x	0	1	x	0	0	35	2	x	0	4	8	14	0	0	0	0	0	0	x	x	0	0	0
0	0	1	0	0	x	0	0	x	x	0	49	4	0	0	3	11	20	0	0	0	x	0	1	x	x	0	0	0
0	0	2	0	0	0	0	0	1	0	0	71	4	2	0	x	4	8	0	0	0	0	0	1	1	x	1	0	0
0	0	3	0	0	x	0	1	x	0	0	36	4	0	0	5	11	29	0	0	0	0	0	x	0	0	0	0	0
0	0	6	0	0	x	0	3	1	0	0	55	3	0	0	2	5	27	0	0	0	0	0	1	x	x	0	x	0
0	x	0	0	0	x	0	1	2	0	0	37	0	1	0	x	11	12	0	0	0	0	0	x	x	0	0	0	0
0	0	7	x	x	x	0	x	x	x	0	52	1	2	0	0	3	12	0	0	0	0	0	x	x	x	0	0	0
0	0	5	x	0	x	0	1	0	0	0	43	1	1	0	3	10	6	0	0	0	0	0	x	0	0	x	0	0
0	x	8	1	x	1	0	2	x	0	0	29	2	0	0	1	5	11	0	0	0	x	0	1	x	0	0	0	0
0	x	4	2	0	x	0	9	x	1	0	6	0	0	0	1	7	21	0	0	0	x	0	x	0	x	x	0	0
0	0	5	1	0	x	0	2	x	0	0	8	x	0	0	4	6	11	0	0	0	x	0	x	0	x	0	0	0
0	1	9	0	0	x	0	1	1	x	0	1	1	6	0	0	7	19	0	0	0	11	0	1	0	x	0	x	0
0	0	4	1	0	x	0	2	x	x	0	18	0	1	0	2	3	30	0	2	0	0	0	x	0	0	0	2	0
0	0	9	1	0	0	0	2	1	x	0	11	x	x	0	4	6	24	0	0	0	x	0	1	1	1	0	2	0
1	1	5	x	0	0	0	x	x	0	0	21	0	2	0	8	4	25	0	0	0	0	0	1	0	0	0	1	0
0	0	7	x	x	0	0	0	x	x	0	39	x	x	0	3	11	17	0	x	0	x	0	x	0	0	0	x	0
0	1	6	0	0	0	0	x	1	x	0	17	0	x	0	8	8	25	0	x	0	x	0	0	0	1	0	x	0
0	x	3	0	x	0	x	1	2	0	0	16	0	1	0	5	11	32	0	0	0	1	0	x	x	x	0	1	0
0	x	4	2	0	0	0	2	1	0	0	11	0	0	0	6	25	15	0	0	0	0	0	0	0	0	0	1	0
0	0	5	1	x	1	0	2	2	0	0	9	0	1	0	7	18	16	0	0	0	x	0	x	x	0	0	3	0
0	1	2	x	1	x	0	1	1	0	0	2	0	2	0	2	9	23	0	x	0	4	0	x	0	0	0	1	0
0	x	4	1	0	1	0	2	1	0	0	x	0	0	0	x	7	37	0	x	0	5	x	0	0	0	0	x	0
0	0	8	x	0	0	0	3	3	0	0	4	0	0	0	8	9	8	0	0	0	2	0	x	x	0	0	x	0
0	1	6	2	x	0	0	x	x	0	0	1	0	0	0	2	17	20	0	x	0	1	0	x	x	1	0	0	0

Composite depth (mcd)	Age (Ma)	*Reticulatosphaera actinocoronata*	Round brown cysts	*Selenopemphix brevispinosa*	*Selenopemphix dionaeacysta*	*Selenopemphix nephroides*	*Selenopemphix porcupensis*	*Selenopemphix quanta*	*Selenopemphix* spp. (pars)	*Spiniferites hyperacanthus*	*Spiniferites mirabilis/membranaceus*	*Spiniferites solidago*	*Spiniferites/Achomosphaera* complex	*Spiniferites* sp. A	*Spiniferites* sp. B	*Spiniferites* sp. C	*Sumatradinium? delectabilis*	*Sumatradinium hamulatum*	*Sumatradinium soucouyantiae*	*Sumatradinium* spp. (pars)	*Tectatodinium pellitum*	*Trinovantedinium glorianum*	*Trinovantedinium ferugnomatum*	*Trinovantedinium harpagonium*	*Trinovantedinium henrietti*	*Tuberculodinium vancampoe*	*Unipontidinium aquaeductus*	Dinocyst sp. A
126.42	13.09	x	0	0	0	x	0	0	0	0	0	0	261	0	0	0	0	0	x	0	0	0	0	0	0	1	3	0
126.61	13.09	x	0	x	0	x	0	0	0	0	0	0	193	0	0	0	0	1	x	0	x	0	0	0	0	1	4	0
126.95	13.10	2	0	0	0	1	0	0	0	4	3	x	193	5	x	0	0	2	1	0	x	0	0	0	x	1	1	0
127.11	13.11	x	0	1	0	x	0	1	0	0	0	0	199	0	0	0	0	x	2	0	0	0	0	0	0	2	0	0
127.42	13.11	x	0	x	0	0	0	x	0	x	3	1	183	6	x	0	0	x	1	0	0	0	0	0	x	1	2	0
127.61	13.12	x	0	x	1	x	0	0	0	0	0	0	169	0	0	0	0	3	2	0	0	0	0	0	0	1	8	0
127.92	13.13	3	0	x	0	2	0	0	0	8	7	0	119	6	x	0	0	3	1	0	0	0	0	0	x	x	3	0
128.11	13.13	1	1	1	0	1	0	0	0	1	2	0	169	7	1	0	0	x	x	0	0	0	0	0	0	0	0	0
128.45	13.14	2	1	0	0	3	0	1	0	2	2	0	141	10	0	0	0	5	1	0	0	1	0	0	0	1	2	0
128.61	13.15	x	0	x	0	4	0	x	0	4	5	x	158	7	x	0	0	1	1	0	x	0	0	0	0	0	3	0
128.92	13.15	2	0	1	0	1	0	x	0	4	4	2	226	9	4	0	0	4	2	0	1	0	0	0	x	0	1	0
129.11	13.16	x	0	x	0	0	0	x	0	14	4	0	157	8	x	0	0	1	1	0	1	0	2	0	1	1	5	0
129.42	13.17	2	x	x	0	0	0	0	0	7	4	1	169	13	0	0	0	1	x	0	1	x	0	0	0	x	2	0
129.61	13.17	1	0	1	0	3	0	0	0	4	1	1	173	8	x	0	1	1	0	0	1	0	0	0	x	x	3	0
129.95	13.18	1	0	1	0	2	0	0	0	9	2	1	131	10	x	0	0	6	x	0	0	0	0	0	0	x	6	0
130.11	13.19	5	0	1	0	x	0	x	0	8	5	2	195	12	3	0	0	x	1	0	1	x	0	0	x	2	11	0
130.42	13.19	4	2	1	0	x	0	0	0	3	2	x	241	4	x	0	0	1	0	0	x	0	0	0	0	x	6	0
130.61	13.20	2	0	1	0	x	0	1	0	1	5	1	166	5	1	0	0	1	x	0	1	0	0	0	x	1	7	0
130.98	13.21	5	0	1	x	x	0	0	0	3	3	2	214	7	2	0	0	1	x	0	x	0	0	0	0	x	5	0
131.1	13.21	3	0	1	0	2	0	0	0	6	7	0	172	0	0	0	0	3	x	0	2	0	1	0	1	0	9	0
131.45	13.22	3	0	x	0	x	0	0	0	8	5	2	143	5	4	0	0	2	1	0	x	0	0	0	0	x	1	0
131.75	13.23	4	0	5	0	2	0	0	0	6	2	2	118	12	2	0	0	5	2	0	1	0	0	0	1	x	6	0
131.81	13.23	x	0	x	0	2	0	0	0	5	4	1	215	10	6	0	0	1	x	0	1	x	0	0	x	2	1	0
132.21	13.24	4	1	0	0	1	0	0	0	1	4	1	159	12	6	0	0	2	1	0	x	0	0	0	1	2	4	0
132.75	13.26	1	1	1	0	2	0	0	0	0	0	1	133	9	9	0	0	1	4	0	x	0	0	0	x	x	4	0
133.17	13.27	1	0	1	0	2	0	0	0	6	1	x	102	10	2	0	0	x	x	0	x	0	0	x	x	x	2	0
133.65	13.55	1	0	2	0	2	2	x	0	14	3	0	182	2	x	0	0	1	x	0	x	0	0	x	x	x	6	0
134.17	13.58	5	0	2	0	1	0	0	0	15	3	1	177	4	3	0	0	1	x	0	1	x	1	0	0	x	6	0
134.67	13.60	1	0	2	0	2	0	0	0	6	3	1	188	11	5	0	0	1	2	0	x	x	0	0	0	x	1	0
135.13	13.63	2	0	3	0	5	x	0	0	4	4	0	166	0	0	0	0	1	4	0	1	1	0	0	x	1	2	0
135.68	13.66	x	0	1	x	2	0	1	0	5	4	2	194	7	2	0	0	3	2	0	1	0	0	0	1	x	2	0
136.17	13.69	1	0	3	0	1	x	x	0	5	2	x	216	7	3	0	0	2	5	0	x	x	0	x	2	x	8	0
136.63	13.72	2	2	2	x	4	x	0	0	6	0	2	218	8	x	0	0	x	2	0	1	2	0	0	x	3	2	0
137.18	13.75	2	0	2	0	2	0	2	0	5	1	1	158	7	x	0	0	1	x	0	1	1	0	x	2	x	2	0
137.67	13.78	5	0	0	0	3	0	0	0	5	x	1	205	4	0	0	0	1	x	0	0	x	0	0	x	x	4	0
138.13	13.81	x	0	2	0	x	0	0	0	2	x	0	140	4	x	0	0	3	x	0	x	1	0	0	0	1	4	0
138.69	13.84	5	0	3	0	4	0	x	0	4	2	3	143	6	2	0	0	x	3	0	0	1	0	0	x	2	x	0
139.17	13.87	2	0	2	0	1	1	0	0	1	1	1	115	5	x	0	0	2	1	0	1	0	0	x	1	1	9	0
139.63	13.89	3	x	1	0	2	x	1	0	2	x	3	160	3	1	0	0	2	x	0	x	3	0	0	x	1	2	0
140.17	13.92	1	1	0	0	x	0	x	0	6	x	3	146	1	4	0	0	3	2	0	1	2	0	0	0	x	11	0
140.67	13.95	0	0	x	0	1	0	0	0	5	3	3	155	4	2	0	0	3	2	0	x	0	0	0	x	1	7	0
141.1	13.98	1	0	x	0	1	0	0	0	11	1	1	176	4	1	0	0	1	1	0	x	0	0	0	x	x	3	0
141.54	14.00	1	0	0	0	1	x	x	0	2	x	x	167	1	5	0	0	3	4	0	x	x	x	0	x	x	1	0
142.01	14.03	3	x	1	0	x	1	0	0	6	5	0	172	3	2	0	0	4	2	0	1	2	x	0	3	3	2	0
142.51	14.06	2	0	x	0	x	x	x	0	10	2	0	192	9	5	0	0	2	x	0	x	0	0	x	1	1	5	0
143.05	14.09	4	0	1	0	1	x	1	0	1	2	0	184	7	3	0	0	1	2	0	x	1	1	0	x	3	0	0
143.51	14.12	1	0	3	0	x	1	1	0	17	1	0	165	9	6	0	0	1	3	0	0	1	0	x	x	2	3	0
144.01	14.15	3	0	x	0	1	0	x	0	0	3	0	223	9	4	0	0	x	4	0	x	x	0	x	2	x	1	0
144.55	14.18	3	x	3	0	6	x	x	0	3	1	0	145	9	3	0	0	2	x	0	0	x	0	0	2	x	1	0
145.01	14.20	1	1	2	0	x	x	1	0	0	5	0	201	5	5	0	0	1	x	0	x	0	0	0	x	3	x	0
145.51	14.23	2	2	1	0	3	0	0	0	1	1	x	161	5	3	0	0	1	1	0	x	x	0	0	x	x	1	0
146.04	14.26	2	0	2	0	2	x	0	0	2	1	1	165	6	1	0	0	2	3	0	x	1	0	x	1	x	1	0
146.51	14.29	1	3	6	0	5	0	x	0	2	4	1	135	3	x	0	0	x	2	0	x	1	0	0	1	x	1	0
147.01	14.32	1	2	2	0	1	0	x	0	9	2	1	177	6	10	0	0	x	2	0	x	0	0	x	x	1	1	0
147.54	14.35	1	0	x	0	x	0	0	0	2	x	x	240	3	3	0	0	x	3	0	x	x	0	0	0	2	1	0
148.05	14.38	6	0	5	0	1	0	0	0	5	2	x	245	4	1	0	0	2	2	0	x	x	0	1	1	x	1	0
148.51	14.41	3	0	x	0	x	0	0	0	1	4	2	182	2	2	0	0	1	x	0	x	0	0	0	2	x	1	0

Dinocyst sp. B	Dinocyst sp. C	Dinocyst sp. D	Dinocyst indet.	P-cyst indet.	Reworked dinocysts	Total in situ dinocysts	Acritarchs	*Cyclopsiella elliptica / granosa*	*Nannobarbophora gedlii*	*Nannobarbophora walldalei*	*Palambages*	*Paralecaniella indentata*	*Quadrina? condita*	Skolochorate acritarchs	Acritrach sp. A	Acritarch sp. B	Acritarch sp. C	Acritarch sp. D	Acritarch sp. E	Acritarch sp. F	Acritarch sp. G	Green algae	*Botryococcus*	*Cymatiosphaera baffinensis*	*Cymatiosphaera* spp. (pars)	*Leiosphaeridia rockhallensis*	Other prasinophyte algae	*Pediastrum*	*Pterospermella*	*Tasmanites*	Other marine acritarchs
0	2	0	4	0	11	363		1	5	0	x	2	0	36	x	0	0	0	0	0	0		0	0	3	0	0	0	0	x	
15	0	0	4	x	0	375		3	5	0	0	0	0	63	0	0	0	0	0	0	0		0	0	21	1	0	0	0	0	
2	4	0	6	1	2	381		11	23	x	0	0	0	94	0	2	0	0	0	0	0		0	1	8	5	0	0	0	0	
9	0	0	1	1	6	404		1	13	0	0	x	0	58	0	0	0	0	0	0	0		0	0	9	2	x	0	0	0	
0	6	0	5	1	1	354		5	33	0	0	1	0	120	0	0	1	x	0	0	0		0	0	4	5	0	0	0	0	
2	9	0	1	1	6	355		1	22	0	0	1	0	46	0	x	0	0	0	0	0		0	1	11	1	0	0	0	0	
5	1	0	10	0	7	325		1	21	0	0	0	0	73	0	x	2	1	0	0	0		0	3	8	x	1	0	0	x	
2	4	0	8	1	3	321		0	65	0	0	0	0	65	0	2	0	0	0	0	0		0	1	6	2	x	0	1	0	
6	4	0	6	1	3	351		4	41	0	0	0	0	111	x	1	3	2	0	0	0		0	1	7	3	x	0	0	1	
3	9	0	3	4	1	354		0	67	0	0	x	0	150	0	x	6	2	0	0	0		0	1	2	1	0	0	0	1	
x	6	0	3	0	2	401		0	43	0	0	0	0	162	0	0	3	1	0	0	0		0	0	2	2	x	0	0	0	
1	5	0	6	2	3	324		1	42	0	0	0	1	88	x	2	4	1	0	0	0		0	x	12	2	0	0	0	0	
5	7	0	8	0	2	357		0	35	0	0	0	0	76	0	2	0	0	0	0	0		0	x	8	5	x	0	0	0	
2	11	0	7	1	1	383		0	61	1	0	0	0	127	2	x	7	0	0	0	0		0	3	5	4	0	0	0	0	
4	4	0	6	0	6	350		0	34	0	0	0	0	51	2	0	1	0	0	0	0		0	x	11	4	0	0	0	1	
4	6	0	2	1	5	390		0	22	0	0	0	0	85	0	x	0	0	0	0	0		0	1	8	5	x	0	x	0	
4	5	0	9	0	2	412		0	19	0	0	0	x	83	0	1	1	1	0	0	0		1	2	7	22	0	0	0	0	
5	4	0	2	1	0	340		0	7	0	x	0	0	53	0	1	2	0	0	0	0		0	4	7	6	0	0	0	0	
7	6	0	7	0	0	380		0	9	0	0	0	0	39	0	0	1	0	0	0	0		0	2	8	4	x	0	0	0	
4	11	0	6	1	5	368		0	12	0	0	0	0	91	0	0	1	0	0	0	0		0	3	12	3	0	0	0	0	
10	10	0	2	1	2	354		0	18	0	0	0	1	76	x	1	0	x	0	0	0		0	2	8	3	0	x	0	0	
1	9	0	4	2	3	339		0	25	0	0	3	0	85	0	11	1	1	0	0	0		0	3	4	11	0	1	0	0	
9	1	0	8	0	3	445		0	51	0	0	0	0	82	2	0	2	0	0	0	0		0	0	2	4	x	0	0	1	
3	3	0	8	1	5	374		0	16	1	0	x	0	55	0	1	0	0	0	0	1		0	10	4	3	x	0	0	0	
6	5	0	4	2	5	343		0	9	0	0	0	1	60	0	1	1	0	0	0	0		0	2	7	4	x	0	0	x	
6	7	0	12	2	4	357		x	12	0	0	0	1	78	0	x	1	0	0	0	1		0	3	6	3	0	0	0	0	
5	3	4	5	0	5	430		22	13	0	0	0	0	171	2	1	1	0	0	0	0		0	1	8	0	0	0	0	0	
1	9	1	3	1	2	444		3	26	3	0	1	0	147	1	4	0	0	0	0	1		0	1	7	x	0	0	0	x	
1	9	2	11	2	2	437		15	15	0	x	0	0	87	2	8	0	0	0	0	0		0	2	6	1	0	0	0	0	
3	8	1	3	0	4	428		1	19	1	0	0	0	58	1	9	0	0	0	0	0		0	1	4	x	x	0	0	1	
1	7	2	0	0	7	470		21	27	1	0	0	0	80	7	12	0	x	x	0	0		0	1	4	0	0	0	0	0	
2	1	x	7	1	5	475		15	25	0	0	0	0	69	3	5	1	0	0	0	x		0	x	1	x	x	0	0	0	
1	3	3	7	0	9	445		374	14	1	0	0	0	77	3	6	0	0	0	0	0		0	1	3	3	0	0	0	x	
0	2	x	4	0	0	349		178	26	0	0	1	0	71	0	9	0	0	0	0	1		0	1	4	1	1	0	0	0	
2	3	2	1	1	6	427		138	12	0	0	0	x	48	2	11	0	0	0	0	0		0	2	5	0	0	0	0	0	
0	0	0	2	0	11	323		51	13	0	0	0	0	50	0	8	0	0	0	0	x		0	1	5	0	0	0	0	0	
0	2	0	2	0	5	335		33	19	0	0	0	0	58	0	10	0	0	x	0	0		0	1	2	0	1	0	0	0	
3	2	7	2	1	2	346		16	41	1	0	0	0	44	0	12	0	0	0	0	0		0	6	3	1	0	0	0	0	
1	1	x	6	1	2	326		10	27	0	0	0	0	63	1	8	0	x	0	0	0		0	1	x	5	0	0	0	0	
2	6	1	2	1	8	341		3	22	0	0	0	0	43	3	15	0	1	0	0	0		0	1	2	2	0	0	0	0	
3	1	9	5	1	12	349		15	34	0	0	0	0	56	6	11	1	0	0	0	0		0	0	2	5	0	0	0	0	
1	2	3	11	1	9	369		13	22	0	0	0	0	73	5	10	1	0	0	0	0		0	x	1	1	x	0	0	0	
3	1	2	5	2	4	359		74	23	0	0	0	0	80	3	2	0	0	0	0	0		0	4	x	0	1	0	0	x	
3	0	5	5	0	6	345		270	4	0	0	0	0	63	0	7	0	0	0	0	0		0	1	2	0	0	0	0	0	
0	2	1	5	0	3	377		63	15	0	x	0	0	32	1	0	0	0	0	0	0		0	x	4	0	0	0	0	0	
2	3	1	8	0	7	366		26	12	0	0	0	0	54	1	2	0	2	0	0	0		0	1	4	1	0	0	0	0	
0	0	8	1	x	9	376		93	13	0	0	0	0	48	1	5	0	0	0	0	0		1	3	3	0	x	0	0	0	
1	10	10	6	0	8	444		159	18	0	0	0	0	122	1	0	0	0	0	0	0		0	7	7	2	x	0	0	0	
2	0	x	7	0	4	371		33	11	0	0	0	0	35	3	1	1	0	0	0	0		1	3	2	0	1	0	0	0	
3	1	7	2	0	6	405		30	12	0	0	x	0	51	7	1	0	1	0	0	0		0	3	2	0	x	0	x	0	
x	1	19	2	3	7	369		25	15	0	0	0	0	62	13	0	0	0	0	0	0		1	4	3	0	2	0	0	0	
1	x	15	5	0	1	376		97	19	0	0	0	0	63	11	x	0	1	1	0	0		1	5	4	1	0	0	0	0	
0	2	9	4	3	7	329		604	9	0	0	0	0	53	10	0	0	0	0	3	0		0	x	6	0	0	0	0	1	
0	0	5	3	2	2	345		56	9	0	0	2	0	86	8	0	1	1	1	1	0		0	1	x	x	0	0	0	0	
0	0	4	5	0	8	401		9	21	0	0	0	0	36	2	x	0	0	0	0	0		0	x	1	0	0	0	0	1	
0	2	8	3	0	5	416		113	9	0	0	0	0	72	4	0	0	1	0	0	0		1	0	6	0	0	0	0	0	
0	0	3	5	2	1	329		6	27	0	0	0	0	61	x	0	0	x	0	4	0		0	2	1	1	0	0	0	0	

Composite depth (mcd)	Age (Ma)	Crustacean egg	Foraminiferal lining > 4 chambers	Pyritised diatoms	Terrestrial palynomorphs	Bisaccate pollen	Angiosperm pollen	Spores	Reworked spores	Reworked pollen	Fungal threads	Fungal spores	Palynomorph indet.
126.42	13.09	0	4	0		2	0	5	0	0	x	0	1
126.61	13.09	0	4	0		4	1	1	1	0	22	0	5
126.95	13.10	0	2	0		7	3	0	0	0	0	1	0
127.11	13.11	0	5	0		7	4	1	0	0	x	0	2
127.42	13.11	1	1	0		5	2	1	0	0	0	0	2
127.61	13.12	0	5	0		5	3	0	0	0	x	0	6
127.92	13.13	0	11	0		5	3	0	0	0	6	0	0
128.11	13.13	0	14	0		5	1	1	0	0	0	0	6
128.45	13.14	0	18	0		9	5	0	0	0	2	0	3
128.61	13.15	0	14	0		6	2	0	0	0	0	0	3
128.92	13.15	0	12	0		7	0	0	0	0	10	1	2
129.11	13.16	0	10	0		5	3	0	0	0	4	0	2
129.42	13.17	0	14	0		4	4	0	0	0	4	1	2
129.61	13.17	0	26	0		9	3	0	0	0	1	0	6
129.95	13.18	0	16	0		6	5	0	0	0	3	0	1
130.11	13.19	0	9	0		8	6	3	0	0	0	0	2
130.42	13.19	0	25	0		2	2	2	x	0	0	1	2
130.61	13.20	0	11	0		5	4	1	0	0	1	0	4
130.98	13.21	1	31	0		9	2	0	0	0	1	0	1
131.1	13.21	x	40	0		9	1	0	0	0	2	1	2
131.45	13.22	0	14	0		5	7	1	0	0	2	x	1
131.75	13.23	0	22	0		6	0	1	0	0	11	0	3
131.81	13.23	0	11	0		3	1	1	0	0	8	0	1
132.21	13.24	0	13	0		6	1	1	0	0	1	0	4
132.75	13.26	0	16	0		7	3	1	0	0	5	0	5
133.17	13.27	0	14	0		5	3	2	0	0	3	3	0
133.65	13.55	0	6	0		10	4	0	0	0	0	0	2
134.17	13.58	x	8	0		9	7	0	0	0	1	0	4
134.67	13.60	0	9	0		8	3	3	0	0	12	0	3
135.13	13.63	0	3	0		16	6	2	0	0	0	0	4
135.68	13.66	0	1	0		10	2	0	0	0	0	0	3
136.17	13.69	0	9	0		5	2	1	0	0	1	0	6
136.63	13.72	0	4	0		8	0	0	0	0	2	0	9
137.18	13.75	0	7	0		9	2	2	0	0	0	0	0
137.67	13.78	0	13	0		8	0	3	0	0	0	0	1
138.13	13.81	0	11	0		10	0	0	0	0	1	0	2
138.69	13.84	0	20	0		11	0	1	0	0	4	3	3
139.17	13.87	x	10	0		9	5	2	0	0	5	0	5
139.63	13.89	0	15	0		7	0	1	0	0	0	0	3
140.17	13.92	0	10	0		11	1	1	0	0	5	0	2
140.67	13.95	0	10	0		6	2	2	0	0	1	0	1
141.1	13.98	0	8	0		19	11	0	0	0	12	1	4
141.54	14.00	0	4	0		38	2	1	1	0	1	0	8
142.01	14.03	0	9	0		16	2	0	0	0	x	0	13
142.51	14.06	0	11	0		12	4	1	0	0	0	0	7
143.05	14.09	0	11	0		34	9	3	0	0	3	1	22
143.51	14.12	x	8	x		6	10	2	0	0	2	0	6
144.01	14.15	0	14	0		28	7	5	1	0	1	1	25
144.55	14.18	0	12	0		29	5	4	0	0	0	0	1
145.01	14.20	0	17	1		5	2	1	0	0	0	0	4
145.51	14.23	0	13	0		17	2	6	1	0	2	0	6
146.04	14.26	0	17	0		15	8	0	0	0	1	0	21
146.51	14.29	0	13	0		26	10	5	0	0	0	0	10
147.01	14.32	0	6	0		10	7	3	1	0	1	0	13
147.54	14.35	0	9	0		18	2	0	0	0	0	1	12
148.05	14.38	0	23	0		20	3	4	x	0	0	0	14
148.51	14.41	0	4	0		22	2	3	0	0	0	0	15

Supplementary Table 2.2: distribution of calcareous nannofossils in Holes 1318B and 1318C.

Leg	Site	Hole	Core	Type	Section	Top sample interval (cm)	Bottom sample interval (cm)	Core depth (mbsf)	Composite depth (mcd)	Fields of view	*Calcidiscus premacintyrei*	*Calcidiscus sp. (< 10mm)*	*Cyclicargolithus floridanus*	*Coccolithus miopelagicus*	*Coccolithus pelagicus*	*Discoaster adamanteus*	*Discoaster exilis*	*Discoaster variabilis*	*Helicosphaera granulata*	*Helicosphaera kamptneri/carteri*	*Helicosphaera walberdorfensis*	*Helicosphaera waltrans*	*Pontosphaera sp.*	*Rabdospaera sicca*	*Reticulofenestra pseudoumbilicus (<7mm)*	*Reticulofenestra sp. (≤5mm)*	*Sphenolithus dissimilis*	*Sphenolithus heteromorphus*
307	1318	B	14	H	7	2	5	127.29	131.81	100	R		R		A					F	C		R		C	A	F	F
307	1318	C	8	X	1	60	62	126.3	132.21	100				R	A					C	C		R		C	A	F	R
307	1318	C	8	X	2	14	16	127.26	133.17	100	F			R	C	R				C	C				A	A	F	R
307	1318	C	8	X	2	62	64	127.74	133.65	100	R		R		C					F	F		R		A	A		R
307	1318	C	8	X	2	114	117	128.26	134.17	100				R	C		R			R	F			R	R	C		R
307	1318	C	8	X	3	60	62	129.22	135.13	100	R			R	A			R			C			F	F	A		
307	1318	C	8	X	4	14	16	130.26	136.17	100				R	A					F	F			F	F	A		R
307	1318	C	8	X	4	115	117	131.27	137.18	100	F	R	R	R	A	R	R			C	C		R	R	C	A	R	R
307	1318	C	8	X	5	60	62	132.22	138.13	100	R		R	F	A					C	C			R	F	A	F	F
307	1318	C	8	X	5	116	118	132.78	138.69	100		R		F	A					F	C		R	R	F	A	C	F
307	1318	C	8	X	6	114	16	133.26	139.17	100	R		C	R	A					F	C		R	R	R	A	R	F
307	1318	C	8	X	6	60	62	133.72	139.63	100	F		F	R	A					F	C			R	C	A		F
307	1318	C	8	X	7	14	16	134.76	140.67	100	R		C	F	A					C	F				C	A	R	F
307	1318	C	9	X	1	33	35	135.63	141.54	100			F	R	A		R	F		C	F			R	F		R	C
307	1318	C	9	X	1	130	132	136.6	142.51	100	R		C	R	A	R	R	F		C	F		F		F	A	C	C
307	1318	C	9	X	2	34	36	137.14	143.05	100		R	F	F	A			F		C	F				C	A	R	C
307	1318	C	9	X	3	34	36	138.64	144.55	100	R	F	F	F	A			F		C	F				R	A		R
307	1318	C	9	X	4	130	132	141.1	147.01	100			R	R	A		R			C	C	F	R	R	R	A		R
307	1318	C	9	X	6	33	35	143.13	149.04	100			C	R	C			C	R	F	F	C		R	R	A	R	R
307	1318	C	9	X	8	21	23	145.03	150.95	100			F	F	A			F		C	R	F			F	A		R
307	1318	C	10	X	2	83	85	147.23	153.18	100			C	R	C			C		A	F				R	A	R	F
307	1318	B	17	X	1	67	69	148.37	154.52	100			C		A			F		C	F			F	F	A		F
307	1318	C	10	X	3	130	132	149.2	155.15	100			C	R	A			C		C	R	F			C	A	C	F
307	1318	C	10	X	5	31	33	151.21	157.16	100			A	R	A			C		A	R	C		C	C	A	R	F
307	1318	C	10	X	6	130	132	153.7	159.65	100			C	R	A	R		C		C		C		F	A	A	R	F

Supplementary Table 3.1: Distribution of the six newly described acritarch species in Holes 1318B and 1318C.

Leg	Site	Hole	Core	Type	Section	Top sample interval (cm)	Bottom sample interval (cm)	Core depth(mbsf)	Composite depth (mcd)	Age (Ma; ATNTS 2012)	Batch number *Lycopodium* tables	Number of spores per tablet	Number of tablets		*Cometesphaera bullatio*	*Cymatiosphaera? deverteuilli*	*Platycystidia manumii*	*Porcupinea collaris*	*Porcupinea indentata*	*Pusillisphaera solaris*
307	1318	B	10	H	5	50	52	87.50	92.44	12.11	1031	20848	2		0	3	0	0	0	2
307	1318	B	10	H	5	109	111	88.09	93.03	12.13	1031	20848	2		0	2	0	0	0	1
307	1318	B	10	H	6	2	4	88.52	93.46	12.15	1031	20848	2		0	5	0	0	0	x
307	1318	B	10	H	6	50	52	89.00	93.94	12.17	1031	20848	2		0	1	0	0	0	0
307	1318	B	10	H	6	106	108	89.56	94.5	12.18	1031	20848	2		0	x	0	0	0	0
307	1318	B	10	H	7	17	19	90.03	94.97	12.19	1031	20848	2		0	1	0	0	0	0
307	1318	B	11	H	1	47	49	90.97	95.4	12.20	1031	20848	2		0	3	0	0	0	0
307	1318	B	11	H	1	97	99	91.47	95.9	12.22	1031	20848	2		0	x	0	0	0	0
307	1318	B	11	H	2	5	7	92.05	96.48	12.23	1031	20848	2		0	1	0	0	0	0
307	1318	B	11	H	2	55	57	92.55	96.98	12.24	1031	20848	2		0	4	0	0	0	0
307	1318	B	11	H	2	105	107	93.05	97.48	12.25	1031	20848	2		0	2	0	0	0	0
307	1318	B	11	H	3	1	3	93.51	97.94	12.26	1031	20848	2		0	1	0	0	0	0
307	1318	B	11	H	3	51	53	94.01	98.44	12.27	1031	20848	2		0	10	0	0	0	0
307	1318	B	11	H	3	105	107	94.55	98.98	12.30	1031	20848	2		0	8	0	0	1	x
307	1318	B	11	H	4	3	4	95.03	99.46	12.33	177745	18584	2		0	2	0	0	0	0
307	1318	B	11	H	4	52	54	95.52	99.95	12.35	177745	18584	2		0	0	0	0	0	0
307	1318	B	11	H	4	103	105	96.03	100.46	12.38	177745	18584	2		0	0	0	0	0	0
307	1318	B	11	H	5	2	4	96.52	100.95	12.41	177745	18584	2		0	0	0	0	0	0
307	1318	B	11	H	5	52	54	97.02	101.45	12.43	177745	18584	2		0	0	0	0	6	0
307	1318	B	11	H	6	2	4	97.52	101.95	12.46	177745	18584	2		0	0	0	0	0	1
307	1318	B	11	H	6	52	54	98.02	102.45	12.49	177745	18584	2		0	0	0	0	0	1
307	1318	B	12	H	1	30	32	100.30	104.61	12.73	177745	18584	2		0	0	0	0	0	x
307	1318	B	12	H	1	80	82	100.80	105.11	12.73	177745	18584	2		0	0	0	0	x	0
307	1318	B	12	H	1	133	135	101.33	105.64	12.74	177745	18584	2		0	0	0	0	4	4
307	1318	B	12	H	2	30	32	101.80	106.11	12.74	177745	18584	2		0	0	0	0	1	0
307	1318	B	12	H	2	80	82	102.30	106.61	12.75	177745	18584	2		0	0	0	0	3	1
307	1318	B	12	H	2	133	135	102.83	107.14	12.75	177745	18584	2		0	0	0	0	1	x
307	1318	B	12	H	3	30	32	103.30	107.61	12.76	177745	18584	1		0	0	0	0	7	0
307	1318	B	12	H	3	80	82	103.80	108.11	12.76	177745	18584	2		0	0	0	0	2	4
307	1318	B	12	H	3	133	135	104.33	108.64	12.76	177745	18584	1		0	0	0	0	x	0
307	1318	B	12	H	4	30	32	104.80	109.11	12.77	177745	18584	1		0	0	0	0	5	2
307	1318	B	12	H	4	80	82	105.30	109.61	12.77	177745	18584	2		0	0	0	0	2	5
307	1318	B	12	H	4	133	135	105.83	110.14	12.78	177745	18584	1		0	0	0	0	3	1
307	1318	B	12	H	5	30	32	106.30	110.61	12.78	177745	18584	2		0	0	0	0	2	7
307	1318	B	12	H	5	80	82	106.80	111.11	12.78	177745	18584	2		0	0	0	0	1	4
307	1318	B	12	H	5	133	135	107.33	111.64	12.79	177745	18584	2		0	0	0	0	7	3
307	1318	B	12	H	6	30	32	107.80	112.11	12.79	177745	18584	2		0	0	0	0	14	4
307	1318	B	12	H	6	80	82	108.30	112.61	12.80	177745	18584	2		0	0	0	0	4	4
307	1318	B	13	H	1	30	32	109.80	114.66	12.81	177745	18584	2		0	0	0	0	4	6
307	1318	B	13	H	1	90	92	110.40	115.26	12.82	177745	18584	2		0	0	0	0	6	5
307	1318	B	13	H	1	140	142	110.90	115.76	12.82	177745	18584	2		0	0	0	0	4	6
307	1318	B	13	H	2	43	45	111.43	116.29	12.83	177745	18584	2		0	0	0	0	1	2
307	1318	B	13	H	2	90	92	111.90	116.76	12.83	177745	18584	2		0	0	0	0	1	2
307	1318	B	13	H	2	140	142	112.40	117.26	12.84	177745	18584	2		0	0	0	0	4	7
307	1318	B	13	H	3	43	45	112.93	117.79	12.84	177745	18584	2		0	0	0	0	2	3
307	1318	B	13	H	3	90	92	113.40	118.26	12.85	177745	18584	2		0	0	0	0	3	2
307	1318	B	13	H	3	140	142	113.90	118.76	12.85	177745	18584	2		0	0	0	0	1	0
307	1318	B	13	H	4	43	45	114.43	119.29	12.85	177745	18584	2		0	0	0	0	4	1
307	1318	B	13	H	4	90	92	114.90	119.76	12.86	177745	18584	2		0	0	0	0	12	2
307	1318	B	13	H	4	140	142	115.40	120.26	12.86	177745	18584	2		0	0	0	0	1	4
307	1318	B	13	H	5	43	45	115.93	120.79	12.87	177745	18584	2		0	0	0	0	x	3
307	1318	B	13	H	5	90	92	116.40	121.26	12.87	177745	18584	2		0	0	0	0	10	20
307	1318	B	13	H	5	140	142	116.90	121.76	12.88	177745	18584	2		0	0	0	0	16	13
307	1318	B	13	H	6	33	35	117.33	122.19	12.88	177745	18584	2		0	0	0	0	3	5
307	1318	B	13	H	7	18	20	117.65	122.51	12.88	177745	18584	2		0	0	0	0	2	9
307	1318	C	7	H	1	20	22	117.70	123.61	12.96	177745	18584	1		0	0	0	0	7	4
307	1318	B	14	H	1	43	45	119.43	123.95	13.00	177745	18584	2		0	0	0	0	4	4
307	1318	C	7	H	1	70	72	118.20	124.11	13.01	177745	18584	1		0	0	0	0	2	2
307	1318	B	14	H	1	90	92	119.90	124.42	13.03	177745	18584	2		0	0	0	0	0	9
307	1318	C	7	H	1	120	122	118.70	124.61	13.04	177745	18584	1		0	0	0	0	3	1
307	1318	B	14	H	1	140	142	120.40	124.92	13.05	177745	18584	2		0	0	0	0	0	1
307	1318	C	7	H	2	20	22	119.20	125.11	13.05	177745	18584	1		0	0	0	0	2	4
307	1318	B	14	H	2	43	45	120.93	125.45	13.06	177745	18584	2		0	0	0	0	0	11
307	1318	C	7	H	2	70	72	119.70	125.61	13.07	177745	18584	1		0	0	0	0	2	4
307	1318	B	14	H	2	90	92	121.40	125.92	13.07	177745	18584	2		0	0	0	0	0	6

Leg	Site	Hole	Core	Type	Section	Top sample interval (cm)	Bottom sample interval (cm)	Core depth(mbsf)	Composite depth (mcd)	Age (Ma; ATNTS 2012)	Batch number *Lycopodium* tables	Number of spores per tablet	Number of tablets		*Cometesphaera bullatio*	*Cymatiosphaera? deverteuilii*	*Platycystidia manumii*	*Porcupinea collaris*	*Porcupinea indentata*	*Pusillisphaera solaris*
307	1318	C	7	H	2	120	122	120.20	126.11	13.08	177745	18584	2		0	0	0	0	7	0
307	1318	B	14	H	2	140	142	121.90	126.42	13.09	177745	18584	2		0	0	0	0	0	2
307	1318	C	7	H	3	20	22	120.70	126.61	13.09	177745	18584	2		0	0	0	0	15	0
307	1318	B	14	H	3	43	45	122.43	126.95	13.10	1031	20848	2		0	0	0	0	2	4
307	1318	C	7	H	3	70	72	121.20	127.11	13.11	177745	18584	2		0	0	0	0	9	0
307	1318	B	14	H	3	90	92	122.90	127.42	13.11	1031	20848	2		0	0	0	0	0	6
307	1318	C	7	H	3	120	122	121.70	127.61	13.12	177745	18584	2		0	0	0	0	2	9
307	1318	B	14	H	3	140	142	123.40	127.92	13.13	177745	18584	2		0	0	0	0	5	1
307	1318	C	7	H	4	20	22	122.20	128.11	13.13	177745	18584	1		0	0	0	0	2	4
307	1318	B	14	H	4	43	45	123.93	128.45	13.14	1031	20848	2		0	0	0	0	6	4
307	1318	C	7	H	4	70	72	122.70	128.61	13.15	177745	18584	1		0	0	0	0	3	9
307	1318	B	14	H	4	90	92	124.40	128.92	13.15	1031	20848	2		0	0	0	0	x	6
307	1318	C	7	H	4	120	122	123.20	129.11	13.16	177745	18584	1		0	0	0	0	1	5
307	1318	B	14	H	4	140	142	124.90	129.42	13.17	177745	18584	2		0	0	0	0	5	7
307	1318	C	7	H	5	20	22	123.70	129.61	13.17	1031	20848	2		0	0	0	0	2	11
307	1318	B	14	H	5	43	45	125.43	129.95	13.18	177745	18584	2		0	0	0	0	4	4
307	1318	C	7	H	5	70	72	124.20	130.11	13.19	1031	20848	2		0	0	0	0	4	6
307	1318	B	14	H	5	90	92	125.90	130.42	13.19	1031	20848	2		0	0	0	0	4	5
307	1318	C	7	H	5	120	122	124.70	130.61	13.20	1031	20848	2		0	0	0	0	5	4
307	1318	B	14	H	6	13	15	126.46	130.98	13.21	1031	20848	2		0	0	0	0	7	6
307	1318	C	7	H	6	19	21	125.19	131.1	13.21	1031	20848	2		0	0	0	0	4	11
307	1318	B	14	H	6	60	62	126.93	131.45	13.22	1031	20848	2		0	0	0	0	10	10
307	1318	C	8	X	1	14	16	125.84	131.75	13.23	1031	20848	2		0	0	0	0	1	9
307	1318	B	14	H	7	2	5	127.29	131.81	13.23	1031	20848	2		0	0	0	0	9	1
307	1318	C	8	X	1	60	62	126.30	132.21	13.24	1031	20848	2		0	0	0	0	3	3
307	1318	C	8	X	1	114	116	126.84	132.75	13.26	1031	20848	2		0	0	0	0	6	5
307	1318	C	8	X	2	14	16	127.26	133.17	13.27	1031	20848	2		0	0	0	0	6	7
307	1318	C	8	X	2	62	64	127.74	133.65	13.55	1031	20848	2		3	0	0	x	5	3
307	1318	C	8	X	2	114	116	128.26	134.17	13.58	1031	20848	2		1	0	0	x	1	9
307	1318	C	8	X	3	14	16	128.76	134.67	13.60	1031	20848	2		2	0	0	x	1	9
307	1318	C	8	X	3	60	62	129.22	135.13	13.63	1031	20848	2		1	0	0	1	3	8
307	1318	C	8	X	3	115	117	129.77	135.68	13.66	1031	20848	2		4	0	0	x	1	7
307	1318	C	8	X	4	14	16	130.26	136.17	13.69	1031	20848	2		x	0	0	0	2	1
307	1318	C	8	X	4	60	62	130.72	136.63	13.72	1031	20848	2		x	0	0	0	1	3
307	1318	C	8	X	4	115	117	131.27	137.18	13.75	1031	20848	2		x	0	0	1	0	2
307	1318	C	8	X	5	14	16	131.76	137.67	13.78	1031	20848	2		1	0	0	1	2	3
307	1318	C	8	X	5	60	62	132.22	138.13	13.81	1031	20848	2		x	0	0	0	0	0
307	1318	C	8	X	5	116	118	132.78	138.69	13.84	1031	20848	2		x	0	0	0	0	2
307	1318	C	8	X	6	14	16	133.26	139.17	13.87	1031	20848	2		7	0	0	x	3	2
307	1318	C	8	X	6	60	62	133.72	139.63	13.89	1031	20848	2		1	0	0	x	1	1
307	1318	C	8	X	6	114	116	134.26	140.17	13.92	1031	20848	2		3	0	0	x	2	6
307	1318	C	8	X	7	14	16	134.76	140.67	13.95	1031	20848	2		3	0	0	x	3	1
307	1318	C	8	X	8	13	15	135.19	141.1	13.98	1031	20848	2		4	0	0	x	1	2
307	1318	C	9	X	1	33	35	135.63	141.54	14.00	1031	20848	2		1	0	0	0	3	1
307	1318	C	9	X	1	80	82	136.10	142.01	14.03	1031	20848	2		1	0	0	x	3	0
307	1318	C	9	X	1	130	132	136.60	142.51	14.06	177745	18584	2		1	0	0	x	0	2
307	1318	C	9	X	2	34	36	137.14	143.05	14.09	1031	20848	2		1	0	0	x	2	3
307	1318	C	9	X	2	80	82	137.60	143.51	14.12	177745	18584	2		4	0	0	9	0	0
307	1318	C	9	X	2	130	132	138.10	144.01	14.15	1031	20848	2		9	0	0	3	1	10
307	1318	C	9	X	3	34	36	138.64	144.55	14.18	177745	18584	2		1	0	0	x	2	0
307	1318	C	9	X	3	80	82	139.10	145.01	14.20	1031	20848	2		13	0	0	4	3	1
307	1318	C	9	X	3	130	132	139.60	145.51	14.23	1031	20848	2		14	0	1	2	x	1
307	1318	C	9	X	4	33	35	140.13	146.04	14.26	1031	20848	2		10	0	5	3	1	x
307	1318	C	9	X	4	80	82	140.60	146.51	14.29	1031	20848	2		8	0	6	4	0	2
307	1318	C	9	X	4	130	132	141.10	147.01	14.32	177745	18584	2		9	0	1	3	0	0
307	1318	C	9	X	5	33	35	141.63	147.54	14.35	1031	20848	2		3	0	0	x	0	0
307	1318	C	9	X	5	84	86	142.14	148.05	14.38	177745	18584	2		2	0	0	4	0	2
307	1318	C	9	X	5	130	132	142.60	148.51	14.41	1031	20848	2		1	0	4	2	0	0
307	1318	C	9	X	6	33	35	143.13	149.04	14.44	1031	20848	2		8	0	9	3	0	5
307	1318	C	9	X	6	80	82	143.60	149.51	14.47	177745	18584	2		10	0	1	3	0	4
307	1318	C	9	X	6	130	132	144.10	150.01	14.49	1031	20848	2		6	0	2	1	1	8
307	1318	C	9	X	7	32	34	144.62	150.53	14.52	1031	20848	2		3	0	0	x	1	0
307	1318	C	9	X	8	21	23	145.03	150.94	14.55	177745	18584	2		6	0	0	3	0	2
307	1318	C	10	X	1	31	33	145.21	151.16	14.56	1031	20848	2		2	0	1	1	0	2
307	1318	C	10	X	1	80	82	145.70	151.65	14.59	177745	18584	2		1	0	x	x	0	3
307	1318	C	10	X	1	130	132	146.20	152.15	14.62	1031	20848	2		5	0	2	1	0	13
307	1318	C	10	X	2	31	33	146.71	152.66	14.65	1031	20848	2		4	0	1	x	0	8
307	1318	C	10	X	2	83	85	147.23	153.18	14.68	1031	20848	2		13	0	2	x	0	2
307	1318	C	10	X	2	130	132	147.70	153.65	14.71	1031	20848	2		4	0	1	x	0	7
307	1318	B	17	X	1	20	22	147.90	154.05	14.73	1031	20848	2		1	0	x	x	0	1

Leg	Site	Hole	Core	Type	Section	Top sample interval (cm)	Bottom sample interval (cm)	Core depth(mbsf)	Composite depth (mcd)	Age (Ma; ATNTS 2012)	Batch number *Lycopodium* tables	Number of spores per tablet	Number of tablets		*Cometesphaera bullatio*	*Cymatiosphaera? deverteuilii*	*Platycystidia manumii*	*Porcupinea collaris*	*Porcupinea indentata*	*Pusillisphaera solaris*
307	1318	C	10	X	3	33	35	148.23	154.18	14.74	1031	20848	2		10	0	1	0	0	18
307	1318	B	17	X	1	67	69	148.37	154.52	14.76	1031	20848	2		1	0	0	x	0	4
307	1318	C	10	X	3	80	82	148.70	154.65	14.76	1031	20848	2		9	0	12	0	0	12
307	1318	B	17	X	1	120	122	148.90	155.05	14.78	1031	20848	2		4	0	8	0	0	2
307	1318	C	10	X	3	130	132	149.20	155.15	14.78	1031	20848	2		6	0	9	0	0	11
307	1318	B	17	X	2	20	22	149.40	155.55	14.79	1031	20848	2		3	0	1	0	0	2
307	1318	C	10	X	4	33	35	149.73	155.68	14.79	1031	20848	2		13	0	1	0	0	3
307	1318	B	17	X	2	65	67	149.85	156	14.80	1031	20848	2		12	0	x	0	1	2
307	1318	C	10	X	4	80	82	150.20	156.15	14.80	1031	20848	2		16	0	5	0	x	0
307	1318	B	17	X	2	120	122	150.40	156.55	14.81	1031	20848	2		7	0	1	0	0	2
307	1318	C	10	X	4	130	132	150.70	156.65	14.81	1031	20848	2		10	0	2	0	0	7
307	1318	B	17	X	3	18	20	150.88	157.03	14.81	1031	20848	2		12	0	0	0	1	2
307	1318	C	10	X	5	31	33	151.21	157.16	14.82	1031	20848	2		20	0	2	0	0	2
307	1318	B	17	X	3	67	69	151.37	157.52	14.82	1031	20848	2		13	0	1	0	0	3
307	1318	C	10	X	5	80	82	151.70	157.65	14.83	1031	20848	2		10	0	0	0	0	4
307	1318	B	17	X	3	120	122	151.90	158.05	14.83	1031	20848	2		12	0	1	0	0	4
307	1318	C	10	X	5	134	136	152.24	158.19	14.83	1031	20848	2		12	0	0	0	0	3
307	1318	B	17	X	4	8	10	152.28	158.43	14.84	1031	20848	2		9	0	4	0	0	1
307	1318	C	10	X	6	30	32	152.70	158.65	14.84	1031	20848	2		11	0	0	0	0	2
307	1318	C	10	X	6	80	82	153.20	159.15	14.85	1031	20848	1		1	0	0	0	0	3
307	1318	C	10	X	6	130	132	153.70	159.65	14.86	1031	20848	2		10	0	1	0	0	3
307	1318	B	17	X	5	13	15	153.83	159.98	14.87	1031	20848	2		18	0	2	0	1	11
307	1318	C	10	X	7	33	35	154.23	160.18	14.87	1031	20848	2		5	0	0	0	0	6
307	1318	B	17	X	5	63	65	154.33	160.48	14.88	1031	20848	2		19	0	1	0	0	8
307	1318	B	17	X	5	113	115	154.83	160.98	14.89	1031	20848	2		5	0	3	0	0	1
307	1318	B	17	X	6	13	15	155.33	161.48	14.91	1031	20848	2		5	0	0	0	0	0
307	1318	B	17	X	6	60	62	155.80	161.95	14.92	1031	20848	2		6	0	0	0	0	2
307	1318	B	17	X	6	113	115	156.33	162.48	14.93	1031	20848	2		3	0	0	0	0	2
307	1318	B	17	X	7	15	17	156.85	163	14.95	1031	20848	2		5	0	0	0	1	1
307	1318	B	17	X	8	13	15	157.31	163.46	14.96	1031	20848	2		9	0	0	0	0	1
307	1318	B	18	X	1	20	22	157.50	163.65	14.96	1031	20848	2		15	0	2	0	1	7
307	1318	B	18	X	1	120	122	158.50	164.65	14.99	1031	20848	2		4	0	0	0	0	2
307	1318	B	18	X	2	66	68	159.46	165.61	15.02	1031	20848	2		3	0	1	0	0	5
307	1318	B	18	X	3	18	20	160.48	166.63	15.04	1031	20848	2		7	0	1	0	0	5
307	1318	B	18	X	4	13	15	162.43	168.58	15.06	1031	20848	2		13	0	0	0	0	6
307	1318	B	18	X	4	112	114	163.42	169.57	15.07	1031	20848	2		17	0	2	0	1	9
307	1318	B	18	X	5	60	62	164.40	170.55	15.08	1031	20848	2		6	0	0	0	0	4
307	1318	B	18	X	6	13	15	165.43	171.58	15.09	1031	20848	2		2	0	x	0	x	2
307	1318	B	18	X	6	112	114	166.42	172.57	15.10	1031	20848	2		9	0	0	0	0	2
307	1318	B	19	X	1	30	32	167.20	173.35	15.11	1031	20848	1		7	0	0	0	0	3
307	1318	B	19	X	1	133	135	168.23	174.38	15.12	1031	20848	2		2	0	0	0	0	x
307	1318	B	19	X	2	80	82	169.20	175.35	15.13	1031	20848	2		4	0	x	0	0	8
307	1318	B	19	X	3	30	32	170.20	176.35	15.14	1031	20848	2		1	0	x	0	0	4
307	1318	B	19	X	4	30	32	171.20	177.35	15.15	1031	20848	2		7	0	1	0	0	10
307	1318	B	19	X	5	36	38	172.26	178.41	15.17	1031	20848	2		6	0	0	0	2	7
307	1318	B	19	X	5	135	137	173.25	179.4	15.31	1031	20848	2		1	0	0	0	1	5
307	1318	B	19	X	6	79	81	174.19	180.34	15.44	1031	20848	2		3	0	0	0	0	1
307	1318	B	19	X	7	30	32	175.20	181.35	15.58	1031	20848	2		11	0	0	0	1	5
307	1318	B	19	X	8	30	32	176.20	182.35	15.72	1031	20848	2		1	0	0	0	1	9
307	1318	B	20	X	1	43	45	176.93	183.08	15.82	1031	20848	2		5	0	92	0	0	5
307	1318	B	20	X	1	143	145	177.93	184.08	15.96	1031	20848	2		8	0	3	0	0	2
307	1318	B	20	X	2	88	90	178.88	185.03	16.02	1031	20848	2		4	0	60	0	2	6
307	1318	B	20	X	3	41	43	179.91	186.06	16.07	1031	20848	2		4	0	2	0	1	4
307	1318	B	20	X	4	46	48	180.96	187.11	16.12	1031	20848	2		11	0	10	0	0	7
307	1318	B	20	X	5	39	41	181.89	188.04	16.16	1031	20848	2		7	0	2	0	0	2
307	1318	B	20	X	5	141	142	182.91	189.06	16.21	1031	20848	2		0	0	1	0	0	2
307	1318	B	20	X	6	90	92	183.90	190.05	16.26	1031	20848	2		5	0	6	0	0	3
307	1318	B	20	X	7	44	46	184.94	191.09	16.27	1031	20848	2		5	0	8	0	0	1
307	1318	B	20	X	7	140	142	185.90	192.05	16.28	1031	20848	2		3	0	4	0	0	1

On the following pages 158 – 163:

Supplementary Table 4.1: Summary of stable carbon and oxygen isotope measurements for Site U1318.

Leg	Site	Hole	Core	Type	Section	Top sample interval (cm)	Bottom sample interval (cm)	Core depth (mbsf)	Composite depth (mcd)	Age (Ma; ATNTS 2012)	*Cibicidoides pachyderma*			
											$\delta^{13}C$	1 sd $\delta^{13}C$	$\delta^{18}O$	1 sd $\delta^{18}O$
307	1318	B	10	H	5	50	52	87.5	92.44	12.75	1.018	0.030	1.280	0.078
307	1318	B	10	H	5	109	111	88.09	93.03	12.76				
307	1318	B	10	H	6	50	52	89	93.94	12.77	1.414	0.034	1.243	0.082
307	1318	B	10	H	6	50	52	89	93.94	12.77				
307	1318	B	10	H	6	106	108	89.56	94.5	12.78	1.234	0.034	1.204	0.080
307	1318	B	10	H	7	17	19	90.03	94.97	12.78	1.275	0.030	1.337	0.080
307	1318	B	11	H	1	97	99	91.47	95.9	12.79	1.303	0.030	1.095	0.081
307	1318	B	11	H	2	5	7	92.05	96.48	12.80	0.648	0.033	1.428	0.078
307	1318	B	11	H	2	55	57	92.55	96.98	12.81	1.419	0.033	1.120	0.082
307	1318	B	11	H	3	1	3	93.51	97.94	12.82	1.058	0.032	1.006	0.079
307	1318	B	11	H	3	1	3	93.51	97.94	12.82				
307	1318	B	11	H	3	105	107	94.55	98.98	12.84	0.971	0.033	1.033	0.080
307	1318	B	11	H	4	52	54	95.52	99.95	12.85	0.846	0.032	1.127	0.079
307	1318	B	11	H	5	2	4	96.52	100.95	12.87	1.143	0.040	0.913	0.081
307	1318	B	11	H	5	2	4	96.52	100.95	12.87	1.046	0.034	0.974	0.082
307	1318	B	11	H	6	2	4	97.52	101.95	12.88	1.328	0.032	1.249	0.082
307	1318	B	11	H	6	52	54	98.02	102.45	12.89	1.319	0.031	1.097	0.081
307	1318	B	12	H	1	30	32	100.3	104.61	13.01	1.199	0.028	0.865	0.077
307	1318	B	12	H	2	30	32	101.8	106.11	13.06	1.183	0.031	0.901	0.081
307	1318	B	12	H	2	80	82	102.3	106.61	13.08				
307	1318	B	12	H	3	30	32	103.3	107.61	13.12	1.307	0.027	0.608	0.081
307	1318	B	12	H	3	133	135	104.33	108.64	13.16	1.309	0.031	0.822	0.078
307	1318	B	12	H	4	30	32	104.8	109.11	13.17	1.168	0.032	1.250	0.077
307	1318	B	12	H	4	133	135	105.83	110.14	13.20	0.900	0.030	1.084	0.082
307	1318	B	12	H	5	133	135	107.33	111.64	13.24	0.863	0.030	1.002	0.079
307	1318	B	12	H	5	133	135	107.33	111.64	13.24				
307	1318	B	12	H	6	30	32	107.8	112.11	13.25	1.284	0.033	0.866	0.078
307	1318	B	12	H	6	80	82	108.3	112.61	13.26	1.303	0.029	0.975	0.078
307	1318	B	13	H	1	90	92	110.4	115.26	13.33				
307	1318	B	13	H	1	140	142	110.9	115.76	13.34	1.318	0.034	0.960	0.079
307	1318	B	13	H	2	43	45	111.43	116.29	13.36	1.385	0.032	0.941	0.077
307	1318	B	13	H	2	90	92	111.9	116.76	13.37	1.235	0.031	1.136	0.077
307	1318	B	13	H	3	90	92	113.4	118.26	13.39	1.380	0.033	0.708	0.080
307	1318	B	13	H	4	43	45	114.43	119.29	13.41	0.768	0.030	0.909	0.078
307	1318	B	13	H	4	90	92	114.9	119.76	13.42	1.207	0.030	0.706	0.081
307	1318	B	13	H	4	140	142	115.4	120.26	13.43	1.295	0.031	0.580	0.078
307	1318	B	13	H	5	90	92	116.4	121.26	13.45	1.090	0.029	0.364	0.077
307	1318	B	13	H	5	90	92	116.4	121.26	13.45	1.110	0.029	0.262	0.077
307	1318	B	13	H	5	140	142	116.9	121.76	13.46	1.267	0.029	0.293	0.076
307	1318	B	13	H	6	33	35	117.33	122.19	13.47	1.133	0.033	0.342	0.080
307	1318	B	13	H	7	18	20	117.65	122.51	13.47	0.999	0.029	0.685	0.078
307	1318	C	7	H	1	20	22	117.7	123.61	13.49	1.333	0.031	0.994	0.077
307	1318	C	7	H	1	70	72	118.2	124.11	13.50	1.280	0.031	0.992	0.091
307	1318	C	7	H	1	120	122	118.7	124.61	13.51	1.458	0.027	0.683	0.078
307	1318	C	7	H	2	20	22	119.2	125.11	13.52	1.409	0.032	0.761	0.083
307	1318	C	7	H	2	70	72	119.7	125.61	13.53	1.484	0.032	0.807	0.077
307	1318	C	7	H	2	120	122	120.2	126.11	13.54	1.523	0.030	0.600	0.082
307	1318	C	7	H	3	20	22	120.7	126.61	13.55	1.722	0.031	0.594	0.079
307	1318	C	7	H	3	70	72	121.2	127.11	13.56	1.552	0.028	0.527	0.079
307	1318	C	7	H	3	120	122	121.7	127.61	13.56	1.602	0.028	0.870	0.082
307	1318	C	7	H	4	20	22	122.2	128.11	13.57				
307	1318	C	7	H	4	70	72	122.7	128.61	13.58	1.755	0.033	1.060	0.080
307	1318	C	7	H	4	120	122	123.2	129.11	13.59	1.716	0.033	1.037	0.081
307	1318	C	7	H	5	20	22	123.7	129.61	13.60	1.723	0.031	0.979	0.084
307	1318	C	7	H	5	70	72	124.2	130.11	13.61	1.497	0.029	0.942	0.079
307	1318	C	7	H	5	120	122	124.7	130.61	13.62				
307	1318	C	8	X	1	14	16	125.84	131.75	13.65				
307	1318	B	14	H	7	2	5	127.29	131.81	13.65	1.806	0.032	0.771	0.079
307	1318	C	8	X	1	60	62	126.3	132.21	13.66	1.704	0.031	0.888	0.081
307	1318	C	8	X	2	14	16	127.26	133.17	13.68				
307	1318	C	8	X	3	60	62	129.22	135.13	13.72				
307	1318	C	8	X	4	14	16	130.26	136.17	13.75				
307	1318	C	8	X	4	115	117	131.27	137.18	13.77				
307	1318	C	8	X	6	14	16	133.26	139.17	13.81	1.346	0.039	0.282	0.078
307	1318	C	8	X	6	114	116	134.26	140.17	13.83	1.598	0.038	0.357	0.087
307	1318	C	8	X	6	114	116	134.26	140.17	13.83				
307	1318	C	8	X	8	13	15	135.19	141.1	13.86	1.379	0.030	0.407	0.084
307	1318	C	9	X	1	80	82	136.1	142.01	13.88				
307	1318	C	9	X	2	80	82	137.6	143.51	13.91	1.368	0.026	0.042	0.086
307	1318	C	9	X	3	80	82	139.1	145.01	13.94				
307	1318	C	9	X	3	130	132	139.6	145.51	13.95				

Leg	Site	Hole	Core	Type	Section	Top sample interval (cm)	Bottom sample interval (cm)	Core depth (mbsf)	Composite depth (mcd)	Age (Ma; ATNTS 2012)	*Uvigerina* sp.					
											$\delta^{13}C$	1 sd $\delta^{13}C$	Converted $\delta^{13}C$	$\delta^{18}O$	1 sd $\delta^{18}O$	Converted $\delta^{18}O$
307	1318	B	10	H	5	50	52	87.5	92.44	12.75	-0.094	0.035	1.072	1.471	0.086	1.152
307	1318	B	10	H	5	109	111	88.09	93.03	12.76	-0.327	0.031	0.911	1.497	0.079	1.177
307	1318	B	10	H	6	50	52	89	93.94	12.77				1.605	0.089	1.284
307	1318	B	10	H	6	50	52	89	93.94	12.77				1.553	0.085	1.233
307	1318	B	10	H	6	106	108	89.56	94.5	12.78	0.081	0.030	1.193	1.521	0.078	1.201
307	1318	B	10	H	7	17	19	90.03	94.97	12.78						
307	1318	B	11	H	1	97	99	91.47	95.9	12.79	-0.110	0.032	1.061	1.483	0.082	1.164
307	1318	B	11	H	2	5	7	92.05	96.48	12.80	-0.039	0.035	1.110	1.605	0.077	1.284
307	1318	B	11	H	2	55	57	92.55	96.98	12.81						
307	1318	B	11	H	3	1	3	93.51	97.94	12.82	0.005	0.033	1.140	1.366	0.080	1.049
307	1318	B	11	H	3	1	3	93.51	97.94	12.82	-0.024	0.034	1.120	1.366	0.077	1.049
307	1318	B	11	H	3	105	107	94.55	98.98	12.84	-0.427	0.028	0.842	1.415	0.077	1.097
307	1318	B	11	H	4	52	54	95.52	99.95	12.85	-0.282	0.029	0.942	1.381	0.082	1.063
307	1318	B	11	H	5	2	4	96.52	100.95	12.87						
307	1318	B	11	H	5	2	4	96.52	100.95	12.87						
307	1318	B	11	H	6	2	4	97.52	101.95	12.88						
307	1318	B	11	H	6	52	54	98.02	102.45	12.89	-0.017	0.029	1.125	1.539	0.081	1.219
307	1318	B	12	H	1	30	32	100.3	104.61	13.01	0.001	0.030	1.138	1.206	0.083	0.891
307	1318	B	12	H	2	30	32	101.8	106.11	13.06	-0.194	0.030	1.003	1.227	0.078	0.912
307	1318	B	12	H	2	80	82	102.3	106.61	13.08	-0.045	0.034	1.106	1.351	0.082	1.034
307	1318	B	12	H	3	30	32	103.3	107.61	13.12	0.251	0.029	1.311	0.782	0.080	0.474
307	1318	B	12	H	3	133	135	104.33	108.64	13.16						
307	1318	B	12	H	4	30	32	104.8	109.11	13.17	0.058	0.034	1.177	1.355	0.079	1.038
307	1318	B	12	H	4	133	135	105.83	110.14	13.20	0.017	0.033	1.149	1.451	0.077	1.132
307	1318	B	12	H	5	133	135	107.33	111.64	13.24	0.147	0.035	1.239	1.206	0.080	0.891
307	1318	B	12	H	5	133	135	107.33	111.64	13.24	0.199	0.033	1.275	1.193	0.077	0.878
307	1318	B	12	H	6	30	32	107.8	112.11	13.25						
307	1318	B	12	H	6	80	82	108.3	112.61	13.26	0.147	0.028	1.239	1.317	0.080	1.000
307	1318	B	13	H	1	90	92	110.4	115.26	13.33	0.102	0.028	1.208	1.026	0.078	0.714
307	1318	B	13	H	1	140	142	110.9	115.76	13.34						
307	1318	B	13	H	2	43	45	111.43	116.29	13.36						
307	1318	B	13	H	2	90	92	111.9	116.76	13.37	-0.014	0.033	1.127	1.360	0.076	1.043
307	1318	B	13	H	3	90	92	113.4	118.26	13.39	0.186	0.034	1.266	0.941	0.085	0.630
307	1318	B	13	H	4	43	45	114.43	119.29	13.41	-0.408	0.031	0.855	1.407	0.079	1.089
307	1318	B	13	H	4	90	92	114.9	119.76	13.42						
307	1318	B	13	H	4	140	142	115.4	120.26	13.43	0.207	0.031	1.280	0.921	0.078	0.611
307	1318	B	13	H	5	90	92	116.4	121.26	13.45	0.004	0.028	1.140	0.873	0.086	0.564
307	1318	B	13	H	5	90	92	116.4	121.26	13.45						
307	1318	B	13	H	5	140	142	116.9	121.76	13.46						
307	1318	B	13	H	6	33	35	117.33	122.19	13.47	-0.112	0.029	1.060	0.658	0.082	0.352
307	1318	B	13	H	7	18	20	117.65	122.51	13.47	-0.082	0.032	1.080	0.823	0.079	0.514
307	1318	C	7	H	1	20	22	117.7	123.61	13.49						
307	1318	C	7	H	1	70	72	118.2	124.11	13.50	0.137	0.028	1.232	1.267	0.083	0.951
307	1318	C	7	H	1	120	122	118.7	124.61	13.51	0.217	0.029	1.287	1.057	0.076	0.745
307	1318	C	7	H	2	20	22	119.2	125.11	13.52	0.111	0.029	1.214	1.095	0.081	0.782
307	1318	C	7	H	2	70	72	119.7	125.61	13.53	0.283	0.035	1.333	0.995	0.079	0.684
307	1318	C	7	H	2	120	122	120.2	126.11	13.54	0.303	0.031	1.347	0.858	0.078	0.549
307	1318	C	7	H	3	20	22	120.7	126.61	13.55	0.632	0.029	1.575	0.846	0.081	0.537
307	1318	C	7	H	3	70	72	121.2	127.11	13.56	0.460	0.028	1.455	0.899	0.080	0.589
307	1318	C	7	H	3	120	122	121.7	127.61	13.56	0.411	0.033	1.421	1.256	0.086	0.940
307	1318	C	7	H	4	20	22	122.2	128.11	13.57	0.468	0.028	1.461	1.421	0.080	1.103
307	1318	C	7	H	4	70	72	122.7	128.61	13.58	0.589	0.030	1.545	1.403	0.077	1.085
307	1318	C	7	H	4	120	122	123.2	129.11	13.59	0.395	0.033	1.410	1.278	0.080	0.962
307	1318	C	7	H	5	20	22	123.7	129.61	13.60	0.609	0.027	1.558	1.276	0.077	0.960
307	1318	C	7	H	5	70	72	124.2	130.11	13.61	0.430	0.037	1.435	1.347	0.077	1.030
307	1318	C	7	H	5	120	122	124.7	130.61	13.62	0.424	0.028	1.430	1.012	0.083	0.700
307	1318	C	8	X	1	14	16	125.84	131.75	13.65	0.574	0.030	1.534	1.201	0.079	0.886
307	1318	B	14	H	7	2	5	127.29	131.81	13.65						
307	1318	C	8	X	1	60	62	126.3	132.21	13.66	0.829	0.032	1.711	1.270	0.076	0.954
307	1318	C	8	X	2	14	16	127.26	133.17	13.68	0.291	0.028	1.338	1.063	0.079	0.751
307	1318	C	8	X	3	60	62	129.22	135.13	13.72	0.499	0.031	1.483	0.972	0.082	0.661
307	1318	C	8	X	4	14	16	130.26	136.17	13.75	0.583	0.029	1.540	0.819	0.077	0.510
307	1318	C	8	X	4	115	117	131.27	137.18	13.77	0.197	0.028	1.273	0.941	0.082	0.630
307	1318	C	8	X	6	14	16	133.26	139.17	13.81	0.259	0.029	1.316	0.716	0.081	0.409
307	1318	C	8	X	6	114	116	134.26	140.17	13.83	0.120	0.034	1.220	0.663	0.078	0.357
307	1318	C	8	X	6	114	116	134.26	140.17	13.83	0.176	0.037	1.259	0.542	0.097	0.238
307	1318	C	8	X	8	13	15	135.19	141.1	13.86	0.098	0.032	1.205	0.671	0.080	0.365
307	1318	C	9	X	1	80	82	136.1	142.01	13.88	0.227	0.029	1.294	0.822	0.078	0.513
307	1318	C	9	X	2	80	82	137.6	143.51	13.91	0.352	0.031	1.381	0.429	0.076	0.127
307	1318	C	9	X	3	80	82	139.1	145.01	13.94	0.333	0.037	1.367	0.446	0.078	0.143
307	1318	C	9	X	3	130	132	139.6	145.51	13.95	0.547	0.034	1.516	0.675	0.084	0.369

Leg	Site	Hole	Core	Type	Section	Top sample interval (cm)	Bottom sample interval (cm)	Core depth (mbsf)	Composite depth (mcd)	Age (Ma; ATNTS 2012)	*Cibicidoides pachyderma*			
											$\delta^{13}C$	1 sd $\delta^{13}C$	$\delta^{18}O$	1 sd $\delta^{18}O$
307	1318	C	9	X	4	130	132	141.1	147.01	13.99	1.351	0.031	0.195	0.078
307	1318	C	9	X	5	33	35	141.63	147.54	14.00	1.313	0.038	0.322	0.083
307	1318	C	9	X	5	130	132	142.6	148.51	14.02				
307	1318	C	9	X	6	80	82	143.6	149.51	14.04	1.414	0.029	0.303	0.080
307	1318	C	9	X	6	130	132	144.1	150.01	14.05	1.457	0.030	0.383	0.078
307	1318	C	9	X	8	21	23	145.03	150.94	14.08				
307	1318	C	9	X	8	21	23	145.03	150.94	14.08				
307	1318	C	10	X	1	80	82	145.7	151.65	14.09				
307	1318	C	10	X	2	31	33	146.71	152.66	14.11	1.284	0.031	0.244	0.079
307	1318	C	10	X	2	83	85	147.23	153.18	14.13				
307	1318	B	17	X	1	20	22	147.9	154.05	14.15	1.217	0.037	0.150	0.090
307	1318	B	17	X	1	67	69	148.37	154.52	14.16				
307	1318	B	17	X	1	120	122	148.9	155.05	14.18	1.345	0.028	0.281	0.080
307	1318	B	17	X	2	20	22	149.4	155.55	14.22	1.407	0.028	0.088	0.077
307	1318	C	10	X	4	33	35	149.73	155.68	14.23	1.214	0.033	0.216	0.077
307	1318	B	17	X	2	65	67	149.85	156	14.26	1.122	0.031	0.061	0.081
307	1318	C	10	X	4	80	82	150.2	156.15	14.27				
307	1318	B	17	X	2	120	122	150.4	156.55	14.31				
307	1318	B	17	X	3	18	20	150.88	157.03	14.35	1.281	0.032	0.132	0.079
307	1318	B	17	X	3	67	69	151.37	157.52	14.39				
307	1318	B	17	X	3	120	122	151.9	158.05	14.43				
307	1318	C	10	X	6	30	32	152.7	158.65	14.48				
307	1318	C	10	X	6	80	82	153.2	159.15	14.52				
307	1318	B	17	X	5	13	15	153.83	159.98	14.59	1.089	0.033	0.578	0.080
307	1318	B	17	X	5	113	115	154.83	160.98	14.63	0.983	0.027	0.265	0.084
307	1318	B	17	X	6	60	62	155.8	161.95	14.66				
307	1318	B	18	X	1	20	22	157.5	163.65	14.70				
307	1318	B	18	X	1	66	68	157.96	164.11	14.72				
307	1318	B	18	X	1	66	68	157.96	164.11	14.72				
307	1318	B	18	X	1	120	122	158.5	164.65	14.73				
307	1318	B	18	X	2	66	68	159.46	165.61	14.76				
307	1318	B	18	X	4	63	65	162.93	169.08	14.80	1.231	0.030	0.110	0.080
307	1318	B	18	X	4	112	114	163.42	169.57	14.80				
307	1318	B	18	X	7	30	32	166.93	173.08	14.83				
307	1318	B	19	X	1	80	82	167.7	173.85	14.83				
307	1318	B	19	X	2	31	33	168.71	174.86	14.84				
307	1318	B	19	X	2	128	130	169.68	175.83	14.85				
307	1318	B	19	X	3	80	82	170.7	176.85	14.86				
307	1318	B	19	X	4	67	69	171.57	177.72	14.87				
307	1318	B	19	X	5	87	89	172.77	178.92	14.89				
307	1318	B	19	X	6	30.5	32.5	173.705	179.86	14.91				
307	1318	B	19	X	6	129	131	174.69	180.84	14.94				
307	1318	B	19	X	7	79.5	81.5	175.695	181.85	14.97				
307	1318	B	19	X	9	15	17	176.58	182.73	14.99				
307	1318	B	20	X	1	93	95	177.43	183.58	15.02	1.008	0.032	0.165	0.081
307	1318	B	20	X	2	43	45	178.43	184.58	15.04	1.171	0.030	0.236	0.082
307	1318	B	20	X	2	138	140	179.38	185.53	15.06	1.369	0.029	0.237	0.084
307	1318	B	20	X	3	91	93	180.41	186.56	15.08	1.139	0.037	0.133	0.080
307	1318	B	20	X	5	0	2	181.5	187.65	15.11	1.251	0.029	0.109	0.077
307	1318	B	20	X	5	88	90	182.38	188.53	15.13				
307	1318	B	20	X	6	43	45	183.43	189.58	15.15				
307	1318	B	20	X	6	140	142	184.4	190.55	15.18	1.170	0.034	0.081	0.081
307	1318	B	20	X	7	94	96	185.44	191.59	15.23				
307	1318	B	21	X	1	26	28	186.36	192.51	15.27				
307	1318	B	21	X	1	128	130	187.38	193.53	15.32				
307	1318	B	21	X	2	82	84	188.42	194.57	15.37				
307	1318	B	21	X	2	128	130	188.88	195.03	15.39				
307	1318	B	21	X	3	27	29	189.37	195.52	15.42	1.425	0.035	0.351	0.081
307	1318	B	21	X	3	129	131	190.39	196.54	15.47	1.233	0.025	0.170	0.084
307	1318	B	21	X	4	84	86	191.44	197.59	15.52	1.529	0.037	0.580	0.076
307	1318	B	21	X	5	64.5	66.5	192.245	198.4	15.55	1.714	0.034	0.397	0.083
307	1318	B	21	X	7	27.5	29.5	194.375	200.53	15.66	1.874	0.034	0.014	0.077
307	1318	B	21	X	7	128	130	195.38	201.53	15.70	1.671	0.031	0.471	0.077
307	1318	B	22	X	1	68.5	70.5	196.385	202.54	15.75	1.835	0.031	0.306	0.079
307	1318	B	22	X	1	120	122	196.9	203.05	15.78	1.873	0.032	0.200	0.078
307	1318	B	22	X	2	20	22	197.4	203.55	15.80	1.914	0.026	0.059	0.085
307	1318	B	22	X	3	75.5	77.5	199.455	205.61	15.90	1.853	0.032	0.100	0.082
307	1318	B	22	X	6	120	122	203.4	209.55	16.03	1.337	0.031	0.584	0.078
307	1318	B	23	X	1	22	24	205.42	211.57	16.07	1.825	0.032	0.227	0.079
307	1318	B	23	X	1	63.5	65.5	205.835	211.99	16.08	1.729	0.039	0.180	0.079
307	1318	B	23	X	2	20	22	206.9	213.05	16.10	1.599	0.029	0.077	0.084
307	1318	B	23	X	2	120	122	207.9	214.05	16.13	1.613	0.032	-0.104	0.079

Leg	Site	Hole	Core	Type	Section	Top sample interval (cm)	Bottom sample interval (cm)	Core depth (mbsf)	Composite depth (mcd)	Age (Ma; ATNTS 2012)	*Uvigerina* sp.					
											$\delta^{13}C$	1 sd $\delta^{13}C$	Converted $\delta^{13}C$	$\delta^{18}O$	1 sd $\delta^{18}O$	Converted $\delta^{18}O$
307	1318	C	9	X	4	130	132	141.1	147.01	13.99	0.424	0.030	1.431	0.615	0.082	0.310
307	1318	C	9	X	5	33	35	141.63	147.54	14.00	0.443	0.034	1.444	0.607	0.077	0.302
307	1318	C	9	X	5	130	132	142.6	148.51	14.02	0.477	0.033	1.467	0.825	0.077	0.516
307	1318	C	9	X	6	80	82	143.6	149.51	14.04	0.251	0.032	1.311	0.610	0.077	0.305
307	1318	C	9	X	6	130	132	144.1	150.01	14.05	0.308	0.039	1.350	0.647	0.088	0.341
307	1318	C	9	X	8	21	23	145.03	150.94	14.08	0.036	0.028	1.162	0.723	0.075	0.416
307	1318	C	9	X	8	21	23	145.03	150.94	14.08	0.223	0.028	1.291	0.670	0.083	0.364
307	1318	C	10	X	1	80	82	145.7	151.65	14.09	0.396	0.029	1.411	0.611	0.080	0.306
307	1318	C	10	X	2	31	33	146.71	152.66	14.11	0.456	0.032	1.453	0.439	0.086	0.137
307	1318	C	10	X	2	83	85	147.23	153.18	14.13	0.313	0.035	1.354	0.486	0.080	0.183
307	1318	B	17	X	1	20	22	147.9	154.05	14.15	0.334	0.026	1.368	0.255	0.082	-0.044
307	1318	B	17	X	1	67	69	148.37	154.52	14.16	0.479	0.029	1.468	0.432	0.082	0.130
307	1318	B	17	X	1	120	122	148.9	155.05	14.18	0.568	0.029	1.530	0.665	0.078	0.359
307	1318	B	17	X	2	20	22	149.4	155.55	14.22	0.573	0.029	1.534	0.563	0.077	0.259
307	1318	C	10	X	4	33	35	149.73	155.68	14.23						
307	1318	B	17	X	2	65	67	149.85	156	14.26	0.325	0.028	1.362	0.414	0.082	0.112
307	1318	C	10	X	4	80	82	150.2	156.15	14.27	0.138	0.030	1.232	0.389	0.079	0.087
307	1318	B	17	X	2	120	122	150.4	156.55	14.31	0.339	0.031	1.372	0.392	0.082	0.090
307	1318	B	17	X	3	18	20	150.88	157.03	14.35	0.302	0.031	1.346	0.412	0.078	0.110
307	1318	B	17	X	3	67	69	151.37	157.52	14.39	0.143	0.033	1.236	0.544	0.078	0.240
307	1318	B	17	X	3	120	122	151.9	158.05	14.43	0.138	0.029	1.232	0.518	0.082	0.214
307	1318	C	10	X	6	30	32	152.7	158.65	14.48	0.199	0.031	1.275	0.602	0.077	0.297
307	1318	C	10	X	6	80	82	153.2	159.15	14.52	0.335	0.029	1.369	0.535	0.080	0.231
307	1318	B	17	X	5	13	15	153.83	159.98	14.59	0.093	0.030	1.201	0.687	0.080	0.381
307	1318	B	17	X	5	113	115	154.83	160.98	14.63	0.183	0.029	1.264	0.624	0.078	0.319
307	1318	B	17	X	6	60	62	155.8	161.95	14.66	0.080	0.031	1.192	0.698	0.080	0.391
307	1318	B	18	X	1	20	22	157.5	163.65	14.70	-0.172	0.033	1.018	0.320	0.091	0.020
307	1318	B	18	X	1	66	68	157.96	164.11	14.72	-0.025	0.032	1.120	0.168	0.076	-0.130
307	1318	B	18	X	1	66	68	157.96	164.11	14.72	-0.112	0.037	1.059	0.032	0.078	-0.264
307	1318	B	18	X	1	120	122	158.5	164.65	14.73	0.209	0.033	1.282	0.360	0.078	0.059
307	1318	B	18	X	2	66	68	159.46	165.61	14.76	-0.073	0.036	1.086	-0.045	0.079	-0.340
307	1318	B	18	X	4	63	65	162.93	169.08	14.80						
307	1318	B	18	X	4	112	114	163.42	169.57	14.80	0.683	0.032	1.610	0.751	0.083	0.444
307	1318	B	18	X	7	30	32	166.93	173.08	14.83	-0.188	0.037	1.007	0.840	0.082	0.531
307	1318	B	19	X	1	80	82	167.7	173.85	14.83	0.180	0.029	1.262	0.792	0.078	0.484
307	1318	B	19	X	2	31	33	168.71	174.86	14.84	-0.048	0.028	1.104	0.583	0.082	0.278
307	1318	B	19	X	2	128	130	169.68	175.83	14.85	-0.121	0.045	1.053	0.519	0.089	0.215
307	1318	B	19	X	3	80	82	170.7	176.85	14.86	-0.046	0.037	1.105	0.348	0.082	0.047
307	1318	B	19	X	4	67	69	171.57	177.72	14.87	0.250	0.028	1.310	0.432	0.076	0.130
307	1318	B	19	X	5	87	89	172.77	178.92	14.89	-0.204	0.033	0.996	0.247	0.078	-0.052
307	1318	B	19	X	6	30.5	32.5	173.705	179.86	14.91	-0.196	0.034	1.001	0.082	0.133	-0.215
307	1318	B	19	X	6	129	131	174.69	180.84	14.94	-0.128	0.030	1.048	0.029	0.084	-0.267
307	1318	B	19	X	7	79.5	81.5	175.695	181.85	14.97	0.122	0.030	1.221	0.143	0.079	-0.155
307	1318	B	19	X	9	15	17	176.58	182.73	14.99	0.457	0.032	1.453	0.492	0.081	0.189
307	1318	B	20	X	1	93	95	177.43	183.58	15.02	0.281	0.033	1.331	0.530	0.078	0.226
307	1318	B	20	X	2	43	45	178.43	184.58	15.04	0.146	0.032	1.238	0.664	0.077	0.358
307	1318	B	20	X	2	138	140	179.38	185.53	15.06	0.364	0.037	1.389	0.520	0.086	0.216
307	1318	B	20	X	3	91	93	180.41	186.56	15.08	0.153	0.034	1.243	0.419	0.077	0.117
307	1318	B	20	X	5	0	2	181.5	187.65	15.11						
307	1318	B	20	X	5	88	90	182.38	188.53	15.13	0.382	0.036	1.401	0.521	0.083	0.217
307	1318	B	20	X	6	43	45	183.43	189.58	15.15	0.396	0.028	1.411	0.346	0.079	0.045
307	1318	B	20	X	6	140	142	184.4	190.55	15.18	0.111	0.027	1.214	0.415	0.079	0.113
307	1318	B	20	X	7	94	96	185.44	191.59	15.23	0.329	0.028	1.365	0.559	0.080	0.255
307	1318	B	21	X	1	26	28	186.36	192.51	15.27	-0.143	0.033	1.038	0.022	0.080	-0.274
307	1318	B	21	X	1	128	130	187.38	193.53	15.32	-0.026	0.029	1.119	0.047	0.077	-0.249
307	1318	B	21	X	2	82	84	188.42	194.57	15.37	0.155	0.033	1.244	0.129	0.078	-0.168
307	1318	B	21	X	2	128	130	188.88	195.03	15.39	0.053	0.028	1.174	0.160	0.079	-0.138
307	1318	B	21	X	3	27	29	189.37	195.52	15.42						
307	1318	B	21	X	3	129	131	190.39	196.54	15.47	0.478	0.029	1.468	0.534	0.078	0.230
307	1318	B	21	X	4	84	86	191.44	197.59	15.52						
307	1318	B	21	X	5	64.5	66.5	192.245	198.4	15.55						
307	1318	B	21	X	7	27.5	29.5	194.375	200.53	15.66						
307	1318	B	21	X	7	128	130	195.38	201.53	15.70						
307	1318	B	22	X	1	68.5	70.5	196.385	202.54	15.75						
307	1318	B	22	X	1	120	122	196.9	203.05	15.78						
307	1318	B	22	X	2	20	22	197.4	203.55	15.80						
307	1318	B	22	X	3	75.5	77.5	199.455	205.61	15.90						
307	1318	B	22	X	6	120	122	203.4	209.55	16.03						
307	1318	B	23	X	1	22	24	205.42	211.57	16.07						
307	1318	B	23	X	1	63.5	65.5	205.835	211.99	16.08						
307	1318	B	23	X	2	20	22	206.9	213.05	16.10						
307	1318	B	23	X	2	120	122	207.9	214.05	16.13						

Leg	Site	Hole	Core	Type	Section	Top sample interval (cm)	Bottom sample interval (cm)	Core depth (mbsf)	Composite depth (mcd)	Age (Ma; ATNTS 2012)	*Cibicidoides pachyderma*			
											$\delta^{13}C$	1 sd $\delta^{13}C$	$\delta^{18}O$	1 sd $\delta^{18}O$
307	1318	B	23	X	4	20	22	209.9	216.05	16.17	1.626	0.029	-0.217	0.081
307	1318	B	23	X	5	68	70	211.88	218.03	16.21	1.618	0.032	0.091	0.078
307	1318	B	23	X	6	17	19	212.87	219.02	16.24	1.500	0.031	0.108	0.076
307	1318	B	25	X	2	69.5	71.5	225.895	232.05	16.43	1.553	0.034	-0.347	0.082
307	1318	B	26	X	2	11	13	229.92	236.07	16.49	1.649	0.031	0.066	0.079
307	1318	B	26	X	2	112.5	114.5	230.935	237.09	16.50	1.901	0.028	0.206	0.082
307	1318	B	27	X	3	41.5	43.5	238.415	244.57	16.57	1.898	0.032	0.356	0.082
307	1318	B	27	X	3	140	142	239.4	245.55	16.58	1.712	0.035	0.283	0.087
307	1318	B	27	X	4	89.5	91.5	240.395	246.55	16.59	1.961	0.026	0.247	0.077
307	1318	B	27	X	6	25.5	27.5	241.325	247.48	16.60	1.942	0.029	0.196	0.078

Leg	Site	Hole	Core	Type	Section	Top sample interval (cm)	Bottom sample interval (cm)	Core depth (mbsf)	Composite depth (mcd)	Age (Ma; ATNTS 2012)	*Uvigerina* sp.					
											$\delta^{13}C$	1 sd $\delta^{13}C$	Converted $\delta^{13}C$	$\delta^{18}O$	1 sd $\delta^{18}O$	Converted $\delta^{18}O$
307	1318	B	23	X	4	20	22	209.9	216.05	16.17						
307	1318	B	23	X	5	68	70	211.88	218.03	16.21						
307	1318	B	23	X	6	17	19	212.87	219.02	16.24						
307	1318	B	25	X	2	69.5	71.5	225.895	232.05	16.43						
307	1318	B	26	X	2	11	13	229.92	236.07	16.49						
307	1318	B	26	X	2	112.5	114.5	230.935	237.09	16.50						
307	1318	B	27	X	3	41.5	43.5	238.415	244.57	16.57						
307	1318	B	27	X	3	140	142	239.4	245.55	16.58						
307	1318	B	27	X	4	89.5	91.5	240.395	246.55	16.59						
307	1318	B	27	X	6	25.5	27.5	241.325	247.48	16.60						

Supplementary note 5.1

Apart from various taphonomic processes a fossil dinocyst assemblage is dependent from the living dinoflagellate assemblage. Only about 10–20% of the living dinoflagellates produce a fossilizable cyst, but studies on surface sediments have shown that specific dinocysts show good correlations with e.g. sea-surface temperature, -salinity, -productivity, and relative sea-level (*Bonnet et al.*, 2012; *de Vernal et al.*, 2013; *Zonneveld et al.*, 2013). However, working with fossil assemblages opposes the problem that some fossil species do not occur in modern sediments and some modern indicator species do not occur in fossil assemblages. The assumption has to be made that the environmental preferences of extant dinocyst species also apply to fossil assemblages. A comparative study based on Pliocene and Pleistocene dinocyst abundances and Mg/Ca temperatures linked fossil assemblages to modern assemblages identified in core tops and compared the past and present records, confirming most environmental interpretations for the majority of the extant species (*De Schepper et al.*, 2011). A cryptic species appeared to be the cold-water indicator dinocyst *Impagidinium pallidum* that showed a wider temperature range for the past record than is known in present records. This species was kept as a cold-water indicator because changing temperature gradients and related competition between species may have caused *Impagidinium pallidum* to migrate polewards in recent times. For extinct species environmental preferences can also be deduced indirectly, e.g. from temperature reconstructions using other proxies.

Based on these principles several palaeoenvironment indices are available that provide indications of relative environmental change, but no quantitative results. For relative sea-surface temperature changes SST_{dino} or also called the Warm/Cold index (W/C) is available: W/C = nW / (nW + nC), where n is the number of specimens counted, W are warm-water indicating species and C are cold-water indicating species (*Versteegh*, 1994). An overview of the species used in the W/C index is provided in table 2 of *Quaijtaal et al.* (2014).

Bonnet, S., de Vernal, A., Gersonde, R., Lembke-Jene, L., 2012. Modern distribution of dinocysts from the North Pacific Ocean (37-64°N, 144°E-148°W) in relation to hydrographic conditions, sea-ice and productivity. Marine Micropaleontology 84–85, 87–113.

De Schepper, S., Fischer, E.I., Groeneveld, J., Head, M.J., Matthiessen, J., 2011. Deciphering the palaeoecology of Late Pliocene and Early Pleistocene dinoflagellate cysts. Palaeogeography, Palaeoclimatology, Palaeoecology 309, 17–32.

de Vernal, A., Rochon, A., Fréchette, B., Henry, M., Radi, T., Solignac, S., 2013. Reconstructing past sea ice cover of the Northern Hemisphere from dinocyst assemblages: Status of the approach. Quaternary Science Reviews 79, 122–134.

Quaijtaal, W., Donders, T.H., Persico, D., Louwye, S., 2014. Characterising the middle Miocene Mi-events in the Eastern North Atlantic realm: A first high-resolution marine palynological record from the Porcupine Basin. Palaeogeography, Palaeoclimatology, Palaeoecology 399, 140–159.

Versteegh, G.J.M., 1994. Recognition of cyclic and non-cyclic environmental changes in the Mediterranean Pliocene: A palynological approach. Marine Micropaleontology 23, 147–183.

Zonneveld, K.A.F., Marret, F., Versteegh, G.J.M., Bogus, K., Bonnet, S., Bouimetarhan, I., Crouch, E., de Vernal, A., Elshanawany, R., Edwards, L., Esper, O., Forke, S., Grøsfjeld, K., Henry, M., Holzwarth, U., Kielt, J.-F., Kim, S.-Y., Ladouceur, S., Ledu, D., Chen, L., Limoges, A., Londeix, L., Lu, S.-H., Mahmoud, M.S., Marino, G., Matsouka, K., Matthiessen, J., Mildenhal, D.C., Mudie, P., Neil, H.L., Pospelova, V., Qi, Y., Radi, T., Richerol, T., Rochon, A., Sangiorgi, F., Solignac, S., Turon, J.-L., Verleye, T., Wang, Y., Wang, Z., Young, M., 2013. Atlas of modern dinoflagellate cyst distribution based on 2405 data points. Review of Palaeobotany and Palynology 191, 1–197.

Supplementary Table 5.1: summary of BIT-index, SST_{TEX86H}, $SST_{UK'37}$ and SST_{dino} for Site U1318.

Leg	Site	Hole	Core	Type	Section	Top sample interval (cm)	Bottom sample interval (cm)	Core depth (mbsf)	Composite depth (mcd)	Age (ATNTS 2012; Ma)	BIT index	TEX86	TEX86-H temperature	UK37	SST-UK'37	SST-dino	# Cold-water dinocysts	# Warm-water dinocysts
307	1318	B	10	H	5	50	52	87.5	92.44	12.36	0.05	0.54	20.1	0.90	25.9	0.54	11	13
307	1318	B	10	H	5	109	111	88.09	93.03	12.40	0.05	0.53	19.9	0.91	26.3	0.31	29	13
307	1318	B	10	H	6	2	4	88.52	93.46	12.43	0.05	0.53	19.8	0.92	26.4	0.25	40	13
307	1318	B	10	H	6	50	52	89	93.94	12.47	0.06	0.52	19.1	0.90	25.8	0.09	71	7
307	1318	B	10	H	6	106	108	89.56	94.5	12.50	0.05	0.52	19.0	0.92	26.5	0.28	39	15
307	1318	B	10	H	7	17	19	90.03	94.97	12.53	0.05	0.50	18.1	0.91	26.2	0.15	33	6
307	1318	B	11	H	1	47	49	90.97	95.4	12.55	0.07	0.53	19.9	0.92	26.6	0.35	11	6
307	1318	B	11	H	1	97	99	91.47	95.9	12.58	0.06	0.54	20.1	0.92	26.6	0.16	21	4
307	1318	B	11	H	2	5	7	92.05	96.48	12.62	0.07	0.54	20.1	0.94	27.0	0.18	18	4
307	1318	B	11	H	2	55	57	92.55	96.98	12.65	0.09	0.54	20.5	0.93	26.8	0.17	20	4
307	1318	B	11	H	2	105	107	93.05	97.48	12.68	0.08	0.53	19.7	0.93	26.8	0.15	22	4
307	1318	B	11	H	3	1	3	93.51	97.94	12.71	0.07	0.54	20.4	0.93	26.8	0.13	7	1
307	1318	B	11	H	3	51	53	94.01	98.44	12.74	0.05	0.57	21.9	0.94	27.1	0.18	32	7
307	1318	B	11	H	3	105	107	94.55	98.98	12.74	0.06	0.54	20.2	0.94	27.2	0.19	43	10
307	1318	B	11	H	4	3	4	95.03	99.46	12.74	0.05	0.56	21.6	0.94	27.1	0.13	75	11
307	1318	B	11	H	4	52	54	95.52	99.95	12.75	0.07	0.54	20.1	0.93	26.8	0.26	28	10
307	1318	B	11	H	4	103	105	96.03	100.46	12.75	0.06	0.57	21.9	1.00	28.9	0.39	20	13
307	1318	B	11	H	5	2	4	96.52	100.95	12.76	0.06	0.58	22.3	0.97	27.9	0.24	34	11
307	1318	B	11	H	5	52	54	97.02	101.45	12.76	0.07	0.54	20.4	0.95	27.4	0.31	34	15
307	1318	B	11	H	6	2	4	97.52	101.95	12.77	0.05	0.53	19.8	0.94	27.2	0.16	47	9
307	1318	B	11	H	6	52	54	98.02	102.45	12.77	0.04	0.53	19.6	0.94	27.1	0.27	16	6
307	1318	B	12	H	1	30	32	100.3	104.61	12.82	0.04	0.57	21.8	0.96	27.9	0.54	16	19
307	1318	B	12	H	1	80	82	100.8	105.11	12.83	0.04	0.56	21.2	0.96	27.8	0.61	9	14
307	1318	B	12	H	1	133	135	101.33	105.64	12.84	0.04	0.53	19.8	0.99	28.8	0.33	20	10
307	1318	B	12	H	2	30	32	101.8	106.11	12.84	0.04	0.54	20.3	0.94	27.2	0.38	10	6
307	1318	B	12	H	2	80	82	102.3	106.61	12.85	0.05	0.54	20.2	0.95	27.5	0.28	21	8
307	1318	B	12	H	2	133	135	102.83	107.14	12.86	0.04	0.58	22.4	0.97	28.0	0.67	4	8
307	1318	B	12	H	3	30	32	103.3	107.61	12.86	0.05	0.59	22.8	0.96	27.6	0.29	27	11
307	1318	B	12	H	3	80	82	103.8	108.11	12.87	0.04	0.53	19.7	0.94	27.2	0.18	14	3
307	1318	B	12	H	3	133	135	104.33	108.64	12.88	0.05	0.55	20.9	0.95	27.5	0.25	24	8
307	1318	B	12	H	4	30	32	104.8	109.11	12.88	0.07	0.52	19.4	0.94	27.2	0.28	29	11
307	1318	B	12	H	4	80	82	105.3	109.61	12.89	0.05	0.52	19.4	0.93	26.8	0.54	6	7
307	1318	B	12	H	4	133	135	105.83	110.14	12.90	0.04	0.51	18.4	0.90	25.8	0.13	42	6
307	1318	B	12	H	5	30	32	106.3	110.61	12.91	0.04	0.53	19.7	0.93	26.8	0.35	22	12
307	1318	B	12	H	5	80	82	106.8	111.11	12.92	0.04	0.53	19.6	0.94	27.1	0.48	12	11
307	1318	B	12	H	5	133	135	107.33	111.64	12.93	0.04	0.53	19.9	0.94	27.3	0.34	21	11
307	1318	B	12	H	6	30	32	107.8	112.11	12.94	0.05	0.56	21.2	0.94	27.3	0.53	25	28
307	1318	B	12	H	6	80	82	108.3	112.61	12.95	0.04	0.52	19.0	0.92	26.7	0.42	26	19
307	1318	B	13	H	1	30	32	109.8	114.66	12.99	0.06	0.55	21.0	0.95	27.4	0.40	15	10
307	1318	B	13	H	1	90	92	110.4	115.26	13.01	0.06	0.55	20.9	0.94	27.1	0.44	14	11
307	1318	B	13	H	1	140	142	110.9	115.76	13.02	0.05	0.54	20.2	0.95	27.3	0.40	26	17
307	1318	B	13	H	2	43	45	111.43	116.29	13.03	0.05	0.52	19.1	0.92	26.7	0.33	14	7
307	1318	B	13	H	2	90	92	111.9	116.76	13.04	0.07	0.51	18.8	0.92	26.5	0.20	44	11
307	1318	B	13	H	2	140	142	112.4	117.26	13.05	0.04	0.53	19.6	0.92	26.5	0.06	72	5
307	1318	B	13	H	3	43	45	112.93	117.79	13.06	0.06	0.54	20.1	0.94	27.0	0.14	31	5
307	1318	B	13	H	3	90	92	113.4	118.26	13.07	0.05	0.56	21.6	0.94	27.1	0.23	43	13
307	1318	B	13	H	3	140	142	113.9	118.76	13.09	0.08	0.55	20.6	0.94	27.1	0.07	84	6
307	1318	B	13	H	4	43	45	114.43	119.29	13.10	0.05	0.52	19.5	0.96	27.8	0.08	84	7
307	1318	B	13	H	4	90	92	114.9	119.76	13.11	0.05	0.55	21.1	0.94	27.2	0.27	37	14
307	1318	B	13	H	4	140	142	115.4	120.26	13.12	0.05	0.56	21.3	0.95	27.4	0.20	48	12
307	1318	B	13	H	5	43	45	115.93	120.79	13.13	0.04	0.58	22.4	0.95	27.4	0.26	32	11
307	1318	B	13	H	5	90	92	116.4	121.26	13.15	0.06	0.58	22.3	0.95	27.5	0.07	89	7
307	1318	B	13	H	5	140	142	116.9	121.76	13.16	0.05	0.60	23.5	0.96	27.8	0.20	41	10
307	1318	B	13	H	6	33	35	117.33	122.19	13.17	0.06	0.60	23.7	0.96	27.9	0.09	69	7
307	1318	B	13	H	7	18	20	117.65	122.51	13.18	0.06	0.58	22.6	0.95	27.5	0.09	95	9
307	1318	C	7	H	1	20	22	117.7	123.61	13.28	0.07	0.53	19.7	0.95	27.5	0.02	128	3
307	1318	B	14	H	1	43	45	119.43	123.95	13.32	0.07	0.52	19.3	0.95	27.5	0.03	127	4
307	1318	C	7	H	1	70	72	118.2	124.11	13.34	0.08	0.53	19.7	0.96	27.7	0.09	63	6
307	1318	B	14	H	1	90	92	119.9	124.42	13.37	0.08	0.53	19.9	0.92	26.6	0.22	14	4
307	1318	C	7	H	1	120	122	118.7	124.61	13.38	0.06	0.58	22.2	0.97	28.0	0.36	32	18
307	1318	B	14	H	1	140	142	120.4	124.92	13.39	0.08	0.56	21.3	0.95	27.5	0.49	19	18
307	1318	C	7	H	2	20	22	119.2	125.11	13.40	0.07	0.54	20.1	0.97	27.9	0.15	64	11

Leg	Site	Hole	Core	Type	Section	Top sample interval (cm)	Bottom sample interval (cm)	Core depth (mbsf)	Composite depth (mcd)	Age (ATNTS 2012; Ma)	BIT index	TEX86	TEX86-H temperature	UK37	SST-UK'37	SST-dino	# Cold-water dinocysts	# Warm-water dinocysts
307	1318	B	14	H	2	43	45	120.93	125.45	13.41	0.07	0.54	20.5	0.95	27.4	0.14	25	4
307	1318	C	7	H	2	70	72	119.7	125.61	13.42	0.06	0.57	22.1	0.97	27.9	0.27	24	9
307	1318	B	14	H	2	90	92	121.4	125.92	13.43	0.06	0.60	23.5	0.96	27.9	0.44	14	11
307	1318	C	7	H	2	120	122	120.2	126.11	13.44	0.08	0.56	21.5	0.97	28.0	0.37	18	10.5
307	1318	B	14	H	2	140	142	121.9	126.42	13.45	0.06	0.56	21.2	0.96	27.9	0.38	8	5
307	1318	C	7	H	3	20	22	120.7	126.61	13.46	0.06	0.52	19.2	0.94	27.1	0.43	17	13
307	1318	B	14	H	3	43	45	122.43	126.95	13.48	0.07	0.59	22.7	0.96	27.9	0.17	29	6
307	1318	C	7	H	3	70	72	121.2	127.11	13.48	0.09	0.58	22.3	0.95	27.5	0.19	35	8
307	1318	B	14	H	3	90	92	122.9	127.42	13.50	0.08	0.56	21.3	0.95	27.4	0.33	16	8
307	1318	C	7	H	3	120	122	121.7	127.61	13.50	0.06	0.56	21.3	0.95	27.6	0.26	29	10
307	1318	B	14	H	3	140	142	123.4	127.92	13.52	0.08	0.54	20.4	0.94	27.0	0.28	26	10
307	1318	C	7	H	4	20	22	122.2	128.11	13.53	0.08	0.51	18.8	0.95	27.6	0.14	38	6
307	1318	B	14	H	4	43	45	123.93	128.45	13.54	0.07	0.51	18.9	0.94	27.2	0.17	38	8
307	1318	C	7	H	4	70	72	122.7	128.61	13.55	0.07	0.51	18.8	0.96	27.6	0.21	45	12
307	1318	B	14	H	4	90	92	124.4	128.92	13.56	0.08	0.53	19.5	0.96	27.7	0.35	15	8
307	1318	C	7	H	4	120	122	123.2	129.11	13.57	0.08	0.52	19.2	0.96	27.8	0.43	24	18
307	1318	B	14	H	4	140	142	124.9	129.42	13.58	0.09	0.54	20.5	0.96	27.6	0.27	35	13
307	1318	C	7	H	5	20	22	123.7	129.61	13.59	0.08	0.53	19.6	0.96	27.7	0.42	28	20
307	1318	B	14	H	5	43	45	125.43	129.95	13.60	0.10	0.53	19.6	0.95	27.4	0.19	59	14
307	1318	C	7	H	5	70	72	124.2	130.11	13.61	0.08	0.53	19.6	0.94	27.1	0.39	22	14
307	1318	B	14	H	5	90	92	125.9	130.42	13.62	0.09	0.55	20.6	0.96	27.7	0.48	16	15
307	1318	C	7	H	5	120	122	124.7	130.61	13.62	0.10	0.55	20.9	0.96	27.7	0.64	9	16
307	1318	B	14	H	6	13	15	126.46	130.98	13.63	0.10	0.55	20.6	0.96	27.7	0.30	19	8
307	1318	C	7	H	6	19	21	125.19	131.1	13.63	0.11	0.54	20.2	0.95	27.5	0.42	22	16
307	1318	B	14	H	6	60	62	126.93	131.45	13.64	0.09	0.54	20.5	0.92	26.6	0.24	19	6
307	1318	C	8	X	1	14	16	125.84	131.75	13.65	0.11	0.55	20.9	0.93	26.9	0.52	13	14
307	1318	B	14	H	7	2	5	127.29	131.81	13.65	0.07	0.55	20.9	0.97	28.0	0.55	14	17
307	1318	C	8	X	1	60	62	126.3	132.21	13.66	0.08	0.52	19.2	0.94	27.3	0.38	20	12
307	1318	C	8	X	1	114	116	126.84	132.75	13.67	0.06	0.52	19.3	0.95	27.5	0.24	19	6
307	1318	C	8	X	2	14	16	127.26	133.17	13.68	0.06	0.54	20.2	0.96	27.8	0.38	13	8
307	1318	C	8	X	2	62	64	127.74	133.65	13.69	0.08	0.59	22.7	0.97	28.1	0.19	17	4
307	1318	C	8	X	2	114	116	128.26	134.17	13.70	0.07	0.58	22.2	0.98	28.4	0.23	24	7
307	1318	C	8	X	3	14	16	128.76	134.67	13.71	0.08	0.57	21.8	0.97	28.1	0.58	13	18
307	1318	C	8	X	3	60	62	129.22	135.13	13.72	0.08	0.55	20.9	0.97	28.1	0.26	23	8
307	1318	C	8	X	3	115	117	129.77	135.68	13.73	0.07	0.57	21.9	0.97	28.1	0.31	22	10
307	1318	C	8	X	4	14	16	130.26	136.17	13.75	0.07	0.57	22.2	0.96	27.9	0.42	15	11
307	1318	C	8	X	4	60	62	130.72	136.63	13.76	0.08	0.56	21.5	0.98	28.2	0.35	35	19
307	1318	C	8	X	4	115	117	131.27	137.18	13.77	0.08	0.55	21.1	0.97	27.9	0.21	15	4
307	1318	C	8	X	5	14	16	131.76	137.67	13.78	0.09	0.56	21.2	0.98	28.5	0.18	28	6
307	1318	C	8	X	5	60	62	132.22	138.13	13.79	0.08	0.56	21.6	0.97	28.0	0.27	16	6
307	1318	C	8	X	5	116	118	132.78	138.69	13.80	0.10	0.58	22.6	0.98	28.3	0.30	14	6
307	1318	C	8	X	6	14	16	133.26	139.17	13.81	0.10	0.58	22.5	0.98	28.3	0.19	21	5
307	1318	C	8	X	6	60	62	133.72	139.63	13.82	0.10	0.58	22.2	0.98	28.3	0.30	14	6
307	1318	C	8	X	6	114	116	134.26	140.17	13.83	0.10	0.58	22.3	0.97	28.2	0.30	14	6
307	1318	C	8	X	7	14	16	134.76	140.67	13.85	0.10	0.58	22.2	0.97	28.0	0.43	16	12
307	1318	C	8	X	8	13	15	135.19	141.1	13.86	0.08	0.58	22.4	0.97	28.2	0.30	14	6
307	1318	C	9	X	1	33	35	135.63	141.54	13.87	0.06	0.60	23.5	0.98	28.3	0.33	12	6
307	1318	C	9	X	1	80	82	136.1	142.01	13.88	0.07	0.59	22.9	0.97	28.2	0.28	13	5
307	1318	C	9	X	1	130	132	136.6	142.51	13.89	0.06	0.59	22.7	0.97	28.1	0.79	6	22
307	1318	C	9	X	2	34	36	137.14	143.05	13.90	0.07	0.59	22.8	0.96	27.9	0.26	14	5
307	1318	C	9	X	2	80	82	137.6	143.51	13.91	0.06	0.62	24.5	0.99	28.8	0.69	4	9
307	1318	C	9	X	2	130	132	138.1	144.01	13.92	0.06	0.58	22.2	0.97	28.0	0.56	12	15
307	1318	C	9	X	3	34	36	138.64	144.55	13.93	0.07	0.58	22.3	0.97	28.1	0.50	9	9
307	1318	C	9	X	3	80	82	139.1	145.01	13.94	0.08	0.60	23.2	0.96	27.8	0.63	7	12
307	1318	C	9	X	3	130	132	139.6	145.51	13.95	0.07	0.59	23.1	0.97	28.1	0.42	11	8
307	1318	C	9	X	4	33	35	140.13	146.04	13.97	0.06	0.60	23.3	0.97	28.2	0.45	12	10
307	1318	C	9	X	4	80	82	140.6	146.51	13.98	0.06	0.61	23.8	0.99	28.6	0.60	8	12
307	1318	C	9	X	4	130	132	141.1	147.01	13.99	0.07	0.60	23.3	0.97	28.1	0.67	7	14
307	1318	C	9	X	5	33	35	141.63	147.54	14.00	0.07	0.60	23.5	0.97	28.1	0.69	8	18
307	1318	C	9	X	5	84	86	142.14	148.05	14.01	0.07	0.61	23.7	0.98	28.5	0.69	4	9
307	1318	C	9	X	5	130	132	142.6	148.51	14.02	0.07	0.59	22.8	0.97	28.1	0.25	9	3
307	1318	C	9	X	6	33	35	143.13	149.04	14.03	0.07	0.58	22.4	0.97	28.1	0.52	10	11
307	1318	C	9	X	6	80	82	143.6	149.51	14.04	0.08	0.60	23.4	0.98	28.3	0.75	3	9
307	1318	C	9	X	6	130	132	144.1	150.01	14.05	0.09	0.59	23.1	0.97	28.2	0.78	2	7
307	1318	C	9	X	7	32	34	144.62	150.53	14.07	0.06	0.58	22.3	0.97	28.2	0.81	3	13
307	1318	C	9	X	8	21	23	145.03	150.94	14.08	0.07	0.60	23.3	0.98	28.4	0.93	1	13
307	1318	C	10	X	1	31	33	145.21	151.16	14.08	0.09	0.64	25.5	0.98	28.4	0.78	5	18

Leg	Site	Hole	Core	Type	Section	Top sample interval (cm)	Bottom sample interval (cm)	Core depth (mbsf)	Composite depth (mcd)	Age (ATNTS 2012; Ma)	BIT index	TEX86	TEX86-H temperature	UK37	SST-UK'37	SST-dino	# Cold-water dinocysts	# Warm-water dinocysts
307	1318	C	10	X	1	80	82	145.7	151.65	14.09	0.10	0.60	23.2	0.98	28.4	0.72	5	13
307	1318	C	10	X	1	130	132	146.2	152.15	14.10	0.08	0.59	23.1	0.97	27.9	0.70	8	19
307	1318	C	10	X	2	31	33	146.71	152.66	14.11	0.09	0.60	23.5	0.97	28.1	1.00	0	9
307	1318	C	10	X	2	83	85	147.23	153.18	14.13	0.10	0.63	24.8	0.99	28.7	0.87	2	13
307	1318	C	10	X	2	130	132	147.7	153.65	14.14	0.09	0.64	25.1	0.97	28.2	0.83	4	20
307	1318	B	17	X	1	20	22	147.9	154.05	14.15	0.10	0.62	24.5	0.98	28.2	0.81	3	13
307	1318	C	10	X	3	33	35	148.23	154.18	14.15	0.12	0.61	24.0	0.99	28.6	0.50	6	6
307	1318	B	17	X	1	67	69	148.37	154.52	14.16	0.09	0.60	23.4	0.97	28.2	0.92	1	11
307	1318	C	10	X	3	80	82	148.7	154.65	14.16	0.09	0.59	22.9	0.97	27.9	0.58	5	7
307	1318	B	17	X	1	120	122	148.9	155.05	14.18	0.09	0.60	23.4	0.97	28.1	0.60	6	9
307	1318	C	10	X	3	130	132	149.2	155.15	14.19	0.08	0.61	23.8	0.97	28.1	0.79	3	11
307	1318	B	17	X	2	20	22	149.4	155.55	14.22	0.08	0.61	23.9	0.98	28.2	0.50	5	5
307	1318	C	10	X	4	33	35	149.73	155.68	14.23	0.08	0.62	24.2	0.97	28.2	0.67	5	10
307	1318	B	17	X	2	65	67	149.85	156	14.26	0.09	0.62	24.5	0.98	28.3	0.88	2	14
307	1318	C	10	X	4	80	82	150.2	156.15	14.27	0.09	0.62	24.5	0.99	28.6	0.75	2	6
307	1318	B	17	X	2	120	122	150.4	156.55	14.31	0.07	0.60	23.5	0.98	28.3	0.89	2	16
307	1318	C	10	X	4	130	132	150.7	156.65	14.31	0.06	0.62	24.2	0.98	28.2	0.67	4	8
307	1318	B	17	X	3	18	20	150.88	157.03	14.35	0.06	0.60	23.4	0.97	28.1	0.90	1	9
307	1318	C	10	X	5	31	33	151.21	157.16	14.36	0.07	0.61	23.7	0.97	28.2	0.87	2	13
307	1318	B	17	X	3	67	69	151.37	157.52	14.39	0.07	0.59	23.1	0.97	28.1	0.77	3	10
307	1318	C	10	X	5	80	82	151.7	157.65	14.40	0.09	0.61	23.8	0.98	28.3	0.53	7	8
307	1318	B	17	X	3	120	122	151.9	158.05	14.43	0.08	0.59	23.1	0.98	28.2	0.92	1	11
307	1318	C	10	X	5	134	136	152.24	158.19	14.44	0.09	0.62	24.2	0.97	28.0	0.86	1	6
307	1318	B	17	X	4	8	10	152.28	158.43	14.46	0.09	0.61	24.0	0.97	28.0	0.75	3	9
307	1318	C	10	X	6	30	32	152.7	158.65	14.48	0.09	0.61	24.0	0.97	28.0	0.70	3	7
307	1318	C	10	X	6	80	82	153.2	159.15	14.52	0.09	0.59	23.0	0.96	27.8	1.00	0	14
307	1318	C	10	X	6	130	132	153.7	159.65	14.57	0.11	0.57	21.9	0.98	28.2	0.79	3	11
307	1318	B	17	X	5	13	15	153.83	159.98	14.59	0.07	0.56	21.3	0.97	28.1	0.91	1	10
307	1318	C	10	X	7	33	35	154.23	160.18	14.61	0.07	0.56	21.2	0.97	28.1	0.91	1	10
307	1318	B	17	X	5	63	65	154.33	160.48	14.62	0.09	0.58	22.5	0.97	28.1	0.80	2	8
307	1318	B	17	X	5	113	115	154.83	160.98	14.63	0.08	0.57	21.8	0.97	28.1	0.88	1	7
307	1318	B	17	X	6	13	15	155.33	161.48	14.65	0.09	0.58	22.3	0.97	28.0	0.77	3	10
307	1318	B	17	X	6	60	62	155.8	161.95	14.66	0.11	0.56	21.6	0.96	27.9	0.90	1	9
307	1318	B	17	X	6	113	115	156.33	162.48	14.67	0.11	0.59	23.0	0.97	27.9	0.50	4	4
307	1318	B	17	X	7	15	17	156.85	163	14.69	0.07	0.61	24.1	0.97	28.2	1.00	0	13
307	1318	B	17	X	8	13	15	157.31	163.46	14.70	0.06	0.63	24.8	0.98	28.4	1.00	0	8
307	1318	B	18	X	1	20	22	157.5	163.65	14.70	0.09	0.63	24.9	0.98	28.3	0.91	2	21
307	1318	B	18	X	1	120	122	158.5	164.65	14.73	0.06	0.65	25.8	0.99	28.7	1.00	0	12
307	1318	B	18	X	2	66	68	159.46	165.61	14.76	0.09	0.68	27.0	0.98	28.3	1.00	0	15
307	1318	B	18	X	3	18	20	160.48	166.63	14.78	0.06	0.65	26.0	0.98	28.3	0.80	2	8
307	1318	B	18	X	4	13	15	162.43	168.58	14.79	0.11	0.60	23.4	0.97	28.1	0.82	4	18
307	1318	B	18	X	4	112	114	163.42	169.57	14.80	0.14	0.59	23.1	0.98	28.3	0.73	3	8
307	1318	B	18	X	5	60	62	164.4	170.55	14.81	0.10	0.59	23.0	0.97	28.1	0.50	10	10
307	1318	B	18	X	6	13	15	165.43	171.58	14.82	0.12	0.61	24.0	0.98	28.5	0.83	3	15
307	1318	B	18	X	6	112	114	166.42	172.57	14.82	0.15	0.59	22.8	0.97	28.1	0.81	7	30
307	1318	B	19	X	1	30	32	167.2	173.35	14.83	0.13	0.58	22.7	0.97	28.1	0.60	8	12
307	1318	B	19	X	1	133	135	168.23	174.38	14.84	0.11	0.58	22.6	1.00	28.9	0.67	5	10
307	1318	B	19	X	2	80	82	169.2	175.35	14.85	0.10	0.60	23.3	0.98	28.4	0.69	5	11
307	1318	B	19	X	3	30	32	170.2	176.35	14.85	0.14	0.63	24.7	0.98	28.5	0.86	2	12
307	1318	B	19	X	4	30	32	171.2	177.35	14.86	0.13	0.61	24.1	0.99	28.6	0.65	7	13
307	1318	B	19	X	5	36	38	172.26	178.41	14.87	0.16	0.63	25.0	0.98	28.4	1.00	0	7
307	1318	B	19	X	5	135	137	173.25	179.4	14.90	0.09	0.65	25.8	0.99	28.6	0.88	2	14
307	1318	B	19	X	6	79	81	174.19	180.34	14.93	0.07	0.64	25.1	1.00	28.9	1.00	0	20
307	1318	B	19	X	7	30	32	175.2	181.35	14.95	0.08	0.64	25.3	0.98	28.4	0.94	1	16
307	1318	B	19	X	8	30	32	176.2	182.35	14.98	0.12	0.62	24.4	0.98	28.2	0.93	1	13
307	1318	B	20	X	1	43	45	176.93	183.08	15.00	0.11	0.59	23.0	0.98	28.4	0.73	3	8
307	1318	B	20	X	1	143	145	177.93	184.08	15.03	0.11	0.59	22.8	0.98	28.3	0.94	1	16
307	1318	B	20	X	2	88	90	178.88	185.03	15.05	0.21	0.61	24.1	0.99	28.6	0.75	3	9
307	1318	B	20	X	3	41	43	179.91	186.06	15.07	0.12	0.62	24.4	0.99	28.6	0.79	6	23
307	1318	B	20	X	4	46	48	180.96	187.11	15.10	0.12	0.62	24.6	0.99	28.7	0.67	5	10
307	1318	B	20	X	5	39	41	181.89	188.04	15.11	0.16	0.64	25.2	0.99	28.6	0.91	1	10
307	1318	B	20	X	5	141	142	182.91	189.06	15.14	0.11	0.63	24.8	0.99	28.5	0.83	2	10
307	1318	B	20	X	6	90	92	183.9	190.05	15.16	0.12	0.63	24.8	0.99	28.5	0.89	1	8
307	1318	B	20	X	7	44	46	184.94	191.09	15.21	0.16	0.62	24.5	0.98	28.3	0.79	4	15
307	1318	B	20	X	7	140	142	185.9	192.05	15.25	0.18	0.61	23.7	0.98	28.3	1.00	0	39
307	1318	B	21	X	1	26	28	186.36	192.51	15.27	0.10	0.66	26.3	0.98	28.5	0.67	4	8
307	1318	B	21	X	1	128	130	187.38	193.53	15.32	0.08	0.67	26.6	0.99	28.5	1.00	0	12

Leg	Site	Hole	Core	Type	Section	Top sample interval (cm)	Bottom sample interval (cm)	Core depth (mbsf)	Composite depth (mcd)	Age (ATNTS 2012; Ma)	BIT index	TEX86	TEX86-H temperature	UK37	SST-UK'37	SST-dino	# Cold-water dinocysts	# Warm-water dinocysts
307	1318	B	21	X	2	82	84	188.42	194.57	15.37	0.08	0.66	26.3	0.99	28.5	1.00	0	7
307	1318	B	21	X	3	27	29	189.37	195.52	15.42	0.13	0.60	23.4	0.99	28.6	0.96	1	23
307	1318	B	21	X	3	129	131	190.39	196.54	15.47	0.10	0.61	23.8	0.98	28.4	0.96	1	23
307	1318	B	21	X	4	84	86	191.44	197.59	15.52	0.15	0.58	22.5	0.97	28.1	0.71	4	10
307	1318	B	21	X	5	64.5	66.5	192.245	198.395	15.55	0.15	0.58	22.3	0.97	28.2	0.82	3	14
307	1318	B	21	X	6	80.5	82.5	193.405	199.555	15.61	0.10	0.62	24.3	0.98	28.3			
307	1318	B	21	X	7	27.5	29.5	194.375	200.525	15.66	0.13	0.61	23.9	0.98	28.3	0.97	1	30
307	1318	B	21	X	7	128	130	195.38	201.53	15.70	0.12	0.58	22.5	0.97	28.0	0.87	2	13
307	1318	B	22	X	1	68.5	70.5	196.385	202.535	15.75	0.13	0.60	23.2	0.96	27.8	0.95	1	18
307	1318	B	22	X	2	20	22	197.4	203.55	15.80	0.14	0.62	24.4	0.98	28.3	0.92	2	22
307	1318	B	22	X	2	120	122	198.4	204.55	15.85	0.15	0.60	23.5	0.98	28.3			
307	1318	B	22	X	3	75.5	77.5	199.455	205.605	15.90	0.17	0.60	23.7	0.98	28.3	0.88	2	14
307	1318	B	22	X	4	64	66	200.34	206.49	15.94	0.16	0.61	24.1	0.98	28.3			
307	1318	B	22	X	5	75	77	201.45	207.6	15.98	0.16	0.61	23.7	0.98	28.2			
307	1318	B	22	X	6	20	22	202.4	208.55	16.00	0.17	0.61	24.0	0.98	28.3			
307	1318	B	22	X	6	120	122	203.4	209.55	16.03	0.11	0.58	22.4	0.96	27.8	1.00	0	19
307	1318	B	22	X	7	67.5	69.5	204.375	210.525	16.05	0.14	0.58	22.6	0.97	28.2			
307	1318	B	22	X	9	19	21	205.45	211.6	16.07	0.16	0.59	23.1	0.98	28.4			
307	1318	B	23	X	1	63.5	65.5	205.835	211.985	16.08	0.15	0.59	22.8	0.97	28.1	0.84	3	16
307	1318	B	23	X	2	20	22	206.9	213.05	16.10	0.14	0.61	23.7	0.97	28.0	0.71	4	10
307	1318	B	23	X	2	120	122	207.9	214.05	16.13	0.13	0.62	24.3	0.98	28.3	0.77	6	20
307	1318	B	23	X	3	71	73	208.91	215.06	16.15	0.11	0.62	24.4	0.98	28.2			
307	1318	B	23	X	4	20	22	209.9	216.05	16.17	0.12	0.64	25.3	0.98	28.4	0.91	2	20
307	1318	B	23	X	4	120	122	210.9	217.05	16.19	0.16	0.64	25.2	0.99	28.5			
307	1318	B	23	X	5	68	70	211.88	218.03	16.21	0.20	0.63	24.9	0.98	28.4	0.85	3	17
307	1318	B	23	X	6	17	19	212.87	219.02	16.24	0.15	0.61	23.9	0.98	28.3	0.88	3	21
307	1318	B	23	X	7	3	5	213.93	220.08	16.26	0.14	0.64	25.3	0.99	28.6			
307	1318	B	23	X	8	18.5	20.5	214.835	220.985	16.27	0.12	0.65	25.9	0.99	28.6			
307	1318	B	24	X	1	77	79	215.47	221.62	16.27	0.13	0.65	25.9	0.99	28.6			
307	1318	B	24	X	2	18	20	216.38	222.53	16.28	0.12	0.66	26.0	0.99	28.7			
307	1318	B	24	X	2	117	119	217.37	223.52	16.29	0.14	0.66	26.1	0.99	28.7	0.95	1	18
307	1318	B	24	X	3	69.5	71.5	218.395	224.545	16.29	0.13	0.65	25.9	0.99	28.6			
307	1318	B	24	X	4	20	22	219.4	225.55	16.30	0.12	0.65	25.8	0.99	28.6			
307	1318	B	24	X	4	120	122	220.4	226.55	16.31	0.13	0.65	26.0	0.99	28.6			
307	1318	B	24	X	6	63	65	222.83	228.98	16.36	0.11	0.65	25.9	0.99	28.7			
307	1318	B	25	X	1	18	20	223.88	230.03	16.38	0.14	0.67	26.6	0.99	28.7	0.93	1	14
307	1318	B	25	X	1	117	119	224.87	231.02	16.41	0.18	0.68	27.2	0.99	28.7			
307	1318	B	25	X	2	69.5	71.5	225.895	232.045	16.43	0.23	0.67	26.8	1.00	29.0	1.00	0	13
307	1318	B	25	X	3	20	22	226.9	233.05	16.45	0.16	0.67	26.8	0.99	28.6			
307	1318	B	25	X	4	20	22	227.74	233.89	16.47	0.14	0.66	26.3	0.99	28.5			
307	1318	B	26	X	1	58	60	228.88	235.03	16.48	0.14	0.65	25.9	1.00	29.0			
307	1318	B	26	X	2	11	13	229.92	236.07	16.49	0.16	0.64	25.2	0.98	28.5	0.58	8	11
307	1318	B	26	X	2	112.5	114.5	230.935	237.085	16.50	0.14	0.61	24.1	0.98	28.5	0.91	2	21
307	1318	B	27	X	1	40	42	235.4	241.55	16.54	0.14	0.63	25.0	0.99	28.5			
307	1318	B	27	X	1	128	130	236.28	242.43	16.55	0.14	0.63	24.8	0.98	28.5			
307	1318	B	27	X	3	41.5	43.5	238.415	244.565	16.57	0.18	0.60	23.5	0.97	28.1	0.57	9	12
307	1318	B	27	X	3	140	142	239.4	245.55	16.58	0.17	0.59	22.9	0.98	28.3	0.83	4	19
307	1318	B	27	X	4	89.5	91.5	240.395	246.545	16.59	0.14	0.61	23.7	0.98	28.3	1.00	0	29
307	1318	B	27	X	6	25.5	27.5	241.325	247.475	16.60	0.15	0.62	24.3	0.99	28.5	1.00	0	8